UNIVERSITY OF SOUTHAMPTON

FACULTY OF NATURAL & ENVIRONMENTAL SCIENCES

Ocean and Earth Science

Photoacclimation, production and critical depth: a comparison of phytoplankton dynamics in Lagrangian and Eulerian models

by

Melissa Tomkins

Thesis for the degree of Doctor of Philosophy

September 2015

UNIVERSITY OF SOUTHAMPTON

ABSTRACT

FACULTY OF NATURAL & ENVIRONMENTAL SCIENCES

Ocean and Earth Science

Doctor of Philosophy

PHOTOACCLIMATION, PRODUCTION AND CRITICAL DEPTH: A COMPARISON OF PHYTOPLANKTON DYNAMICS IN LAGRANGIAN AND EULERIAN MODELS

by Melissa Sophie Tomkins

Marine phytoplankton growth is controlled by non-linear processes, such as the photosynthetic and photoacclimative response to irradiance. Traditional Eulerian models calculate rates of primary production using the assumption that phytoplankton have identical properties, whereas Lagrangian models simulate phytoplankton as individual particles, tracking their trajectories through the light field. It might therefore be expected that photoacclimation in Lagrangian models would have an impact on seasonal cycles. In this thesis, I construct a Lagrangian ecosystem model, applying it to two questions: whether the individual responses of phytoplankton to their local irradiance affects the overall rates of primary production, and whether Lagrangian models are necessary for the study of the mechanisms surrounding the spring bloom, due to their representation of phytoplankton growth in response to mixing.

The study begins by addressing some of the fundamental assumptions underpinning Lagrangian models, and provides novel solutions for some of the difficulties. The model was set up for Ocean Weather Station India (OWSI) in the North Atlantic, and the predicted seasonal cycles of primary production were shown to not differ from those predicted by an Eulerian equivalent, due to the phytoplankton being mixed too fast to have time to acclimate to local irradiances. Additionally, the results suggested a closer relationship between the timescales of growth and mixing, demonstrating that vertical profiles of phytoplankton could form within a well-mixed layer, resulting in changes to the overall rates of primary production. The model was next used to investigate the controls of the spring bloom at OWSI, by investigating the critical depth, critical turbulence and disturbance-recovery hypotheses. Although the use of Lagrangian model did highlight a possible source of inaccuracy when calculating critical depth with an Eulerian model, overall an Eulerian model could have performed the experiments with the same results, given information about the vertical profile of phytoplankton in the mixed layer. However, the study successfully reconciled the three hypotheses, showing how each describes a mechanism that can affect the critical depth.

Contents

List of tables

List of figures

DECLARATION OF AUTHORSHIP

I, Melissa Tomkins

declare that the thesis entitled *Photoacclimation, production and critical depth: a comparison of phytoplankton dynamics in Lagrangian and Eulerian models* and the work presented in the thesis are both my own, and have been generated by me as the result of my own original research. I confirm that:

- this work was done wholly or mainly while in candidature for a research degree at this University;
- where any part of this thesis has previously been submitted for a degree or any other qualification at this University or any other institution, this has been clearly stated;
- where I have consulted the published work of others, this is always clearly attributed;
- where I have quoted from the work of others, the source is always given. With the exception of such quotations, this thesis is entirely my own work;
- I have acknowledged all main sources of help;
- where the thesis is based on work done by myself jointly with others, I have made clear exactly what was done by others and what I have contributed myself;
- none of this work has been published before submission

Signed: .....

Date:.....

Acknowledgements

First and foremost, I would like to thank my supervisory team of Prof. Tom Anderson, Dr. Adrian Martin, and Prof. Seth Bullock for their patience and support through a somewhat eventful Ph.D. In particular, Prof. Anderson, who has always made himself available for my many questions, remained enthusiastic about the project during times that I lost focus, and whose exemplary standards have taught me so much about the responsibility of being a scientist.

Many thanks also to the Institute of Complex Systems DTC for an amazing 5 years. Thanks to Nicki Lewin and Seth Bullock, I have felt a valued part of a group of scientists involved in a new and exciting collaboration. I am also extremely grateful to the EPSRC for funding the project.

I would also like to thank my sister, Eleanor, for being an amazing Medante, and supporting me so much throughout, and especially at the end of my write-up. Mwah! Also, I am fortunate enough to have a very patient husband, Simon, who has supported me throughout my studies, and stayed wisely quiet when I have vented my frustration at him. Many thanks for food and babysitting duties goes to: Claudia and Joe Stewalt, and Claire and James Hunt.

Also, I would like to acknowledge Tabitha and Magnus, my beautiful children, who haven't seen much of their mother over the last few weeks!

Finally, I would like to thank Prof. John Woods for first introducing me to the field of Lagrangian ecosystem modelling, and for teaching me how to build and run Lagrangian models..

List of Acronyms and Abbreviations

Acronym	Description
OWSI	Ocean Weather Station India. A site in the North Atlantic located at 59°N 19°W
M95	McGillicuddy (1995)
LL89	Lande & Lewis (1989)
HK07	Hellweger & Kianirad (2007)
WW88	Wolf & Woods (1988)
PAR	Photosynthetically active radiation
P-I curve	Curve describing the photosynthetic response to changes in irradiance
DIN	Dissolved inorganic nitrate
NPZD	Nutrient-phytoplankton-zooplankton-detritus
MLD	Mixed layer depth
CDH	Critical depth hypothesis
CTH	Critical turbulence hypothesis
DRH	Disturbance-recovery hypothesis
SI	Super-individual
NABE	North Atlantic Bloom Experiment
ERA40	45-year global atmospheric reanalysis dataset for the period 1 September 1957 to 31 August 2002
KPP model	K profile parameterisation model (Large et al., 1994)

List of Symbols

Symbol	Description	Units
I_C	Compensation irradiance	W m^{-2}
I_S	Saturation onset	W m^{-2}
I_B	Inhibition threshold	W m^{-2}
I_0	Irradiance at the surface	W m^{-2}
Z_{Cr}	Critical depth	m
D_C	Compensation depth	m
P_{SI}, P_{Conc}	Phytoplankton nitrogen (individual, population)	mmol N, mmol N m^{-3}
Chl_{SI}	Super-individual cellular Chl content	mg Chl
Z	Zooplankton state variable	mmol N m^{-3}
D	Detritus state variable	mmol N m^{-3}
DIN	Dissolved inorganic nutrient state variable	mmol N m^{-3}
DIN_0	Sub-thermocline DIN	mmol N m^{-3}
$\theta_{Chl,SI}$	Cellular super-individual Chl:C	g Chl (g C)$^{-1}$
$\mu_{P,SI}$, μ_{Ptotal}, μ_{Pconc}	Growth rate (individual, population, concentration)	d^{-1}
V_{SI}^{PT}	Rate of photosynthesis at current temperature, irradiance	gC (gChl)$^{-1}$ h^{-1}
G_{SI}, G_{Pconc}	Grazing (individual, population)	mmol N d^{-1}, mmol N m^{-3} d^{-1}

$R_{Chl,z}$	Chlorophyll scaling factor	dimensionless
I_Z	Irradiance at depth, z	W m^{-2}
S_{Chl}	Shape function to modify production with depth	dimensionless
V_P	Maximum photosynthetic rate at 0˚C	gC $(gChl)^{-1}$ h^{-1}
V_{PT}	Maximum photosynthetic rate at current temperature	gC $(gChl)^{-1}$ h^{-1}
α_P	Chl-specific initial slope of P-I curve	(gC $(gChl)^{-1}$ h^{-1} $(W\ m^{-2})^{-1}$
k_N	N nutrient uptake half-saturation constant	mmol N m^{-3}
m_P	Phytoplankton respiration rate	d^{-1}
m_{P2}	Phytoplankton mortality rate	d^{-1}
k_P	Phytoplankton mortality half-saturation constant	mmol N m^{-3}
I_{max}	Maximum zooplankton grazing rate	d^{-1}
k_g	Zooplankton grazing half-saturation constant	mmol N m^{-3}
ϕ	Zooplankton grazing inefficiency	dimensionless
m_Z	Zooplankton respiration rate	d^{-1}
m_{Z2}	Zooplankton mortality rate	d^{-1}
k_Z	Zooplankton mortality half-saturation constant	mmol N m^{-3}
ζ	N:C conversion factor (Redfield ratio of 6.625)	mol N $(g\ C)^{-1}$
$\theta_{\max}^{Chl}$	Maximum cellular Chl:C	g Chl $(g\ C)^{-1}$

V_D	Detrital sinking rate	m d^{-1}
m_D	Detrital N remineralisation rate at 0˚C	d^{-1}
k_{mix}	Cross-thermocline mixing rate	m d^{-1}
P_{div}	Threshold for particle division	mmol N
δt	Time step	minutes
H	Depth of the surface mixed layer	m
k_{par}	Vertical light attenuation coefficient	m^{-1}
k_W	Background light attenuation coefficient	m^{-1}
k_C	Phytoplankton light attenuation coefficient	m^{-1}
K_{turb}	Vertical diffusivity coefficient	m^2 s^{-1}
z	Vertical depth	m
w_x	Turbulent velocity scale	m s^{-1}
G	Vertical shape function	dimensionless
κ	von Kármáns constant	dimensionless
u^*	Wind friction velocity	m s^{-1}
U	Wind speed	m s^{-1}

Introduction

"If there is a starting point for thinking about populations, it must be the individual. Individual organisms are born, grow, develop, mature, move, reproduce, and eventually die. The rates at which these processes occur determine whether the population increases or decreases, persists or becomes extinct, expands or contracts, fluctuates or remains stable. The environment affects the population through its effects on these individual processes." (Tuljapurkar & Caswell, 1997)

Phytoplankton are mostly single celled plants that live suspended in either marine or freshwater environments. In the ocean, they constitute a major component of marine primary production, forming the base of the food web that sustains our fisheries, which provide the most important source of protein in many developing countries. In addition, marine photosynthesis provides over 50% of our atmospheric oxygen, while simultaneously providing an important sink for global carbon. There is therefore a great onus on scientists to understand the most important controls on phytoplankton, how they respond to changes in their ecosystem, and how the ecosystem responds in return.

Performing experiments in the ocean is expensive, full of difficulties, and only provides a snapshot of the system at the time the observations are made. Therefore, marine ecosystem models - simplified abstractions of full ocean ecosystems - are useful tools for scientists to use when investigating the complex relationships between the physical forcing, and the biogeochemistry in the ocean. These models have a wide application in the field of oceanography, for the purposes of quantification of the global carbon cycle and its relationship to the climate, using past trends to predict how the current anthropogenic input could influence the ocean in the future, connecting sparse ocean observations in a coherent manner, and understanding and describing the fundamental ecological controls on marine ecosystems.

Developing a model of a marine ecosystem first starts with identifying and understanding the important underlying mechanisms. Many simplifications have to be made, in order to reduce the complex interplay of physics,

chemistry and biology to solvable mathematical expressions. A commonly used simplification in marine ecosystem models is to represent the phytoplankton as a concentration of biomass, evenly distributed through the model space. These Eulerian models, named for Eulerian measurements, which are taken from fixed locations and measure the properties of the water that moves through them, calculate rates of primary production by dividing the water column into vertical bins, averaging the light intensity over each bin, and then calculating the growth rate for each bin by integrating the growth functions over time. They therefore assume that all of the phytoplankton are completely identical. In reality, however, phytoplankton move through fluctuating fields of light, nutrients and predators, which results in variability between the individual cells. For example, phytoplankton are known to regulate their light-harvesting capacity in response to changes in irradiance, by downgrading production of pigments in high irradiance, and increasing it when exposed to lower irradiances, in a process known as photoacclimation. Any one depth in the ocean could therefore be populated by phytoplankton with a range of photosynthetic abilities, depending on the previous light history of each individual cell. Lagrangian models, named for Lagrangian measurements, which follow and measure the properties of individual fluid parcels, track individual phytoplankton particles as they move through space and time. These first integrate over time, using the light history of each phytoplankton cell, and take the rate of production as the ensemble average of the entire community. As averaging non-linear equations before integration does not give the same results as averaging them after integration (Woods & Onken, 1982), these two approaches would be expected to give differing results. This has moved some researchers (Nagai et al., 2003; Ross et al., 2011a; Woods & Onken, 1982) to propose that a Lagrangian approach is more appropriate for accurate representation of primary production.

Whilst the theory behind the use of Lagrangian phytoplankton models is compelling, there currently exists little conclusive evidence regarding their advantage over their Eulerian counterparts. Nevertheless, Lagrangian models are becoming a popular choice, due to their ability to depict individual processes that Eulerian models are unable to capture. Unfortunately, Lagrangian models can be computationally expensive, often requiring more resources for their development and maintenance than for their actual

application (Fulton et al., 2003). The lack of standards for Lagrangian models means that most are created from scratch, and each decision needs to be carefully thought out and justified. Therefore, before implementing a Lagrangian approach, it is important to ensure that it is necessary for the problem at hand.

In this thesis, I construct a new Lagrangian ecosystem model, and use it to investigate three topics:

1. The fundamental assumptions underpinning Lagrangian models, and their potential effects on the resulting ecosystem dynamics (Chapter 2). This chapter details the construction of the Lagrangian model, and in the process, describes new methods for handling the interactions between Lagrangian phytoplankton and an Eulerian ecosystem.
2. The relationships between photoacclimation, photosynthesis and the turbulent mixing of the ocean surface layer (Chapter 3). A first of its kind Eulerian-Lagrangian intercomparison study involving a model with a full ecosystem parameterised for a site in the ocean (Ocean Weather Station India) demonstrates that these two model formulations do not give differing predictions. The reason for this is investigated by an in-depth analysis using simplified fixed-slab models, which shows that the rates of photoacclimation are too slow to allow phytoplankton time to acclimate to local irradiances. In addition, a closer relationship is found between the rates of photosynthesis and mixing, and this is shown to have a greater control on rates of primary production when mixing is low.
3. The controls of the spring bloom in the North Atlantic. Lagrangian models include information regarding the rates at which phytoplankton are mixed through the water column, making them ideal for the exploration of the hypotheses surrounding the controls of the spring bloom. In this chapter, the three main hypotheses (critical depth, critical turbulence, and disturbance-recovery) are thoroughly investigated, to explore the conditions that result in each one describing the main controls on net production, and then they are reconciled as all being extensions of the critical depth hypothesis.

In addition, Chapter 1 provides the general background for each of the above topics, and the implications of this work, along with potential avenues for future research are discussed in Chapter 5.

Chapter 1: General background

"A model is a simple representation of a complex phenomenon. It is an *abstraction,* and therefore does not contain all the features of the real system. However, a model does comprise all the characteristic ones, those essential to the problem to be solved or described."

(Soetaert & Herman, 2008)

Model design generally starts with two questions: what is the purpose of the model, and what are the essential characteristics of the system to be modelled? This thesis approaches this process the other way around – the model is built based on the assumption that a Lagrangian approach will allow for greater accuracy in the resulting predictions, and is then used to test this assumption in a number of different ways, including an Eulerian-Lagrangian model intercomparison study, extensive exploration of individual phytoplankton behaviour within controlled fixed-slab models, and through its application for testing current ecological theory.

In this chapter, the relevant background for the study is presented. The underlying theme of the thesis concerns the influence of molecular level processes on large scale patterns of primary production, and the structure of this introduction reflects this progression. The cellular level process of interest is the acclimation of phytoplankton to changes in their local irradiance, and this chapter introduces the underlying mechanisms controlling this. Whilst this process is very well understood in the laboratory, it is less clear how it impacts on overall rates of primary production in the ocean, in particular with respect to whether phytoplankton physiology and photosynthetic efficiency is continually adjusting to the fluctuations in irradiance experienced by phytoplankton as they travel through the mixed layer. The relationship between primary production and mixing has been previously investigated both through empirical experimentation, and through the use of modelling methods, both of which are discussed in respect to the current study. The study site - the Ocean Weather Station India in the North Atlantic - and the reasons for its choice are then described and discussed. Finally, the

applicability of a Lagrangian approach for the investigation of the spring bloom in the North Atlantic, involving the three current main hypotheses surrounded the processes that govern this phenomenon – the critical depth, the critical turbulence and the disturbance-recovery hypothesis, is discussed.

1.1 Mixing, growth and photoacclimation

Marine phytoplankton use sunlight to synthesise foods from carbon dioxide and water, in a process known as photosynthesis. Chlorophyll, and other accessory pigments, absorb sunlight and convert it to usable energy through carbon fixation. The relationship between the rate of carbon fixation and the intensity of the irradiance is commonly described by the use of a curve, known as a photosynthesis-irradiance (P-I) curve. Figure 1shows a typical P-I curve, as well as some of its common features.

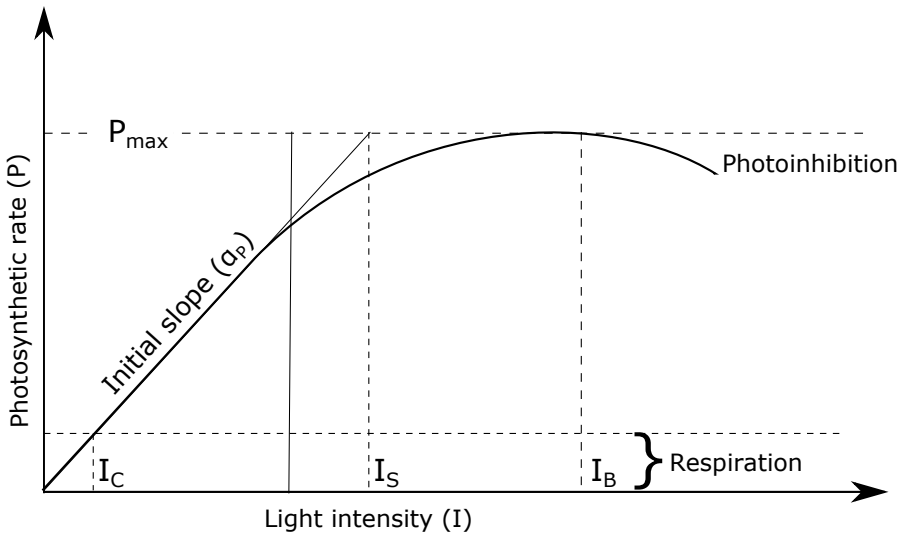

Figure 1: Typical shape of a P-I curve representing the response in phytoplankton production to light. The marked irradiances are I_c = compensation irradiance, I_s = saturation onset, and I_B = inhibition threshold

At low irradiances, the rate of photosynthesis is usually proportional to light intensity (with slope α_P), because photosynthesis is limited by the rate at which the light photons can be absorbed. Once the saturation threshold is reached (I_S), the algae become 'light-saturated', and the rate of photosynthesis is limited by the rate of the reactions following the capture of photons. This is the maximum rate of photosynthesis, P_{max}, and is independent of light intensity. Once an inhibitory threshold is reached (I_B), the rate of

photosynthesis starts to decrease with light intensity, due to the deactivation of key proteins in the photosynthetic units, known as photoinhibition (Béchet et al., 2013). Also shown in Figure 1, is the *compensation irradiance* (I_C), which is the irradiance at which the rate of photosynthesis exactly matches the rate of respiration (and other losses) in a phytoplankton cell. The depth at which this occurs in the ocean is known as the *compensation depth*, and is often taken to mark the base of the euphotic zone.

1.1.1 What is photoacclimation?

Photoacclimation describes a series of related physiological and biochemical changes that allow algal cells to optimise their harvesting and utilisation of available light. This enables phytoplankton to survive under dim light when transported to the depth of the water column, whilst avoiding photodamage when exposed to the intense surface radiation (Pinchasov-Grinblat et al., 2011). This thesis uses the terminology recommended by Falkowski & Raven (2013) who differentiate between short-term *acclimation* processes, and physiological *adaptations* which occur on longer time-scales, through genetic modifications. Photoacclimation is important for phytoplankton because of the extreme temporal and spatial variations in their light field. Even though terrestrial vegetation is also exposed to daily and annual cycles of irradiance, these are amplified in aquatic environments due to the attenuation of light by water and the substances and particles dissolved and suspended in it (Dubinsky & Stambler, 2009). This means that as phytoplankton are vertically mixed through the water column, they experience a wide range of light intensities. In order to maximise growth under sub-optimal conditions, and also to limit the damage that may be incurred through exposure to high irradiances, phytoplankton alter their chlorophyll production dependent on the light regime. To prevent excess energy from being absorbed that could potentially damage the photosynthetic system, phytoplankton downgrade the production of chlorophyll in high light. At the same time, phytoplankton in low light conditions increase their production of chlorophyll (Geider et al., 1998) .

Photoacclimation can be assessed by measuring differences in the physiology and photosynthetic efficiency of phytoplankton grown at different light intensities (Moore et al., 2006). P-I curves provide a useful mechanism for depicting changes to phytoplankton growth rates due to photoacclimation, because they differentiate between light-limited and light-saturated growth. However, whether growth is normalised to chlorophyll, carbon or is cell-specific can provide different impressions of the effects of photoacclimation (MacIntyre et al., 2002). This can be seen in Figure 2, which shows the response curves for cultures of the marine diatom *Skeletonema costatum,* grown at either a high (1200 µmol photons m^{-2} s^{-1}), or a low (50 µmol photons m^{-2} s^{-1}) irradiance. Plotting chl *a* specific photosynthetic rates against irradiance (A) shows similar initial slopes for the high and low light acclimated cells, although the point at which the light saturates differs greatly. High light acclimated cells have a higher chl *a* specific light saturated photosynthetic rate, although this is because chl *a* is a much lower proportion of total mass in high light cells, and rather than the

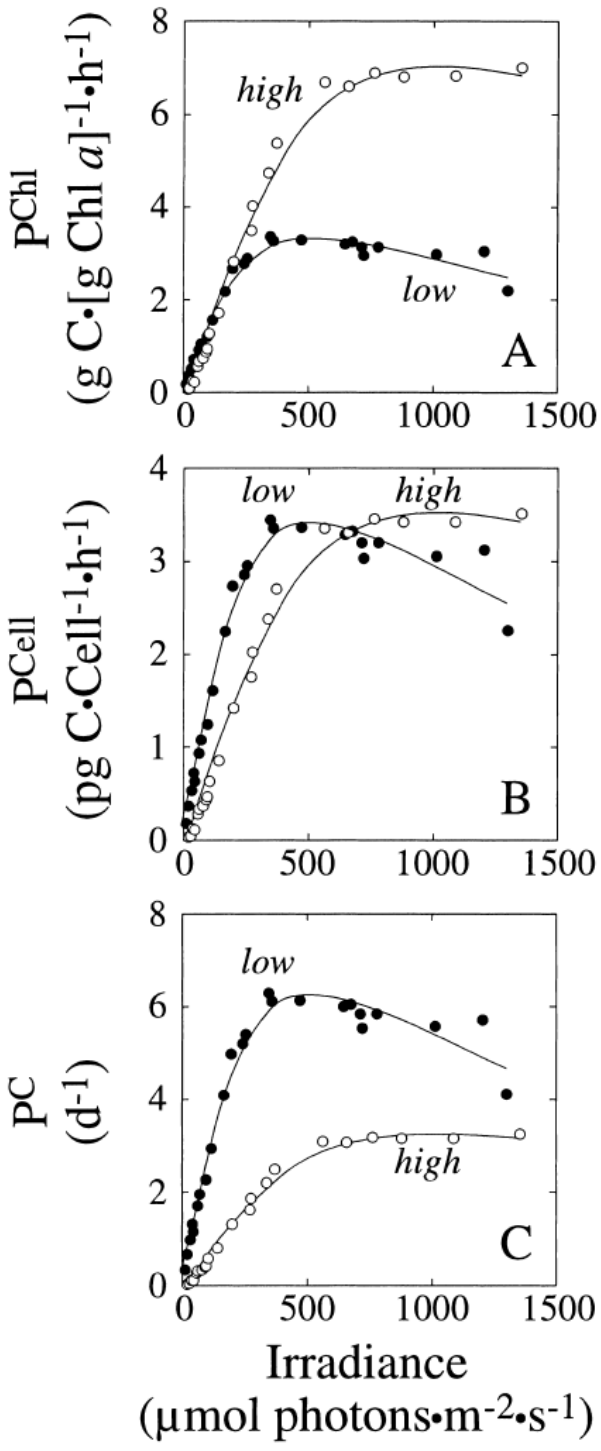

Figure 2: P-I response curves for high light (1200 µmol photons m-2 s-1) and low light (50 µmol photons m-2 s-1) acclimated nutrient replete cultures of the diatom *Skeletonema costatum*. A) Chl a-specific photosynthesis B) Cell-specific photosynthesis C) Carbon specific photosynthesis. Figure taken from MacIntyre (2002) of data from Anning (2000)

high light acclimated cells outperforming the low light acclimated ones. Rates of photosynthesis can also be expressed on a per cell basis (B). However, changes to the environmental conditions can result in changes to the average mass of the cells, confusing the relationship between growth rate and cell-specific photosynthetic rate. A third approach is to represent rates of photosynthesis normalised to carbon content (Figure 2C). This allows for the rates of photosynthesis to be directly compared to growth rates (MacIntyre et al., 2002). Figure 2C shows how when the photosynthetic response curves are represented on a carbon-specific basis, the two cell cultures show a difference in both the initial slope and the maximum rate of photosynthesis.

1.1.2 Modelling photoacclimation

Phytoplankton growth models can be used to replicate laboratory data of the response of phytoplankton cells to changes in their irradiance. Marra (1978) compared rates of primary production from experimental bottles suspended at a series of fixed depths, with rates of primary production from bottles circulated through the water column. He found that the vertically cycled bottles gave estimates of integral photosynthesis that were significantly higher than those of the stationary bottles. He then conducted laboratory experiments, where he measured the rates of photosynthesis for a marine diatom grown under three different light regimes: constant, simulated diurnal variation, and fluctuating. He discovered that the rates of photosynthesis were higher in the simulations with fluctuating light. He proposed that the parameters that control the rates of photosynthesis are time dependent. Above some threshold irradiance, rates of photosynthesis will decrease over time, with the sharpest decrease occurring at the highest light intensities. He suggested that this allowed phytoplankton to optimise the fluctuations imposed by a turbulent environment by taking advantage of the brief exposures to the surface light intensity, but that if a phytoplankter remained at a shallow depth, then the rate of photosynthesis would decay over time.

Marra's results led to the development of phytoplankton growth models that included a time dependence of the rates of photosynthesis. The parameters that control the rate of photosynthesis (i.e. that define the shape of the P-I curve), α_P, P_{max} and β, where α_P represents the initial slope of the P-I curve, P_{max} the maximum rate of photosynthesis, and β controls the current state of

photoinhibition, are modified over time. A function (usually logistic) describes the way the steady state values of each function vary with irradiance. These parameters then move towards their steady state values, depending on a prescribed rate of acclimation (e.g. Barkmann & Woods (1996a) Cullen & Lewis (1988), Falkowski & Wirick (1981), Lande & Lewis (1989), Wolf & Woods (1988) and Woods & Barkmann (1993)). Two examples of these, the model described by Lande & Lewis (1989), and the model used in Wolf & Woods (1988) are given in detail in the next section. Although these models can produce good fits to empirical data, they are parameterised according to specific scenarios, which makes them difficult to use for different locations.

Mechanistic phytoplankton growth models, on the other hand, include explicit representation of underlying phytoplankton processes, such as the allocation of energy between growth, storage and pigment production under variable irradiance and nutrient conditions. They predict not only rates of photosynthesis, but also the current cell composition in regards to the ratios of pigment and biomass (Flynn, 2001; Geider et al., 1997; Geider et al., 1996; Geider et al., 1998; Zonneveld, 1998). These have the advantage of being easily adaptable to different ocean locations, plus they produce additional data (i.e. chl-to-carbon ratios) that can be verified against empirical observations. The dataset obtained by Anning et al. (2000) (some of which is shown in Figure 2) has proved highly useful for the testing of these models, as it includes information not only about the rates of photosynthesis under varying light conditions, but also about changes to cell composition (e.g. ratios of chl-to-carbon, and nitrogen-to-carbon). The phytoplankton growth model used in this thesis is based on the mechanistic model described in Geider et al. (1997), and is fully described in the next chapter.

1.1.3 Photoacclimation in the ocean.

Phytoplankton photoacclimation has been the focus of many laboratory studies (a good review of these can be found in MacIntyre et al. (2002)) and the response of phytoplankton under laboratory conditions is well understood, but uncertainty still exists as to how the response of individual phytoplankton affects overall rates of primary production in the ocean. This is an important question for researchers, because phytoplankton growth rates are often calculated using incubation bottle experiments, which involve taking a sample

of phytoplankton from the ocean, and then incubating it in bottles at fixed depths (or irradiances). If the physiological changes made by phytoplankton as they move vertically through the water column affects their rates of photosynthesis at each depth, then fixed incubation bottles will give inaccurate estimates of primary production. Conducting experiments in the open ocean is obviously both costly and time-consuming, and so previous studies have used models in order to investigate the relationship between mixing and rates of primary production. However, the results from these studies seem far from clear cut. Differences in the way that photoacclimation is represented, plus the fact that some models also include a separate function for damage incurred through photoinhibition, has resulted in a great deal of confusion surrounding modelling studies that have investigated the effects of mixing on rates of primary production. For example, Barkmann & Woods (1996b) and Ross et al., (2011a,b) both conducted modelling studies using Lagrangian phytoplankton models, and concluded that fixed incubation methods overestimate primary production, although they differed in their calculations of the magnitude of this overestimation, with Barkmann and Woods (1996) suggesting it was by up to 40%, and Ross et al., (2011a,b) predicting an overestimation of up to 25%, although less than 15% in the majority of cases. In contrast, modelling studies by Franks & Marra (1994) and Kamykowski et al. (1994) both proposed that rates of photosynthesis in the mixed layer actually increase with increasing wind stress, and therefore higher rates of mixing. Finally, Falkowski & Wirick (1981) used a random walk simulation model to investigate whether the total daily primary productivity in a mixed layer is influenced by the variations in light regimes experienced by individual phytoplankton cells. Their model predicted that primary productivity is not significantly affected by variations in light regimes due to turbulence.

1.1.4 Eulerian-Lagrangian model intercomparison studies

The previous section has described how the different modelling methods for representing photoacclimation have resulted in some confusion in the literature regarding the effects on rates of primary production of mixing. Another method to determine whether accounting for the individual photoresponse of phytoplankton results in changes to the population growth rates, would be to directly compare equivalent models that account for

individual variability (Lagrangian models), and those that base primary production on average photoacclimative properties (Eulerian models). There are three main studies that have directly compared Eulerian and Lagrangian implementations of phytoplankton models: Lande & Lewis (1989), McGillicuddy (1995) and Hellweger & Kianirad (2007).

The first study was performed by Lande & Lewis (1989), who created analytical models of photoacclimation and photosynthesis, based on data on the photosynthetic physiology of an ocean diatom, *Thalaisiosira pseudonana*. Their model was set in a mixed layer depth that was assumed to be significantly deeper than the euphotic zone. The rate of photosynthesis, *P*, was calculated as a function of the ambient light intensity, *I*, using the equation:

$$P(I;\alpha,P_s,\beta) = P_s\left(1-e^{\left(\frac{-\alpha I}{P_s}\right)}\right)e^{\left(\frac{-\beta I}{P_s}\right)} \quad (1.1)$$

Photoacclimation was then represented by α, P_s and β being assumed to have fully adapted values, Γ_i^*, which were linear functions of the logarithm of the light intensity. The instantaneous values shown by the individual phytoplankton cells were then calculated according to first order reaction kinetics:

$$\frac{\partial \Gamma_i}{\partial t} = \gamma_i\left(\Gamma_i^* - \Gamma_i\right) \quad (1.2)$$

where γ_i = constant rate of acclimation. The cells were assumed to move via a Brownian motion diffusion process reflected at the sea surface, with mean equal to zero and variance equal to $2K_{turb}$, where K_{turb} = the diffusivity constant, which was set to 0.01 $m^2\ s^{-1}$. Surface irradiance was a constant 2000 $\mu E\ m^{-2}\ s^{-1}$, and light was attenuated with depth by a constant parameter, k_{par}, which was 0.04 m^{-1} (i.e. attenuation due to water only, no self-shading). The time of day was early afternoon, so that the vertical profiles of the photosynthetic parameters had equilibrated to the noon irradiance. There was assumed to be a constant, evenly distributed number of cells in the water column.

They used their model to calculate the mean, variances and covariances of the photoacclimation properties (α, P_s and β) for the single cell model, and then

used these values to calculate the approximate average rates of photosynthesis at each depth. These results were then compared to an equivalent Eulerian model. They found no predicted difference in the photoacclimative properties in the two models, and less than 1% difference between the predicted rates of photosynthesis. They concluded that the similarity of the rates of photosynthesis predicted by the two models was a consequence of the rapid photoacclimation of the photosynthetic traits in *T. pseudonana*, which occurs on time scales of a few hours. Therefore, on a clear day, vertical mixing by turbulent diffusion does not prevent cells from being nearly fully acclimated to the ambient irradiance, at least on average. They suggested that vertical mixing would have a larger impact on the rate of depth-integrated primary production for species with slower rates of acclimation.

The second study comparing Eulerian and Lagrangian implementations of phytoplankton models was undertaken by McGillicuddy (1995), hereafter M95, who implemented numerical Eulerian and Lagrangian versions of the Lande and Lewis (1989) model (hereafter, LL89). M95 also implemented Eulerian and Lagrangian versions of a model taken from Wolf & Woods (1988), (hereafter, WW88), and compared the predictions of each model under different mixing regimes.

WW88 used a simple photoacclimation model, whereby the energy (irradiance) absorbed by each Lagrangian Ensemble individual (or super-individual) is calculated using an 'efficiency factor', $\varepsilon = \exp\left(\frac{-I}{I_m}\right)$, based on the average irradiance experienced by the super-individual over a defined period of acclimation I_m, which they took to be 5 hours.

M95 set the models in an idealized 1D simulation, using a constant mixed layer depth (100m), and a diel cycle of irradiance consistent with conditions during the vernal equinox at 40°N. The Lagrangian simulations were initialized with a concentration of 1.0×10^6 cells l^{-1}, which was initially distributed between 50 particles. The particles were assumed to be randomly distributed on a time scale characteristic of the mixing layer:

$$\varepsilon \sim \frac{u^3}{l} \qquad (1.3)$$

where ε = the rate of dissipation, u = the velocity scale, and l = length scale of large eddies (set by depth of mixed layer). The turbulent velocity was then calculated, using an estimate of the rate of dissipation, with the turnover time of the mixing layer, τ_m, then being given by:

$$\tau_m = \frac{l}{u}. \qquad (1.4)$$

The Lagrangian trajectories of the cells are calculated assuming that the particles in the mixing layer are uniformly distributed on this timescale, i.e. a new turbulent velocity between –(u/2) and (u/2) is randomly chosen for each particle in the mixed layer after every turnover time. Thus, the velocity of the individual particles changes once every ($\tau_m/\Delta t$) time steps. In order to ensure a sufficient number of phytoplankton super-individuals in the simulation at any one time, if the number of individuals in any one 1-metre layer fell below 20, then all of the individuals in that layer were divided into two equal individuals. He investigated two mixing regimes - one weak (K_{turb}=0.01m^2 s^{-1}) and one strong (K_{turb}=4.64m^2 s^{-1}). He found little difference in the predicted growth rate (<5%) for the different model formulations with relatively weak mixing, but that there was a significant reduction in the mean growth rate of the WW88 Lagrangian model version (~20%) in vigorously mixed conditions, whereas the LL89 model showed only slight differences (~3%) under an increased mixing regime. M95 concluded that the difference shown by WW88 was due to their use of exponential photoacclimative reaction kinetics. Although this would result in the phytoplankton reaching a fully acclimated state faster than the phytoplankton in LL89, the initial slope of the curve showing the photosynthetic response to changes in irradiance is much steeper, meaning that the phytoplankton show greater immediate losses to photosynthetic efficiency in response to changes in light intensity. Due to the fact that the timescale of mixing was much faster than that of acclimation under the vigorously mixed conditions, this meant that the phytoplankton were always in this early part of the photoresponse curve, and the WW88 phytoplankton were continually in a state of light shock. Were both models to use the same kinetics, then this discrepancy would be alleviated, and M95 suggested that the first-order kinetics used by LL89 seemed to be more supported by previous literature.

The third study that directly compares Lagrangian and Eulerian implementations of phytoplankton models was performed by Hellweger & Kianirad (2007), hereafter HK07. HK07 explored the effect of Lagrangian formulations on cell quota models, and, in particular, those scenarios where intra-population variability in natural systems leads to differences between Lagrangian and Eulerian models. They used a simple growth model, where the growth rate (μ) was a function of the cell quota (mmol P mmol C^{-1}):

$$\mu = \mu_{\max} \cdot \min\left[\left(1 - \frac{q_0}{q}\right), LH\right] \quad (1.5)$$

where q_0 = subsistence quota (μ=0) and LH = limitation threshold (accounts for limitation by a nutrient not explicitly represented).

HK07 proposed that applying Eulerian and Lagrangian models to heterogenous phytoplankton populations would produce differing results, because of a mathematical phenomenon known as 'Jensen's inequality'. They argued this through the description of an idealised case, where the phytoplankton population was split into two equally sized sub-populations, A and B, with cell quotas of q_0 and $3q_0$, respectively. An Eulerian model would average out the cell quotas before calculating the growth rate, resulting in:

$\mu = \mu_{\max}\left(1 - \frac{q_0}{av\left[q_0, 3q_0\right]}\right) = 0.5\mu_{\max}$. A Lagrangian model would first calculate the growth rate of each sub-population, and then average the resulting rates:

$$\mu(A) = \mu_{\max}\left(1 - \frac{q_0}{q_0}\right) = 0.0 \text{ and } \mu(B) = \mu_{\max}\left(1 - \frac{q_0}{3q_0}\right) = 0.67\mu_{\max}$$

The average growth rate in the Lagrangian model is therefore $av\left[0.0, 0.67\right]\mu_{\max} = 0.33\mu_{\max}$, which is significantly lower than the growth rate calculated using the Eulerian model.

They constructed equivalent Eulerian and Lagrangian models, and applied them to a realistic field scenario. The results of their model appeared to confirm their hypothesis, as the Lagrangian representation showed a decreased averaged growth rate. However, as they pointed out, this discrepancy was a result of the limitation threshold, which states that when a

cell quota is above the threshold, the photosynthetic rate is at the attainable maximum. For the whole population, the average cell quota is above the threshold, and the Eulerian approach would predict a population photosynthesis rate at the attainable maximum. For many of the individuals, the cell quota is also above the threshold and their photosynthesis rate is at the attainable maximum. However, a significant number of individuals have cell quotas below the threshold, and their photosynthesis rate is below the attainable maximum. As a result, the population average photosynthetic rate is also below the attainable maximum.

1.2 The current study

The main objective of the study is to investigate the changes to the photoacclimative state of phytoplankton as they travel vertically through the surface mixed layer of the ocean. Therefore, the two most important model components were the turbulence model, and the photoacclimative model. It was crucial to find methods that would produce realistic timescales of mixing and acclimation, whilst keeping the model as simple as possible, in order to both allow comparison with an equivalent Eulerian implementation, and to be able to strip the model back to basics in order to clearly understand the behaviour of the phytoplankton.

1.2.1 Photoacclimation model

The phytoplankton photoacclimation model needed to be sensitive to short-term changes in irradiance, whilst still being simple enough to allow for thorough examination of the response of the phytoplankton. In addition, setting the model up for OWS India would require the ability to adjust the photoacclimative parameters in a meaningful fashion. As has been previously discussed, using a mechanistic model would both allow for individual changes in phytoplankton physiology to be represented, and produce further output for validation with empirical data, such as the cellular ratios of chl-to-carbon.

Flynn et al. (2001) compared the performance of different versions of two N-based mechanistic models of photoacclimation, concluding that the implementation that best describes the response of phytoplankton to changes in their irradiance was a set-up based on the model version described in Geider

et al. (1998). This model is first described in Geider et al. (1996), and describes how phytoplankton growth rate and chl-to-carbon ratio change in response to variations in irradiance. The production of chlorophyll in the model depends upon the ratio of the energy supply from light absorption and photosynthetic energy conversion, to the energy demand for growth. At high irradiances, the rate of light absorption exceeds the rate at which it is assimilated, and chlorophyll production is downgraded. The model was then extended in Geider et al. (1997) to include temperature and nutrient concentration dependence, with the result that reductions in the growth rate due to temperature or low nutrient concentrations could also lead to a reduction in the chl-to-carbon ratio. The model was later extended again, to allow for unbalanced growth, in Geider et al. (1998), through the inclusion of a variable ratio of nitrogen-to-carbon. A further, cell-based implementation was then introduced in Ross & Geider (2009). Although this latter version is designed for implementation in Lagrangian models, it was deemed not to be suitable for the current study, as it would be difficult to perform a direct comparison with an equivalent Eulerian model, and also it would be difficult to strip the model back in order to fully understand how each change affected the behaviour of the phytoplankton. However, one important difference between the cell-based model version and the previous Geider models was in the ability of the phytoplankton to synthesise chlorophyll in the absence of irradiance from energy stored during the day. Previously, chlorophyll production could only take place at the same time as photosynthesis, so that chl-to-carbon ratios remained constant overnight. A model that allowed for photoacclimation in the absence of light could produce different results from those presented in this thesis, and this is discussed in more detail in Chapter 3.

Although Flynn et al. (2001) recommended the model described in Geider et al. (1998), the inclusion of variable ratio of nitrogen-to-carbon was not needed for the current study, plus, one advantage of the Geider et al. (1997) version is the ability to create an analytical equation describing the steady-state chl-to-carbon ratio of phytoplankton to any irradiance. In addition, the two models showed little variation in their behaviour in terms of predictions of chl-to-carbon (Figure 3), so the simpler model was chosen for the current study.

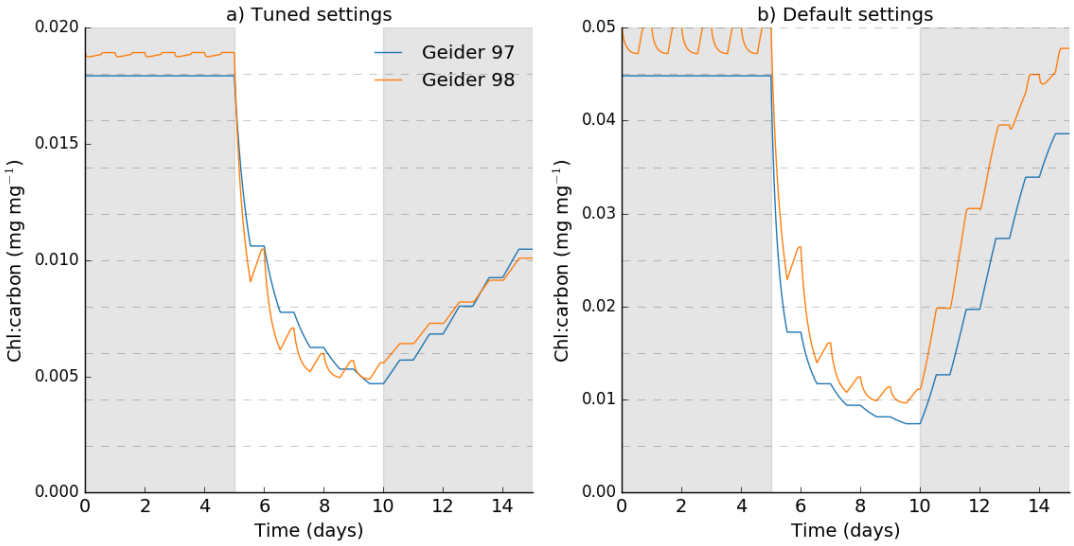

Figure 3: The response of G97 and G98 to changes in irradiance. The models are run for 5 days at low irradiance, 5 days at high irradiance, and then 5 days low irradiance, with a 12h light, 12h dark diurnal cycle. For G98, when irradiance is 0, photosynthesis was also set to 0 (to avoid divide by zero errors in the equations). The two plots show a) the parameter settings used to reproduce the phytoplankton cycles at OWS India (θ_{Chl}^{max}=0.02, θ_{N}^{max}=0.1), as well as the default parameters settings (θ_{Chl}^{max}=0.05, θ_{N}^{max}=0.389), where θ_{Chl}^{max} and θ_{N}^{max} represent the maximum ratios of chl-to-carbon, and chl-to-nitrogen, respectively.

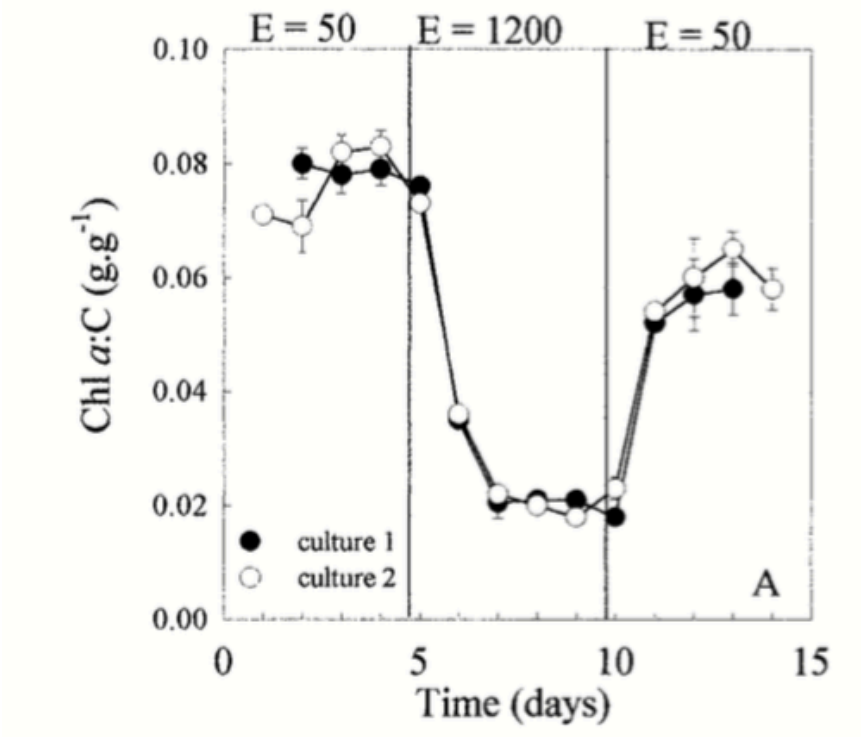

Figure 4: Phytoplankton response to changes in irradiance between high and low light regimes in the laboratory. Taken from Anning et al. (2000)

1.2.2 Turbulence model

The upper surface boundary layer of the ocean comprises the interface between the ocean and atmosphere. Mixing occurs at this interface at a wide range of scales, from the formation of small bubbles formation, to heat-driven convective mixing (Figure 5). Turbulence models can therefore range from those that attempt to simulate all mixing at all levels (direct numerical simulation), to those that perform some kind of averaging of the mixing processes (statistical and empirical turbulence models).

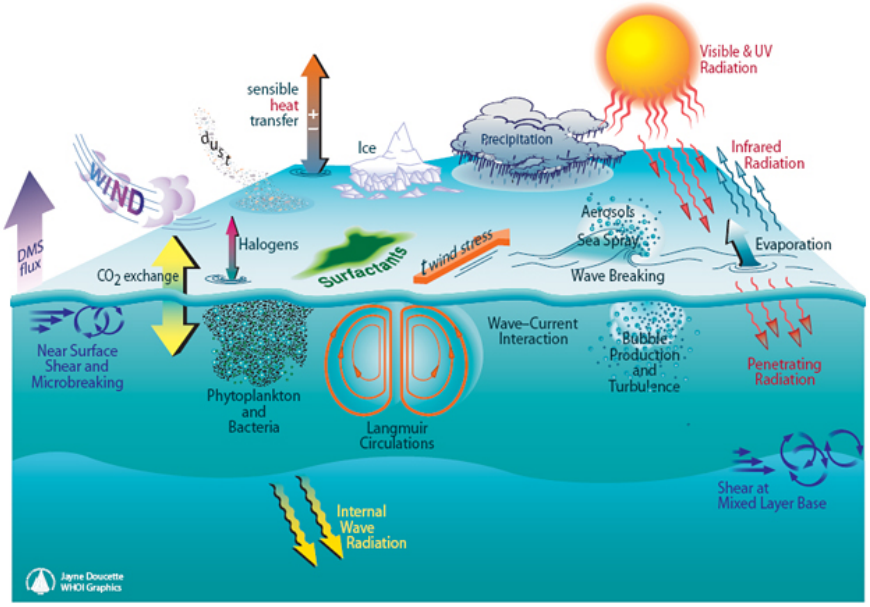

Figure 5: The large and small scale processes affecting the level of turbulence in the ocean surface boundary later of the ocean. Image taken from https://www.whoi.edu/ooi_cgsn/page.do?pid=53278&tid=1621&cid=70189&article=43126

Choosing the correct turbulence model for a simulation depends upon the types of processes under investigation, and on finding a suitable balance between accuracy and computational cost. For example, as the current study is only concerned with mixing in the vertical, there is no need to simulate lateral motion. Therefore, a highly computationally intensive method, such as direct numerical simulation, which solves the Navier-Stoke equations for all scales of motion in a turbulent flow, would be unnecessary.

A more commonly used technique for simulations that require a high resolution is Large Eddy Simulation (LES). This method is based on the underlying concept that large eddies migrate across the flow, carrying smaller scale disturbances with them. The larger eddies, which carry out most of the

mixing are computed, and then the smaller eddies, which dissipate the energy cascading from the large eddies, are represented through the use of sub-grid scale models. This reduces the computational cost by avoiding representing all of the smaller scale processes. However, as one of the aims of the current study is to strip the model back to basics, in order to fully understand the behaviour of the phytoplankton, use of an LES would not have been suitable. Instead, it was decided to move the phytoplankton using a random walk, parameterised by the rate of turbulent diffusivity in the surface mixed layer; a commonly used method in Lagrangian phytoplankton modelling (Falkowski & Wirick, 1981; Ross et al., 2011a; Ross et al., 2011b; Visser, 1997). The mixing rates can then be obtained through the use of statistical or empirical models of turbulence. Statistical models of turbulence calculate averages of the Navier-Stokes equations, through the use of turbulence closure techniques. These can be divided into three main classes: bulk models that assume homogeneity of the mixed layer; one equation closures, which resolve TKE in the vertical based on eddy length scale; and two equation closures, which use an additional equation for length scale or related quantity. Empirical models are similar to statistical turbulence models, but use entirely empirical knowledge of fluxes, rather than approximating turbulence fluxes through the use of closure techniques. Therefore, the accuracy of the empirical turbulence models depends upon the accuracy of the empirical measurements (Paskyaci & Fer, 2010).

For this study, an empirical model of turbulence, the non-local K-profile Parameterization (KPP), was chosen. This was an ideal choice for the study, as the model could be tailored for OWS India, using empirical data on surface wind speed and the annual cycle of mixed layer depth. It is relatively insensitive to vertical resolution, making it a suitable method for low-resolution configurations. In their review of oceanic turbulence models, which included description and testing of the KPP model, Large et al. (1994) showed that the KPP model can perform as well, or in some cases, even better than other models in its class, and, most importantly, if given the correct surfacing forcing, will distribute properties properly in the vertical.

1.2.3 The study site

As previously mentioned, one of the aims of the study was to gain understanding of how cellular level processes impact upon rates of primary production in the ocean. Although good data describing the response of phytoplankton cells to variations in irradiance in the laboratory exist, it is not clear whether phytoplankton in the open ocean will respond in the same way as those in a laboratory setting. Therefore, the model parameters controlling the photoacclimative response of the phytoplankton were obtained by tuning the model predictions to available empirical data for an ocean site, which described both the chlorophyll concentrations, and the pigment:biomass ratios. Only one station was explored, as this was sufficient to achieve the aim of examining photoacclimation in an environmental rather than a laboratory setting.

The chosen study site is Ocean Weather Station India in the North Atlantic (59N, 19W), which is part of the network of ocean weather stations that were established after World War II, in order to collect long-term observations of ocean water and atmospheric properties (Send el al., 2001). It is situated between the Hatton Bank and the Iceland Basin, in a water depth of 2000m. The site is characterized by a deep winter mixed layer, followed by stratification in spring accompanied by a phytoplankton bloom. It is an ideal site for this study, due to its clear seasonal cycle of phytoplankton, which includes a very large spring bloom

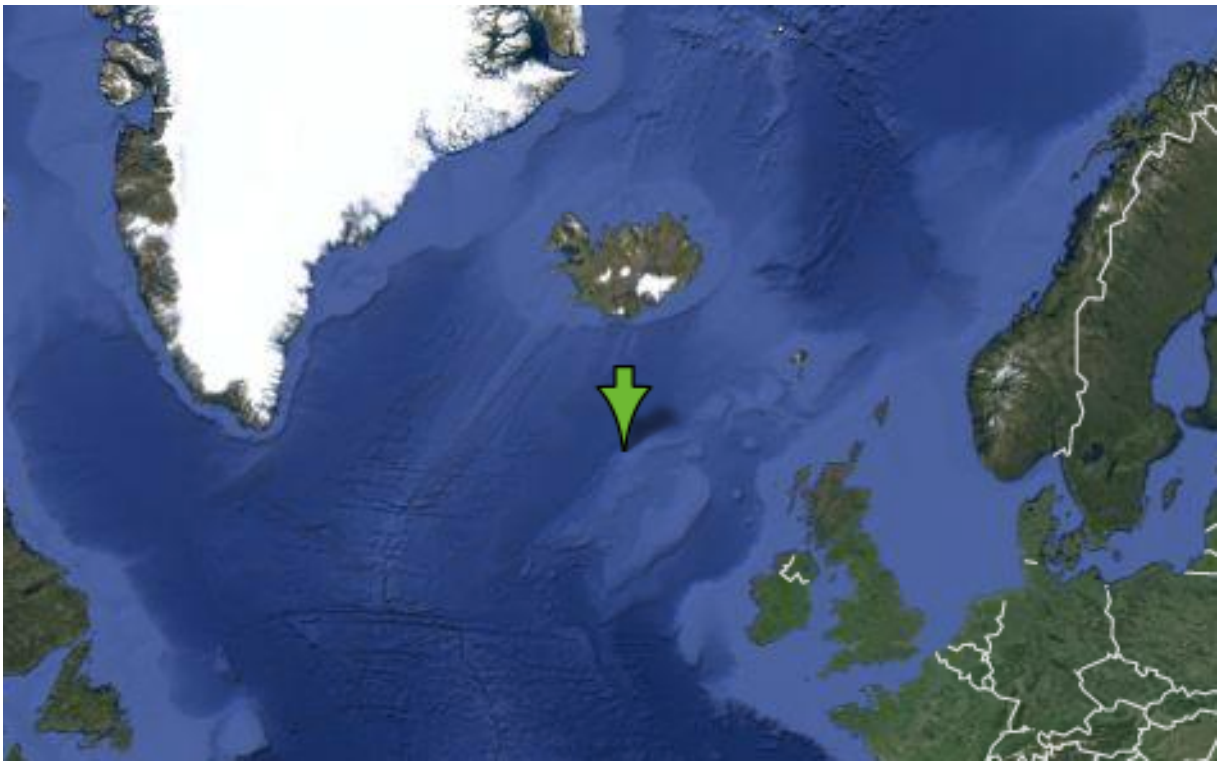

Figure 6: Ocean Weather Station India. Source: "OWSI" 59° 0' 0"N, 19° 0' 0"W. Google maps. 2014

The spring bloom results in visible changes to the phytoplankton concentration at the surface of ocean, which can be measured using satellite imagery (Figure 7).

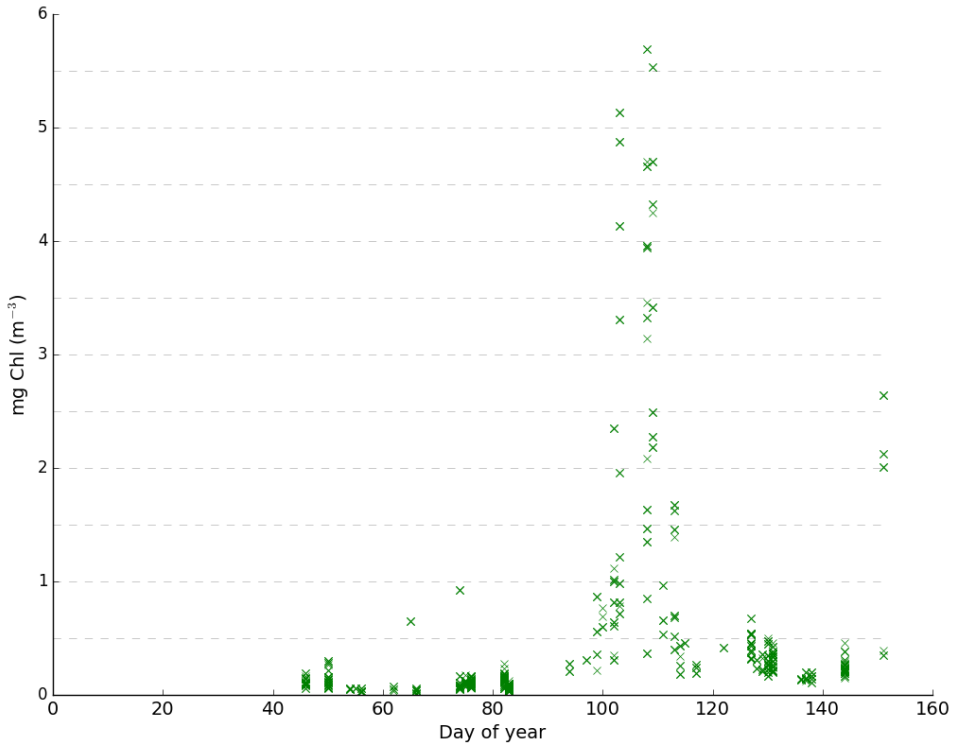

Figure 7: Satellite measurements of surface chlorophyll taken between 58.5 and 59.5N and 18.5 and 19.5W in 2015 (2016)

Models generally look at predictions of integrated biomass, which can be give a misleading impression of a bloom, as this surface growth is not constant, but varies on a daily basis depending on the weather (overcast days, wind) and the ocean (fronts, eddies) conditions. Figure 8 shows how the evolution and peak of the spring bloom (days 90 to 114 of 2015) looked in the area surrounding OWS India in 2015.

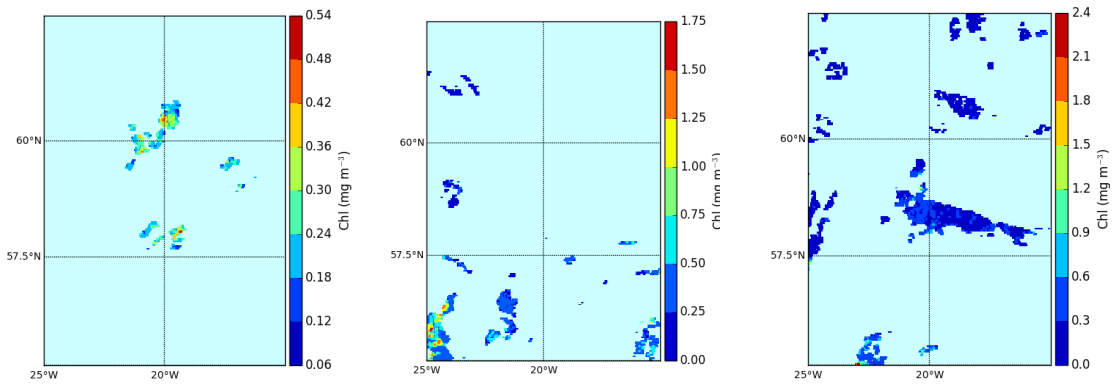

Day 90 Day 92 Day 94

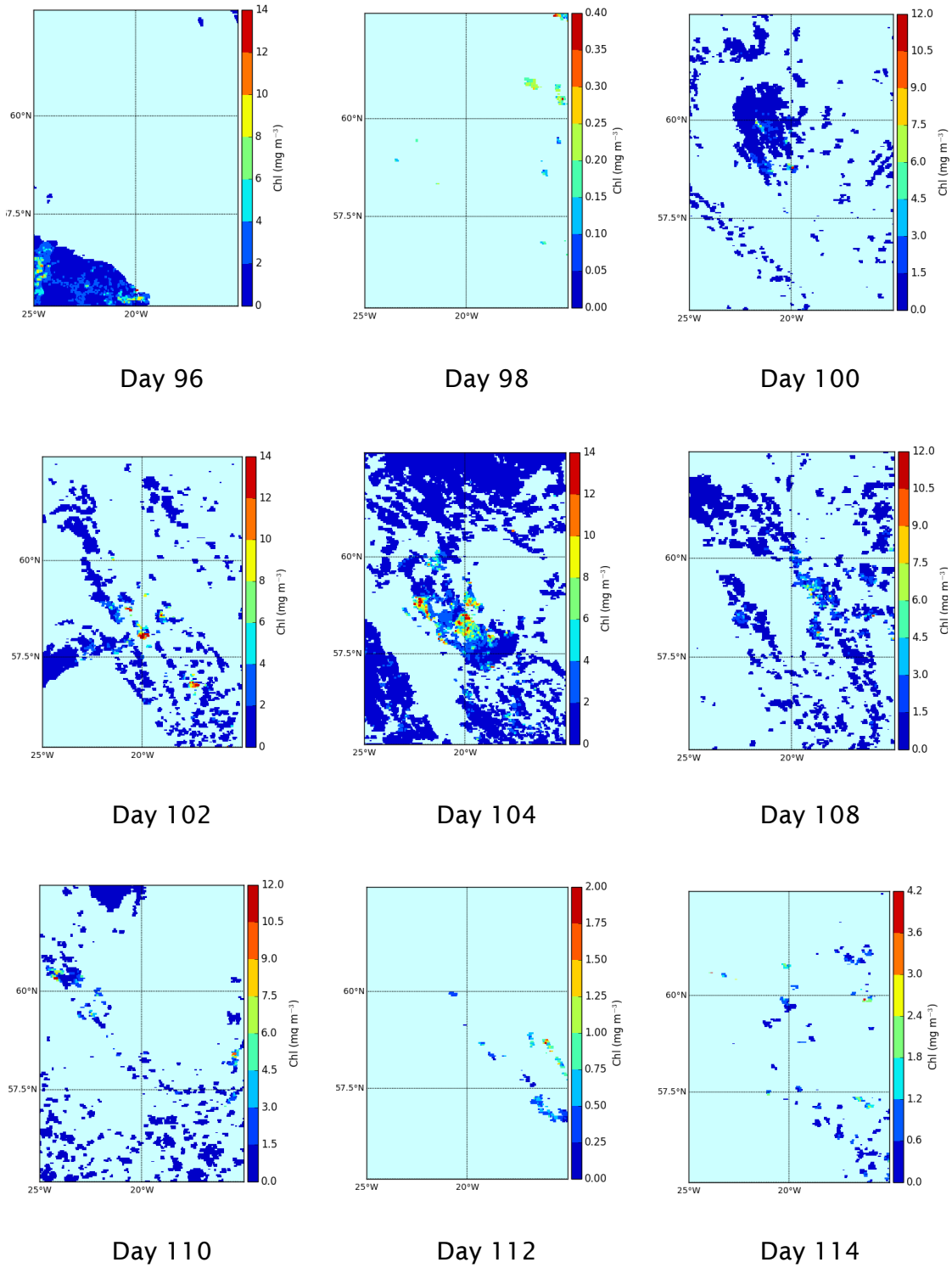

Figure 8: Surface chlorophyll measurements taken from satellite observations in 2015 (2016)

1.2.4 The timing of the onset of the spring bloom in the North Atlantic

Understanding the mechanisms of the spring bloom holds great importance both in terms of ecosystem dynamics, with implications for carbon export

efficiency and food availability for higher trophic levels, and for detecting changes in the ecosystem from natural or anthropogenic forcing (Cole et al., 2015)., The second part of the study was therefore concerned with determining the controls of the spring bloom in the North Atlantic.

Although the North Atlantic is a good testing ground for models of the spring bloom, due to its clear cycle of phytoplankton, it is not typical of the subpolar global basins. It has very deep winter mixed layers, and differs from the North Pacific and Southern Ocean, which have permanent haloclines and are iron limited (Cole et al., 2015). However, as the current study focuses on determining the conditions that best describe the three main hypotheses of the causes of the initiation of the spring bloom, rather than determining one absolutely cause for spring bloom initiation, OWS India is a suitable study site.

The three theories under investigation are based around two different concepts: that the spring bloom results from a temporary decoupling of the growth-loss cycles of the phytoplankton (disturbance-recovery hypothesis), or that changes in physical factors such as mixing rates, mixed layer depth, and surface irradiance, trigger rapid increases to net production (critical depth, critical turbulence hypotheses).

1.2.5 Sverdrup's critical depth hypothesis

The critical depth hypothesis was first proposed by Sverdrup (1953), as a formalisation of ideas already advanced by Gran and Braarud (1935) and by Riley (1946, 1942). The idea behind it is simple: if the turbulence within the surface mixed layer of the ocean is high enough to evenly distribute the phytoplankton, then the rate at which the phytoplankton are moving will result in them experiencing the average irradiance in the mixed layer, I_D, which is a function of the surface irradiance and its attenuation with depth. Assuming that all losses are constant with depth, there exists a vertically averaged irradiance at which the rate of phytoplankton growth is exactly balanced by the sum of the losses. Above this irradiance, the vertically averaged growth rate is positive, below this irradiance, it is negative. Or, to put it another way, there exists a mixed layer depth, above which the average irradiance is high enough to support positive net growth, and below which there is insufficient irradiance for growth to exceed loss. These concepts are fully depicted in Figure 9.

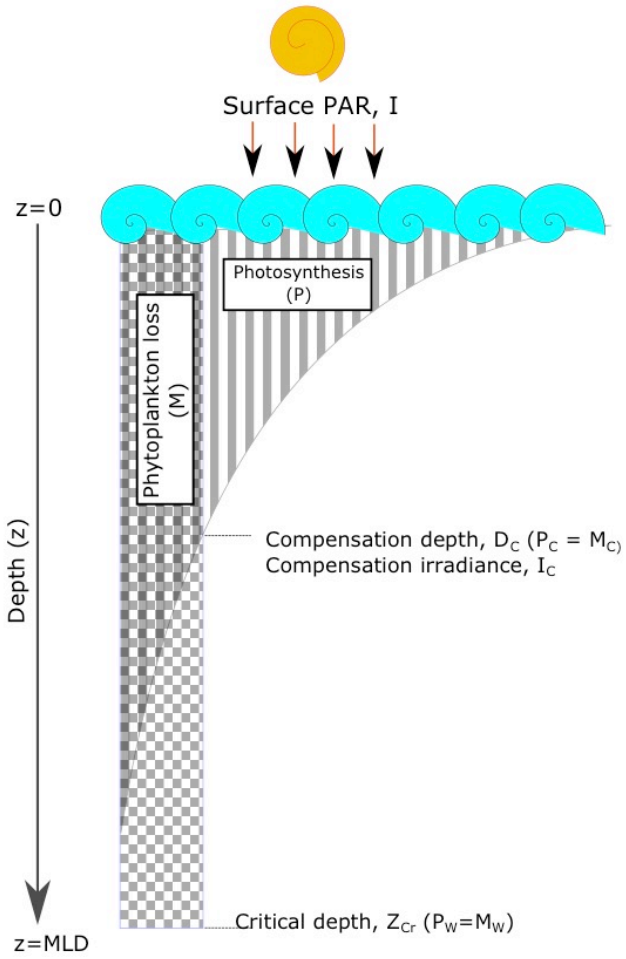

Figure 9: The relationship between the compensation irradiance and the critical depth. At the compensation depth (D_c), the irradiance is such that the photosynthesis of a single phytoplankton cell (P_c) is equal to the sum of its losses (M_c). Above this depth there is a net gain from photosynthesis ($P_c > M_c$), below it there is a net loss ($P_c < M_c$). As phytoplankton are mixed above and below the compensation depth, they experience an average irradiance (ID) in the water column. The depth at which ID equals IC is the critical depth (Z_{cr}) where photosynthesis through the water column (P_w) equals phytoplankton respiration throughout the water column (M_w). The chequered area represents phytoplankton loss (respiration, mortality, grazing, mixing), and the striped area represents photosynthesis; these two areas are equal at the critical depth. Figure redrawn from Lalli and Parsons (1997).

Sverdrup stated that it would be possible to predict the critical depth, using several assumptions, including:

1. The mixed layer experiences turbulence strong enough to evenly distribute the phytoplankton

2. The phytoplankton are not nutrient-limited

3. Phytoplankton loss rates are constant with depth

4. The coefficient for light attenuation, k_{par}, is constant

5. The value for the compensation irradiance, I_C, is known

The compensation irradiance, I_C, is the irradiance at which the growth rate of a phytoplankton cell exactly balances all its losses (Figure 9). As phytoplankton within a well-mixed layer experience the average irradiance within that layer, the average irradiance from the surface down to the critical depth, I_D, is equal to the compensation irradiance, I_C. This represents the lowest irradiance at which the phytoplankton can grow, and varies from species to species. Currently, values for I_C are often obtained from culture experiments that measure the minimum irradiance required for a population to survive. These have been criticised for taking no account of many of the loss processes found in the ocean, and tend to range over an entire order of magnitude from 0.35 to 3.5 mol photons m^{-2} d^{-1} (~0.9 to 9 W m^{-2}) (Siegel et al., 2002). Sverdrup defined the compensation irradiance as being the balance between growth and loss. If the rate of production is proportional to the irradiance, with slope α_P, then the rate of change of production with time, *t*, is:

$$\frac{dp}{dt} = \alpha_P \cdot I_z \tag{1.6}$$

If the loss rate, *m*, is assumed to be a constant, then the loss over the same time period is:

$$\frac{dr}{dt} = m_p \tag{1.7}$$

Therefore, by definition, $I_z = I_c$ at the depth where $dp = dr$. Therefore:

$$I_C = \frac{m_P}{\alpha_P} \tag{1.8}$$

However, as the mortality rate depends upon both the concentration of the phytoplankton and the grazing populations, it seems unlikely that I_C is a constant.

Once the above assumptions have been accounted for, the critical depth, Z_{cr} (m), can be calculated using the equation:

$$\frac{Z_{cr}}{1-e^{-kZ_{cr}}} = \frac{1}{k_{par}} \frac{I_0}{I_c} \tag{1.9}$$

where I_c represents the compensation irradiance, and I_0 represents the irradiance at the surface.

The critical depth hypothesis has gained a number of critics, although some of these are due to misinterpretations of its assumptions. For example, Sverdrup's use of the term 'respiration' to account for all phytoplankton losses (e.g. mortality, grazing, mixing) has led to some confusion. In addition, studies testing the critical depth hypothesis often neglect the assumption of a fully mixed layer. For instance, Townsend et al., (1992) reported that in the offshore waters of the Gulf of Maine, the spring bloom could precede the onset of seasonal stratification. They proposed that the combination of the deepening of light penetration in the clear waters during spring with the lack of, or weak vertical mixing, could maintain cell growth rates that could exceed the mixing rates, thus leading to a bloom. They further suggested that the scattering and absorption of irradiance by the phytoplankton could enhance the warming of the surface waters, and the development of the thermocline could be a consequence of the spring bloom, rather than a trigger. However, this scenario is not a valid test of the hypothesis, as weak vertical mixing would not result in the phytoplankton being evenly distributed with depth. This has led some researchers (e.g. Chiswell, 2011; Franks, 2014) to differentiate between a mixed layer, which is generally measured through changes in density, using proxies such as salinity or temperature, and a mixing layer, which is a source of active turbulence. For example, at the end of winter, a measurable deep mixed layer resulting from convection and winter storms may still exist, but with the end of surface cooling and a reduction in wind stress, the vertical mixing within the layer could be considerably reduced compared to the wintertime values (Chiswell, 2011). This distinction is not new to the literature, Yamazaki and Kamykowski (1991) also separated the idea of a characteristically similar mixed layer, and an active turbulent mixing layer. In fact, some authors suggest that few studies have properly tested Sverdrup's hypothesis, as this would require knowledge of both the phytoplankton growth

rates and the measurements of turbulence, as it is the turbulence that move the phytoplankton through the vertical light gradient (Franks, 2014).

Smetacek and Passow (1990) criticised Sverdrup's use of a constant loss rate over both depth and the diurnal cycle, pointing out that dark respiration is known to be highly variable, with regard to both species and growth conditions. Cells within a deep mixed layer can experience prolonged periods of darkness, resulting in changes to rates of dark respiration. In addition, most species can produce resting stages, some of which remain photosynthetically active (Lindemann & St John, 2014). Smetacek and Passow were further concerned that focussing on phytoplankton respiration in this manner diverts attention to the lower reaches of the euphotic zone, whereas spring bloom induction is far more likely to be governed by processes occurring close to the surface. They concluded that the 'critical depth' of importance to bloom development is found in the upper, rather than the lower, third of the euphotic zone.

Lindemann et al. (2015) used a Lagrangian phytoplankton model to investigate the effects of a variable rate of respiration and sinking on predictions of primary production. Respiration was proportional to photosynthesis in the light, but decreased in the dark, with the rate of decrease reducing exponentially over time. They found that using variable rates for respiration (and sinking) allowed the model to capture both the observed phytoplankton concentration during deep convective mixing, and the timing and magnitude of the onset of the spring bloom. In order to achieve the same result from a model with fixed rates of respiration and sinking required the use of unrealistic parameters.

1.2.5.1 The critical turbulence hypothesis

Huisman et al. (1999) proposed that critical depth theory is insufficient in itself to predict net phytoplankton production in cases where there is weak to moderate turbulence. Their model relaxed the assumption of phytoplankton homogeneity, allowing the dynamics of phytoplankton growth and turbulent mixing to determine the distribution of phytoplankton with depth. They argued that critical depth is only relevant for water columns with high enough levels of turbulence to result in well-mixed phytoplankton populations. Once the turbulence falls below some critical value, phytoplankton growth rates can

exceed vertical mixing rates, resulting in net production, regardless of the depth of the mixed layer.

This critical turbulence hypothesis was then extended by Taylor and Ferrari, (2011) who suggested that it could be used to predict net phytoplankton growth from meteorological conditions. They proposed that there is a window in time between the winter deep mixing and the spring stratification, where mixing can occur close to the surface, while the deeper mixed layer still retains its homogenous properties. Under these conditions, the density defined mixed depth does not give an accurate representation of the actual mixing depth, and surface blooms can occur. They therefore believed that the crucial control on phytoplankton growth rates is related to the switch of seasonal thermal forcing from net cooling to net warming, and that shutting off of atmospheric cooling could trigger a phytoplankton bloom, regardless of the details of biological or physical response (Ferrari et al, 2014).

1.2.5.2 The disturbance-recovery hypothesis

The previous theories describe the triggers of the spring bloom as a consequence of abiotic factors, such as sunlight, nutrients and temperature, increasing the phytoplankton growth rate. However, Behrenfeld and Boss (2014) proposed that there is no evidence in the literature for any correlation between the rate of phytoplankton biomass accumulation and phytoplankton growth (which they defined as cell division) rates, and that the bloom is a result of disturbances in the balance between phytoplankton growth and loss rates, in particular, grazing. They termed this the disturbance-recovery hypothesis.

The idea that spring blooms result from disturbances to the phytoplankton seasonal cycle of growth and loss was first proposed by Evans and Parslow (1985). They used a simple, NPZ model to demonstrate that, unlike the classical view of phytoplankton blooms being due to rapid changes in phytoplankton growth rates due to sudden stratification, blooms were actually a result of rapid changes in the specific growth rates. This meant that, although a sudden, rapid change in phytoplankton growth could result in a high enough specific rate of change to result in a bloom, a very low growth rate during the winter (i.e. resulting from deep mixed layers), will also result in a high specific rate of change through spring, causing a bloom to develop.

This idea was expanded on in the dilution-recoupling hypothesis, proposed by Behrenfeld (2010), which describes the spring bloom as being a result of the decoupling of phytoplankton biomass from zooplankton grazing pressure over winter. The deepening mixed layer dilutes the concentration of phytoplankton and zooplankton, leading to a reduction in grazing pressure, due to the density dependence of grazing. As the water column begins to stratify in early spring, the ability of the zooplankton to remain within the mixed layer increases grazing pressure once more, recoupling the predator-prey relationship, but only after the phytoplankton have had time to accumulate significant biomass. However, due to the deepening of the mixed layer, the increase in phytoplankton biomass before the onset of stratification is not apparent. This is also an important source of carbon export, as the phytoplankton cells below the depth of spring stratification do not contribute to the spring bloom, as they are detrained and lost to the deep ocean (Lindemann & St John, 2014). The disturbance-recovery hypothesis then extends this idea to include other sources of disruption to the phytoplankton growth – loss balance, such as deep winter mixing, freshwater input, upwelling, or polar night (Behrenfeld et al., 2013). They define the start of a bloom as the point when the net integrated growth first becomes positive, stating that the peak of the spring bloom is just the final stage. Unlike the critical depth hypothesis, which focuses on bottom-up control, the disturbance-recovery hypothesis looks at top-down controls of the phytoplankton concentrations.

1.2.5.2.1 Modelling the hypotheses describing the controls of the spring bloom

Non-linear processes, such as photoacclimation, and the relationship between photosynthesis and irradiance, control phytoplankton growth. As a result, the way that phytoplankton move through the fluctuating fields of nutrients and irradiance will impact upon their photoacclimative state, and their growth rate. Therefore, Franks (2014) proposed that in order for a model to properly test the critical depth hypothesis (and therefore also the critical turbulence, and disturbance-recovery hypotheses) it needs to include information about the rates of turbulent mixing, as well as the rates of phytoplankton growth.

Lévy (2015) used an Eulerian NPZ model, to investigate the necessary conditions to model the critical depth, critical turbulence, and disturbance-recovery hypotheses. She started with a simple simulation, based on Sverdrup's original model, and then gradually increased the complexity through the addition of light saturated growth, nutrient limitation, vertical mixing, grazing, self-shading, and a seasonal cycle of mixed layer depth. However, her study was unable to obtain an exact match between the predicted (critical depth equation) and modelled (point where the net growth first became positive) bloom onset, even when using the simple set of assumptions proposed by Sverdrup, which she concluded was due to the way that the Sverdrup solved the critical depth equation (i.e. for steady-state).

She found that including the vertical mixing, allowed the model to reproduce the conditions described in the critical turbulence hypothesis – i.e. reduced mixing resulted in a vertical profile of phytoplankton, with more biomass maintained near the surface. Increasing the biomass near the surface of the mixed layer increased the overall rates of photosynthesis, allowing for net production, even when the mixed layer was deeper than the critical depth. The addition of grazing, and a seasonal cycle of mixed layer depth, where the depth of the mixed layer deepened between the end of summer and winter, created the conditions necessary for the disturbance-recovery hypothesis. Based on this, she identified four key areas that studies wishing to investigate these three hypotheses should include:

1. A distinction between the *mixed* and the *mixing* layer
2. A full season cycle, to account for the evolution of the physical parameters from the previous summer
3. Seasonal evolution of surface irradiance
4. Variable loss, through grazing

However, Lévy concluded that the conclusions drawn within the study were limited through not exploring all of the physical and biological parameter spaces, plus that the model had not incorporated photoacclimation.

The model used in the current study, which will be introduced in the next chapter, fulfils the four requirements recommended by Lévy (2015), and, additionally, includes representation of the photoreponse of individual phytoplankton particles to changes in their environment.

1.2.6 How the current study differs from previous studies

The previous studies have not provided a definitive answer as to whether Lagrangian and Eulerian implementations of phytoplankton based ecosystem models provide differing predictions of rates of photosynthesis and biomass. Furthermore, even though LL89, and M95 both agree that there is little difference between the predicted growth rates of the Lagrangian and Eulerian models, LL89 suggest that it is because the phytoplankton are close to fully acclimated at all times, whereas M95 states that the mixing rates are much faster than the acclimation rates. In Chapter 3, I use a Lagrangian phytoplankton ecosystem model, described in Chapter 2, along with an equivalent Eulerian model, in order to address some of these questions. Both the model I am using and the analysis I perform are unique in a number of ways:

1. LL89 and M95 only investigated phytoplankton growth, with no ecosystem, and HK07 only implicitly represented zooplankton. The model designed for this study includes explicit representation of phytoplankton, detritus, nutrient concentration, and also zooplankton, allowing for not only the effects of the model formulation on phytoplankton growth to be examined, but also the consequences for the ecosystem as a whole.
2. Whilst LL89 used a constant surface PAR, M95 used a diel cycle based on one time of year, and HK07 neglected irradiance completely, my study uses a full, annual cycle of irradiance, based on a specific ocean location (Ocean Weather Station India).
3. Photoacclimation is represented by simple growth models in LL89, and M95, whereas is it omitted completely in HK07, who looked at a quota model of phosphate to carbon. My model uses a phytoplankton growth model which represents photoacclimation based on . This is a well known and well tested method that has been used in a large number of ecosystem studies (for example: Fennel et al. (2006); Lima and Doney (2004); Patara et al. (2011); Spitz et al. (2001); Vichi et al. (2007); Yool et al. (2013, 2011)). This not only allows the model to be directly compared with previous modelling studies, but the nature of the growth equations allows for predictions of the steady-state values of the photoacclimative properties, which can then be compared to the

individual states of phytoplankton photoacclimation. In addition, extra verification of the model can be achieved by comparing the resulting ratios of chl-to-carbon to empirical observations.

4. The movement rules in LL89 and M95 are based on Brownian motion, using a constant rate of dissipation, whereas, although the movement rules in HK07 are based on explicit particle tracking routines (ECOMSED v. 1.3), there is little detail as to how these routines are parameterised. The model in this study uses a random walk based on Visser (1997), with the diffusivity calculated from the surface wind speed and mixed layer depth as per the ocean boundary layer model described in Large et al. (1994). The model is parameterised using mixed layer depths taken from World Ocean Atlas (Antonov et al., 2010) and 5 year averaged wind speed data from the ERA 40 data set for OWSI. This means that it is able to represent changes in mixed layer depths, and also deeper mixed layer depths (i.e. the 500m+ depths observed at OWSI) unlike LL89, which doesn't use a specific mixed layer depth, M95 which looks at a fixed 100m depth, and HK07, which is more interested in horizontal distribution, and use a fixed depth of 10m.

1.3 Project Objectives

The above summary has demonstrated several questions that have not yet been satisfactory resolved in the literature: the effect of mixing on primary production, the relationships between the rates of photoacclimation and mixing, and the controls of the timing of the spring bloom. The current study will address these questions through examination of the central question to this study: will predictions of primary production from a Lagrangian model, that takes into account the previous histories of the individual phytoplankton particles, differ from that of an equivalent Euerian model?

Some of the other issues that will be addressed in the course of this thesis are:

- what is the best practice for setting up Lagrangian phytoplankton models?

- how do decisions regarding the underlying assumption of Lagrangian models impact on the resulting predictions for phytoplankton growth and the consequences for the ecosystem as a whole?
- will Eulerian and Lagrangian implementations of a marine ecosystem model differ in their predictions?
- how do the timescales of growth and acclimation compare to the timescales of mixing, and what consequences does this have for predictions of primary production?
- what can a Lagrangian approach tell us about the timing of the spring bloom in the North Atlantic

Chapter 2: Fundamental Assumptions

2.1 Introduction

This chapter has two main objectives: firstly, to introduce the Eulerian-Lagrangian hybrid ecosystem model that forms the basis of the rest of this thesis, showing how it can simulate the cycles of plankton and nutrients at a particular ocean site, and secondly to understand and test some of the basic assumptions of Lagrangian modelling.

Using an Eulerian-Lagrangian hybrid, rather than a full Lagrangian model, allows for important processes to be represented in a Lagrangian manner (e.g. how individual phytoplankton physiological states influence overall primary production), whilst still enabling an Eulerian-Lagrangian comparison. The hybrid model comprises Lagrangian phytoplankton particles embedded within an Eulerian ecosystem. It uses simple, 2-layer slab physics, with the ecosystem being simulated within a seasonally varying mixed layer, above a deep, nutrient containing layer. Slab models are a good choice for this type of study, as they are sufficiently well formulated to permit realistic and insightful simulation of marine ecosystems, while being simple enough to run multiple times without incurring high computational time or cost. In addition, the lack of complexity makes the resulting model predictions relatively easy to analyse (Anderson et al., 2015). The model parameters are then tuned to produce the cycles of plankton and nutrients observed at Ocean Weather Station India (59°N 19°W) in the North Atlantic. Finally, the model is used to investigate some basic Lagrangian assumptions, such as the model design and structure, and the particle movement rules.

2.2 Model design

2.2.1 The physical model

The slab physics are based on Evans & Parslow (1985), and use a 2-layer slab structure (Anderson et al., 2015). The upper layer, the depth of which varies

seasonally, contains the ecosystem, with the lower layer containing only nutrient (Figure 10).

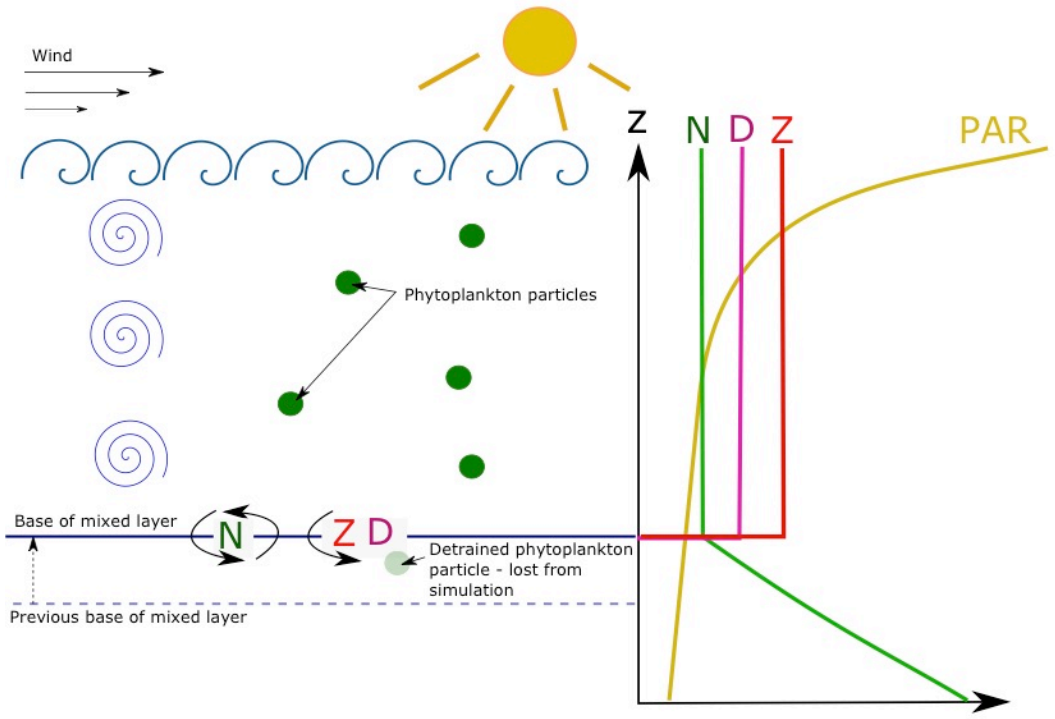

Figure 10: Structure of the ecosystem (redrawn from Ross & Sharples (2007))

There was assumed to be a gradient of nutrient with depth, which was represented using a simple linear equation:

$$DIN_0 = a_N \cdot H + b_N \qquad (2.1)$$

where DIN_0 represents the nutrient below the mixed layer (mmol N m^{-3}) , H represents the depth of the mixed layer (m), and the regression coefficients (a_N = 0.0074, b_N = 10.85) were taken from Anderson et al. (2015) and were fitted from World Ocean Atlas data for OWSI (Antonov et al., 2010) for NO_3 at the base of the thermocline. The mixed layer depths were also taken from the World Ocean Atlas data, and were updated daily (Figure 11).

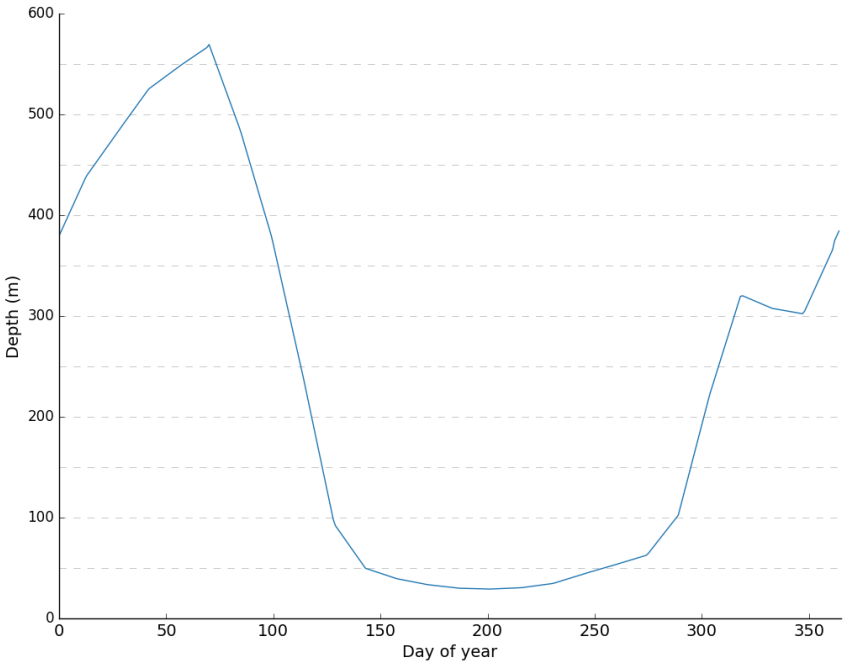

Figure 11: Seasonal cycle of mixed layer depth

The noon irradiance was calculated as a function of the latitude and the time of year, using standard equations (Brock, 1981). Figure 12 shows the predicted seasonal cycle of noon photosynthetically active radiation (PAR).

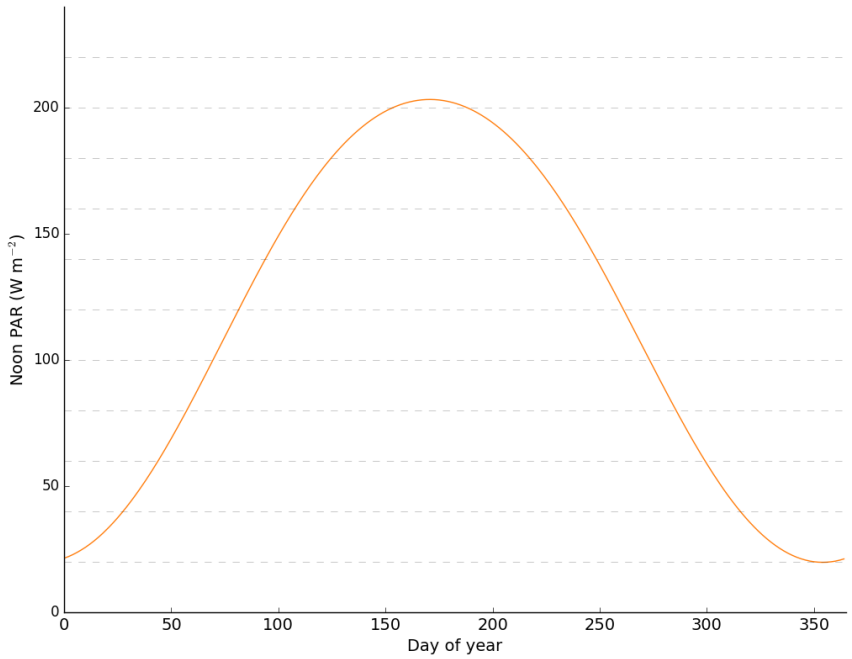

Figure 12: Seasonal cycle of noon PAR for OWSI used in the model

Irradiance varied throughout the day according to a sinusoidal function, and the reduction of insolation due to cloud cover was calculated using the model of Reed (1977) This calculates a number less than 1 by which the solar irradiance is multiplied, using the equation $1-0.62C+0.0019\alpha$, where C represents the cloud cover in tenths (C = 6 oktas), and α the noon solar altitude (degrees). Reed suggested that this model is appropriate for cloud covers of 0.3 and greater, although he pointed out that mean cloud amounts 0.2 and less could be neglected for practical purposes. Thus, the model has a day-night cycle in which phytoplankton have zero growth during night hours.

2.2.2 Parameterizing turbulence

The rate at which the phytoplankton are mixed through the surface mixed layer depends upon the turbulence. This is parameterized through the use of a diffusivity coefficient, K_{turb}, which is set as being constant throughout the water column. This simplification, which allows for greater ease in understanding the phytoplankton's trajectories, would not be expected to be seen in the ocean, where local rates of mixing change depending on conditions. The value for K_{turb} is updated daily, based on the surface wind speed and the depth of the mixed layer. The calculations are taken from the KPP model by Large et al. (1994),

which calculates a profile of diffusivity as the product of a depth dependent turbulent velocity scale, w_x, and a nondimensional vertical shape function $G(\sigma)$, where σ = a dimensionless vertical coordinate that varies from 0 to 1 in the boundary layer .

As the model assumes a homogeneous vertical turbulence profile, i.e. a single value of K_{turb} throughout the water column, there is no vertical profile, $G(\sigma)$, and instead a constant, G, is used. The value of this constant represents the average of the turbulence profile, and is set to 0.1.

$$K_{turb} = w_x \cdot H(t) \cdot G \tag{2.2}$$

The turbulent vertical velocity scale is calculated from:

$$w_x = \kappa \cdot u^* \tag{2.3}$$

where κ = von Kármán's constant (0.4), u^* is the wind friction velocity (~ $1E^{-3} \cdot U$), with U wind speed. The wind speed, U, is updated daily, based on a sinusoidal function fitted using non-linear least squares to an annual cycle obtained by averaging ERA 40 data over the years 1997 to 2001, inclusive (Figure 13).

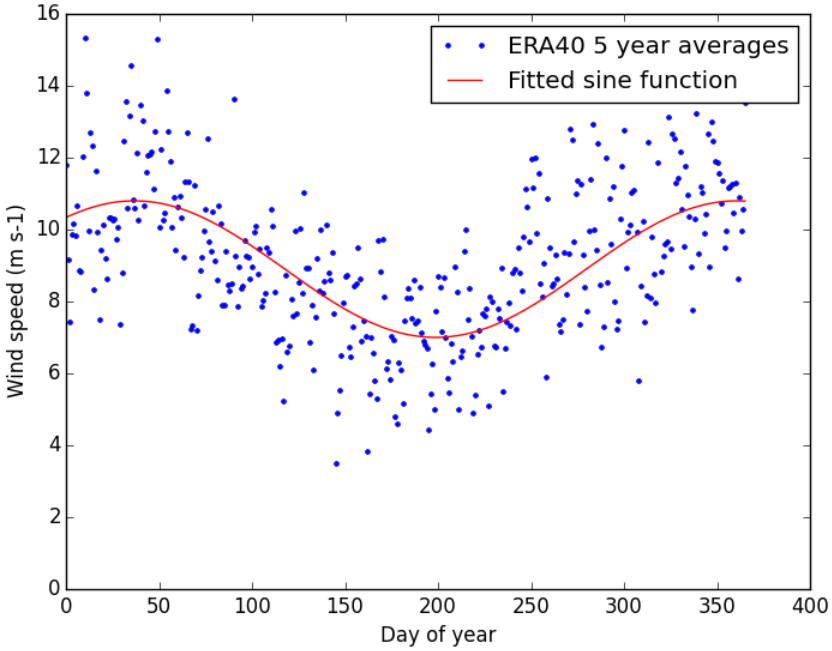

Figure 13: Sinusoidal function for wind speed on each day of the year, compared to wind data calculated from the ERA40 u and v components measured at 10m above sea level.

Table 1: Parameters used in the KPP model for calculating the diffusivity coefficient (K_{turb})

K_{turb}	turbulent diffusivity coefficient ($m^2\ s^{-1}$)	Eq. (2.2)
w_x	turbulent velocity scale ($m\ s^{-1}$)	Eq. (2.3)
G	vertical shape function (dimensionless)	0.1
κ	von Kármán's constant (dimensionless)	0.4
u^*	wind friction velocity ($m\ s^{-1}$)	$1e^{-3}U$
U	Wind speed ($m\ s^{-1}$)	function of day of year (see text)

The calculation for u^* is based on the equation:

$$u^* = \sqrt{\frac{\tau}{\rho}} \tag{2.4}$$

where τ represents the wind stress ($N\ m^{-1}$), and ρ the density of the seawater ($kg\ m^{-3}$). This was found by Large et al. (1994) to be well represented by the use of $1*10^{-3}U$.

2.2.3 Particle movement rules

The phytoplankton particles are assumed to be moved by turbulence only, without taking into account potential changes in buoyancy, or phytoplankton motility. The simplest method to represent this movement is to randomly redistribute the particles within the water column every time step, an approach used in Nogueira et al. (2006), Sinerchia et al. (2012), Woods et al. (2005) and Woods & Barkmann (1993a). This random position movement algorithm is simple to implement and understand, but may not always be an appropriate solution – especially for models with deep mixed layers. The is because the choice of model time step implies the maximum speed of the particles, as the time step is the length of time that it could theoretically take a particle to move from the surface to the base of the water column. In reality, the distance travelled should relate to the level of turbulence in the water column, not the model time step.

An often used alternative is the random walk (e.g. Broekhuizen (1999), Cianelli et al. (2004), Falkowski & Wirick (1981), Franks & Marra (1994), Kamykowski et al. (1994), Lande & Lewis (1989), Lizon et al. (1998), Ross et al. (2011a,b) Ross & Sharples (2004), and Visser (1997)), which involves particles being moved a certain distance in a random direction each time step. The formulation of these walks can vary in complexity. For example, they can move in any number of planes, or their current move can depend upon previous moves. However, even the simplest random walks, where each move is entirely independent of the previous moves, and the particles can only move in one plane, can be complicated to implement and require careful testing to ensure that design considerations are not having unexpected effects on the model predictions. This study used a simple random walk that represents the turbulence in the ocean through a turbulent diffusivity coefficient, K_{turb}, a method seen in studies such as Falkowski & Wirick (1981), Ross & Sharples (2004), and Visser (1997). This parameter provides a reasonable representation of some of the statistical properties of turbulence, such as mean length and time scales (Ross and Sharples, 2004). However, it also compares two different formulations of the same random walk - one as described in Falkowski & Wirick (1981) and the other in Visser (1997) - with the random position method of phytoplankton redistribution. These methods all appear in the literature, but there are currently no studies that directly compare how they affect model predictions.

2.2.4 Description of the random walk

Two random walk formulations were investigated, and then compared to an algorithm that simply randomised the position of the phytoplankton each time step. The random walk assumes that phytoplankton movement is solely based on turbulence, neglecting individual motility and buoyancy control. The only change experienced by the phytoplankton is in their light field, as all other environmental variables (grazing, DIN) are represented as Eulerian concentrations, so only vertical movement was represented. The equations are based on the collective motion of Brownian particles, and express the mean squared displacement in terms of the time elapsed and the diffusivity:

$$\frac{d}{dt} = \left(z^2\right) \equiv 2K_{turb} \tag{2.5}$$

This follows Einstein's arguments that the displacement of a Brownian particle is not proportional to the elapsed time, but rather to its square root (Einstein, 1905). Two different methods for representing this were investigated, the first of which is described in Falkowski & Wirick (1981). In these equations, the distance travelled by each particle is the same for each time step, but there is an equal probability that the particle will move up or down:

$$z_{n+1} = z_n \pm \left(2K_{turb} \cdot \partial t\right)^{\frac{1}{2}} \tag{2.6}$$

where z = depth (m), K_{turb} = eddy diffusivity ($m^2\ s^{-1}$). I will refer to this as a *discrete* random walk, as the distance moved by each particle is the same, and only the direction is randomly varied.

The second is described by Visser (1997), and is based on the same equations, but a random process, ranging from -1 to 1, modifies the resulting displacement. The distance moved by each particle is therefore not the same every time step.

$$z_{n+1} = z_n + \frac{R}{\sqrt{r}}\left(2K_{turb} \cdot \partial t\right)^{\frac{1}{2}} \tag{2.7}$$

Here, R represents a random process, with 0 mean, and variance *r* (e.g. here, R is a uniform distribution between +1 and -1, so r = 1/3, due to the properties of a uniform distribution, i.e. the second moment of the distribution is the variance.). The equations in Visser (1997) also included a function for redistributing the particles from areas of low turbulence, but this has not been included here, because the diffusivity is assumed to be constant throughout the water column. This can be thought of as a *continuous* random walk, because there are, theoretically, an infinite number of possibilities as to the distance moved each time step. However, both the discrete and continuous random walks are essentially the same – the mean squared displacement is always equal to $2K_{turb}\delta t$.

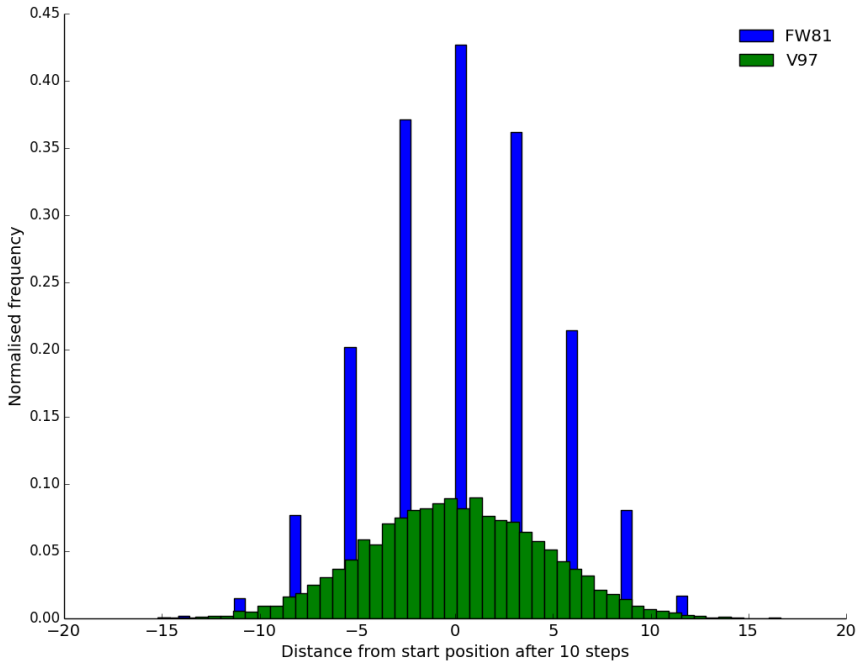

Figure 14: Normalised frequency histogram showing the distance from the starting position (0) after 10 steps for each model, for K_{turb} = 1 m^2 s^{-1} , N = 10,000 (N = number of super-individuals)

Figure 14 shows the distribution of the particles after 10 steps for both the discrete and continuous random walk model. In the discrete model, due to the fixed step size, the particles can only be in one of a number of different positions. Conversely, in the continuous model, the particles can move to any place in the water column, and this is reflected in the smooth curve of the bins in the histogram. The more bins used, the smoother this curve will become (assuming a high enough number of particles to prevent statistical errors).

The distance moved each time step is therefore a function of the surface wind speed and the depth of the mixed layer, which changes over the course of the year. Figure 15 shows the average step length taken by the super-individuals over the annual cycle, using a range of different time steps.

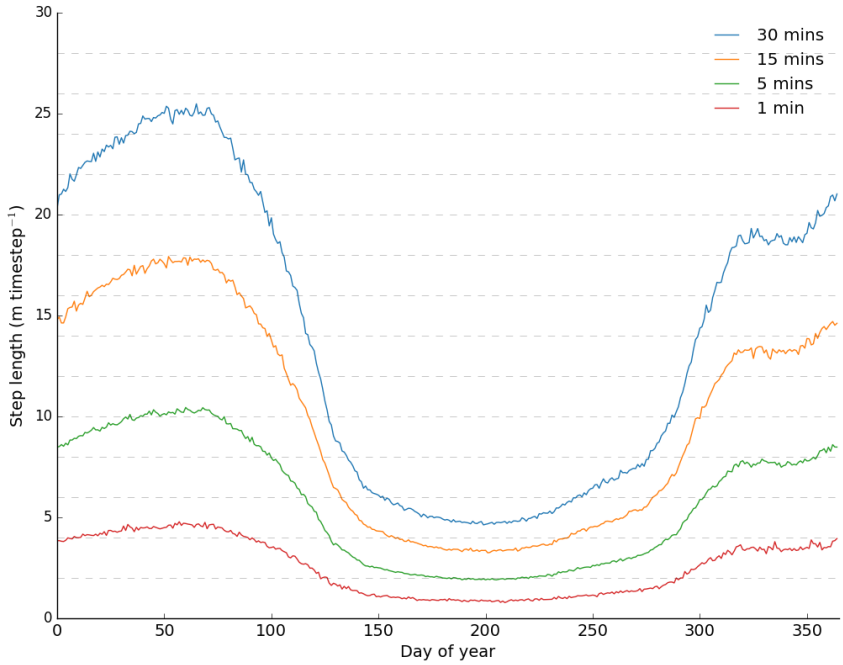

Figure 15: Average step length taken by the super-individuals in response to the annual cycles of surface wind and mixed layer depth timesteps of 30 mins, 15 mins, 5 mins and 1 min.

Both boundaries (the surface and the based of the mixed layer) were assumed to be reflecting.

2.2.5 The biological model

2.2.5.1 The Eulerian-Lagrangian hybrid model

A true Lagrangian plankton ecosystem model that represented every organism individually, and simulated interactions, such as grazing, at a cellular level, would be computationally impossible, due to the extremely high numbers of organisms. A simpler solution was therefore used, whereby only the phytoplankton biomass was represented using a Lagrangian framework, and all other aspects of the ecosystem were simulated using an Eulerian formulation. This is essentially a hybrid approach that embeds Lagrangian phytoplankton into an existing nutrient-phytoplankton-zooplankton-detritus (NPZD) model, previously used in Broekhuizen (1999); Cianelli et al. (2004); Cianelli et al. (2009); Ross & Sharples (2007). However, the model used by Broekhuizen (1999) ignored photoacclimative responses, and none of the previous models explicitly represented zooplankton. The novel aspect of this

work is the use of an NPZD model that both includes explicit representation of all of the model components, and also includes photoacclimation. Classical NPZD models are relatively simple in structure, making them easy to analyse, but have a proven track record in simulating ecosystems (Fasham et al., 1990). The NPZD model chosen for this study explicitly represents both chlorophyll and nitrogen, and has parameterisations based on the MEDUSA model (Yool et al., 2011; Yool et al., 2013). This is a good choice due to its robust equations, plus its explicit representations of internal chlorophyll quotas allows for simulation of phytoplankton light acclimation (see model description in section 2.2).

2.2.6 Super-individuals

The simplest and most natural way to divide the phytoplankton population into a number of particles, would be for each single particle to represent one phytoplankton cell. However, as phytoplankton density can reach thousands of cells per ml (Hirose et al., 2008; Jacquet et al., 2002), it is impossible to consider modelling every individual cell in a column of water in the open ocean, due to computational limits. An alternative approach was presented by Woods & Onken (1982), who proposed that each Lagrangian particle should represent a population of phytoplankton cells, rather than a single cell. In this way, the computational cost of each model could be tailored through simply increasing or decreasing the number of cells represented by each particle. They called this the *Langrangian-ensemble* method of modelling primary production, as the total primary production is estimated from the ensemble of individual particles. The cells are assumed not to change in size (or biomass content per cell), but the particle biomass changes as the number of cells changes. Cell division and mortality can then be represented through simply increasing or decreasing the number of cells the particle represents.

Lagrangian-ensemble models allow researchers to represent individual changes in phytoplankton physiology, without incurring excessive computational costs. However, incorporating these individual-based models into a full ecosystem model raises several issues. The most difficult of these is how the model handles grazing, which is generally assumed to be a non-linear function of phytoplankton concentration: increases in phytoplankton concentrations will increase predator-prey encounter rates, until the zooplankton reach a

maximum, saturating rate. The most 'realistic' solution would be to use Lagrangian zooplankton, however this not only substantially increases the complexity of the model, but also requires some method of representing the dynamics of zooplankton grazing on a cellular level. In addition, grazing at a cellular level tends to happen on a time scale of seconds, whereas model time steps tend to be minutes or hours. One solution is to not explicitly represent zooplankton, but to include losses through grazing in the phytoplankton mortality terms (e.g. Hellweger & Kianirad (2007)). Other models have included explicit zooplankton, and based grazing rates on cell number (e.g. Sinerchia et al. (2012); Woods et al. (2005)), however there is a lack of data surrounding grazing rates in the open ocean against which to verify such models. Grazing rates in ecosystem models tend to be biomass-based, due to the nature of the observations from which they are derived. In order to translate traditional N-based grazing kinetics for an individual-based phytoplankton model, the grazing in the current study is calculated based on the average phytoplankton biomass, and then applied proportionally to each phytoplankton particle (full details and consequences in section 2.2.7). This means that the equations for the ecosystem model used in conjunction with the Lagrangian phytoplankton were formulated in terms of phytoplankton concentration, rather than individual cells. Therefore, each phytoplankton particle (or super-individual (SI) after Scheffer et al. (1995) represented a quantity of biomass, with no information regarding number of cells, or cell size.

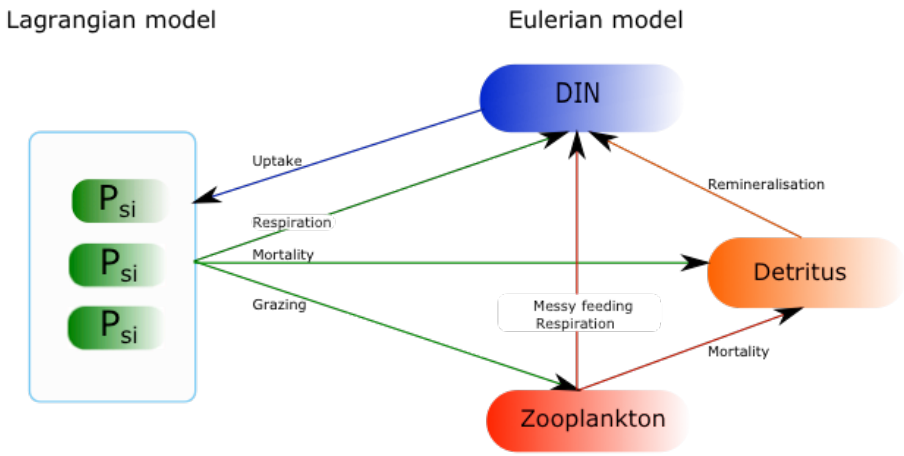

Figure 16: The structure of the hybrid model, showing how the Lagrangian and Eulerian parts interact. The full ecosystem equations are given in section 1.3.2.

The hybrid model represents phytoplankton nitrogen (and chlorophyll) in three different ways: P_{SI}, P_{total} and P_{conc}. P_{sI} represents the nitrogen content of each super-individual, and is expressed in mmol N. P_{total} then represents the total phytoplankton nitrogen in the water column ($P_{total} = \sum P_{sI}$) and P_{conc} represents the average phytoplankton concentration, and is calculated from $P_{conc} = \frac{P_{total}}{H}$, where H represents the depth of the mixed layer. Variables, such as production, are handled in the same way, with phytoplankton production being calculated for each super-individual, $\mu_{P,SI}$, summed up for the total, $\mu_{P_{total}} = \sum \mu_{P,SI} \cdot P_{SI}$, and divided by the mixed layer depth to get the depth averaged new production, $\mu_{P_{conc}} = \frac{\mu_{P_{total}}}{H}$

Integrating the grazing in the Lagrangian model is a little more complicated. In reality, grazing is a binary process where individual cells are grazed or not. In the model in the current study, grazing is handled in an Eulerian fashion, where it impacts on each and every super-individual, removing a fraction of its biomass. The average grazing, G_{Pconc} (mmol N m^{-3} d^{-1}) is calculated from P_{conc}, and is applied to each super-individual proportionally, i.e. $G_{SI} = G_{Pconc} \frac{P_{SI}}{P_{conc}}$. This method was also used for the other density-dependent process, non-linear mortality, to keep the model consistent. As a result, super-individuals do not die off and their number is maintained in the water column (with the exception of those detrained when the mixed layer shallows above them). Representing non-linear processes in this way simplifies the model analysis, allowing for direct comparison between the hybrid model and a fully Eulerian model, which was one of the main aims of this thesis.

The main model currency is nitrogen (N, mmol m^{-3}). However, photosynthesis is driven by chlorophyll which is also explicitly represented, using a variable Chl:C ratio (and a fixed C:N ratio). The super-individuals are moved, individually, around the water column using particle movement rules (see section 2.2.3). While the nutrient environment is uniform in the mixed layer (Eulerian), each super-individual will experience its own unique light

environment, depending on depth and self-shading from other super-individuals above it in the water column.

Super-individuals never die off due to grazing or mortality because these processes only remove a fraction of the biomass (see above). Physics aside, the number of super-individuals is therefore maintained. However, super-individuals are lost, binary fashion, by detrainment out of the mixed layer, decreasing their number. This is implemented by simply removing any particles at a depth lower than the mixed layer depth, once its new position has been calculated each time step. In order to maintain a representative number of super-individuals in the water column, when super-individuals reach a threshold size, they split into two, equally sized super-individuals. Although this is primarily to replace those super-individuals lost through detrainment, it also prevents errors that can arise from the use of a constant number of super-individuals due to over dominance by a single or small number of super-individuals (see section 2.3.2). This splitting is purely a physical method of controlling the number of super-individuals within the simulation, and is in no way meant to represent biological cell division. Figure 17 shows how the numbers of phytoplankton SIs gained through division, lost through detrainment, and the total number throughout the year, are affected by changes to the maximum particle size, P_{div}.

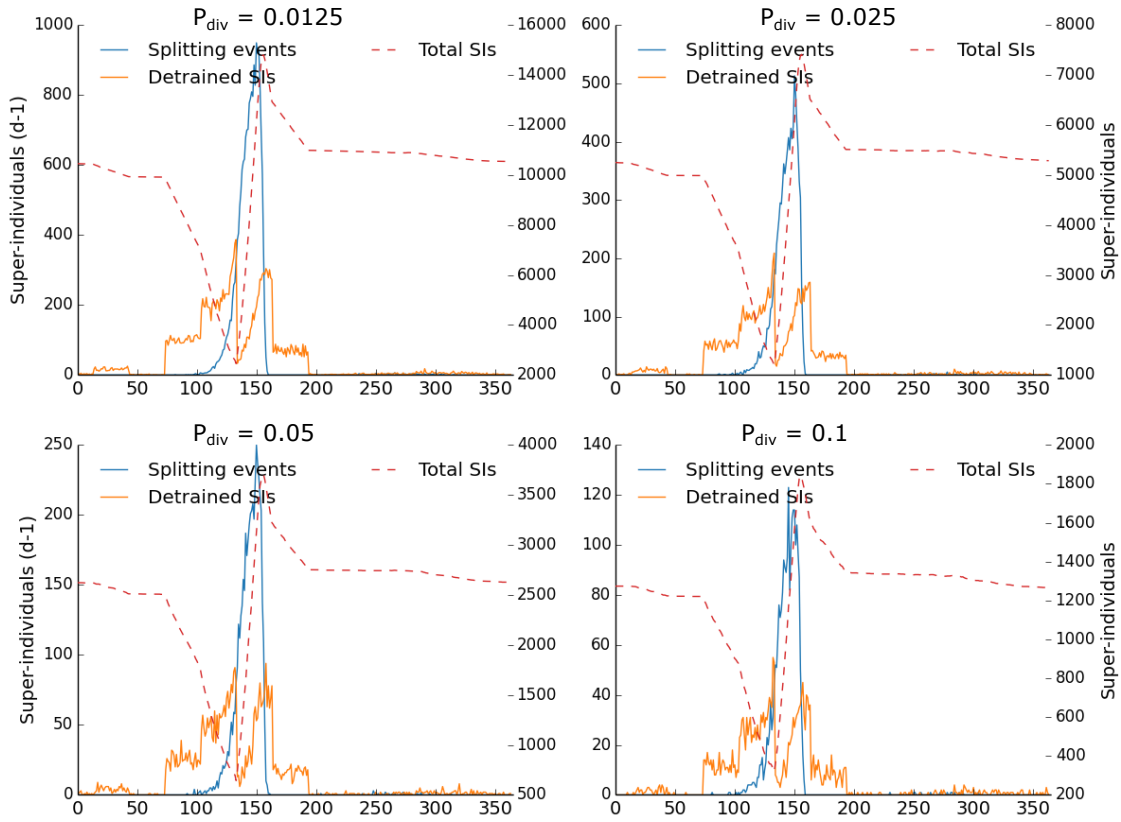

Figure 17: Super-individuals lost through detrainment, and gained through splitting, per day, in response to changes to the P_{div} (mmol N). Also plotted is the total number of SIs in the simulation at any one time. Visser random walk (see section 2.2.4).

2.2.7 Model equations and parameters

The NPZD model chosen for this study includes phytoplankton biomass and pigment growth processes based on Geider et al. (1997), and parameterisations based on the MEDUSA model. MEDUSA incorporates two functional types for both zooplankton and phytoplankton – small and large – but this level of complexity was not necessary for the current study, so the model was scaled down to only one functional type for phytoplankton and one functional type for grazers. Combining two size classes into one functional type in the hybrid model means that some of the parameter values required tuning in order to achieve a good fit to the data (see section 2.2.8 for full description).

2.2.7.1 Phytoplankton growth model

Phytoplankton have two state variables – nitrogen and chlorophyll - both of which represent the total content in each super-individual, P_{SI} and Chl_{SI}. Two

other properties can then be derived from these: the amount in the entire mixed layer, P_{total} and Chl_{total}; and the average concentration in the mixed layer, P_{conc} and Chl_{conc}.

2.2.7.1.1 Nitrogen

The rate of change in the nitrogen biomass for each super-individual is calculated using the equation:

$$\frac{dP_{SI}}{dt} = \mu_{P,SI} P_{SI} - G_{SI} - m_P P_{SI} - M2_{SI} - k_{mix} \frac{P_{SI}}{H(t)} \quad (2.8)$$

where the terms represent production, grazing, respiration, non-linear mortality, and mixing losses, respectively, and H denotes the depth of the mixed layer. The linear loss term is attributed to respiration, but can be thought of as covering both metabolic losses and natural mortality. The non-linear term represents density-dependent loss, for example mortality from infection by viruses, whose abundance is dependent on the density of potential host cells (Anderson et al., 2015). The non-linear loss terms (both grazing and mortality) are calculated and applied in an Eulerian fashion, based on the depth-averaged concentration of phytoplankton nitrogen biomass. This is fully described in section 2.2.6, and the implications are discussed in section 2.3.2. The parameter descriptions and values can be found in Table 3.

Phytoplankton production depends on the supply of dissolved inorganic nutrients, *DIN*, according to Michaelis-Menten kinetics, and on the availability of photosynthetically active light.

The rate of production, $\mu_{P,SI}$ (h^{-1}), is given by:

$$\mu_{P,SI} = \theta_{Chl,SI} \cdot V_{SI}^{PT} \cdot \frac{DIN}{k_N + DIN} \quad (2.9)$$

where k_N is the half-saturation coefficient for nutrient uptake, *DIN* is the average concentration in the mixed layer (represented on a Eulerian framework, so assumed to be homogeneous), and the rate of photosynthesis, V_{SI}^{PT}, is a function of the irradiance at the depth of each super-individual, and is calculated using a Smith function (Smith, 1936):

$$V_{SI}^{PT} = \frac{V^{PT} \cdot \alpha_{P,SI} \cdot I_{SI,z}}{\left(V^{PT^2} + \alpha_{P,SI}{}^2 \cdot I_{SI,z}{}^2\right)^{\frac{1}{2}}} \quad (2.10)$$

where V^{PT} is the temperature specific maximum photosynthetic rate, and is the initial slope of the P-I curve (gC (g chl)$^{-1}$ h^{-1} (W m^{-2})$^{-1}$. $\alpha_{P,SI}$ is chlorophyll rather than carbon specific, necessitating the explicit treatment of chlorophyll in the model.

$I_{SI,Z}$ takes into account both seasonal and diurnal patterns of irradiance arriving at the ocean surface, and attenuation of irradiance with depth. The light profile is calculated using the Beer-Lambert equation:

$$I_z = I_0 \exp(-k_{par} z) \quad (2.11)$$

where I_Z is the light at depth z, I_0 is the surface irradiance and k_{par} is the vertical attenuation coefficient. The value for k_{par} is calculated as in (Anderson, 1993; Anderson et al., 2015). Each 1-metre layer has its own spectrally averaged k_{par}, which is denoted k_L for layer L. In addition, the water column is divided into 3 regions, i_1, i_2 and i_3, which are 0 to 5m, 6 to 23m, and > 23m, respectively. The irradiance for each interval is calculated based on the coefficient for that region, i, and the chlorophyll within that layer, L, and the layers above. The chlorophyll is calculated for each 1 metre layer through the summation of all of the chlorophyll contained in super-individuals within that layer, i.e. $chl_L = \sum chl_{SI}$ for interval L

$$k_L = b_{0,i} + b_{1,i} c_L + b_{2,i} c_L{}^2 + b_{3,i} c_L{}^3 + b_{4,i} c_L{}^4 + b_{5,i} c_L{}^5 \quad (2.12)$$

where $c_L = chl_L{}^{\frac{1}{2}}$

using the coefficients shown in Table 2. This gave the attenuation coefficient for each 1 metre layer, and then this was used, along with equation (2.11) to calculate the attenuation at the exact depth of each super-individual. This meant that the loss of irradiance due to attenuation by the water for phytoplankton between the surface and 1m depth was represented.

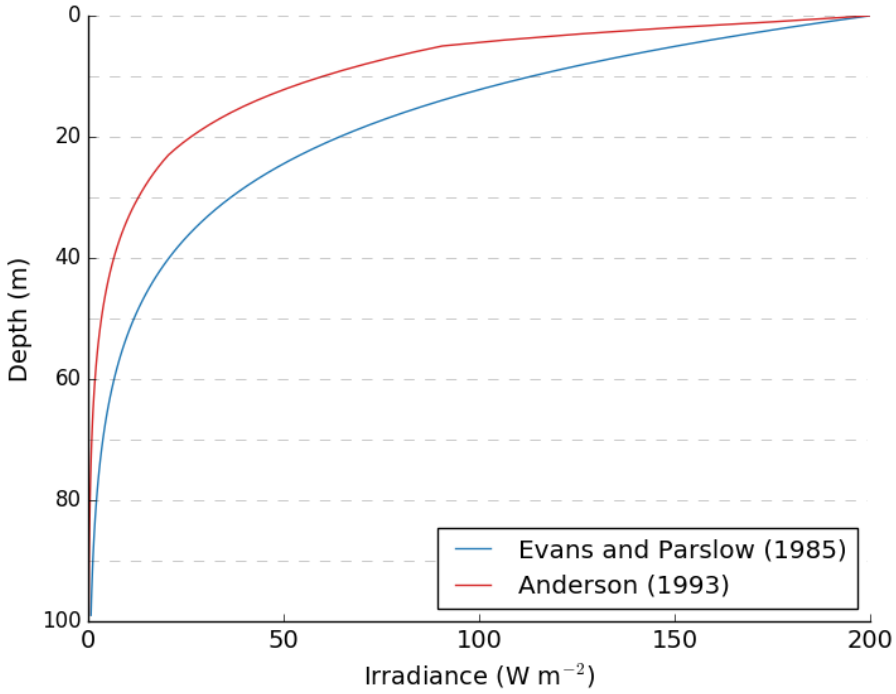

Figure 18: Comparing the model of light attenuation described in Anderson (1993) with a simpler attenuation model, as used in Evans and Parslow (1985)

How this method differs from models that calculate attenuation assuming a constant coefficient for attenuation with depth (as in Evans and Parslow (1985)) can be seen in Figure 18, which demonstrates the difference in predicted light attenuation for the two attenuation models, using two slab models, with constant mixed layer depth (100 m) and constant surface PAR (200 W m^{-2}). The main difference can be seen in the surface layers, where the Anderson method results in a higher rate of attenuation. This method was chosen because it provides a significantly more accurate representation of light attenuation in the water column, a key aspect of the work here given the focus on photoacclimation in response to light (Anderson, 1993; Anderson et al., 2015). However, throughout the thesis, results will also be shown using the method of attenuation based on a constant coefficient for attenuation, calculated from the concentration of phytoplankton in the mixed layer (referred to as the Evans and Parslow (1985) light model).

Table 2: Polynomial coefficients relating k_L to square root of pigment in region *i*.

i	$b_{0,i}$	$b_{1,i}$	$b_{2,i}$	$b_{3,i}$	$b_{4,i}$	$b_{5,i}$
1	0.13096	0.030969	0.042644	-0.013738	0.0024617	-0.00018059
2	0.041025	0.036211	0.062297	-0.030098	0.0062597	-0.00051944
3	0.021517	0.050150	0.058900	-0.040539	0.0087586	-0.00049476

The maximum phytoplankton photosynthetic rate is related to the temperature, *T*, as described by (Eppley, 1972):

$$V^{PT} = V^{P} \cdot 1.066^{T} \tag{2.13}$$

Grazing is calculated using an Eulerian approach, as described in section 2.2.6. It is first calculated as an averaged quantity throughout the mixed layer, Eulerian-style, and then applied proportionately across all the super-individuals. Therefore, the grazing loss for each super-individual is calculated by:

$$G_{SI} = G_{Pconc} \cdot \frac{P_{SI}}{P_{conc}} \tag{2.14}$$

where G_{Pconc} is the average zooplankton grazing rate (mmol m^{-3}), and is calculated throughout the mixed layer, on an Eulerian basis. It is defined as:

$$G_{Pconc} = \frac{I_{\max} \cdot {P_{conc}}^{2} \cdot Z}{{k_g}^{2} + {P_{conc}}^{2}} \tag{2.15}$$

where I_{max} is the maximum grazing rate, and k_g is the half-saturation constant for grazing.

Mortality is also treated in the same way as grazing, using this semi-Eulerian approach:

$$M2_{SI} = \left(m_{P2} \frac{P_{conc}}{\left(k_P + P_{conc}\right)} \right) \frac{P_{SI}}{P_{conc}} \tag{2.16}$$

2.2.7.1.2 Chlorophyll

Chlorophyll biomass is subject to the same growth and losses as the nitrogen biomass, namely grazing, respiration, mortality and mixing. These occur at the same specific rate as for the nitrogen biomass.

$$\frac{dChl_{SI}}{dt} = \mu_{P,SI} R_{Chl,SI} Chl_{SI} - \left(\theta_{Chl,SI} \cdot \xi^{-1} \left[G_{SI} + m_P P_{SI} + M2_{SI} + k_{mix} \frac{P_{SI}}{H(t)} \right] \right) \quad (2.17)$$

where ξ (mol N (g C)$^{-1}$) represents the conversion factor between nitrogen and carbon, assuming a Redfield ratio of 6.625. The rate of chlorophyll production is a function of nitrogen production, but is also affected by the current ratio of chl-to-carbon, $\theta_{Chl,SI}$, and the current irradiance. The change of the Chl:C in response to irradiance is known as photoacclimation, a process which both maximises growth in low light, and prevents photodamage in high light (fully detailed in Chapter 1). This is represented through the use of a growth scaling factor, $R_{Chl,SI}$, as described in Geider et al. (1997)

$$R_{Chl,SI} = \theta^{Chl}_{\max} \frac{\mu_{P,SI}}{\alpha_{P,SI} \cdot I_{SI,z} \cdot \theta_{Chl,SI}} \quad (2.18)$$

where $\theta_{Chl,SI}$ is the chlorophyll to carbon ratio of the super-individual, and is calculated from:

$$\theta_{Chl,SI} = \frac{Chl_{SI}}{P_{SI} \cdot \zeta} \quad (2.19)$$

and $\theta^{Chl}_{\max}$ is the maximum ratio of Chl : C (g Chl a g N^{-1}) observed in cells acclimated to extremely low light. $R_{Chl,SI}$ is therefore regulated by the ratio of achieved to maximum potential photosynthesis, as defined by the term $\frac{\mu_{P,SI}}{\alpha_{P,SI} \cdot I_{SI,z} \cdot \theta_{Chl,SI}}$. Here, the numerator is ultimately constrained by the maximum rate of photosynthesis, V_{PT}, whereas the denominator is effectively unconstrained, because of the inclusion of $I_{SI,z}$. Therefore, $R_{chl,SI}$ declines when the instantaneous light harvesting capacity (i.e. $\alpha_{P,SI} \cdot I_{SI,z} \cdot \theta_{chl,SI}$) exceeds the instantaneous rate of photosynthesis. This results in lower values of $\theta_{chl,SI}$ in

high irradiance, and higher values of $\theta_{chl,SI}$ as irradiance decreases. This model is explained in more detail in section 1.2.1 in the previous chapter.

2.2.7.2 Zooplankton

The zooplankton are assumed to graze only the phytoplankton, and the equation can be written as:

$$\frac{dZ}{dt} = (1-\phi)G_{Pconc} - m_z Z - \left(m_{z2} \frac{Z}{k_Z + Z} Z \right) - \frac{\left(k_{mix} + H'(t)\right)Z}{H(t)} \qquad (2.20)$$

Here, the terms refer to growth (grazing minus losses from messy feeding, ϕ), respiration (linear), mortality (non-linear), and physical losses resulting from mixing at the base of the mixed layer, and dilution. Dilution occurs when the rate of change of the depth of the mixed layer is positive $\left(H'(t) = \max\left(\frac{\partial H}{\partial t}, 0 \right) \right)$ i.e. the mixed layer is deepening. The zooplankton population is assumed to be zero below the mixed layer, so when the mixed layer deepens, more water will be introduced into the mixed layer, and the overall concentration of zooplankton will decrease. This is not explicitly represented in the phytoplankton equations, because the phytoplankton are simulated as a finite number of super-individuals. Therefore, deepening the mixed layer will automatically decrease the concentration, as the same quantity of phytoplankton biomass will be contained in a larger volume. If the mixed layer shallows, then phytoplankton caught below the new mixed layer depth are lost from the simulation, and so the overall concentration is unchanged.

2.2.7.3 Dissolved inorganic nitrate

The changes in nitrate concentration (mmol N m^{-3}) are calculated from:

$$\frac{dDIN}{dt} = -\frac{\sum \mu_{P,SI} P_{SI}}{H(t)} + m_P P_{conc} + \phi G_{Pconc} + m_z Z + m_{DT} D + \frac{\left(k_{mix} + H'(t)\right)\left(DIN_0 - DIN\right)}{H(t)}$$

(2.21)

DIN is taken up by phytoplankton, and returned through both phytoplankton and zooplankton respiration. The other biological inputs are the fraction of grazing lost through messy feeding, and the remineralised detritus. The final term represents mixing between the deep and surface layers, and also changes

due to changes in the depth of the mixed layer, which result in nutrient either being gained or lost from the mixed layer, due to entrainment.

2.2.7.4 Detritus

The equation for detritus is:

$$\frac{dD}{dt} = m_{P2}P_{conc}{}^{2} + m_{z2}\frac{Z}{k_z + Z}Z - m_{DT}D - \frac{\left(k_{mix} + H'(t) + v_D\right)D}{H(t)} \qquad (2.22)$$

Detritus is produced by both phytoplankton and zooplankton mortality. It is lost through remineralisation, which occurs at a temperature dependent rate:

$$m_{DT} = m_D \cdot 1.066^T \qquad (2.23)$$

It is also affected by mixing, changes due to the seasonal cycle of mixed layer depth, and sinking (v_D).

2.2.8 Obtaining the default parameter set for Station India

The initial parameter set was taken, where possible, from the description of the MEDUSA model in Yool et al. (2013), and the parameters used for the EMPOWER model, described in Anderson et al. (2015). Parameters were initially chosen to give the closest match to chlorophyll and nitrate data for Station India, taken for a characteristic year (2006) from SeaWiFS 8-day averages (see Anderson et al. (2015)). The nitrate data are from World Ocean Atlas (Antonov et al., 2010). The full list of parameters is given in Table 3, and the variables along with their initial values in Table 4.

Each simulation was started with 1000 super-individuals, evenly distributed throughout the mixed layer. This number was chosen based on the model output's sensitivity to the number of super-individuals (discussed in section 2.3.4), and the threshold for particle division, P_{div}, was chosen so as to ensure that the number of super-individuals in each simulation was greater than 2,000, but did not exceed 10,000. As the number of super-individuals in any simulation is variable, all the following plots include information about the number of super-individuals in the simulation on the final day. The phytoplankton nitrogen biomass was initialised as 0.15 mmol N m^{-3}, and this was distributed evenly between each super-individual (i.e.

$P_{SI} = P_{conc} \cdot \frac{H(t)}{\text{number of super-individuals}}$). *DIN* was initialised as 14 mmol m^{-3}, and both detritus and zooplankton as 0.1 mmol m^{-3}. The model is relatively insensitive to the initial conditions.

Table 3: Parameters (initial guesses, in parentheses, and final fitted values)

Parameter	Description	Value	Source
V_P	maximum phytoplankton growth rate at 0˚C gC $(gChl)^{-1}$ h^{-1}	2.0	Anderson et al. (2015)
α_P	chl specific initial slope of P-I curve (gC $(g\ chl)^{-1}$ h^{-1} $(W\ m^{-2})^{-1}$	0.12	Anderson et al. (2015)
k_N	N nutrient uptake half-saturation constant mmol N m^{-3}	0.75	Yool et al. (2013)
m_P	phytoplankton respiration rate d^{-1}	0.02	Yool et al. (2013)
m_{p2}	phytoplankton mortality rate d^{-1}	0.1	Yool et al. (2013)
k_p	phytoplankton loss half saturation constant (mmol N m^{-3})	0.5	Yool et al. (2013)
I_{max}	maximum zooplankton grazing rate d^{-1}	1.0	Anderson et al. (2015)
kg	zooplankton grazing half-saturation constant mmol N m^{-3}	0.5	Anderson et al. (2015)
ϕ	zooplankton grazing inefficiency	0.20	Yool et al. (2013)
m_z	zooplankton respiration rate d^{-1}	0.04 (0.02)	Yool et al. (2013)

m_{z2}	zooplankton mortality rate d^{-1}	0.4 (0.1)	adjusted
k_z	zooplankton loss half-saturation constant mmol N m^{-3}	0.5	Yool et al. (2013)
ζ	N:C conversion factor (Redfield ratio of 6.625) mol N (g C)$^{-1}$	79.5	Yool et al. (2013)
θ^{chl}_{max}	maximum Chl:C ratio g chl (g C)$^{-1}$	0.02 (0.05)	adjusted
v_D	detrital sinking rate m d^{-1}	10.0	Fasham et al. (1990)
m_D	detrital N remineralisation rate d^{-1} at 0˚C	0.016	Yool et al. (2013)
k_{mix}	cross-thermocline mixing rate (m d^{-1})	0.1	Fasham et al. (1990)
P_{div}	Threshold for particle division (mmol N)	0.025	
dt	Time step (minutes)	1,30	

Table 4: List of variables and initial values

Variable	Description	Initial values
P_{SI}, P_{conc}	Phytoplankton N state variable: SI (mmol N), population (mmol N m^{-3})	0.089, 0.15
Chl_{SI}, Chl_{conc}	Phytoplankton Chl state variable: SI (mg Chl) population (mg Chl m^{-3})	0.07, 0.12

C_{SI}, C_{conc}	Phytoplankton C state variable: SI (mg C), population (mg C m^{-3})	7.06, 12.0
$\theta_{Chl,SI}$	SI Chl:C (mg Chl (mg C^{-1}))	0.01
DIN	Dissolved inorganic nitrate (mmol N m^{-3})	14.0
Z	Zooplankton state variable (mmol N m^{-3})	0.1
D	Detritus state variable (mmol N m^{-3})	0.1
$\mu_{P,SI}$, μ_{PConc}	Growth rate (d^{-1})	-
G_{SI}, G_{Pconc}	Grazing: SI (mmol N), concentration (mmol N m^{-3})	-
V_{SI}^{PT}	SI photosynthesis (gC $(gChl)^{-1}$ d^{-1})	-
V_{PT}	Rate of photosynthesis at temperature	-

The model is coded in Fortran 90, a general-purpose programming language that is especially suited to numeric computation and scientific computing. The equations are solved each time step using a simple, first-order integration (Euler method). The model was run for three years, using a time step of 30 minutes, by which time a repeating annual cycle of plankton dynamics was generated. The last year of simulation is compared to data for chlorophyll and nitrate in Figure 19.

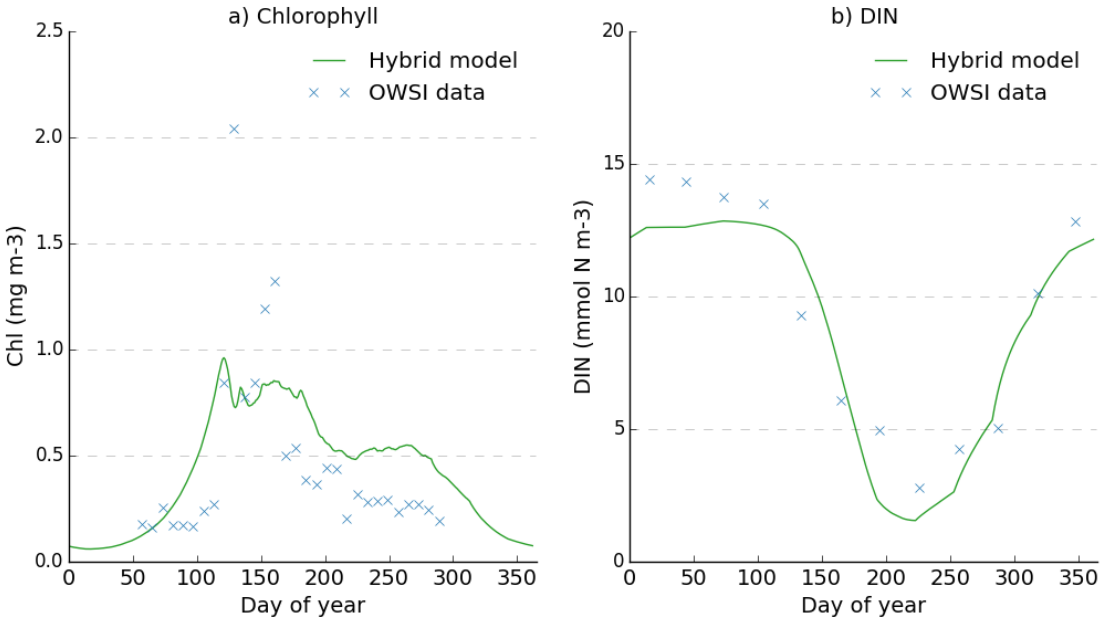

Figure 19: Simulation for OWSI using first-guess parameters compared to data (year 2006) for (a) chlorophyll and (b) DIN. Visser random walk. Final number of super-individuals: 4352

The cycle of nitrate shows a reasonably good match to the data, but the chlorophyll cycle is less well matched (Figure 19). The predicted spring bloom was much lower than expected, and the predicted chlorophyll biomass in the second half of the year was too high, by a factor of 2. In addition, the predicted seasonal cycle of chl : carbon was also high for Station India (Figure 20 and Figure 21).

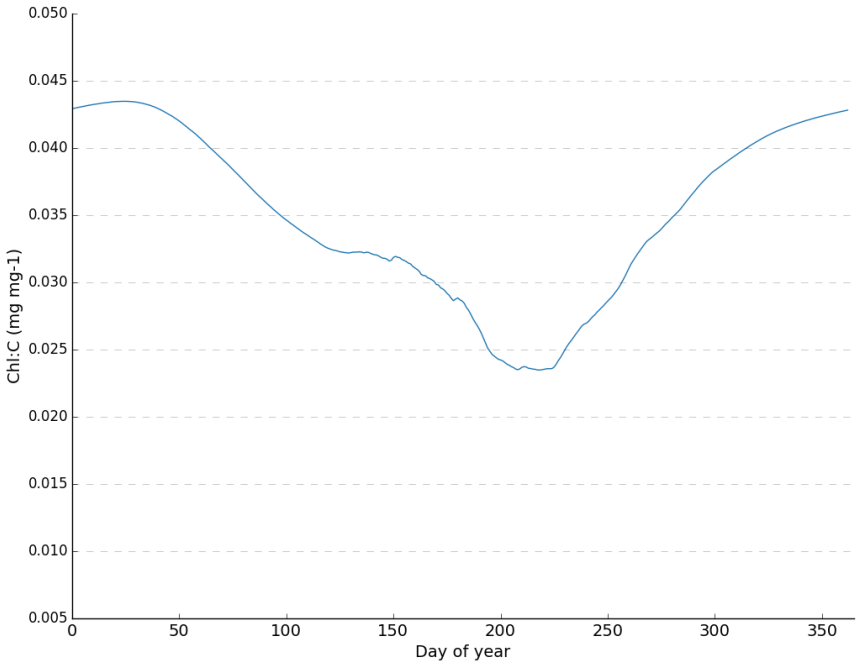

Figure 20: Predicted seasonal cycle of chlorophyll to carbon ratio using the initial parameters for the model at OWS India

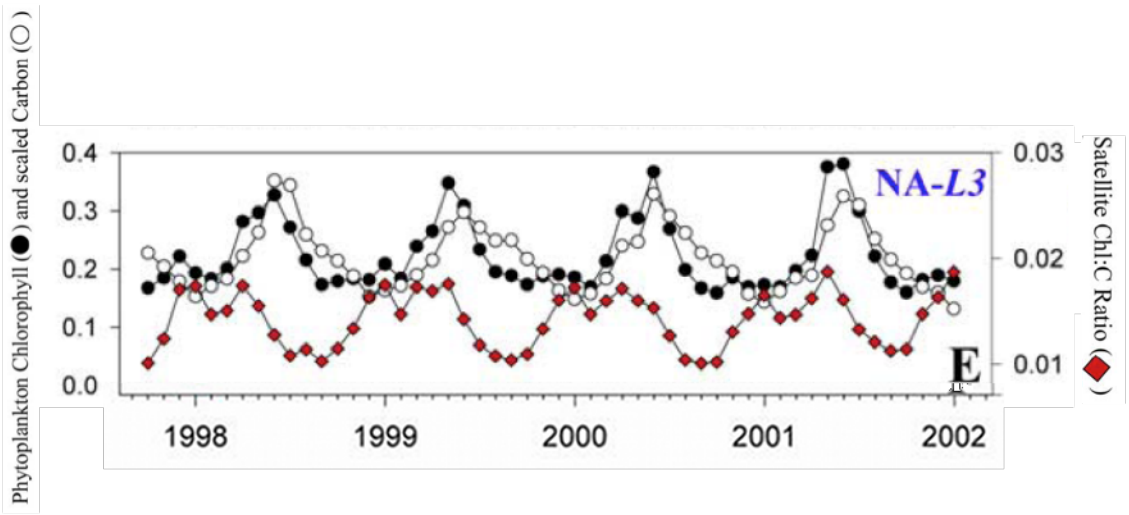

Figure 21: The basic temporal patterns in regional phytoplankton chlorophyll (Chl; solid circles) and carbon (C; open circles) biomass and Chl:C ratios (red diamonds; mg mg^{-1}) in the North Atlantic basin. Taken from Behrenfeld et al. (2005).

The strategy was now to undertake model tuning to fit the data, using strategically chosen parameters. The first parameter altered was the maximum ratio of chlorophyll to carbon ($\theta^{chl}_{\max}$). This value is taken to be the highest measured ratio of chlorophyll to carbon in phytoplankton acclimated to low

irradiances. However, the values tend to be taken from laboratory experiments, which yield different values to those observed in the ocean (Behrenfeld et al., 2005). Behrenfeld et al. showed that satellite derived data suggested that chl:C values in the ocean were much lower than those in the laboratory. I therefore took $\theta_{\max}^{chl}$ from the satellite data in Figure 21, which shows a maximum value of ~0.02 mg Chl (mg C^{-1}). In addition, observations from the North Atlantic Bloom Experiment (NABE) suggest that small nanoplankton dominate the pre-bloom conditions at Station India, accounting for >50% of the daily productivity (Joint et al., 1993). These smaller species tend to show lower maximum ratios of chlorophyll to carbon (~0.013 mg Chl (mg C^{-1})) (Sathyendranath et al., 2009).

Changing the maximum Chl:C gave a much better ratio of Chl:C, but lowered the overall rate of production. In order to improve the fit to the data, I increased the parameters controlling the zooplankton mortality.

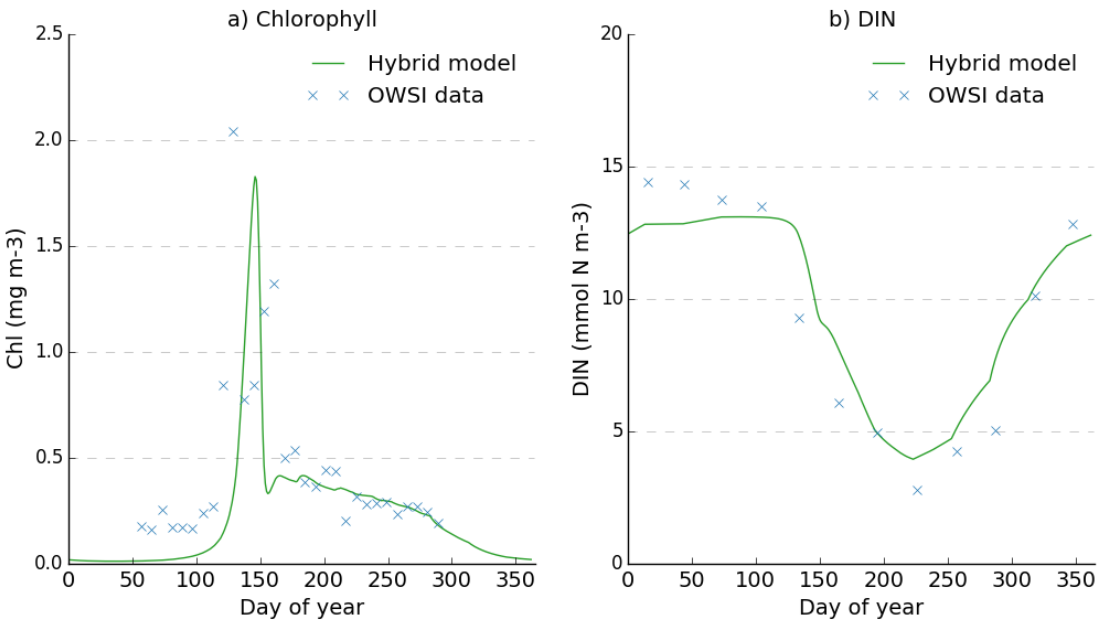

Figure 22: Simulation for OWSI after parameter tuning (see text): (a) chlorophyll, (b) DIN. Visser random walk. Final number of super-individuals: 4585

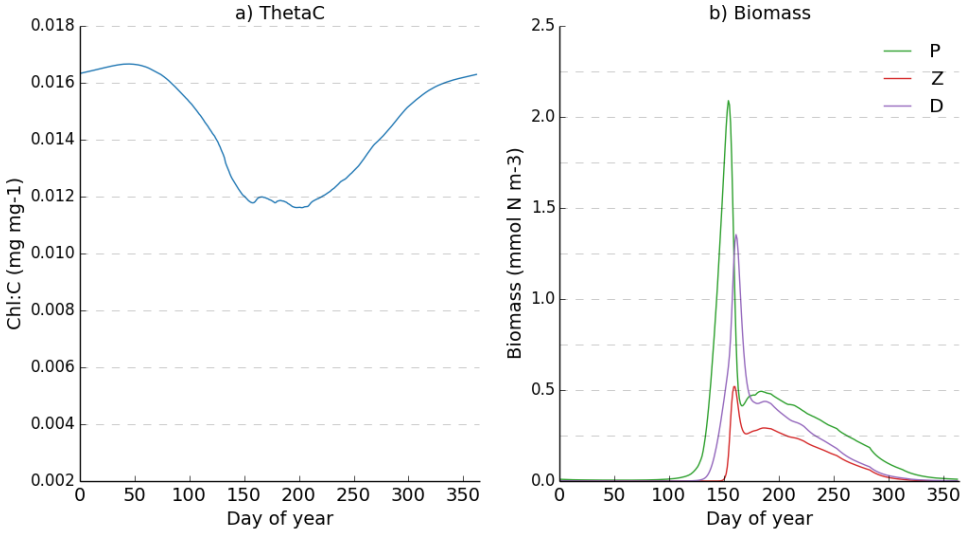

Figure 23: Predicted state variables and chl : carbon ratio for the station India simulation: (a) chlorophyll : carbon and (b) P, Z and D.

One important consideration is then how changing the maximum chl-to-carbon ratio impacts on the results. Reducing the maximum value decreases the range of possible ratios shown by the phytoplankton particles, which could theoretically mask any differences between the Lagrangian and Eulerian model implementations. This will be investigated in the Eulerian – Lagrangian model comparison in the next chapter, by comparing the model predictions both for a model using the original value of $\theta_{\max}^{chl}$ = 0.05 mg Chl (mg C)$^{-1}$, and for the fitted value of $\theta_{\max}^{chl}$ = 0.02 mg Chl (mg C)$^{-1}$.

Table 5: Ecosystem model equations

Phytoplankton

$$\frac{dP_{SI}}{dt} = \mu_{P,SI} P_{SI} - G_{SI} - m_P P_{SI} - M2_{SI} - k_{mix} \frac{P_{SI}}{H(t)}$$

$$\frac{dChl_{SI}}{dt} = \mu_{P,SI} R_{Chl,SI} Chl_{SI} - \left(\theta_{Chl,SI} \cdot \xi^{-1} \left[G_{SI} + m_P P_{SI} + M2_{SI} + k_{mix} \frac{P_{SI}}{H(t)} \right] \right)$$

$$\mu_{P,SI} = \theta_{Chl,SI} \cdot V_{SI}^{PT} \cdot \frac{DIN}{k_N + DIN}$$

$$M2_{SI} = \left(m_{P2} \frac{P_{conc}}{\left(k_P + P_{conc}\right)} \right) \frac{P_{SI}}{P_{conc}}$$

$$V_{SI}^{PT} = \frac{V^{PT} \cdot \alpha_{P,SI} \cdot I_{SI,z}}{\left(V^{PT^2} + \alpha_{P,SI}{}^2 \cdot I_{SI,z}{}^2 \right)^{\frac{1}{2}}}$$

$$R_{Chl,SI} = \theta_{\max}^{Chl} \frac{\mu_{P,SI}}{\alpha_{P,SI} \cdot I_{SI,z} \cdot \theta_{Chl,SI}}$$

$$I_z = I_0 \exp(-k_{par} z)$$

$$\theta_{Chl,SI} = \frac{Chl_{SI}}{P_{SI} \cdot \zeta}$$

$$V^{PT} = V^P \cdot 1.066^T$$

$$G_{SI} = G_{Pconc} \cdot \frac{P_{SI}}{P_{conc}}$$

Zooplankton

$$\frac{dZ}{dt} = (1-\phi) G_{Pconc} - m_z Z - \left(m_{z2} \frac{Z}{k_Z + Z} Z \right) - \frac{\left(k_{mix} + H'(t)\right) Z}{H(t)}$$

$$G_{Pconc} = \frac{I_{\max} \cdot P_{conc}{}^2 \cdot Z}{k_g{}^2 + P_{conc}{}^2}$$

Detritus

$$\frac{dD}{dt} = m_{P2} P_{conc}{}^2 + m_{z2} \frac{Z}{k_z + Z} Z - m_{DT} D - \frac{\left(k_{mix} + H'(t) + v_D\right) D}{H(t)}$$

$$m_{DT} = m_D \cdot 1.066^T$$

DIN

$$\frac{dDIN}{dt} = -\frac{\sum \mu_{P,SI} P_{SI}}{H(t)} + m_P P_{conc} + \phi G_{Pconc} + m_z Z + m_{DT} D + \frac{\left(k_{mix} + H'(t)\right)\left(DIN_0 - DIN\right)}{H(t)}$$

2.3 Testing Lagrangian assumptions

This section investigates how some of the basic assumptions underlying the construction of Lagrangian models impact upon the resulting predictions. This kind of analysis does not appear in the current and previous literature, and

could greatly help with the development of Lagrangian modelling standards. More information about individual model components could allow researchers to make informed decisions about model design, selecting from pre-existing components and modifying where necessary, rather than building each Lagrangian model from scratch. This would be similar to the way that Eulerian models are constructed.

These experiments involve a simplified physical version of the model, which has the seasonal cycles of irradiance and mixed layer depth removed. Using a simple, fixed slab model like this allows for the model behaviour to be more clearly seen, without the complications of the external forcing. The fixed slab model uses the same ecosystem formulation as for Station India, with the parameter settings obtained from the above parameter fixing exercise (section 2.2.8).

2.3.1 Testing the models of turbulence and phytoplankton movement

The predicted annual cycle of turbulence diffusivity can be seen in Figure 24.

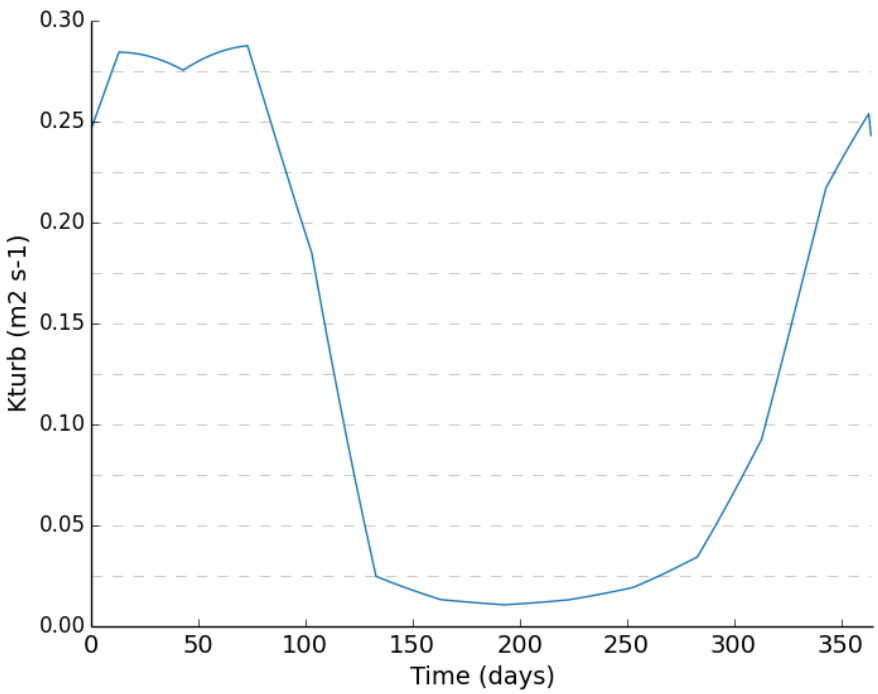

Figure 24: Annual cycle of vertical eddy diffusivity estimated by the model for OWSI

These values can then be compared to values predicted by previous models that have represented OWS India. Figure 25 shows the predicted vertical

diffusivity profile for the location of OWS India taken from the MEDUSA model (Yool et al., 2011; Yool et al., 2013). In this model, the depth of the mixed layer is calculated from physical forcing, rather than being prescribed by observations, and can be see in Figure 25 by the sharp delineation between the well mixed region (orange, red and yellow) and the region of low mixing (purple). The turbulent diffusivity reaches as high as 10 m^2 s^{-1} in winter, early spring, and late autumn. In addition, Oschlies & Garcon (1999) presented results for a transect of the ocean 10°W of OWS India, that showed mixed layer depths of 300m in May, with diffusivities of up to 1 m^2 s^{-1}.

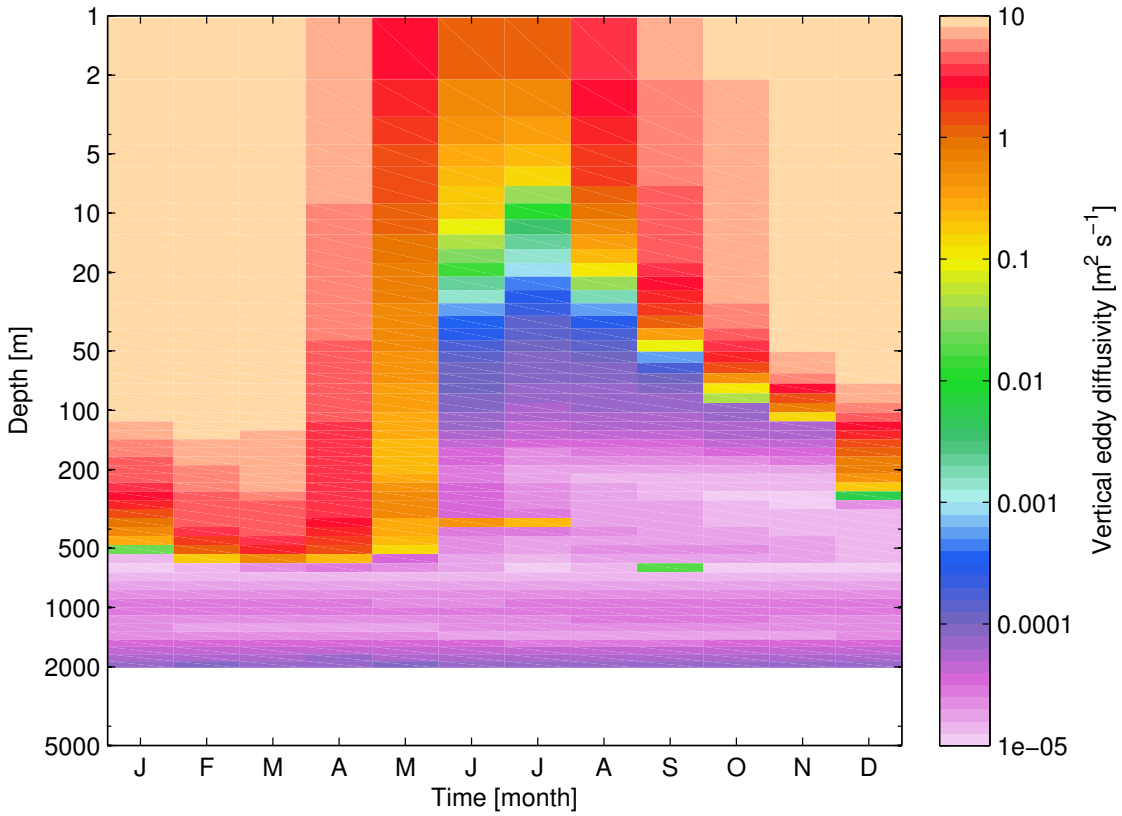

Figure 25: Predictions of vertical eddy diffusivity for OWSI taken from the MEDUSA model (Yool et al., submitted)

The values for turbulent diffusivity predicted by the current model are somewhat lower than these previous modelling studies, with maximum winter rates of < 0.3 m^2 s^{-1}. This could result from the fact that the mixing is based on the depth of the mixed layer and the surface wind speed only, and takes no account of convective overturning. However, there is some evidence in the literature that these lower rates of turbulence could be closer to the conditions in the ocean. The values predicted by the model are just low enough for a

vertical profile of phytoplankton to begin to form, due to the proximity of the timescales of growth and mixing. While few data exist on the vertical profiles of phytoplankton around OWS India, measurements for another location in the same oceanic province (as defined by Longhurst (1998) who partitioned the ocean into geographically identifiable regions based on ecological principles relating phytoplankton growth cycles to ocean physics) show a vertical profile of chlorophyll for a mixed layer depth of 80 m, over the spring.

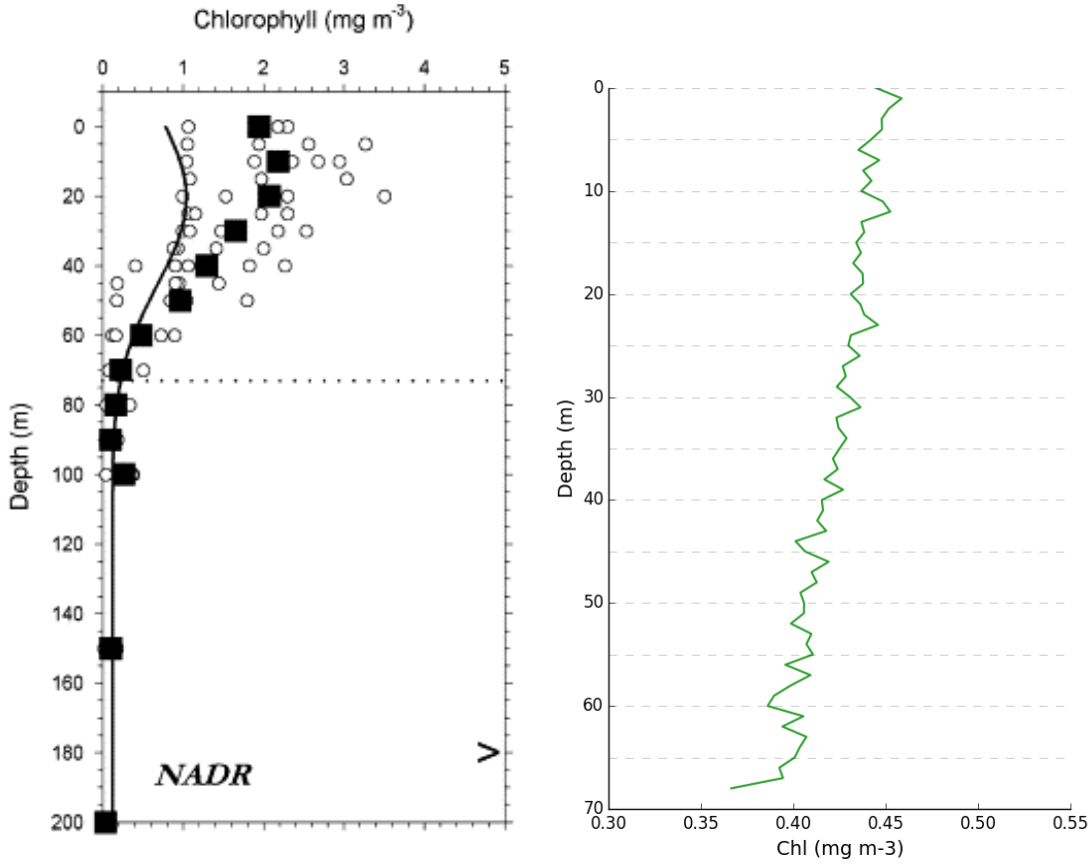

a) NADR observations **b) OWS I model**

Figure 26: Depth profiles of chlorophyll for a) three stations in NADR and b) the OWS India model over the same period. In a) the averages at 10 m depth intervals are shown by the solid square symbols, the smooth curve depicts the profile established by Longhurst (1998) and the horizontal dashed line show the mixed layer depth based on density. Figure a) taken from Li & Harrison (2001)

This suggests that the rates of mixing in North Atlantic, whilst sufficient to produce a well-mixed layer of temperature and density, are not sufficient to overcome the phytoplankton growth rates, lending support to the values obtained for this study. It also indicates that the assumption that

phytoplankton are distributed uniformly through a mixed surface layer may not always be valid. Based on the results of this study, therefore, parameterisations of turbulence should take account of empirical forcing data from the location under investigation, and then verification of the model should include comparison of the resulting vertical phytoplankton profiles to observations, rather than using an assumption that phytoplankton are always uniformly distributed within a surface mixed layer.

2.3.2 Particle splitting and the consequences of the grazing parameterisation

Particle splitting is included in the model for two reasons: firstly to replace those particles lost through detrainment and ensure a sufficient number of particles in the simulation, and secondly to prevent individual particles from growing too large and biasing the results. As pointed out in Ross & Sharples (2007) some phytoplankton particles in Lagrangian models can be 'luckier' than others, spending more time in the productive waters near the surface of the water column and allowing growth to continue unchecked (i.e. no particle splitting) could result a disproportionately large fraction of the total biomass being contained in one phytoplankton. In order to prevent this from occurring, particle splitting was also included in the current model; however, it is important to highlight an extra feedback mechanism on the growth of the phytoplankton, resulting from the grazing parameterisation.

In section 2.2.6, the difficulties in implementing explicit, Eulerian zooplankton grazing on Lagrangian phytoplankton were described. In order to simplify this process, the average grazing rate (mmol N m^{-1} d^{-1}), based on the average phytoplankton biomass (mmol N m^{-1}) in the mixed layer was applied, proportionally, to each super-individual. However, there are consequences to using this method, which require careful handling. For example, running the model with an unchanging numbers of particles (i.e. no detrainment and no splitting), would result in an uneven distribution of biomass between the super-individuals. Those super-individuals experiencing slightly better conditions (i.e. spending slightly longer near the surface) on average, would grow larger than their counterparts. This effect is then exacerbated by the grazing, because as the biomass contained in one individual increases, the average phytoplankton biomass in the water column increases, which, in turn,

increases the overall loss rate. At the same time, the smaller individuals are effectively reducing the loss rate in relation to the large individuals, meaning that there is less grazing pressure on large super-individuals. This creates a positive feedback effect, ensuring that the largest individuals keep increasing in size, whilst the smallest keep decreasing, until all of the phytoplankton biomass is effectively contained in one super-individual.

This can be demonstrated by running a fixed slab version of the model, with a constant mixed layer depth, 100 super-individuals, and no particle splitting.

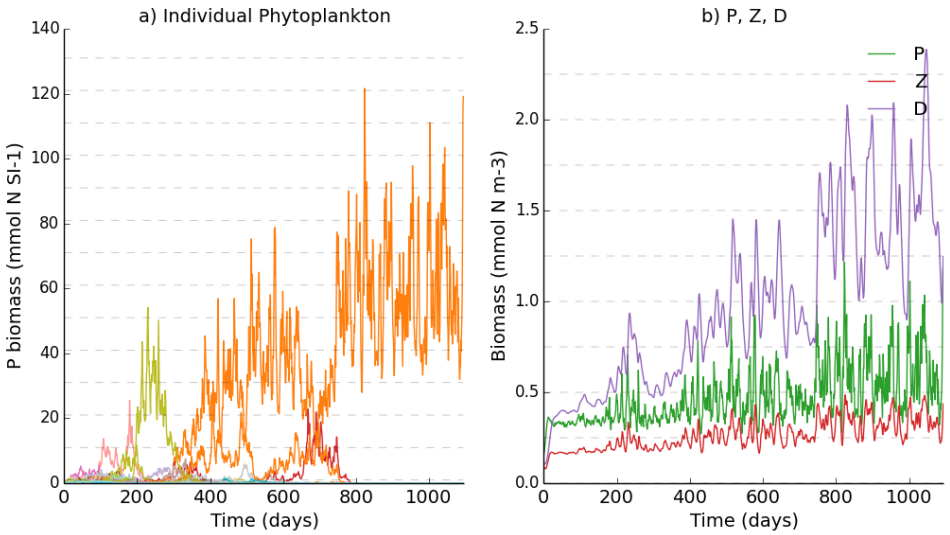

Figure 27: Model predictions for a) super-individual biomass and b) average values for P, Z, D, for a fixed slab model with a mixed layer depth of 100m, surface PAR of 50 W m^{-2}, 100 super-individuals, and no particle splitting

A great deal of the potential advantage to super-individuals higher in the water column can be removed through removing the light attenuation due to chlorophyll. This would completely remove the advantage / disadvantage due to shading, as the differences in light would be only due to the rate at which it is attenuated by water. In order to simulate this, I fixed the light attenuation coefficient to 0.04 m^{-1} (i.e. the value for the attenuation of light by water).

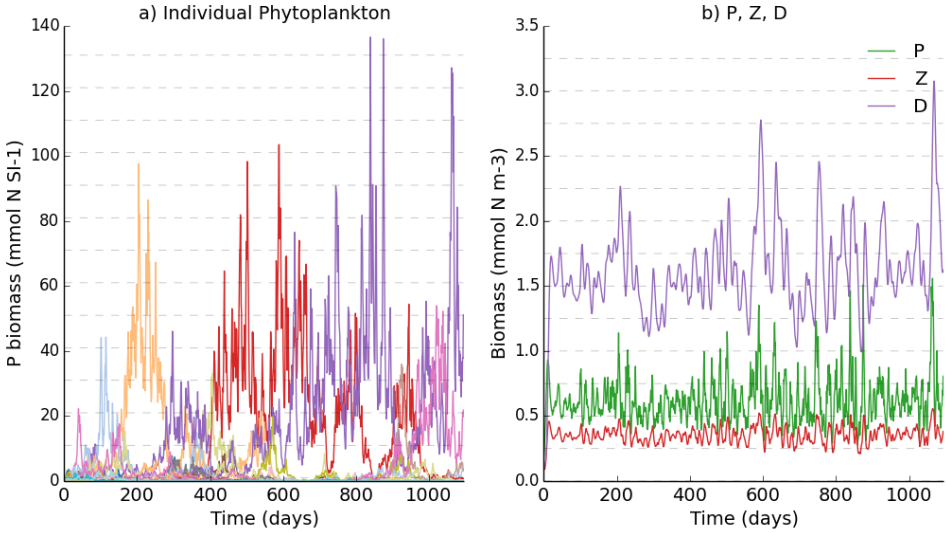

Figure 28: Fixed slab model with a constant mixed layer depth of 100m, a constant irradiance of 50 W m^{-2}, no particle splitting (100 super-individuals) and a fixed attenuation coefficient (k_{par} = 0.04 m^{-2}). Visser random walk.

Figure 28 shows that the shading of super-individuals by those higher up in the water column is not the only advantage that the phytoplankton can exploit. Although removing the light attenuation due to phytoplankton does significantly improve the spread of the biomass, it is still clear a small number of super-individuals still dominate each simulation.

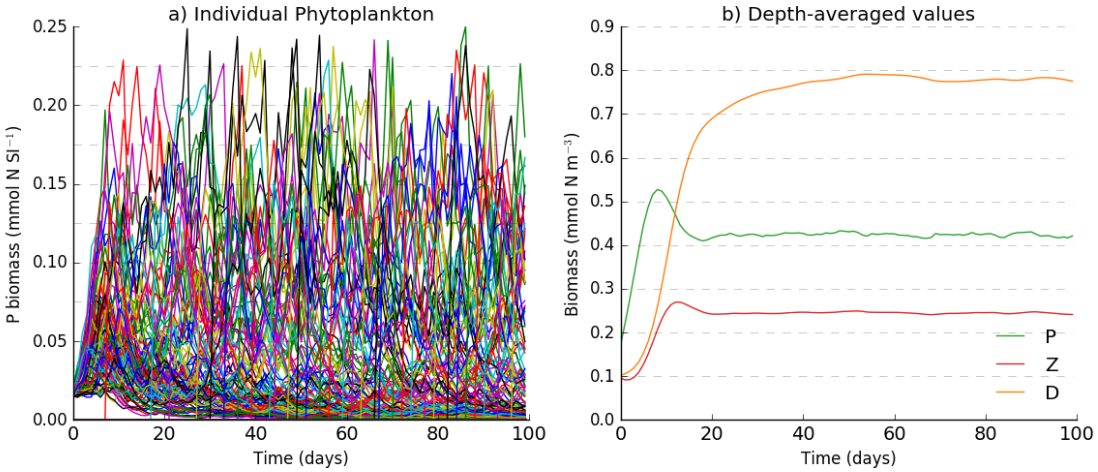

Figure 29: Fixed slab model with a constant mixed layer depth of 100m, a constant irradiance of 200 W m^{-2}, particle splitting (Pmax = 0.25 mmol N, final number of SIs = 5818). Visser random walk. For sake of clarity in the plots, only every 10th particle is plotted in a)

One of the most dramatic differences between Figure 27 and Figure 29, is in the predicted biomass. There is a significant increase in the steady state value

for phytoplankton biomass when the entire population is contained in one individual. This is a result of the way that shading is represented in the model. Essentially, phytoplankton are only shaded by those phytoplankton that are above them in the water column. If the entire population is contained within one individual, it is essentially no longer subject to shading. Although this is obviously an extreme scenario, it does demonstrate how a skewed distribution of biomass in the water column can result in decreased pressure on larger super-individuals, and increased pressure on smaller individuals. It also shows that the aim of including particle splitting is not necessarily just to keep an adequate supply of super-individuals within the simulation, but also to restrict the size to which each individual can grow.

To further demonstrate the effect the grazing and non-linear loss terms have on the phytoplankton, I ran a fixed slab model with a mixed layer depth of 100m, a constant surface PAR of 200 W m^{-2}, and 100 super-individuals – one per 1-metre layer. I kept the super-individuals stationary throughout the simulation, and did not include particle splitting. Running the model to a steady-state took a very long time (2000 days), due to the transient effect shown in Figure 30. The phytoplankton super-individual with the most advantage would dominate the simulation, but the depth at which that individual was situated changed, due to the changes in irradiance resulting from the changes in chlorophyll. Eventually all of the phytoplankton biomass is contained in the super-individual at the depth with the greatest advantage.

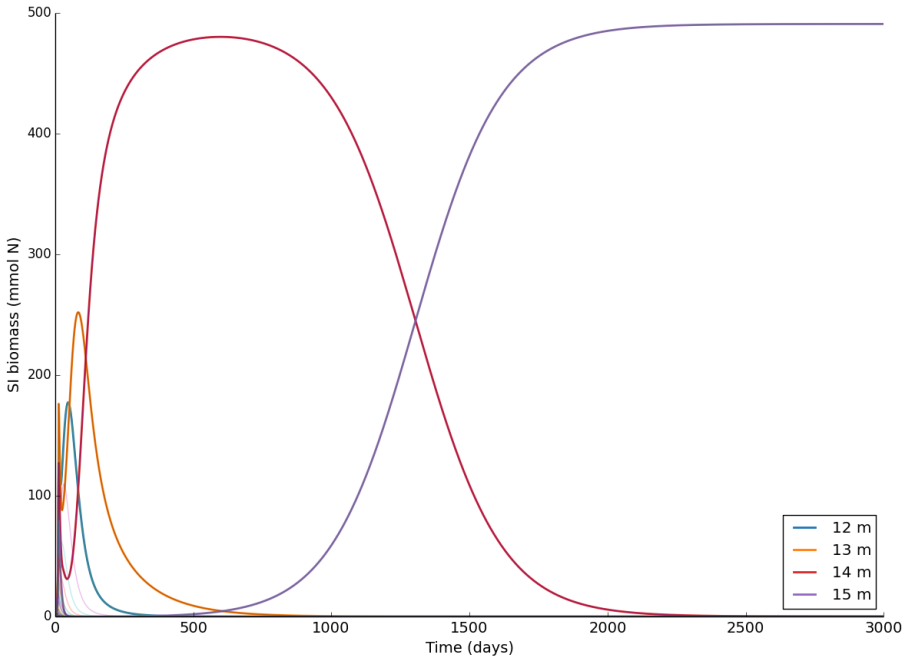

Figure 30: The transient increase shown by the nitrogen biomass at each depth in a fixed slab model, with no mixing. Each 1-metre layer contains a single SI. PAR = 200 W m-2, mld = 100m

That this is a result of the application of non-linear loss terms using linear proportionality can be demonstrated by running the same simulation shown in Figure 30, but this time without grazing by zooplankton, and with the non-linear mortality equation applied to each individual, based on their individual biomass i.e.:

$$M2_{SI} = m_{p2}\frac{P_{SI}}{\left(k_P + P_{SI}\right)} \qquad (2.24)$$

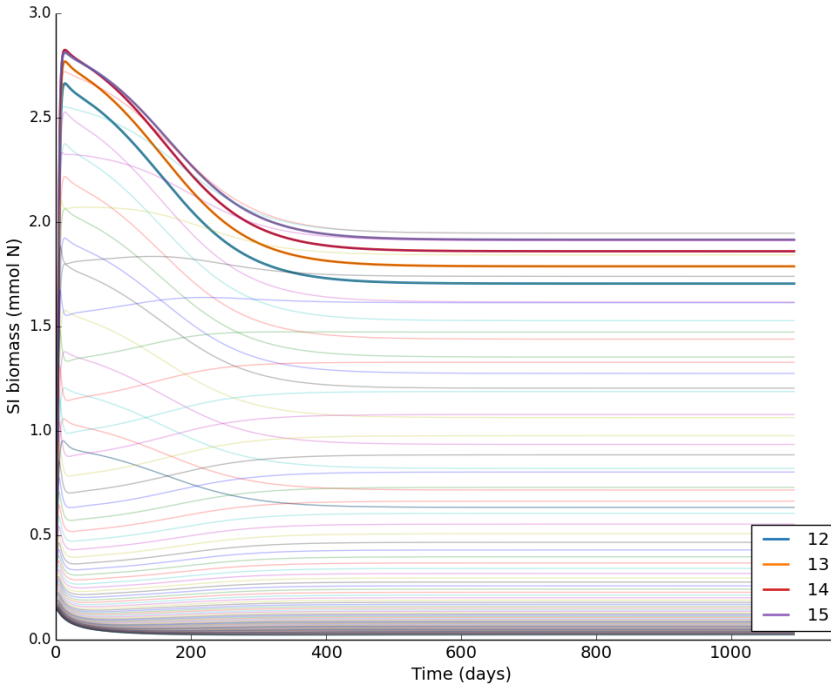

Figure 31: Nitrogen biomass contained in each super-individual, for a fixed slab model with no mixing, a surface PAR of 200 W m-2, and a mixed layer depth of 100 m. Each 1-metre layer contains a single SI, and the loss rate is calculated on an individual basis.

The simulation shown in Figure 31 does not include cell division or phytoplankton movement, yet a steady-state solution is achieved relatively quickly, and no single phytoplankton dominates the simulation. However, this solution has three disadvantages: firstly, implementing individual phytoplankton mortality and grazing makes a comparison with the Eulerian model more complicated, secondly, the Lagrangian model predictions (including the chl-to-carbon ratios) are then highly sensitive to the threshold for particle splitting, and finally, there are difficulties in implementing grazing on a particle level. Therefore, although in Chapter 3 individual based phytoplankton mortality is used to ascertain the rates of acclimation in individual phytoplankton super-individuals for scenarios with little or no mixing, it is not used for predicting rates of primary production.

2.3.3 Considerations for the movement rules

2.3.3.1 Choice of time step

The choice of time step depends upon the rate of the fastest processes. If the time step is too long, then some of the finer detail could be missed. In order to determine the appropriate time step, the model was run using a range of time steps, to find the point at which reducing the time step further made no difference to the results. The profiles of chlorophyll, nitrogen and pigment to biomass ratios in a steady-state simulation, as well as the depth-averaged values for a dynamic simulation were examined.

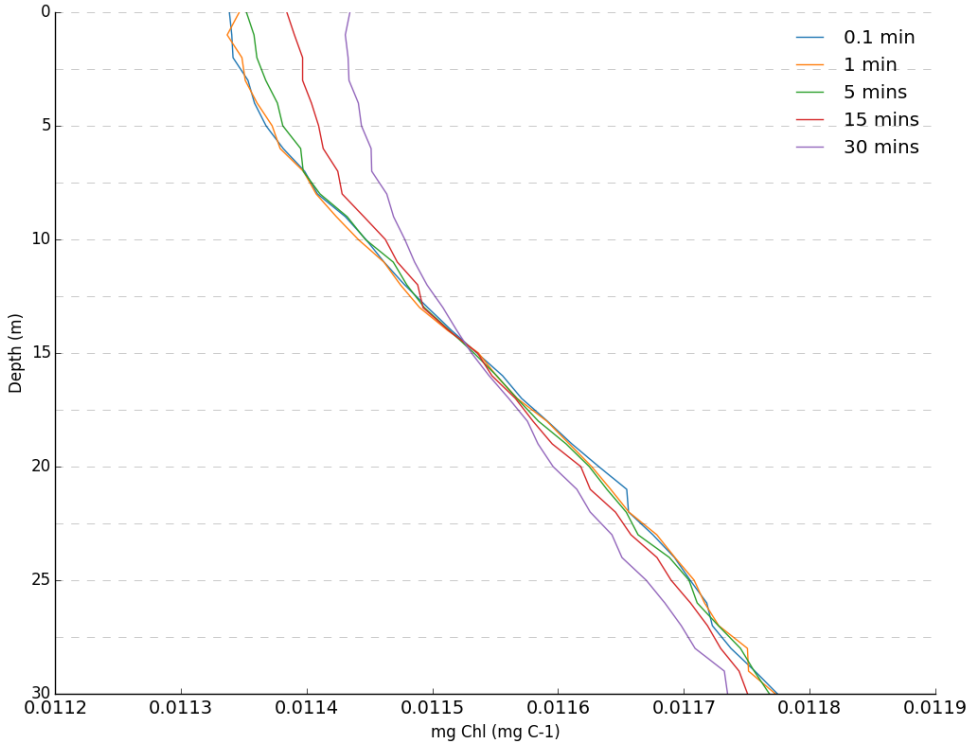

Figure 32: Steady-state chlorophyll profile for a model run with a constant mixed layer depth (100m) and constant surface irradiance (200 W m-2) under a range of different time steps (0.1 mins, 1 min, 5 mins, 15 mins and 30 mins)

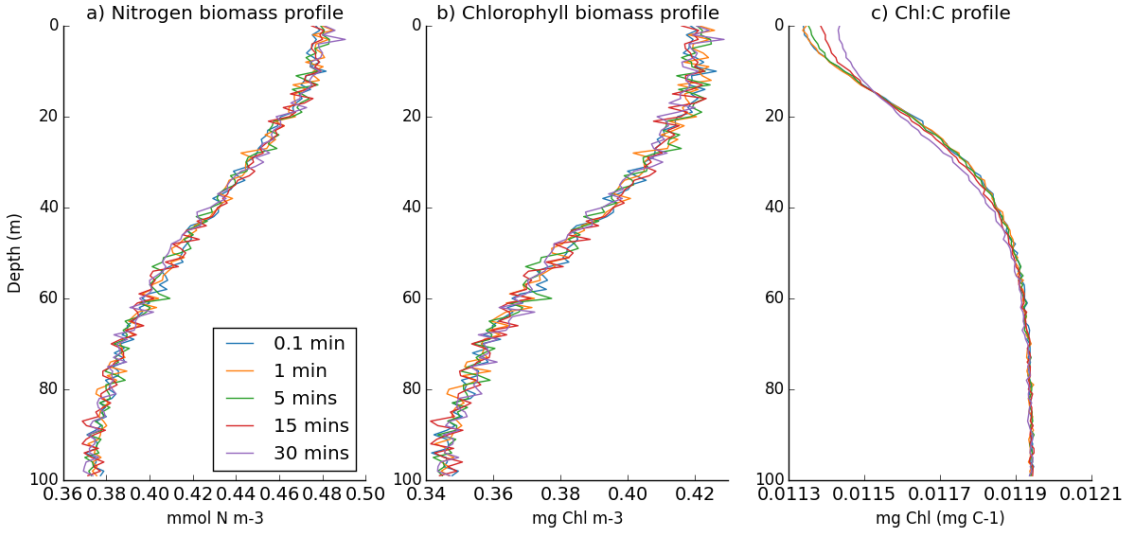

Figure 33: Predicted steady-state profiles for a) nitrogen biomass, b) chlorophyll biomass and c) chl:carbon for a model with a constant mixed layer depth (100m) and a constant surface irradiance (200 W m-2) under different time steps (0.1 mins, 1 min, 5 mins, 15mins and 30 mins)

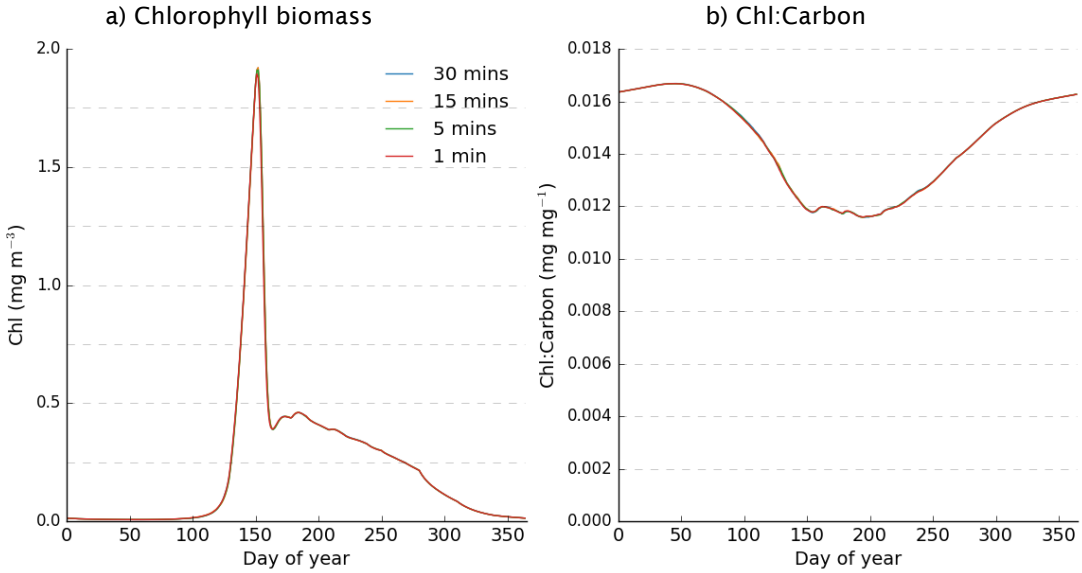

Figure 34: Predictions of a) integrated chlorophyll and b) chl-to-carbon ratios for the OWS I model, under four different time steps (1 min, 5 mins, 15 mins and 30 mins)

Figure 32 shows the steady state chlorophyll profile for a model with a constant mixed layer depth (100m) and a constant surface irradiance (200 W m^{-2}). Only the profile over the top 30m is shown, in order to best display the differences between the predictions of each model set-up. The models with the longer time steps (> 1 min) do show a slight increase in the steady-state chlorophyll near the surface, although this does not appear to affect the result

predicted when using a model with a full seasonal cycle for OWS India (Figure 34). Therefore, although a time step of 30 mins appears sufficient in order to achieve a good accuracy for most of the simulation runs, those which looked at the rates of photoacclimation in individual phytoplankton particles were run with a time step of 1 min, in order to allow for the greatest possible accuracy.

2.3.3.2 Random position movement algorithm

The first mechanism for redistributing the phytoplankton particles I investigated involved randomizing their vertical positions every time step. Although this represents a simple and easily reproducible representation of phytoplankton movement within the mixed layer, it does assume that the length of the time step is the length of time in which one particle could theoretically travel the entire depth of the mixed layer. Therefore, changing the time step effectively changes the speed of the super-individual.

I first investigated the effect of the time step on the model predictions of chlorophyll biomass using the fixed slab model. Figure 35 shows the model predictions for three different length time steps: 1 min, 30 min, and 300 min. These correspond to maximum speeds of ~1.7, ~0.06 and ~0.006 m s^{-1}, respectively (maximum speed calculated as the time step / depth of the mixed layer), and diffusivities of 20, 0.69, and 0.069 m^2 s^{-1} respectively. The plot shows the last year of data from a three year run.

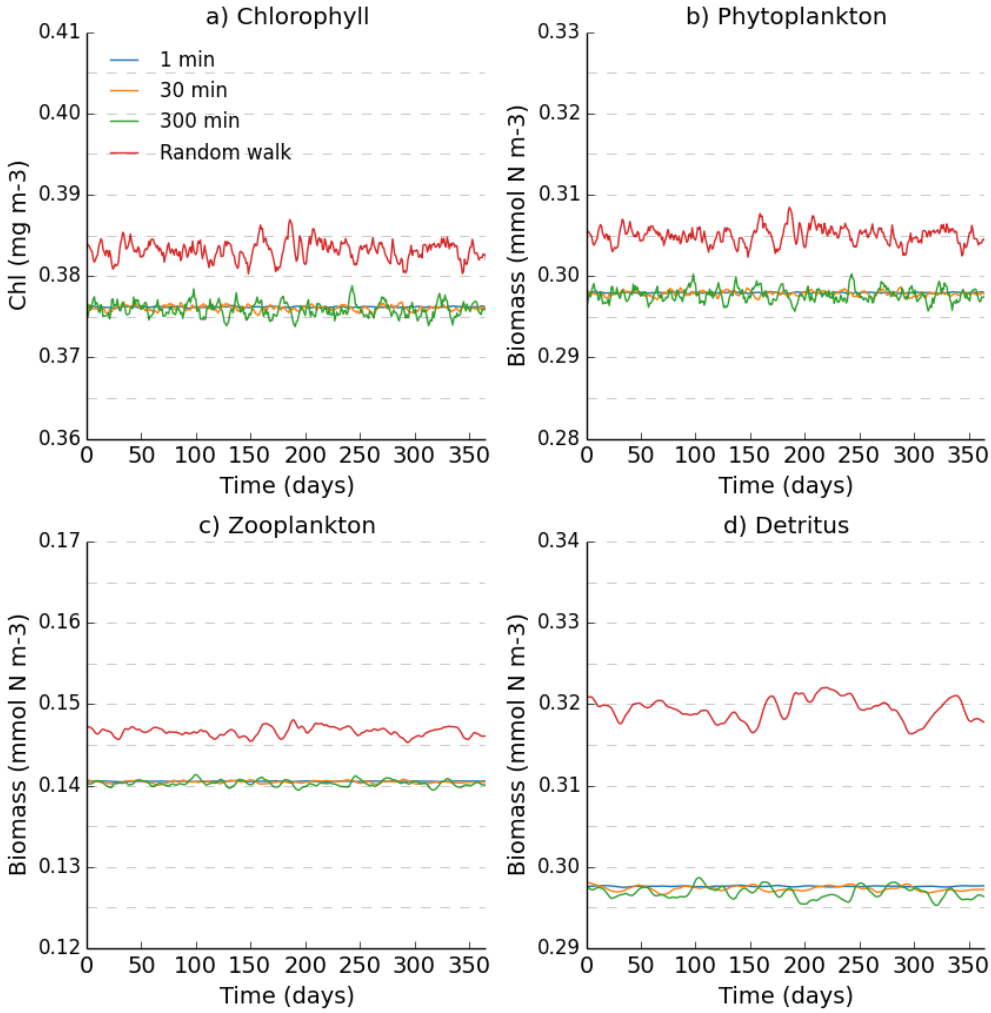

Figure 35: Predicted a) averaged chlorophyll and b) phytoplankton, c) zooplankton and d) detritus biomass from a fixed slab model (mld = 100m, surface PAR = 50W m^{-2}), using random position super-individual movement, for differing time step lengths (final super-individual numbers: 2769, 3629 and 6283, respectively). Random walk uses a time step of 30 minutes, and K_{turb} = 0.04m^2 s^{-1}

Figure 35 suggests that changing the time step from 1 minute to 300 minutes does not have a significant impact on the results. This is a surprising result, as reducing the mixing rate should allow the phytoplankton more time to acclimate to each depth in the mixed layer, which would be expected to result in changes to the growth rate and therefore the predictions biomass. Increasing the time step to 300 minutes does increase the level of noise in the results, but not to any great level. The random oscillations in Figure 35 only vary the average value by ~±0.5%.

The effect of the mixing rate on the phytoplankton can be further illustrated by plotting the vertical profiles of nitrogen, chlorophyll and the chl-to-carbon ratio. These profiles were obtained by averaging the variables over the last year of the three year simulation (Figure 36).

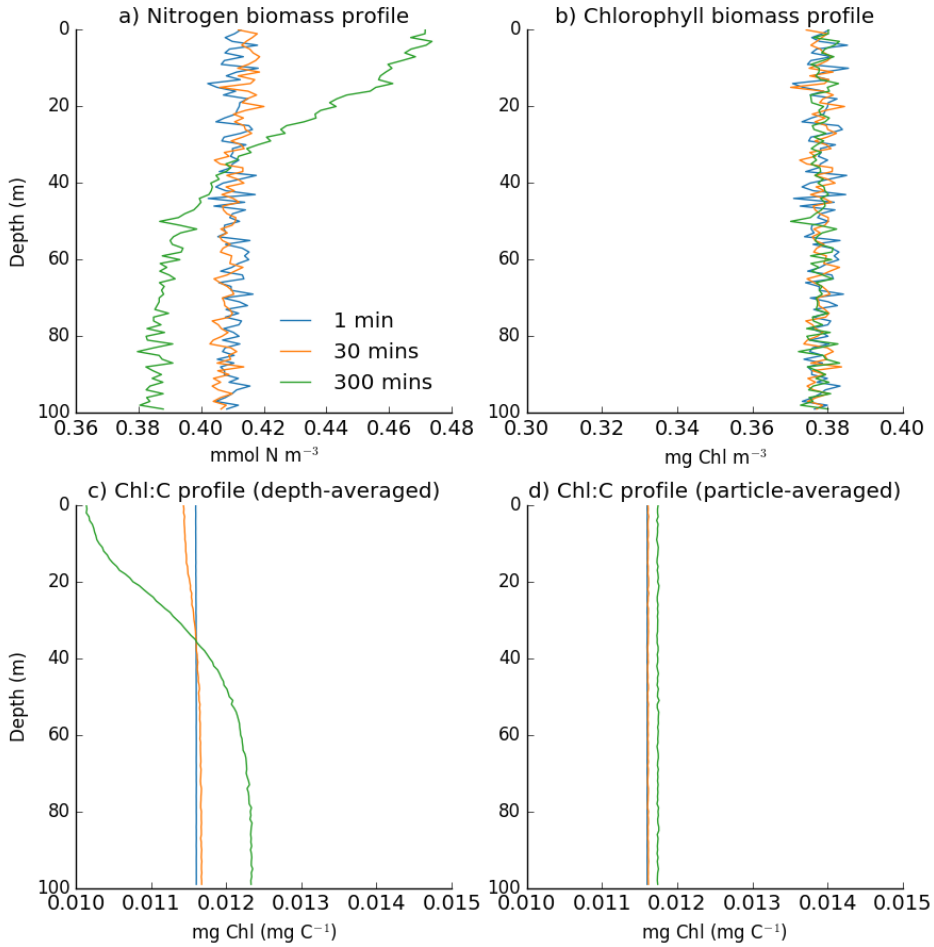

Figure 36: Vertical profiles of a) phytoplankton nitrogen biomass, b) chlorophyll and c) chl-to-carbon ratio for random position model runs with time steps of 1, 30 and 300 mins. Fixed mixed layer depth of 100m, fixed irradiance of 200 W m^{-2}, θ_{Chl}^{Max} = 0.02 mg Chl mg^{-1} C

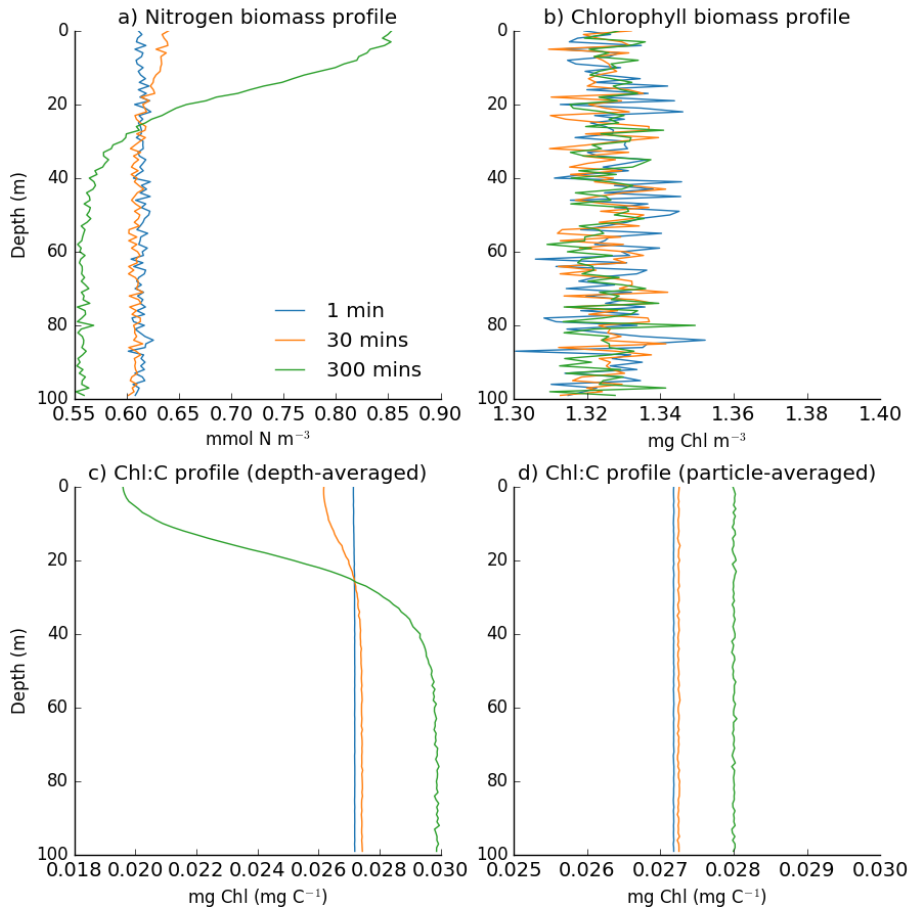

Figure 37: Vertical profiles of a) phytoplankton nitrogen biomass, b) chlorophyll and c) chl-to-carbon ratio for random position model runs with time steps of 1, 30 and 300 mins. Fixed mixed layer depth of 100m, fixed irradiance of 200 W m^{-2}, θ_{Chl}^{Max} = 0.05 mg Chl mg^{-1} C

Figure 36 shows that there is no variation in the chl-to-carbon ratio with depth for the simulations with the randomly positioned phytoplankton super-individuals. Figure 37 shows that this result does not change for a higher value for the maximum ratio of chl-to-carbon (θ_{Chl}^{max} = 0.05 mg Chl mg^{-1} C). This suggests that 300 minutes is not sufficient time for the phytoplankton to acclimate to the irradiance. Chapter 3 includes a more detailed analysis of the relationship between the rates of mixing and acclimation. However, one interesting feature of Figure 36 is the difference in profile of chl-to-carbon ratio, when averaged by the particles at each depth, or by the biomass at each depth. This can be explained by particles at the surface being able to grow rapidly and produce more nitrogen biomass. There is no corresponding increase in chlorophyll, as chlorophyll production is downgraded at higher irradiances. The overall chl-to-carbon ratio of the individual particle is also unaffected, as each phytoplankton super-individual will only experience the

irradiance for one time step, before being mixed back into the water column. Also of interest is the fact that the vertical profile of nitrogen biomass does not result in a different steady-state average nitrogen biomass (Figure 35). Finally, the differences in the values of chl-to-carbon between the phytoplankton that are randomly repositioned every 30 minutes, and those repositioned every 300 minutes do not result in a difference in the predicted steady-state values for averaged chlorophyll or nitrogen (Figure 35). This suggests that the difference in model predictions between the models that randomly position the super-individuals, and the random walk model is not due to phytoplankton photoacclimation. This topic is explored in more depth in Chapter 3.

The same experiment was performed with the full OWS India model (Figure 38).

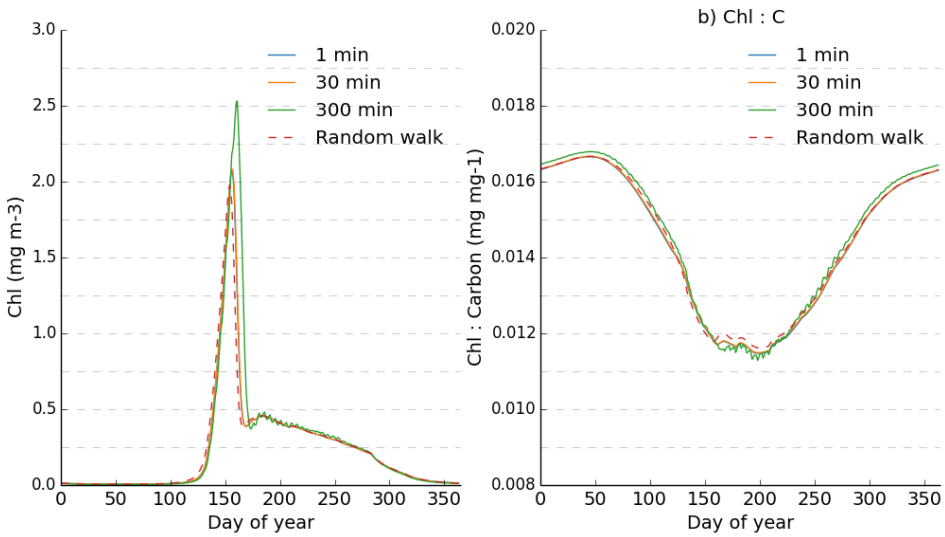

Figure 38: Model predictions for a randomisation model with different time steps. Final super-individual numbers: 2109, 2342, 1701

Again, there is little difference for the predicted seasonal cycle of chlorophyll, with the exception of the magnitude of the chlorophyll peak in the model using the time step of 300 minutes.

This is an interesting result, because, as the rate of mixing is essentially a function of the time step, the fact that altering the time step has no significant effect on the photoacclimative processes would suggest that these are not affected by the mixing rate. However, in order to directly compare the random walk and random position models, some way of quantifying the diffusivity in

the random position model is required. An estimation of the diffusivity can be obtained by rearranging equation (2.6), taking the average step length to be half of the depth of the mixed layer ($H/2$):

$$K_{turb} = 0.5 \cdot \frac{\left(\frac{H}{2}\right)^2}{\partial t} \tag{2.25}$$

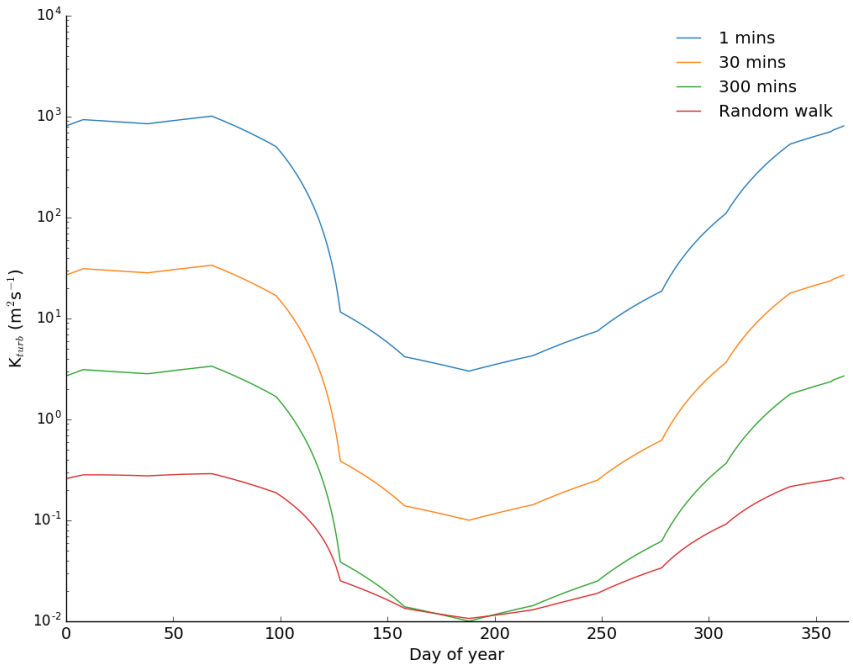

Figure 39: Estimated cycle of diffusivity for the random position model with different time steps, compared to the seasonal cycle of diffusivity for the random walk model

Figure 39 shows the estimated cycles of diffusivity for the random position model with different time steps, based on equation (2.25). It suggests that, even when the time step is increased to 300 minutes, the estimated diffusivity is still higher than for the random walk model. In addition, reducing the time step in the random walk model increases the possibility of each particle staying near its previous location, due to the reduction in step length. This is something that is not seen in the random position, because with each move, the phytoplankton can be relocated to any depth in the mixed layer. This can be demonstrated by initialising a model with 1000 super-individuals, all at the same point in the water column, running the model for 5 time steps, and then plotting the frequency of their final positions (Figure 40).

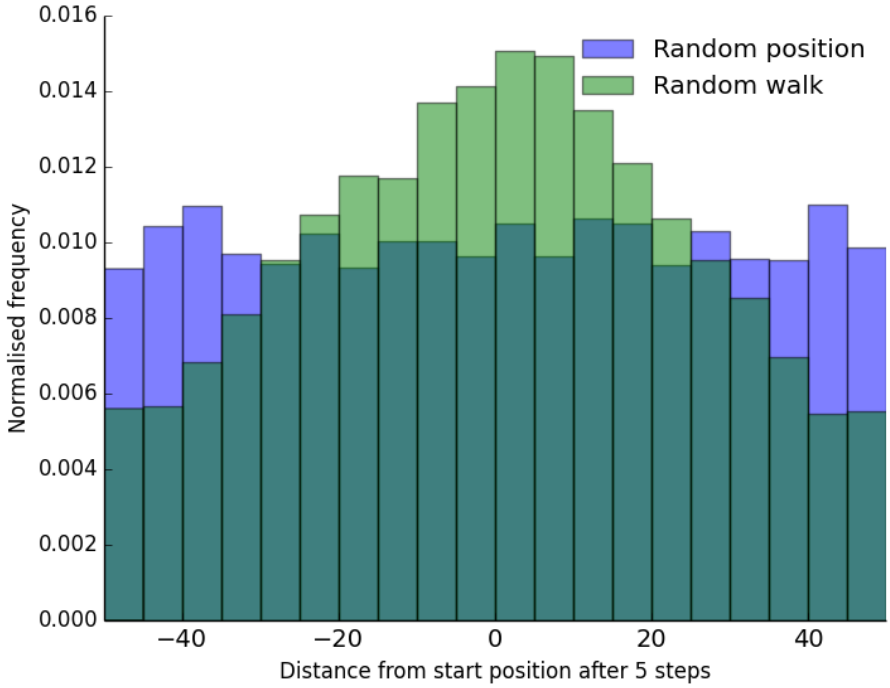

Figure 40: The distance from the start position after 5 time steps for the random position model, and a random walk model with K_{turb} = 1 m^2 s^{-1}, using a time step of 1 min.

Figure 40 shows how the phytoplankton in the random walk model follow a normal distribution around the start point, whereas the random position model super-individuals are evenly distributed throughout the mixed layer. Therefore, even though the estimated diffusivity of the random position is close to the diffusivity of the random walk, the lack of connectivity between each step in the random position model mean that these two methods of movement are not comparable.

2.3.3.3 Random walk

The advantage of using a random walk is that the step length can be determined by the depth of the mixed layer, which makes it a better option for a model with a seasonal cycle. However, measuring the diffusivity coefficient, K_{turb}, is time consuming and rarely, if ever, collected over seasons. The model used in this study takes its basic turbulence equations from the KPP model (Large et al., 1994), and only considers the surface wind speed (Eq. (2.2)).

2.3.3.3.1 Sensitivity to wind speed

Empirical measurements of ocean mixing can vary by up to four or five orders of magnitude, depending on the wind speeds. For example, a 10-15m deep mixed layer can have measurements of K_{turb} = 1.9 x 10^{-5} m^2 s^{-1} in low winds (5 m s^{-1}), but up to 1.9 x 10^{-3} m^2 s^{-1} in higher winds (15 m s-1) (Denman & Gargett, 1983). Figure 41 and Figure 42 show how changing the wind speed affects the model predictions of chlorophyll for a fixed slab model and the OWS I model, respectively, and Figure 43 shows how each of these wind speeds compares to wind speed data taken from the ERA40 dataset for 2001. The wind speeds are calculated from the u and v component of the wind velocity measured at 10m above the ocean, $windspeed = \sqrt{u^2 + v^2}$.

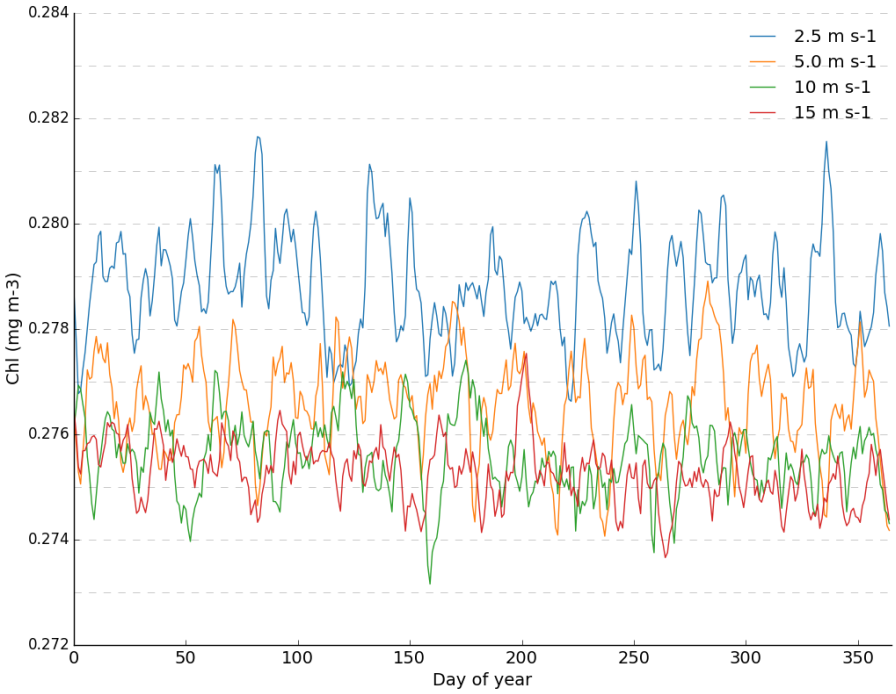

Figure 41: Chlorophyll predictions for fixed slab model with varying wind speeds, Visser random walk. Final super-individual numbers: 19582, 11467, 6692, 4972.

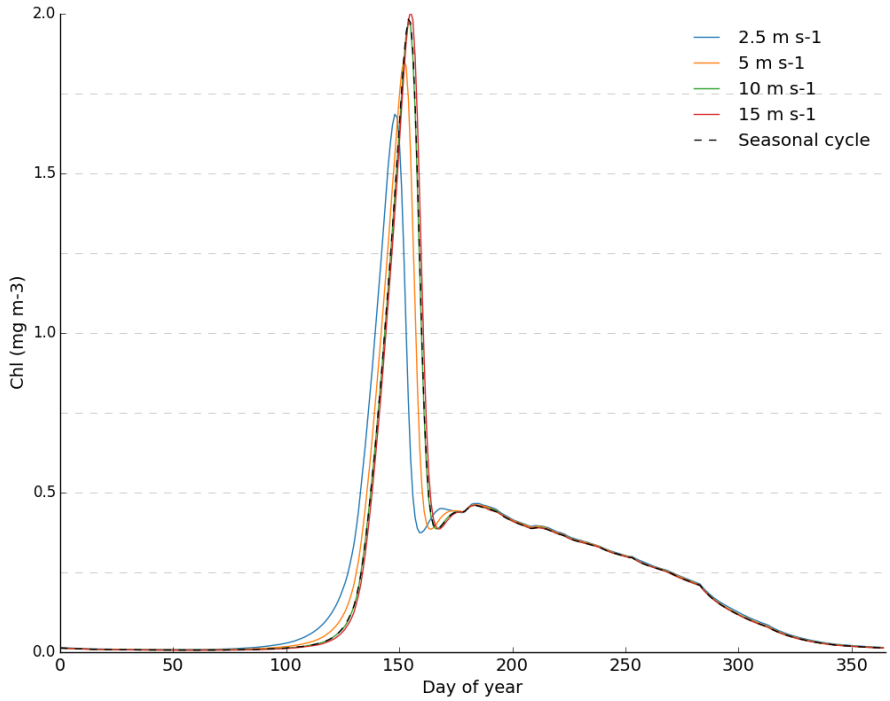

Figure 42: Chlorophyll predictions for Station India model with varying wind speeds, Visser random walk. Final super-individual numbers: 3312, 2807, 2654, 2460. The standard model run uses a seasonal cycle of wind speed.

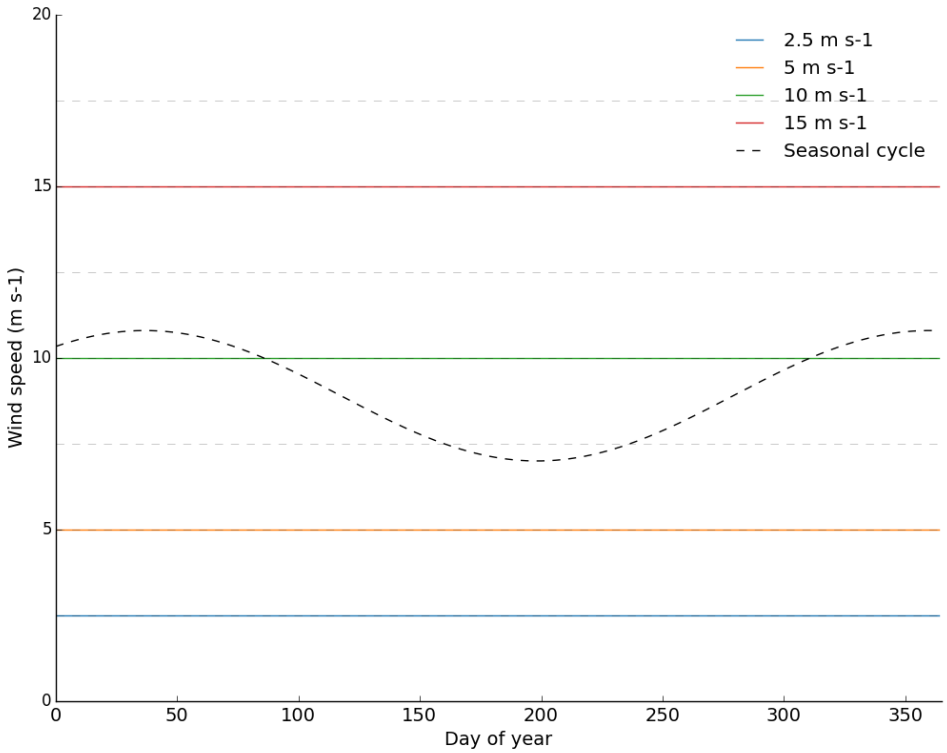

Figure 43: The wind speeds used in Figure 42 compared to the sinuisodal curve used to represent the seasonal cycle of wind speed

There is little difference in the chlorophyll predictions when increasing the wind speed from 10m s^{-1} to 15 m s^{-1}, which suggests that a wind speed of 10 m s^{-1} results in a mixing rate which is fast enough to overcome any phytoplankton processes, such as photoacclimation, which could be affected by the mixing rates.

2.3.4 Number of super-individuals used in a simulation

The compromise between model precision and run time in Lagrangian models is most clearly seen in the number of super-individuals chosen to represent the phytoplankton population. Even though this decision has the greatest and most direct influence on model run time, it has never been fully explored in the literature.

Early Lagrangian phytoplankton models were limited by the lack of available processing power and data storage, and the number of phytoplankton particles was therefore dictated by the available technology. Numbers tended to be relatively low, ranging from 1-200 (e.g. Falkowski & Wirick (1981) and Lizon et al., (1998)) to 1-2000 (e.g. Barkmann & Woods (1996a); Broekhuizen (1999); Cianelli et al. (2004); Franks & Marra (1994)). Dippner (1991) conducted a sensitivity test on a simple Lagrangian model, which concluded that 10 particles was sufficient for a mixed layer 10 m deep. The majority of studies include little or no justification for the numbers used, and only fleeting reference to particle number: for example, Barkmann & Woods (1996a) suggested that 20 particles per metre was a minimum model requirement, and that increasing the number of particles beyond this did not change the results significantly. Cianelli et al. (2004) proposed that “a significant number of cells” needed to be simulated in order to “represent the realistic dynamics of a phytoplankton population with an IBM”, but without clarifying what a significant number actually was.

Although more recent models are less restricted by computing power, there still appears little mention in the literature as to how changes in particle number affect model results. Woods (2005) has stated that 200 particles per layer (1m) is necessary, and Ross et al. (2011b) used 80,000 particles when simulating mixed layers deeper than 60m, stating that this high number was

necessary in order to obtain reliable statistics each metre, but there currently exists no data surrounding how low numbers of particles affect model predictions.

In this section, I show how the average number of super-individuals used to represent the phytoplankton population in a simulation can influence the model predictions, and how the optimal number was chosen. The definition of an 'optimal' number of individuals was a number that would give accurate and consistent results, whilst allowing for the model to run quickly, as the experiments for which it was designed would require a number of runs. The average number of super-individuals in each simulation is controlled by the threshold for particle splitting (P_{div}). Increasing P_{div} means that the super-individuals are allowed to grow to a larger size before they are divided in two, which means that there will be a smaller number of individuals in the simulation, and decreasing P_{div} will have the opposite effect, resulting in a higher number of super-individuals.

The fixed slab model was used, with a constant mixed layer depth of 100m, constant surface PAR of 100 W m^{-2}. Using a fixed slab model means that there is no loss through detrainment, so the starting number of super-individuals was reduced from 1000 to 100, because some of the runs would require average super-individual numbers below 1000. The models were run for 3 years, and the final year of data was used.

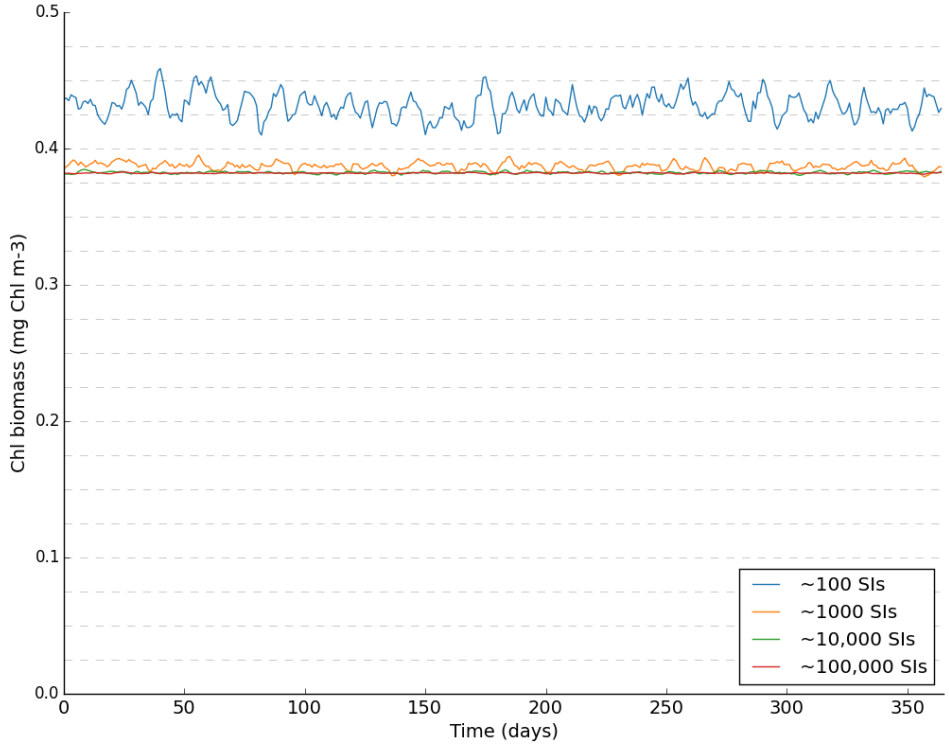

Figure 44: Model predictions of steady state chlorophyll for fixed slab model with different numbers of super-individuals. Super-individual numbers: 91, 1033, 9723, 97487

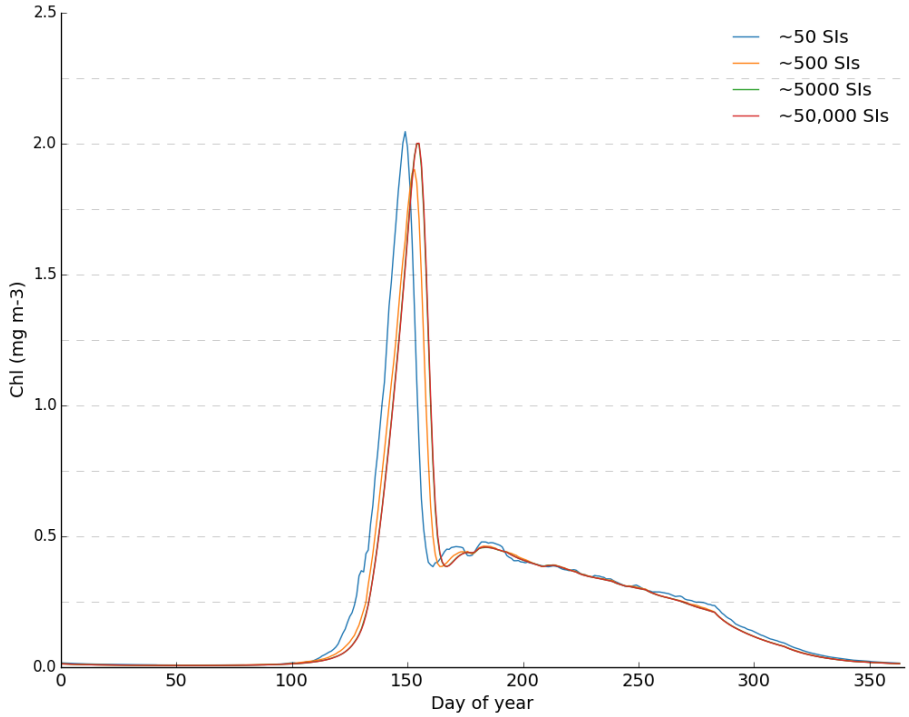

Figure 45: Comparing model predictions of integrated chlorophyll for a model with varying numbers of super-individuals: Final numbers: 55, 499, 5293, 53400. Visser random walk.

Both models appear to be less sensitive to the particle number than expected. The steady state model shows only a small changes in predictions when the SI number falls to 1000 (Figure 44) and the full seasonal cycle shows no significant change to the model predictions, until the particle numbers fall below 500 (Figure 45). The increase in the predicted chlorophyll biomass with the decrease in average super-individual numbers backs up the results in section 2.3.2, because increasing the threshold for splitting increases the potential size to which the super-individuals can grow. Super-individuals do not shade themselves, therefore, an individual that comprises a large proportion of the total phytoplankton population is always unaffected by the attenuation of light by a large proportion of the total phytoplankton chlorophyll. This results highlights that, not only is it necessary to include particle splitting, it is also important to ensure that splitting occurs at a low enough threshold to prevent a skewed distribution of biomass.

However, overall, the results indicate that the model predictions are not overly sensitive to the numbers of super-individuals, and that little accuracy is gained by increasing the numbers past ~1000 individuals. For the OWS India runs, the threshold for splitting was therefore set at a level that would result in between 2,000 and 10,000 super-individuals being simulated at any one time (i.e. P_{div} = 0.025 mmol N).

2.4 Conclusion

This chapter was designed to address two main objectives: firstly to create a Lagrangian phytoplankton-based ecosystem model and use it to replicate the seasonal dynamics at Station India, and secondly to use the model to investigate some of the basic assumptions of Lagrangian modelling. In line with previous studies, an Eulerian-Lagrangian hybrid is used for the study, as a good compromise between complexity and accuracy. The solution to the difficulties surrounding how to represent the high numbers of individual phytoplankton cells found in the ocean is addressed, as by previous researchers, by the use of a Lagrangian Ensemble modelling method (or super-individuals), which allows for the representation of individual physiological changes, whilst keeping individual numbers manageable. However, one new finding here is that it is not necessary to explicitly represent and keep track of

individual cell numbers, each super-individual can represent a quantity of biomass, rather than a number of individual phytoplankton cells.

The section investigating some of the basic assumptions of Lagrangian models, describes several findings, some of which are new to this field. Firstly, models that do not include some form of particle splitting are shown to run the risk of highly skewed biomass distributions between super-individuals, which can lead to inaccuracies in the model predictions, as observed by Ross & Sharples (2007). In addition, although the number of super-individuals does not significantly impact on the model predictions, it is important to ensure that there is an appropriate limit on the maximum size of each individual, to ensure that a significant proportion of the phytoplankton population is not contained within a small number of individuals. A second important and previously unseen finding is that the use of random position models of movement is not appropriate for models that rely on photoacclimation. In random position models, the implied mixing rate is a function of the time step, and the results here show that changes to this implied mixing rate, through changes in the length of the time step, have no significant effect on the individual photoacclimative properties of the phytoplankton.

Determining whether effects such as those explained above are the result of biological processes, or are merely statistical artefacts is of crucial importance, but is not something that is currently seen in the literature. The more studies like this that are carried out, the more researchers can work towards developing well-tested Lagrangian modelling standards, which could eventually result in Lagrangian models that are more easily communicated, replicable, and directly comparable.

In the next chapter, I compare the model described here with an equivalent Eulerian formulation, in order to examine whether Eulerian and Lagrangian models differ in their predictions, and whether these differences are due to the inclusion of photoacclimation.

Chapter 3: Modelling growth and acclimation in Lagrangian phytoplankton

3.1 Introduction

Lagrangian models are more complicated to design and implement, and incur greater computational running and maintenance costs than Eulerian models. Therefore, before deciding to represent phytoplankton using a Lagrangian framework, it is important to ascertain whether a Lagrangian approach is necessary, or whether a simpler Eulerian approach would be adequate for the job at hand. The arguments advocating the use of a Lagrangian approach are based on the fact that integrating non-linear equations before averaging them gives a different result than first averaging and then averaging them (Woods and Onken, 1982). However, the few studies that have investigated comparisons between Eulerian and Lagrangian models demonstrating conflicting results. In this chapter, I perform a direct comparison between equivalent Eulerian and Lagrangian implementations of a phytoplankton-based ecosystem model, in order to determine whether their predictions differ due to the differences in the way that the overall rates of primary production are calculated: i.e. integrated through the mixed layer, or as the summation of photosynthesis from individual phytoplankton.

A Lagrangian approach is believed to offer more accurate representation of the photophysiological response, due to its ability to track the individual light histories of the phytoplankton super-individuals (Ross et al., 2011a). Phytoplankton cells change their physiology in response to irradiance, downgrading rates of chlorophyll production in high irradiance, and increasing it under lower irradiances (MacIntyre et al., 2002). In theory, therefore, a phytoplankton cell that has been mixed to the surface from deeper in the water column will photosynthesise at a different rate to one that has been close to the surface for a length of time. Eulerian models are unable to capture these individual differences in physiology resulting from the individual trajectories and light exposure experienced by phytoplankton cells as they move through the mixed layer.

For acclimation to have a significant impact on individual rates of photosynthesis, phytoplankton need to have time to acclimate to their local irradiance, before being mixed up or down in the mixed layer. Therefore, the relationship between the rates of acclimation and the rates of mixing are extremely important, and this relationship is investigated by plotting the trajectories of super-individuals through the irradiance field, along with their resulting chl-to-carbon ratios. This is then compared to predicted, steady state values, to give a clear illustration of how quickly the phytoplankton are acclimating in relation to the rates of mixing.

For comparison, another mechanism by which Lagrangian and Eulerian models can differ is also investigated: the vertical profile of phytoplankton in the mixed layer. The Eulerian model uses the assumption that the mixed layer is fully mixed at all times, and so there is a homogeneous vertical profile of phytoplankton. There are no such assumptions in the Lagrangian model, and so a heterogeneous profile develops in response to changes in the mixing rates. I investigate the sensitivity of the overall rates of primary production to the vertical distribution of phytoplankton, demonstrating that this has a greater impact on the differences between Lagrangian and Eulerian models than the individual rates of acclimation.

3.1.1 Objectives

This chapter addresses the following questions:

1. Is there any difference between the predictions of average phytoplankton population growth from an ecosystem model implemented in two different formulations: Lagrangian (hybrid model) and Eulerian?
2. If the model predictions do differ, is it due to photoacclimation (and if not, what is the explanation)?
3. What is the relationship between the timescales of mixing and acclimation?
4. What are the consequences for the ecosystem model as a whole?

3.2 Model description

The Lagrangian hybrid model, fully described in Chapter 2, essentially comprises Lagrangian phytoplankton super-individuals, set within an otherwise fully Eulerian ecosystem. Each super-individual has a vertical position in the water column, which is updated every time step via a random walk. Growth is both a function of the external irradiance and nutrient concentrations, and the internal pigment-to-biomass ratios, the latter of which changes in response to the ambient irradiance. In this way, the ratio of pigment to biomass, and therefore the potential maximum photosynthetic rate, is a result of the previous light history experienced by each super-individual.

The Eulerian model uses the same equations as the Lagrangian hybrid model, which are fully described in Chapter 2. The growth rate, μ_P, and the chlorophyll growth-scaling factor, R_{Chl}, are calculated at depth intervals of 1 m. The new chlorophyll and phytoplankton nitrogen production are then calculated at each interval, and the total average new production of chlorophyll and nitrogen is the average of these values. For each depth, z (m), in the mixed layer, the growth rate, μ_P (h^{-1}), is:

$$\mu_{P,Z} = \theta_{Chl} \cdot \frac{V^{PT} \cdot \alpha_P \cdot I_Z}{\left(V^{PT^2} + \alpha_P{}^2 \cdot I_Z{}^2\right)^{0.5}} \cdot \frac{DIN}{k_N + DIN} \tag{3.1}$$

and the chlorophyll growth scaling factor:

$$R_{Chl,Z} = \theta_{\max}^{chl} \cdot \frac{\mu_{P,Z}}{\alpha_P \cdot I_Z \cdot \theta_{Chl}} \tag{3.2}$$

Therefore, for each 1 metre interval (i.e. z, where 0<=z<=H, and H is the depth of the mixed layer (m)):

$$\frac{dP_Z}{dt} = \mu_{P,Z}P - G - m_P P - m_{P2}\frac{P}{P + k_P} - k_{mix}\frac{P}{H(t)} \tag{3.3}$$

$$\frac{dChl_Z}{dt} = \mu_{P,Z}R_{Chl}Chl - \left(\theta_{Chl} \cdot \xi^{-1}\left[G + m_P P + m_{P2}\frac{P}{P + k_P} + k_{mix}\frac{P}{H(t)}\right]\right) \tag{3.4}$$

The averaged, new production of chlorophyll and nitrogen for the entire water column is then the average of the new production at each depth interval.

Growth rate is therefore a function of the average pigment-to-biomass ratio, and the question is whether the summation of the individual growth rates based on individual physiologies in the Lagrangian phytoplankton will differ from the integrated growth rate based on the average pigment-to-biomass in the Eulerian model. In order to aid comparison, the models were kept as simple as possible, and all of the code was written in the same language (Fortran 90). The model parameters and the full model description can be found in Chapter 2.

3.3 Comparing Lagrangian and Eulerian formulations of OWSI

The first experiment compares the Lagrangian model run shown in Chapter 2 to an equivalent Eulerian simulation. Ocean Weather Station India is an ideal location in which to examine potential differences between Eulerian and Lagrangian model implementations, due to the clear seasonal cycle of nutrients and phytoplankton, lack of a sub-surface chlorophyll maximum, and deep mixed layer, which is observed to reach depths of over 500m. The first experiment compared the seasonal cycles of integrated chlorophyll biomass, and the average chl-to-carbon ratios (averaged per metre in both simulations). The phytoplankton moved via a random walk algorithm, with the step length based on the turbulent diffusivity, which was parameterised based on the mixed layer depth (prescribed from observations) and the surface wind speed (based on ERA40 data). A 30 minute time step was used, and the model was run for 2 spin-up years before data were recorded and plotted. The full description of the physical and biological model can be found in Chapter 2.

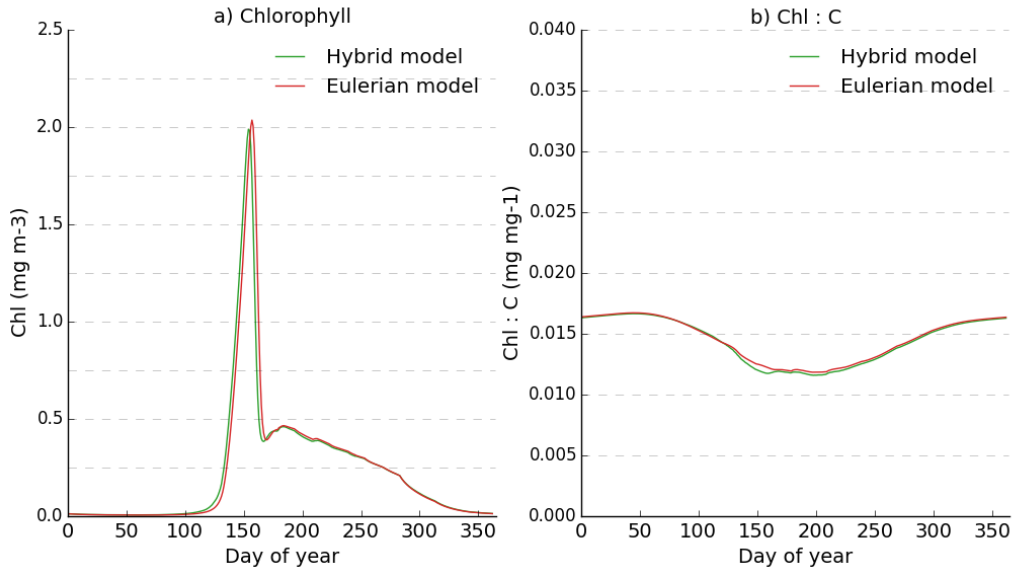

Figure 46: Seasonal cycles of a) chlorophyll and b) chl:carbon predicted by the Eulerian and Lagrangian-Eulerian hybrid formulations of the model.

Figure 46 shows that there is little difference between the seasonal cycles of integrated chlorophyll or averaged chl-to-carbon ratios predicted by each model formulation. In addition, Figure 46 (b) shows that while each model does predict seasonal variation in Chl:C, there is little variation between the Eulerian and Lagrangian models. This was also true for the phytoplankton, zooplankton and detrital nitrogen biomass in the ecosystem (Figure 47).

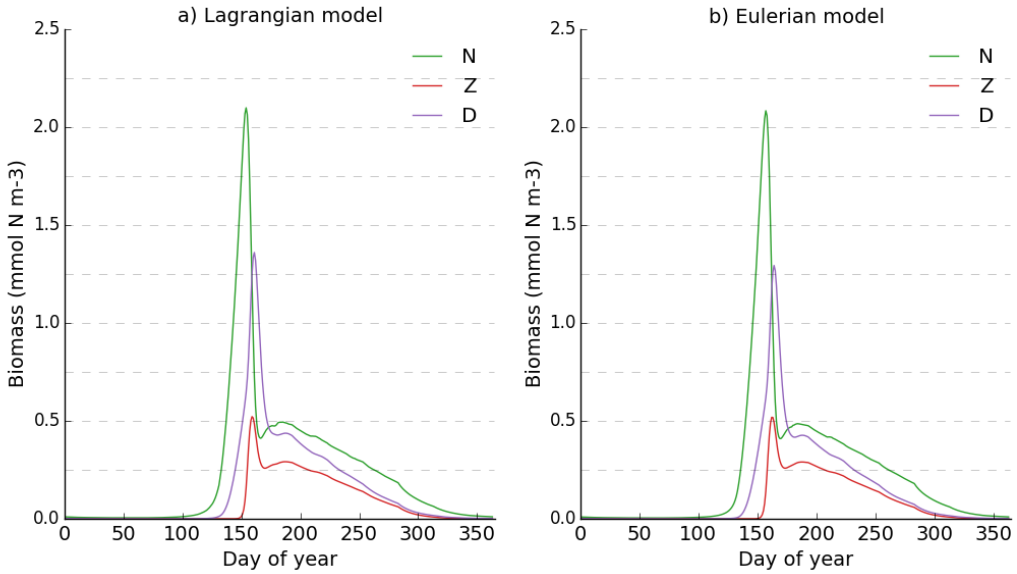

Figure 47: Seasonal cycle of biomass for phytoplankton, zooplankton and detrital nitrogen biomass in a) the Lagrangian model and b) the equivalent Eulerian model

Figure 46 (b) shows that there is little variation between the average Chl:C values, but gives no information about the spread of Chl:C values in the Lagrangian model. Plotting the individual Chl:C values for 100 randomly selected individuals, along with the average value, shows the range of chl-to-carbon ratios over the annual cycle..

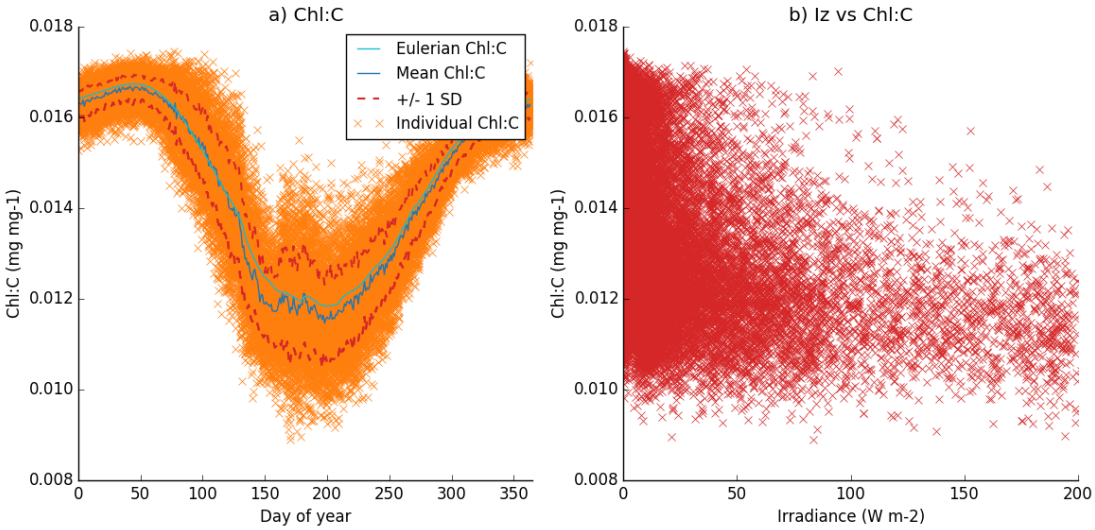

Figure 48: The seasonal cycle of mean values of Chl:C (blue line) with ± two standard deviations (red dashed lines), along with the individual Chl:C values taken from 100, random individuals (orange crosses). Also shown is the instantaneous relationship between the individual chl-to-carbon ratios of the phytoplankton particles and the local irradiance at their depth (b).

Figure 48a shows the range of chl-to-carbon ratios displayed by the super-individuals. Figure 48b gives a 'snapshot' of the relationship between the chl-to-carbon ratio of the individuals, and the irradiance at their current depth. It is interesting to note the wide spread of values displayed by phytoplankton experiencing no irradiance, which could suggest that the phytoplankton are not acclimating to their irradiance. There are more data points for phytoplankton experiencing lower irradiances, as phytoplankton are more likely to experience lower irradiances than higher irradiances, especially over winter when the mixed layer is deep. However, there is also a relationship indicated between the irradiance and the chl-to-carbon ratio in Figure 48b, although, whether this is due to the phytoplankton being fully acclimated at all times (as suggested by Lande & Lewis (1989)), or whether these differences are not significant, and the super-individuals have relatively similar properties, due to the mixing rate being faster than the rate of acclimation (as suggested by

McGillicuddy (1995)) is unclear. Fortunately, the use of a Lagrangian model allows for all the properties of the super-individuals to be tracked, and the trajectory of three, random SIs through the water column, along with their chl-to-carbon ratios, is shown in Figure 49.

Figure 49: Seasonal cycle of chl-to-carbon for three randomly selected SIs in the OWS India model

There is little change in the chl-to-carbon ratio for the SIs in the early and latter parts of the year, because the lower irradiance and deeper mixed layers mean that the phytoplankton are continuously close to the maximum chl-to-carbon ratio. Once the mixed layer shallows and the irradiance increases, the phytoplankton spend the majority of the time in the euphotic zone, and the chl-to-carbon ratio shows more variability. I therefore examined one 10-day section, when the noon irradiance is at its highest, and the mixed layer depth at its shallowest (Figure 50).

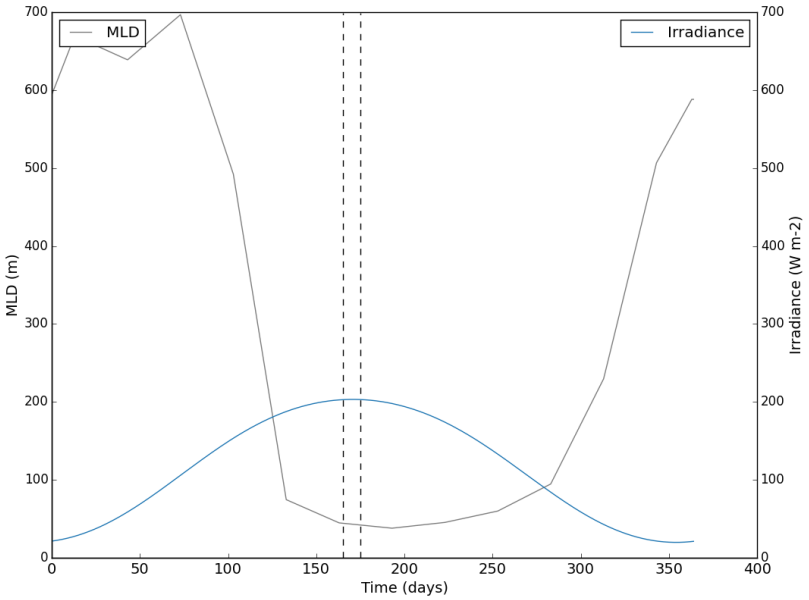

Figure 50: The section of the seasonal cycle used in the plots below (between dotted lines)

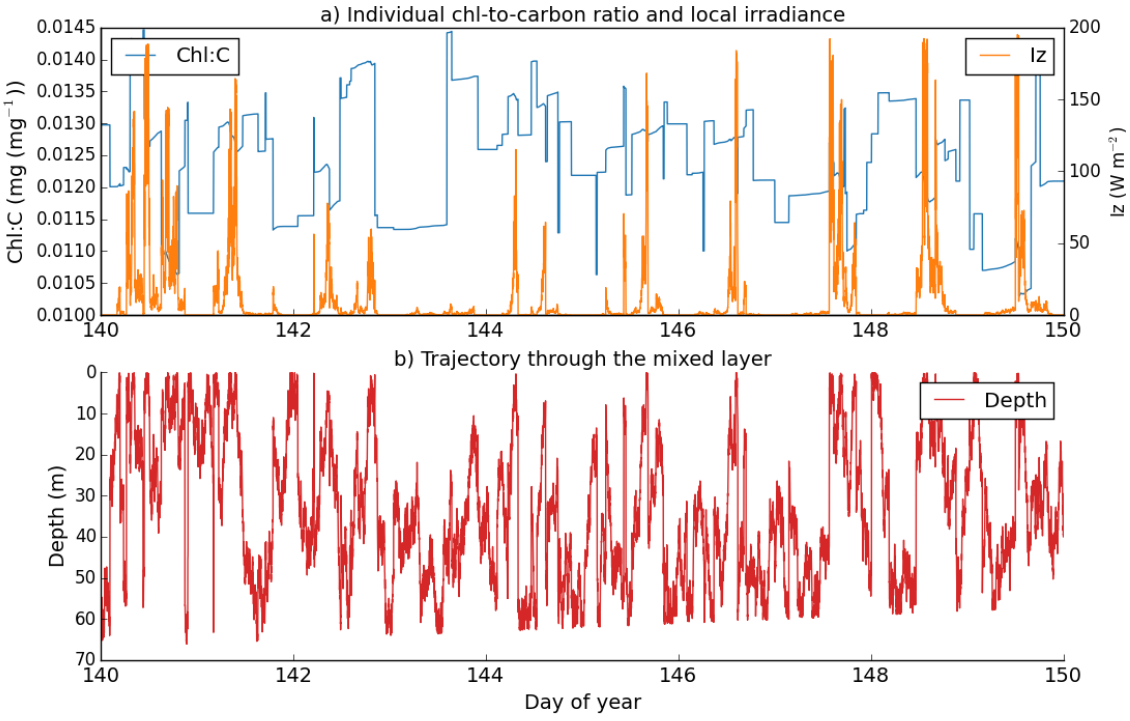

Figure 51: Following the trajectory of irradiance and depth experienced by a single SI, and its resulting chl-to-carbon ratio, for a randomly chosen SI in a simulation set at OWSI over days 140 to 150

Figure 51 shows that the phytoplankton SI is acclimating to changes in irradiance. The chl-to-carbon ratio increases during days where the SI experiences low irradiance, decreases after days where it has been closer to surface, experiencing high irradiance, and shows no change during the night, when there is no irradiance. The rate of change of chl:carbon is a function of the growth rate, so at night, when there is no irradiance, there is no photosynthesis, so therefore, no change to the chl-to-carbon ratio. This can be seen in Figure 51 as the horizontal sections of the red line representing the chl-to-carbon ratio.

It appears, then, that the phytoplankton are acclimating to their ambient irradiance, and, consequently, display a wide range of photoacclimative properties, but that the average of these properties does not differ greatly from the predicted average chl-to-carbon ratio in the Eulerian model. Performing a full sensitivity analysis can help to understand the rate at which phytoplankton acclimate, what affects this rate, and how changes to the rate of photoacclimation affect the ecosystem as a whole. However, analysing the full model has several complications: firstly, the loss of super-individuals through detrainment when the mixed layer shallows can make tracking an individual SI difficult, secondly, understanding the sensitivity of the model to factors such as irradiance and mixed layer depth is complicated when using a seasonal cycle of forcing, and finally, the constant fluctuations of mixed layer depth and irradiance mean that it is not possible to achieve steady-state values which can then be compared to predicted steady-state values. For this reason, the analysis was first performed on a fixed-slab version of the model, using a constant mixed layer depth and surface PAR, in order to get a clear picture of how each component reacts, before performing the same analysis on the full model.

3.4 Sensitivity analysis of the fixed-slab model

This section demonstrates how external forcing, such as the mixed layer depth, the surface irradiance and its attenuation through the mixed layer, and the mixing rates affect the model predictions of phytoplankton pigment and biomass. This is achieved by running the fixed slab model to steady state, under a range of different scenarios. The use of a Lagrangian model allows

investigation of, not only the integrated pigment and biomass, but also their vertical profiles, and super-individual chl-to-carbon ratios.

3.4.1 Steady-state averaged biomass, production, and chl-to-carbon ratios

The first scenario investigated the response of the model predictions of average chlorophyll biomass and chl-to-carbon ratios to changes in the mixing rate. This involved running a fixed slab model to steady state using a range of values for the turbulent diffusivity. The rate of mixing only affects the movement of the phytoplankton through the mixed layer – everything else (i.e. nutrients, zooplankton and detritus) is assumed to be fully mixed at all times. The phytoplankton move via a random walk that is parameterised based on the vertical diffusivity coefficient, K_{turb}, which is proportional to both the depth of the mixed layer, and the strength of the surface wind speed. The mixed layer was assumed to be constant for these simulations (100 m), so changes to the mixing rate represent differing surface wind speeds. A range of different speeds, from 0.01 m s^{-1} up to 100 m s^{-1} (to put these wind speeds in context – the surface wind speed averages for OWSI range from ~ 7 m s^{-1} to ~ 11 m s^{-1}), was investigated. Super-individual division was included in all of the model runs, and the temperature (in order to determine the maximum rate of photosynthesis, V_{PT}, was set to 10˚C (V_{PT} = 3.79 g C (g Chl^{-1}) h^{-1}). The surface irradiance was assumed to be constant throughout the simulation – i.e. no diel or seasonal cycle – and was set to 200 W m^{-2}. An Eulerian fixed-slab model was also run using the same conditions, for comparison.

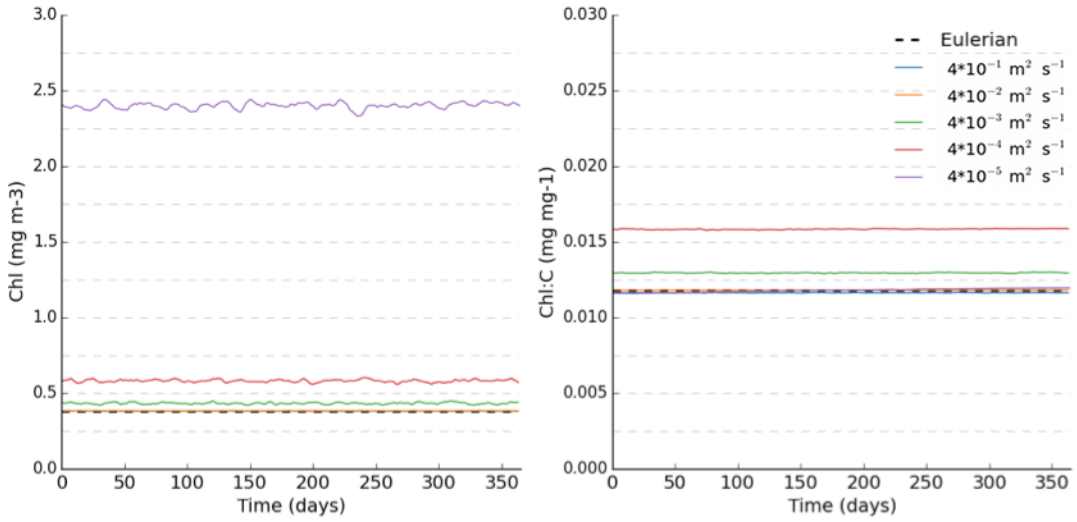

Figure 52: Steady-state predictions of a) chlorophyll and b) Chl:Carbon for the Eulerian and Lagrangian versions of a fixed-slab model, under different mixing regimes. The mixing rates were based on wind speeds of 100 m s^{-1}, 10 m s^{-1}, 1 m s^{-1}, 0.1 m s^{-1}, and 0.01 m s^{-1}, which resulted in turbulent diffusivity coefficients of $4•10^{-1}$, $4•10^{-2}$, $4•10^{-3}$, $4•10^{-4}$, and $4•10^{-5}$ m^2 s^{-1} respectively. Light attenuation is based on Anderson (1993).

Each simulation was run for a year, after reaching equilibrium, and Figure 52 shows this final year of data. The first observation is that decreasing the mixing rate increases the predicted integrated chlorophyll biomass. This does not appear to be a result of the chl-to-carbon ratios, because, as shown in Figure 52b, the slowest rate of mixing has the highest predicted chlorophyll biomass, but the predicted average chl-to-carbon ratio does not differ from that predicted by the Eulerian model. The increase in chlorophyll biomass is a result of the vertical profile of phytoplankton that develops in the mixed layer, when the rate of mixing is decreased. Slower moving super-individuals have more time to grow in areas of high irradiance, and, conversely, more time to decline in areas of low irradiance, resulting in the profiles of biomass and pigment-to-biomass ratios shown in Figure 53.

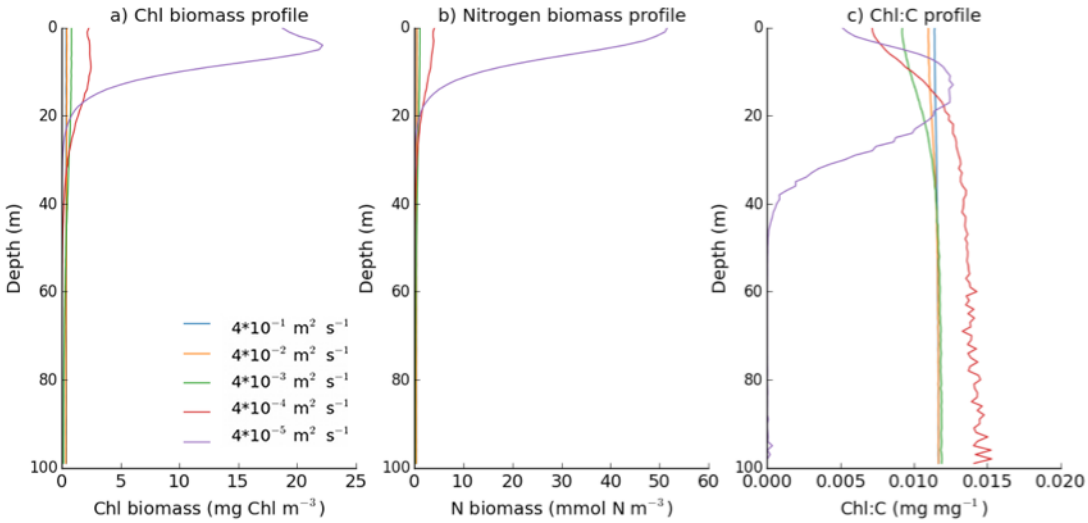

Figure 53: Vertical profiles of a) Chl biomass, b) Nitrogen biomass and c) Chl:C for the mixing regimes show in Figure 52

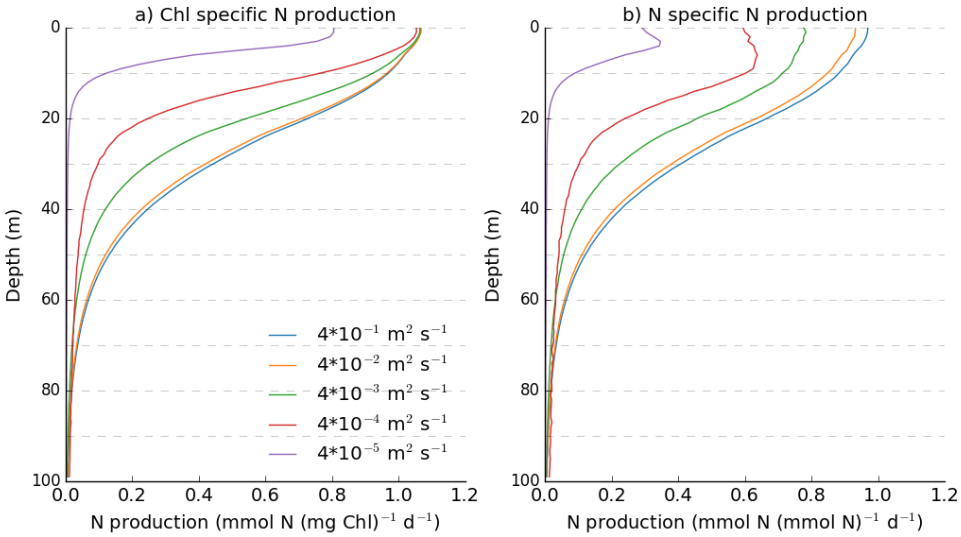

Figure 54: Vertical profiles of a) Chl-specific N production and b) N-specific N production for the mixing regimes shown in Figure 52

The vertical profile of chl-to-carbon shown in Figure 53c shows several important features:

1. The phytoplankton in the simulations with higher mixing rates show no variation of chl:carbon with depth. This is because these well-mixed phytoplankton never have time to acclimate to the irradiance at any one depth, and therefore every individual acclimates to the average irradiance in the water column (technically the average irradiance in the euphotic zone – see section 3.4.2).

2. Decreasing the mixing rate decreases the chl-to-carbon ratio near the surface. A decrease in the mixing rate increases the length of time the phytoplankton near the surface have to acclimate to the higher irradiance. At the same time, the phytoplankton lower down in the water column have more time to acclimate to the lower irradiance, resulting in the increase in chl-to-carbon ratio observed (apart from when the mixing rate is decreased to a wind speed of 0.01m s^{-1} – see below)
3. Below ~40m, all simulations show little variation in chl-to-carbon ratios with depth. Changes to the chl-to-carbon ratio are a function of the growth rate, so once most of the irradiance has been attenuated, the chl-to-carbon ratio remains constant, because respiration affects both chlorophyll and carbon stores at the same rate, so has no effect on their ratio
4. Simulations with decreased mixing rates initially show an increased chl-to-carbon ratio in the lower portion of the mixed layer, until the mixing rate is decreased to the lowest value investigated (based on a wind speed of 0.01 m s^{-1}), at which point chl:carbon in the lower portion of the mixed layer falls to a value closer to that predicted by the models with the high mixing rates.

This final point initially seems counterintuitive: decreasing the mixing rates increases the surface phytoplankton biomass, which should result in less irradiance reaching those deeper in the water column, where the chl-to-carbon ratios would be expected to increase. However, chlorophyll production is scaled relative to nitrogen production using the equation:

$$R_{chl,SI} = \theta^{chl}_{\max} \cdot \frac{\mu_{P,SI}}{\alpha_{P,SI} \cdot I_{SI,z} \cdot \theta_{chl,SI}} \qquad (3.5)$$

This represents the balance between the rate of production, $\mu_{P,SI}$, and the instantaneous light harvesting capacity of the phytoplankton, $\alpha_{P,SI} \cdot I_{SI,z} \cdot \theta_{chl,SI}$. If the achieved rate of photosynthesis is less than the current potential maximum, then $R_{chl,SI}$ decreases, reducing the rate of chlorophyll production in relation to nitrogen production, and therefore there is a decrease in the chl-to-carbon ratio. Therefore, increasing a variable in the denominator of the fraction (i.e. irradiance), will decrease the calculated $R_{chl,SI}$, and decrease the

ratio of chl-to-carbon. However, the phytoplankton production, $\mu_{P,SI}$, is also a function of the average concentration of nutrient (DIN) in the mixed layer. An increase in the steady-state prediction of phytoplankton biomass results in a decrease in the steady-state concentration of DIN, which reduces the achieved rate of production. The steady state values for DIN for the simulations in Figure 52:Figure 54 are shown in Figure 55. The maximum potential rate of photosynthesis shown in eq. (3.5) is based on no nutrient limitation, so a simulation with a lower concentration of DIN will have a lower achieved-to-maximum rate of photosynthesis, which will result in a lower value for $R_{chl,SI}$ and a decreased rate of chlorophyll production in relation to nitrogen production, which will lower the overall chl-to-carbon ratio.

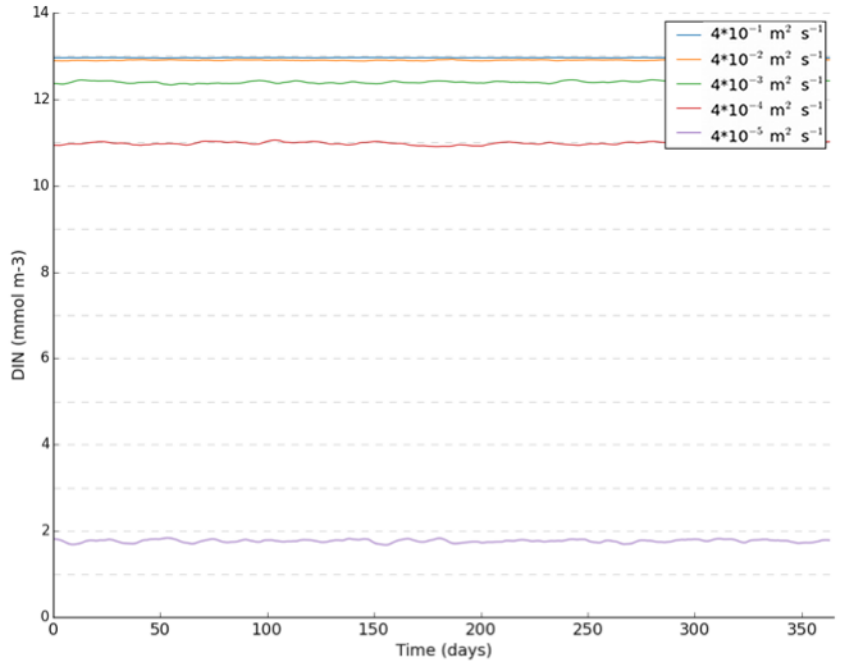

Figure 55: Steady-state DIN concentrations for the simulations shown in Figure 52:Figure 54

Although the above plots give some idea as to the steady-state predictions of both the integrated and vertical profile of chl-to-carbon ratios, there is still not enough information about the rates of acclimation, and whether they reach the predicted, optimal steady-state chl-to-carbon values. As previously mentioned, one advantage of using an existing Eulerian model for this study, is that it allows for mathematical analysis of the model. It is possible to solve the growth equations for the condition of balanced growth in order to produce a

predicted relationship between irradiance and chl:carbon (steady-state solution provided by Prof. T. Anderson):

$$\theta_{chl} = \frac{V_P \cdot \theta_{\max}^{chl}}{\left(V_p^{\,2} + \alpha_P^{\,2} \cdot I^2\right)^{0.5}} \tag{3.6}$$

This gives a predicted steady state value for θ_{chl}, for any value of I, which can be compared to the predictions of θ_{chl} for super-individuals, under different mixing regimes. If the phytoplankton were responding as expected, then running a simulation with no mixing (stationary phytoplankton) should result in the phytoplankton acclimating to the values predicted by eq. (3.6), which would provide a good test that the model was behaving as it should. However, in order to do this, I had to modify the model in several ways:

1. Removal of nitrogen dependence. The steady-state chl-to-carbon equation (3.6) uses the maximum rate of photosynthesis, V_{PT}, so in order to be able to compare the model predicted values with the optimal values, there has to be no nutrient limitation
2. Change to the attenuation model. The Anderson (1993) attenuation model splits the water column into three regions (0m to 5m, 6m to 23m, and <23m), and calculates the attenuation coefficient for each region, based on the chlorophyll concentration. However, these coefficients are calculated using polynomial expressions, which, in Anderson (1993) are tested using chlorophyll concentrations up to 16 mg m^{-3}. Running a fixed-slab model with stationary phytoplankton (i.e. no mixing) results in unrealistically high levels of chlorophyll concentrations (>50 mg m-3), which are outside the useable limits of these polynomials. Therefore, the coefficients were assumed to be constant above a concentration of 16 mg m^{-3} (i.e. if the chlorophyll concentration at a particular depth exceeded 16 mg m^{-3}, the coefficient was calculated using a value of 16 mg chl m^{-3}).

   In addition, some of the experiments involve changing the turbidity of the water in a quantifiable manner, and for that a simpler light attenuation model (as in Evans et al. (1985)) was implemented:

$$k_{par} = k_w + k_c \cdot P_{conc} \tag{3.7}$$

where k_{par} represents the light extinction coefficient, k_w the background turbidity, and k_c the attenuation due to phytoplankton (self-shading). This calculates attenuation based on the average concentration, rather than the concentration at each depth in the mixed layer, and the effect of this light attenuation model on the entire ecosystem is fully explored in section 3.6.1.

3. Changes to the mortality. As described in the Chapter 2, phytoplankton losses through grazing and the non-linear mortality rate are calculated using the average biomass (mmol N m^{-3}) in the mixed layer, rather than the biomass contained within each super-individual. As the biomass contained in one individual increases, the average phytoplankton biomass in the water column increases, which, in turn, increases the loss rate. At the same time, the smaller individuals are effectively reducing the loss rate in relation to the larger individuals, meaning that there is less grazing pressure on larger super-individuals. This creates a positive feedback effect, ensuring that the largest individuals keep increasing in size, whilst the smallest keep decreasing, until all of the phytoplankton biomass is effectively contained in one super-individual. Allowing the super-individuals to divide into 2 super-individuals, each contained half the biomass of the original, alleviates this problem in the full model, however, this does not work with a model with no mixing. If there is no phytoplankton movement, then each 1-metre layer is analogous to one super-individual, as the biomass contained within the layer is the same, regardless of how many super-individuals it is divided between. Therefore, the mortality was applied to each individual, using a simple quadratic equation:

$$M_{SI} = m_P P_{SI}^{\ 2} \tag{3.8}$$

where m_P = 0.3 d^{-1}, which was a value chosen in order to allow the simulations to reach steady-state, without resulting in excessive levels of chlorophyll and nitrogen biomass.

3.4.2 Relationship between the mixing rate and individual chl-to-carbon ratios: random walk movement rules

In order to attain a picture of how well acclimated the super-individuals were to their local irradiance at any one point during the simulation, I plotted the chl-to-carbon ratios of super-individuals against the irradiance at their current depth, and compared these points to the steady-state predictions obtained using eq. (3.6). As explained previously, the model used was a simplified version of the fixed-slab model, with no dependence of photosynthetic rate on DIN concentration, and with the non-linear mortality calculated for each super-individual, based on its biomass. A simple quadratic equation (eq. (3.8)) was used for mortality (M_{SI}), and both linear mortality and grazing were neglected.

The first set of simulations focussed on the relationship between the rates of mixing and photoacclimation. A range of mixing rates was investigated, based on wind speeds of 100m s^{-1}, 10m s^{-1}, 1m s^{-1}, 0.1m s^{-1}, 0.01m s^{-1}, and 0 m s^{-1} (i.e. no mixing), which correspond to diffusivities of K_{turb} = $4•10^{-1}$, $4•10^{-2}$, $4•10^{-3}$, $4•10^{-4}$, $4•10^{-5}$ and 0 m^2 s^{-1}, respectively. For comparison, the study by McGillicuddy (1995) used mixing rates based on turbulent diffusivities of 0.01 m^2 s^{-1} and 4.64m^2 s^{-1}, and Lande et al. (1989) investigated a single value of 0.01 m^2 s^{-1} . Increasing the diffusivity coefficient beyond $4•10^{-1}$ m^2 s^{-1} did not result in any further changes to the steady-state predictions, as the rate of mixing was high enough to ensure that the phytoplankton were evenly distributed at all times.

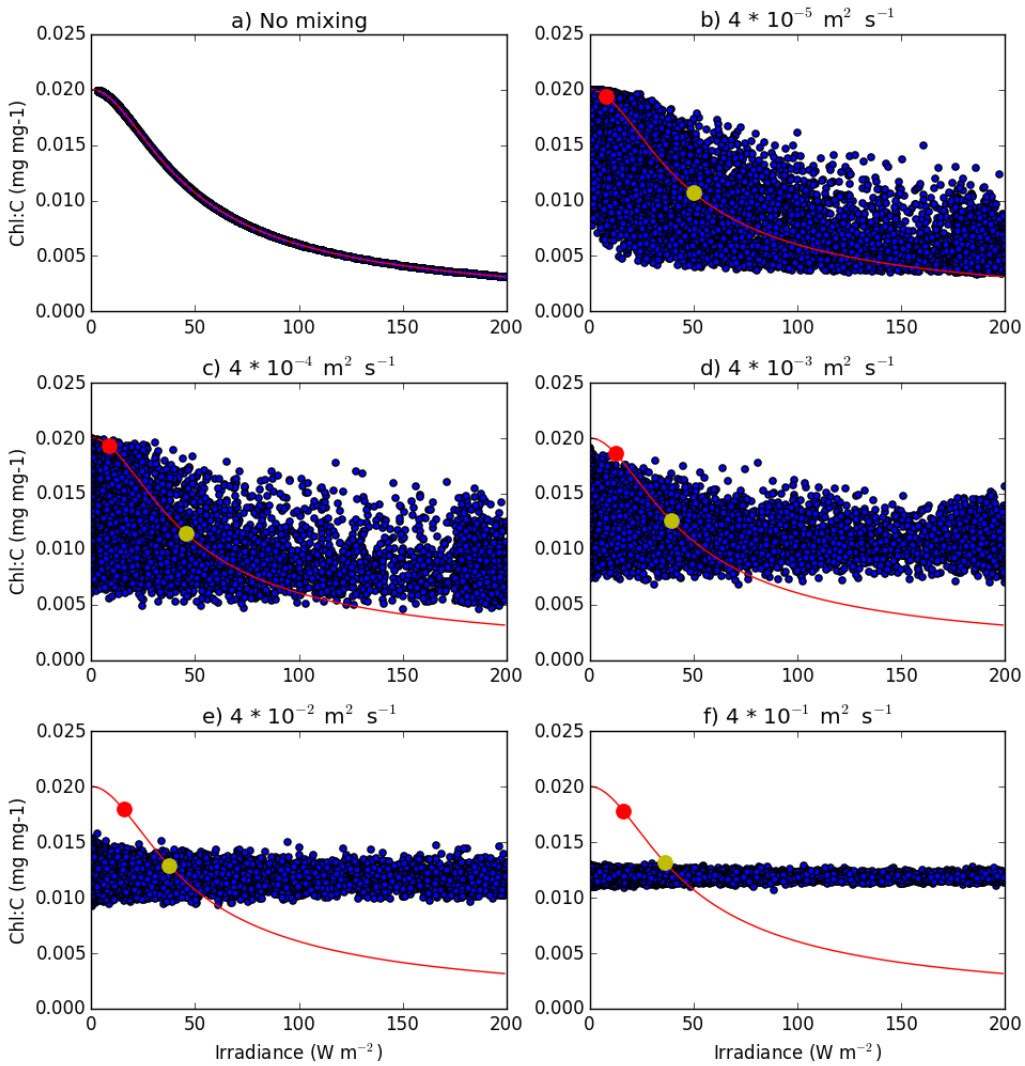

Figure 56: The relationship between irradiance and Chl:C for 100 super-individuals using a range of mixing rates. The red line shows the predicted steady state value, using equation (3.6), the red dot shows the predicted Chl:C based on the average irradiance in the water column, and the yellow dot shows the predicted Chl:C based on the average irradiance in the euphotic zone (surface to 1% of surface irradiance).

Figure 56 shows how far the chl-to-carbon ratio of each super-individual is from the predicted steady-state value for its current irradiance. Each blue circle represents the chl-to-carbon ratio and current irradiance of a single SI. The red line represents the predicted, steady-state relationship between chl:carbon and irradiance, using equation (3.6). If an individual SI is currently fully acclimated to its irradiance, then it will fall on the red line. If the model is responding in a predictable fashion, then removing the mixing should result in all phytoplankton achieving the predicted steady-state values of chl:carbon, which can indeed be seen in Figure 56a).

Several important observations and questions highlighted by Figure 56 are:

1. There appears to be little acclimation to the local irradiance until the wind speed falls to 0.1 m s^{-1} (K_{turb} = 4•10^{-4} m^2 s^{-1})
2. For diffusivities of 4•10^{-3} m^2 s^{-1} and above, the range of chl-to-carbon ratios decreases with increasing mixing rates
3. The phytoplankton in scenarios with wind speeds of 1 m s^{-1} (K_{turb} = 4e^{-3} m^2 s^{-1}) and above, show no correlation between chl-to-carbon ratio and irradiance, although they exhibit a wide range of values for Chl:C.

- There are two values of Chl:C also shown in the plots: the red circle, which corresponds to the predicted steady-state chl-to-carbon ratio for the average irradiance in the mixed layer, and the yellow dot, which shows the predicted steady-state chl-to-carbon ratio for the average irradiance in the euphotic zone (taken as stretching from the surface to the depth at which the irradiance falls to 1% of the surface value). The average acclimation appears to be closer to the value suggested by the irradiance in the euphotic zone. This is because changes to the ratio of chl-to-carbon depend upon phytoplankton growth – chlorophyll production is increased or decreased relative to nitrogen production. If there is no irradiance, then there will be no production, and the ratios will be unaffected. Therefore, when the phytoplankton are in complete darkness, then their chl-to-carbon ratios will remain fixed at the same value, until they move back into the light.

Although these plots show the relationship between the instantaneous rates of acclimation, they don't provide information about how the previous history of irradiance has impacted on the current chl-to-carbon ratios. This can be illustrated by plotting the trajectory of irradiance exposure against the chl-to-carbon ratio of a random super-individual, and then comparing this to the optimal chl-to-carbon ratio for each plotted irradiance point, as predicted by equation (3.6).

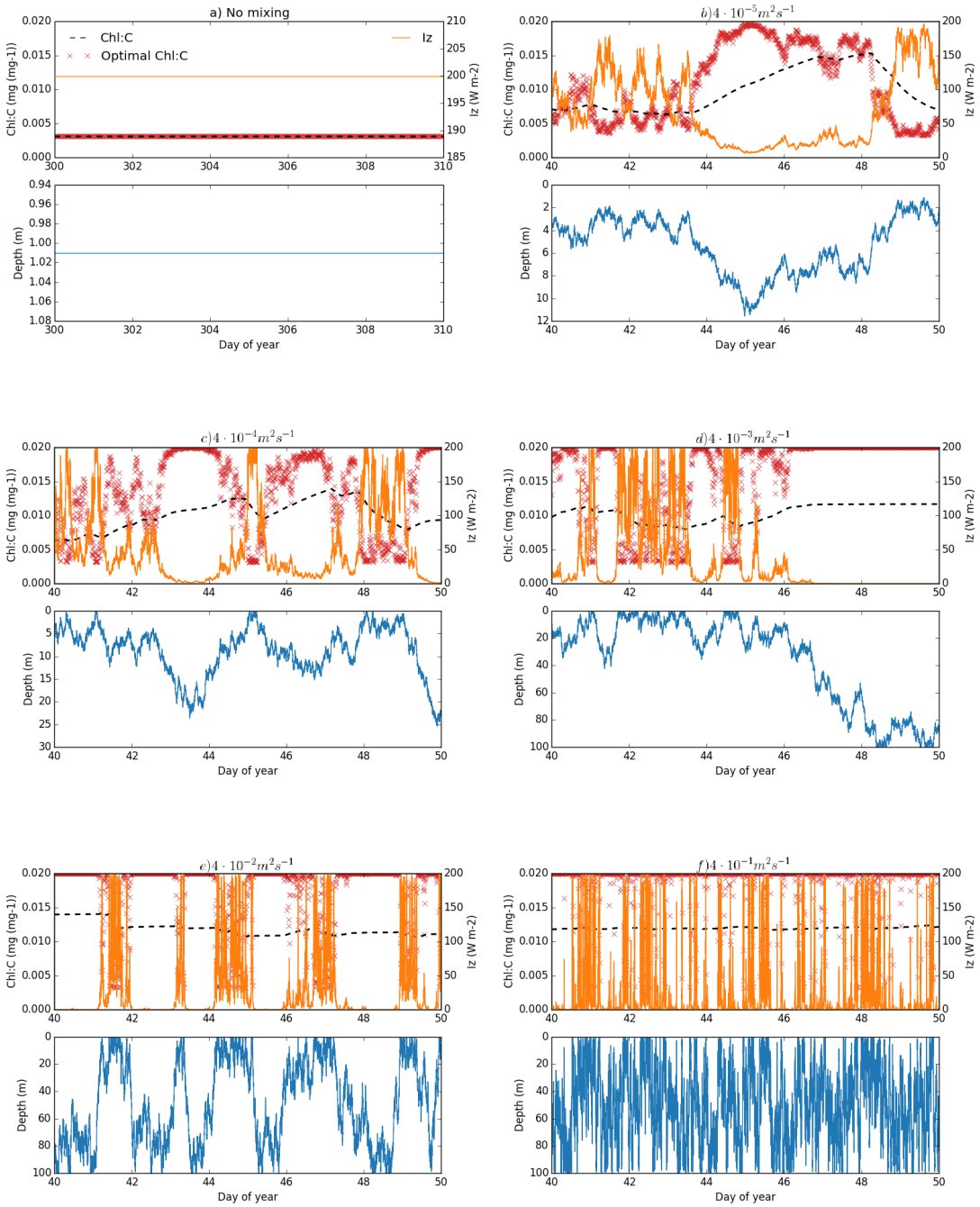

Figure 57: The trajectories of irradiance and depth followed by a single super-individual over the course of 10 days, along with the resulting chl-to-carbon ratios. Also shown are the predicted, steady-state chl-to-carbon values for each irradiance experienced by the super-individual.

Figure 57 illustrates more clearly what is happening in Figure 56. As the rate of mixing decreases, the changes in irradiance decrease, and the phytoplankton have time to acclimate to their local light field. The timescales of acclimation seem to be on the order of days, rather than hours, for example, in Figure 57d,

the predicted steady state chl-to-carbon ratio is never reached, even when the irradiance has changed very little over a number of days. However, the phytoplankton do appear to be acclimating towards the steady-state chl-to-carbon ratios, which would explain the range of chl-to-carbon values shown in Figure 56. The time necessary for the phytoplankton to fully acclimate to their irradiance can be seen in Figure 58, which shows the specific change in chl-to-carbon ($\theta_{Chl,sp}$) ratio each time step (30 minutes), for a single super-individual at different constant irradiances, assuming no nutrient dependence. This is calculated for each individual, by dividing the absolute change in chl-to-carbon ratio, by the chl-to-carbon ratio at the beginning of the time step. This is then averaged out over the entire population.

Full acclimation takes on the order of 8-10 days, although most of the acclimation is complete in 5 days.

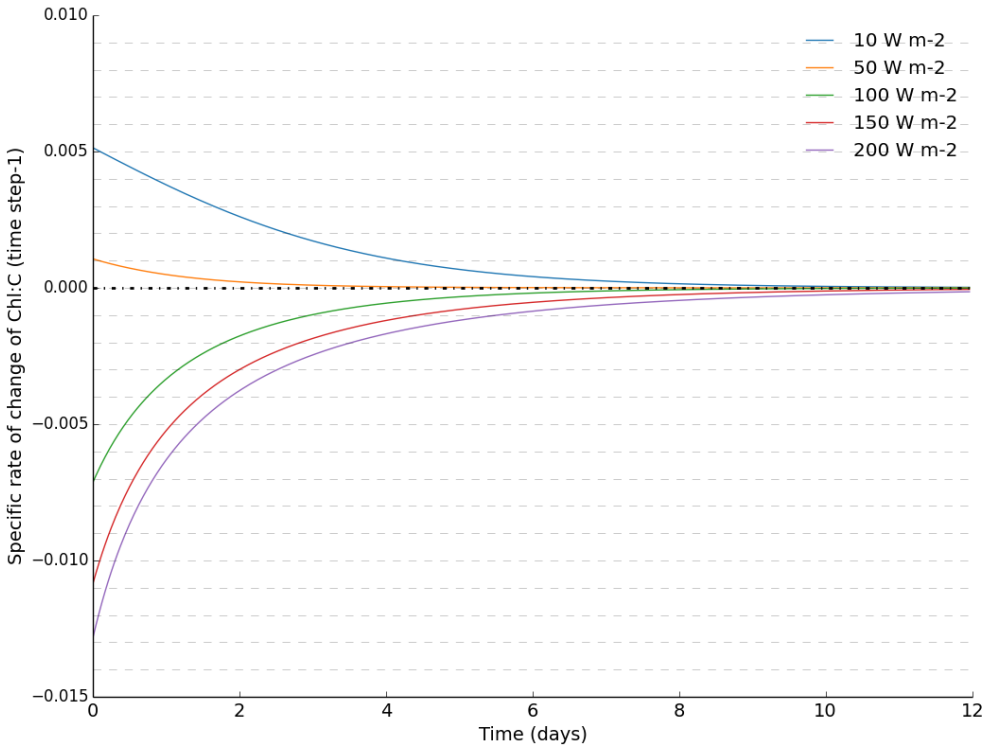

Figure 58: Specific rate of change of chl-to-carbon, $\theta_{Chl,sp}$, under different irradiances, assuming no nutrient limitation for a super-individual with an initial θ_{Chl} = 0.01 mgChl (mg C)$^{-1}$

3.4.3 Relationship between the mixing rate and individual chl-to-carbon ratios: random position movement algorithm

Next, the rates of acclimation in a simulation using the random position movement algorithm were investigated. As stated in Chapter 2, the mixing rate in the random position model of movement is a function of the time step, as that is the implied time taken for a super-individual to move from the surface to the base of the mixed layer. There were four different time steps investigated: 1 min, 30 minutes, 300 minutes, and 1000 minutes. Using the method to estimate the diffusivity described in Chapter 2 gives values of K_{turb} = 20.8m^2 s^{-1}, 0.7m^2 s^{-1}, 0.07m^2 s^{-1}, and 0.02m^2 s^{-1}, respectively. Decreasing the mixing rate should result in the chl-to-carbon ratios falling closer to the theoretical values calculated by equation (3.6).

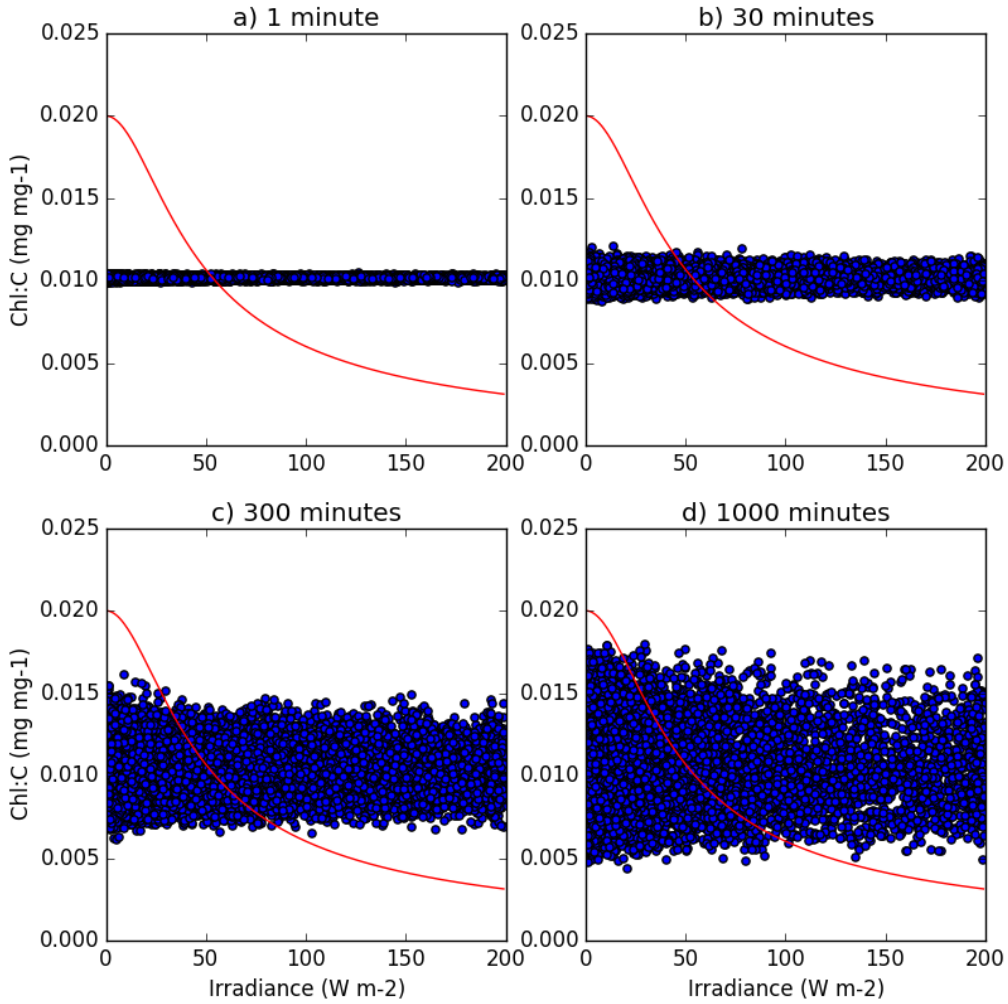

Figure 59: The relationship between irradiance and Chl:C for 100 super-individuals using the randomisation movement, with differing time steps. The red line shows the predicted steady state value, using equation (3.6). Time steps correspond to estimated diffusivities of a) 20.8m^2 s^{-1}, b) 0.7m^2 s^{-1}, c) 0.07m^2 s^{-1}, and d) 0.02m^2 s^{-1}.

The results shown in Figure 59 are inconclusive. Increasing the time step (and therefore decreasing the rate of mixing) does not result in any visible individual acclimation (i.e. the blue circles do not fall on the red line). However, the minimum estimated mixing rate – for the time step of 1000 minutes – was 0.02m^2 s^{-1}, which would not be low enough to cause significant acclimation in the random walk model, where visible acclimation was not seen until the mixing rates fell to < $4 \bullet 10^{-3}$ m^2 s^{-1}. Unfortunately, increasing the model time step beyond 1000 minutes moved the model outside of its workable boundaries. Therefore, in order to investigate estimated rates of mixing that

are comparable to those used with the random walk movement algorithm in Figure 56, the simulation was run again, but for a shallower mixed layer of 10m. Using a shallower mixed layer depth meant that the phytoplankton were assumed to be moving a shorter distance each time step, so that the calculated diffusivities for each time step length were lower. In order to make sure that the phytoplankton were exposed to a wide range of irradiances within such a shallow depth, the Evans and Parslow model of light attenuation was used, with the background attenuation coefficient, k_w, increased from the standard value of 0.04m^{-1}, to 0.4m^{-1}.

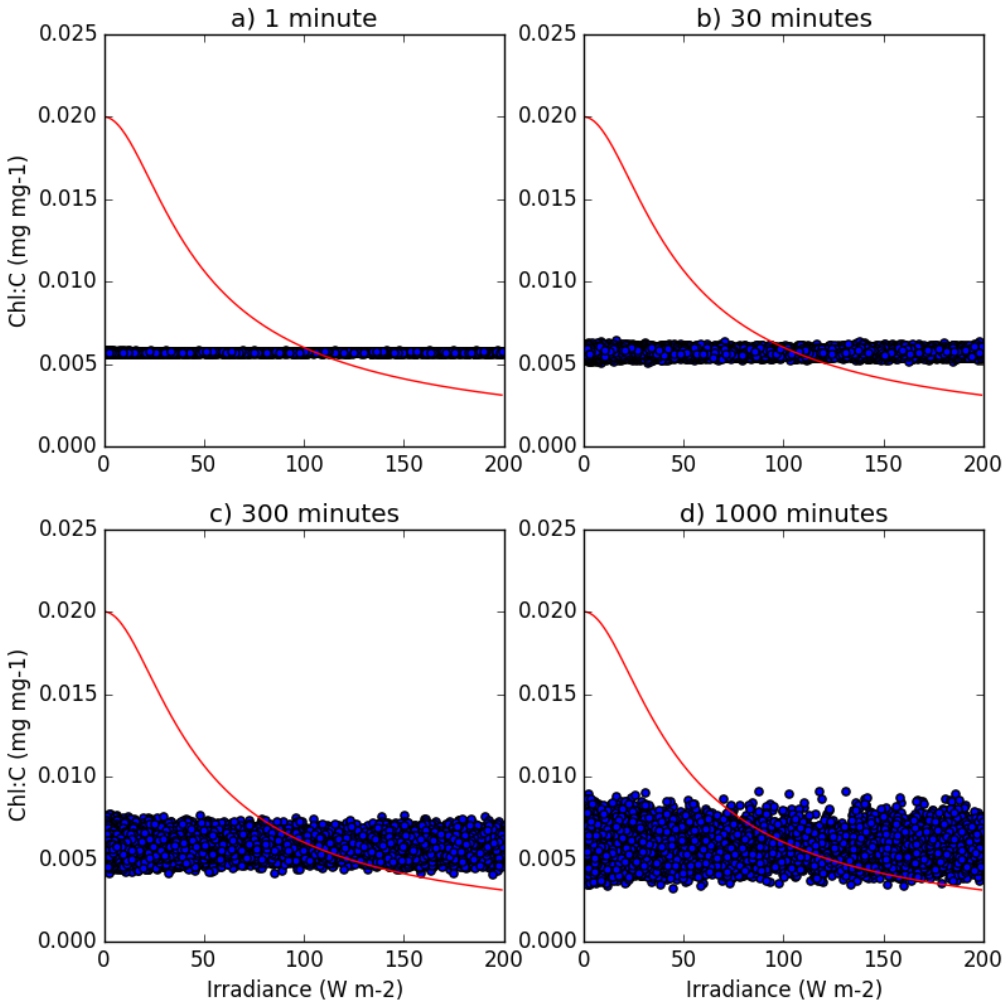

Figure 60: The relationship between irradiance at Chl:C for 100 individuals in a simulation using the random position movement algorithm, for a mixed layer depth of 100m, a surface PAR of 200 W m^{-2}, and a background attenuation coefficient, k_w = 0.4 m^{-1}. Four different time

steps are investigated: 1 min, 30 mins, 300 mins and 1000 mins, which correspond to estimated diffusivities of $2 \bullet 10^{-1} m^2 s^{-1}$, $7 \bullet 10^{-3} m^2 s^{-1}$, $7 \bullet 10^{-4} m^2 s^{-1}$, and $2 \bullet 10^{-4} m^2 s^{-1}$, respectively.

Decreasing the mixing rate results in a small increase in the range of chl-to-carbon ratios, but not to the same extent as in the simulation using the random walk model. This is because there is no correlation between each step taken by the phytoplankton. For this reason, the mixing rate estimated for the random position model, from the depth of the mixed layer and the time step, is not comparable to the mixing rates of the random walk model.

3.4.4 Relationship between the mixed layer depth and the individual chl-to-carbon ratios

The next set of simulations was designed to see whether there is a relationship between the depth of the mixed layer and the chl-to-carbon ratios of the super-individuals. Again, the super-individuals were simulated in the simple fixed slab model, although this time, using a range of different mixed layer depths, and a constant mixing rate, based on a wind speed of 10 m s^{-1}. Changing the depth of the mixed layer also results in a change to the turbulent diffusivity, as described in Chapter 2.

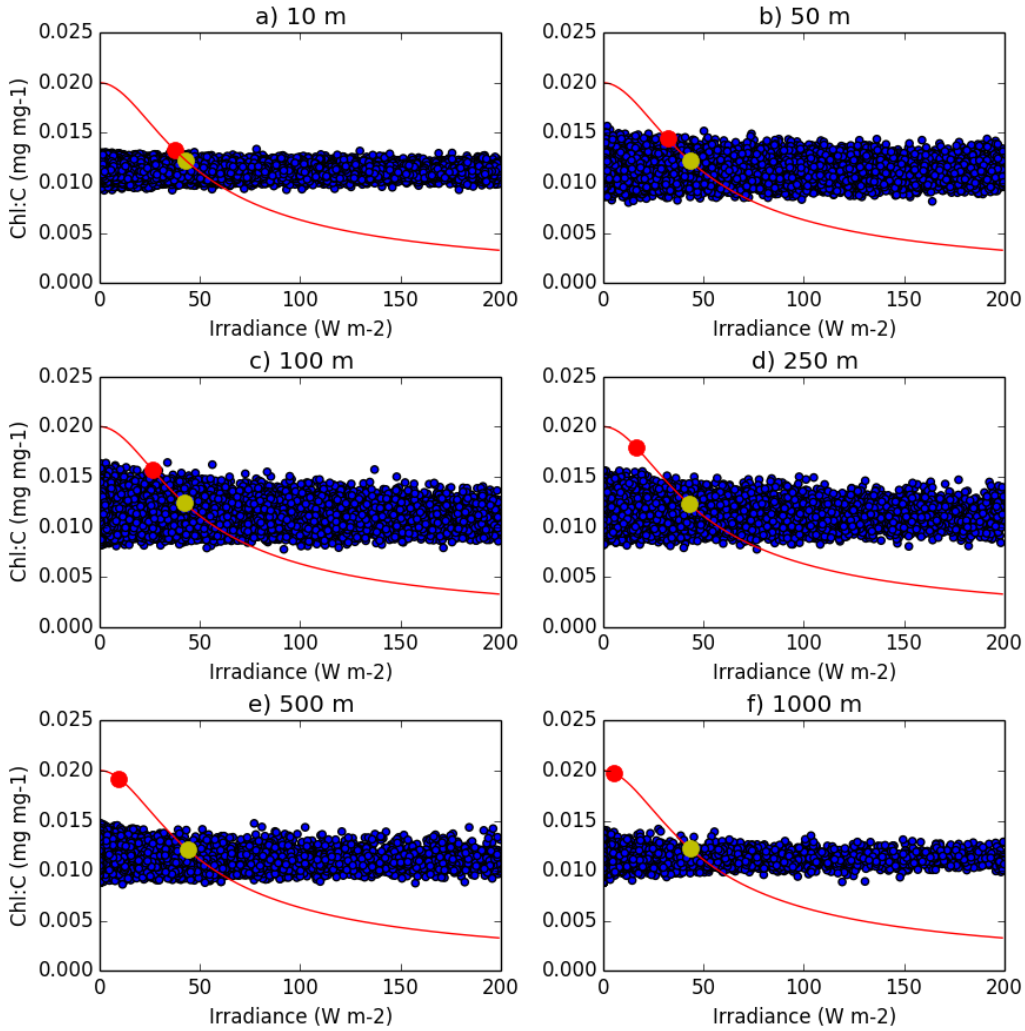

Figure 61: The relationship between irradiance and Chl:C for 100 super-individuals using the random walk movement, with differing mixed layer depths. The red line shows the predicted steady state value, using equation (3.6), the red dot shows the predicted Chl:C based on the average irradiance in the water column, and the yellow dot shows the predicted Chl:C based on the average irradiance in the euphotic zone (surface to 1% of surface irradiance).

The diffusivities used in Figure 61 are based on the standard settings: a surface wind speed of 10 m s^{-1} and the depth of the mixed layer. Mixed layer depths of 10m, 50m, 100m, 250m, 500m, and 1000m correspond to diffusivities of $4 \cdot 10^{-3}$ m^2 s^{-1}, $2 \cdot 10^{-2}$ m^2 s^{-1}, $4 \cdot 10^{-2}$ m^2 s^{-1}, $2 \cdot 10^{-1}$ m^2 s^{-1}, $2 \cdot 10^{-1}$ m^2 s^{-1}, and $4 \cdot 10^{-1}$ m^2 s^{-1}, respectively. The range of values of Chl:C observed in the phytoplankton super-individuals is low when the mixed layer is 10m deep, but then increases until the mixed layer is 100m deep. Once the mixed layer deepens beyond 250m, this range decreases again. This is to do with the irradiance conditions experienced by the phytoplankton in each mixed layer.

When the mixed layer is only 10m deep, the range of irradiances experienced by the phytoplankton is low, because the light is only attenuated over 10 m. The maximum range of irradiances experienced by the phytoplankton will be achieved once the mixed layer depth has deepened to include the entire euphotic zone. However, deepening the mixed layer significantly beyond this depth means that the phytoplankton will spend the majority of their time in the dark. This means that, on average, they will spend less time in the euphotic zone, and will have less time to acclimate to the irradiance.

Figure 61 also clearly demonstrates the difference between the average irradiance in the euphotic zone, and the average irradiance in the entire mixed layer. Even though the average irradiance in the mixed layer is very low, and the predicted steady state chl-to-carbon ratio is very high (red circle), below the euphotic zone, the phytoplankton are not photosynthesizing, and are therefore also not producing chlorophyll, so there is no change to their chl-to-carbon ratios. The average values of chl-to-carbon ratios displayed by the phytoplankton is therefore dependent on the average irradiance in the euphotic zone (predicted steady-state chl-to-carbon shown by the yellow circle).

3.4.5 Relationship between the light attenuation and the individual chl-to-carbon ratios

The final simulations looked at how the rate at which irradiance is attenuated through the water column affects the chl-to-carbon ratios of the super-individuals. In order to increase the turbidity of the water in a quantifiable manner, the Evans and Parslow light attenuation model was used, with increasing levels of background turbidity. Three different values were investigated: k_w = 0.08m^{-1}, 0.16m^{-1}, and 0.32m^{-1}. The simulations were run in a 100m deep mixed layer, with a constant surface PAR of 200 W m^{-2}, and assuming nutrient replete conditions (i.e. no nutrient limitation term).

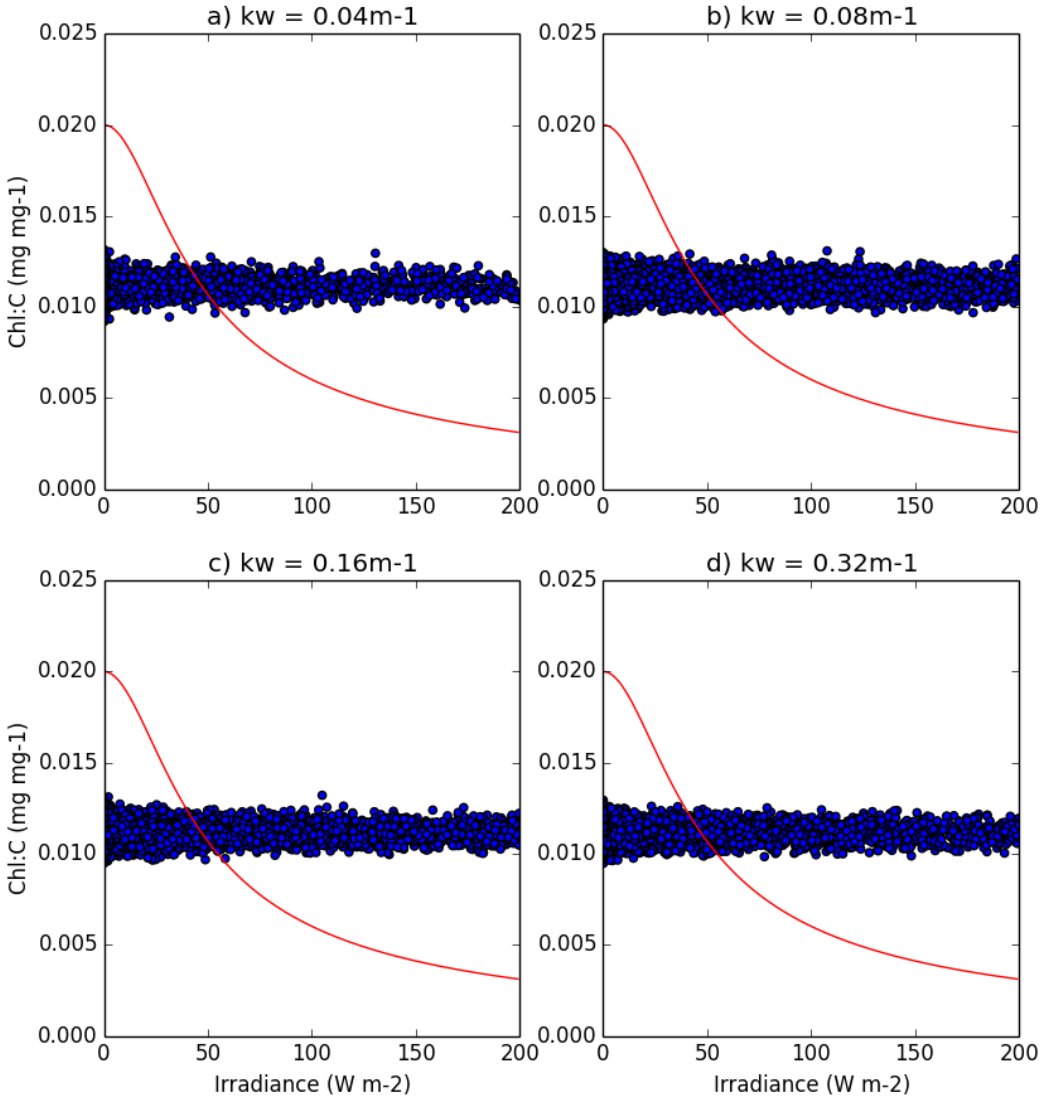

Figure 62: The relationship between irradiance and Chl:C for 100 super-individuals using the random position movement, for different levels of background attenuation, representing increasingly turbid conditions.

The range of chl-to-carbon ratios was not sensitive to the background attenuation. This is because changing the attenuation does not affect the range of irradiances experienced by the phytoplankton – 100 m is deeper than the euphotic zone for all cases, so each scenario involves a range of values from 200 W m^{-2} at the surface, to 0 at the base of the mixed layer.

3.4.6 Determining the timescale between photoacclimation and mixing.

The timescales for acclimation are shown to be on the order of 7-10 days Figure 58. However, this is the time taken for a phytoplankton to fully acclimate to a constant irradiance, a situation that is unlikely to occur in the

ocean, where the surface irradiance is constantly fluctuating. Therefore, the effect of the degree of correlation between steps on the time taken for acclimation was investigated, by simulating two extreme scenarios:

1. A simple trajectory with a strong correlation between each step. A single super-individual was exposed to an irradiance level that oscillated between 0 and 200 W m^{-2}. The irradiance increased by 1 W m^{-2}, until a value of 200 W m^{-2} was reached, at which point it started to decrease. The irradiance increased or decreased by 1 W m^{-2} every *n* time steps, using time steps of 1 minute. The value of *n* was then increased, until the chl-to-carbon ratios shown by the super-individual matched those predicted by the steady-state equation.

2. The second simulation was designed to represent a simulation using the random position movement algorithm, where each irradiance has no relationship with previous levels of irradiance. The irradiance experienced by the super-individual was updated using a randomly selected value between 0 and 200 W m^{-2} every *n* time steps.

The aim was to estimate the length of time necessary for an individual to acclimate to any changes in its irradiance field, for both a highly correlated trajectory and one with no correlation between steps (random position movement). Both movement rules were investigated, to show the rates of acclimation in models where the individuals move in small increments (i.e. random walk), so that the current chl-to-carbon ratio would be influenced by the history of irradiance, and also in models where the changes in irradiance were sudden and random (i.e. random position).

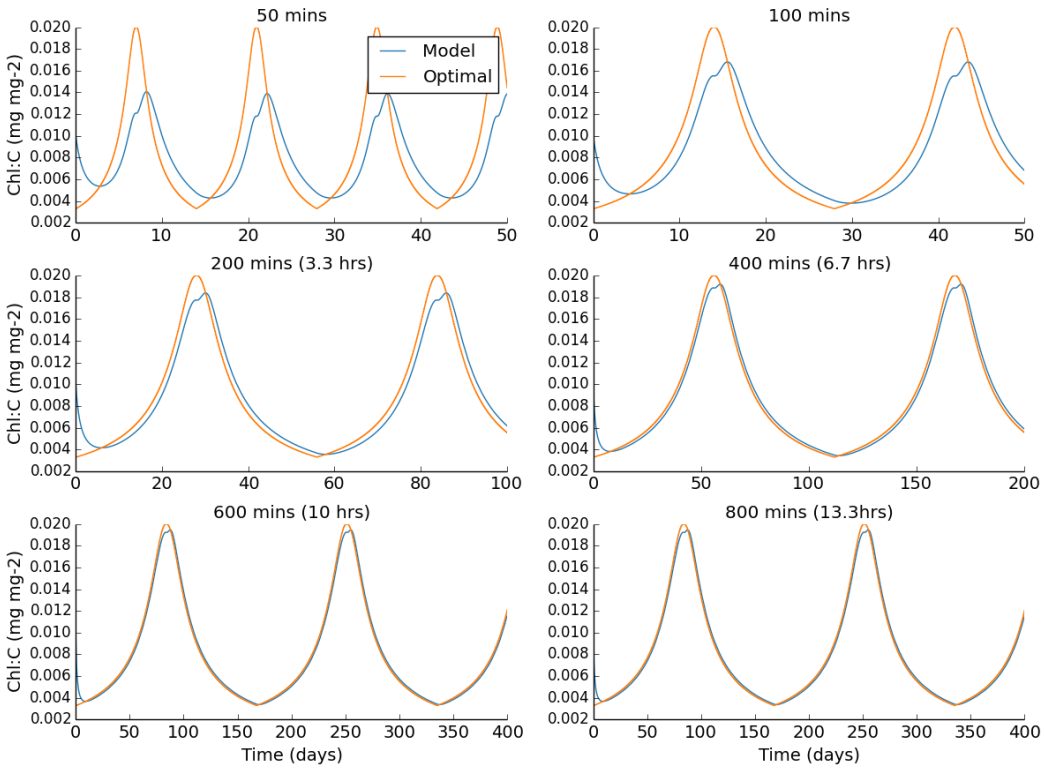

Figure 63: A single phytoplankton super-individual exposed to a series of irradiances, whilst oscillating between the surface and the base of the mixed layer. The irradiance starts at 200 W m-2, and is then decreased by 1 W m-2 every *n* time steps until 0 W m-2 is reached, at which point it is increased by 1 W m-2 every *n* time steps (*n* = 50, 100, 200, 400, 600, 800). The chl-to-carbon ratio predicted by the model (blue line) is then compared to the calculated steady-state chl-to-carbon ratio for each irradiance (orange line). MLD = 100m

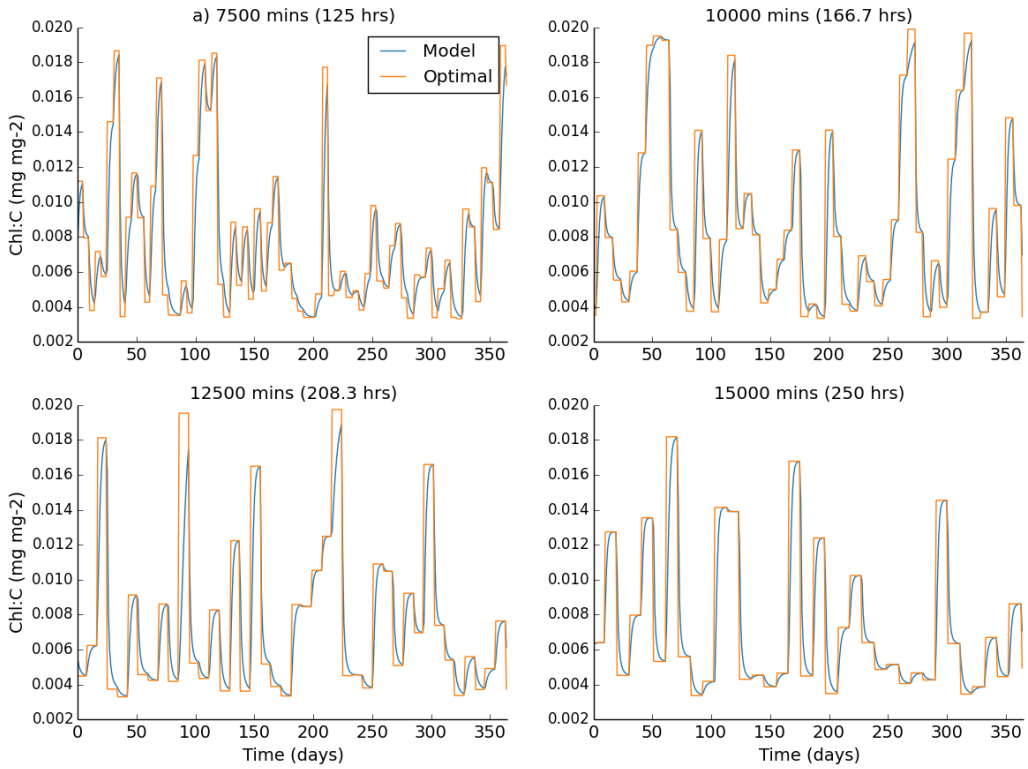

Figure 64: A single phytoplankton super-individual exposed to a series of irradiances, designed to represent a random position movement. The irradiance is updated every *n* time steps (*n* = 7500, 10000, 12500, 15000) to a random value between 0 and 200 W m-2. The chl-to-carbon ratio predicted by the model (blue line) is then compared to the calculated steady-state chl-to-carbon ratios for each irradiance (orange line). MLD = 100m, time step = 1 minute

Figure 63 and Figure 64 suggest that phytoplankton in a model using realistic rates of mixing, are unlikely to ever be fully acclimated to their irradiance. Even though the phytoplankton in Figure 63 are showing significant acclimation after only 50 minutes under each irradiance, their ambient irradiance is only changing a small amount (1 W m^{-2}) every 50 minutes, so little change is needed to acclimate to the new irradiance. At the other end of the scale, the phytoplankton using the random position model (Figure 64) require 250 hours (~10 days) to acclimate to every change in their ambient irradiance. Phytoplankton in the ocean are being constantly mixed through fluctuating irradiance levels, that depend not only on their depth in the ocean, but also on the annual and diel cycles of irradiance. It seems unlikely that there will be significant differences in phytoplankton photoacclimative properties resulting from differences in their irradiance histories. Photoacclimation is still important seasonally, but can be adequately captured through the use of an

Eulerian model. However, Figure 52 shows that steady state predictions from fixed slab Eulerian and Lagrangian models do diverge with wind speeds of less than 1 m s^{-1}, suggesting that there is a mechanism causing model divergence under lower mixing regimes. In the next section, I propose and provide evidence for an alternative hypothesis for the cause of differences between Eulerian and Lagrangian phytoplankton models, based on the vertical profile of phytoplankton biomass.

3.5 The relationship between growth and mixing rates: vertical phytoplankton profiles

The previous section has demonstrated that the rates of acclimation are slow – on the order of days, rather than hours – and, as a consequence, low rates of mixing are necessary to result in the phytoplankton developing a range of chl-to-carbon ratios. However, it is not clear whether differences in the range of chl-to-carbon ratios displayed by the super-individuals results in differences to the overall rates of primary production. The model predicts that decreasing the mixing rate increases the overall steady state values of chlorophyll, but it also shows a strong vertical profile of phytoplankton, which would result in an increase in production.

Determining how much of the increase in production can be accounted for by the vertical profile of phytoplankton can be achieved by calculating the distribution of phytoplankton in the Lagrangian model, and then simulating the same distribution in an Eulerian model. A fixed slab model with a mixed layer depth of 100m, and a surface irradiance of 200 W m^{-2}, using a range of different mixing rates (as in section 3.4.1) results in different relationships between the chl-to-carbon ratios and the irradiance (Figure 65).

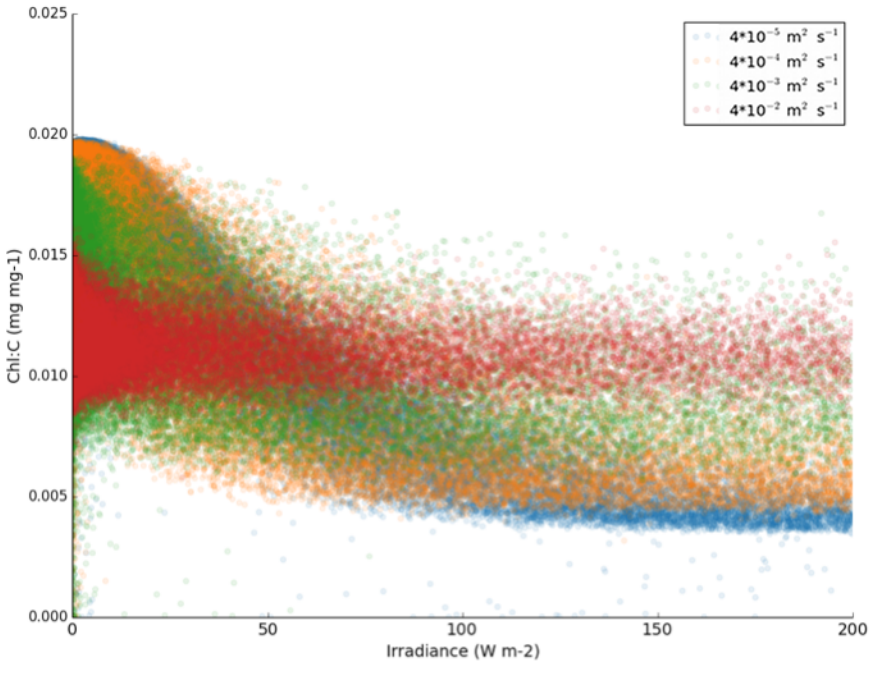

Figure 65: The relationship between the individual chl-to-carbon ratios for 100 super-individuals and their local irradiance, for a fixed slab simulation where H = 100m, surface PAR = 200 W m^{-2}

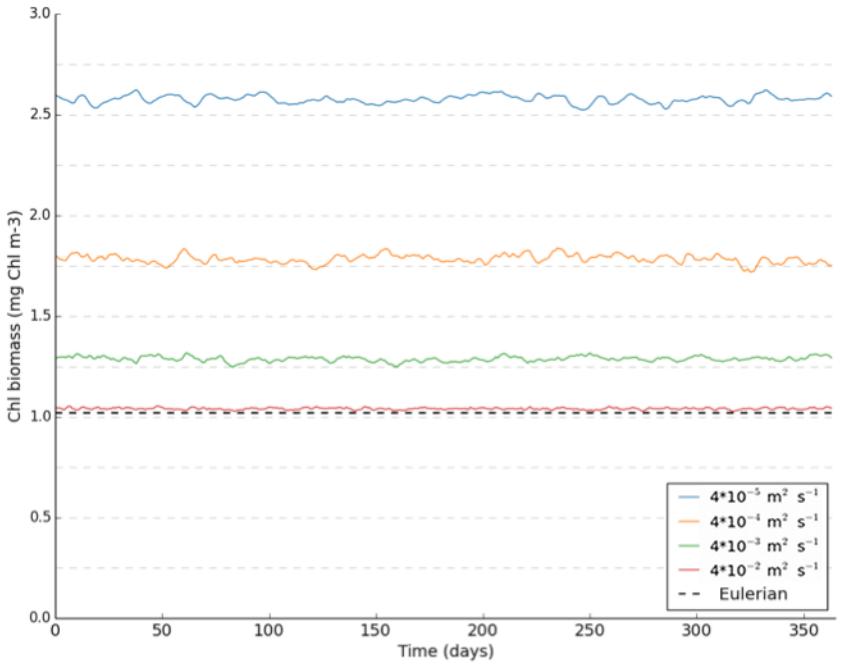

Figure 66: Steady state predictions of chlorophyll for the simulations shown in Figure 65

Figure 65 shows that changing the mixing rate changes the relationship between the local irradiance of a super-individual, and its current chl-to-carbon ratio. The steady-state chlorophyll predictions for each of the mixing rates depicted in Figure 65 are shown in Figure 66, and it is clear that decreasing the mixing rate increases the steady state values.

Reducing the mixing rate allows phytoplankton to remain at, or close to, one depth for longer. This means that phytoplankton near the surface can grow for longer, and those deeper in the water column stay in conditions unsuitable for growth longer, and so decline more. The resulting vertical profiles for the 3 reduced mixing rates, K_{turb} = 4•10^{-5} m^2 s^{-1}, 4•10^{-4} m^2 s^{-1} and 4•10^{-3} m^2 s^{-1}, are shown in Figure 67.

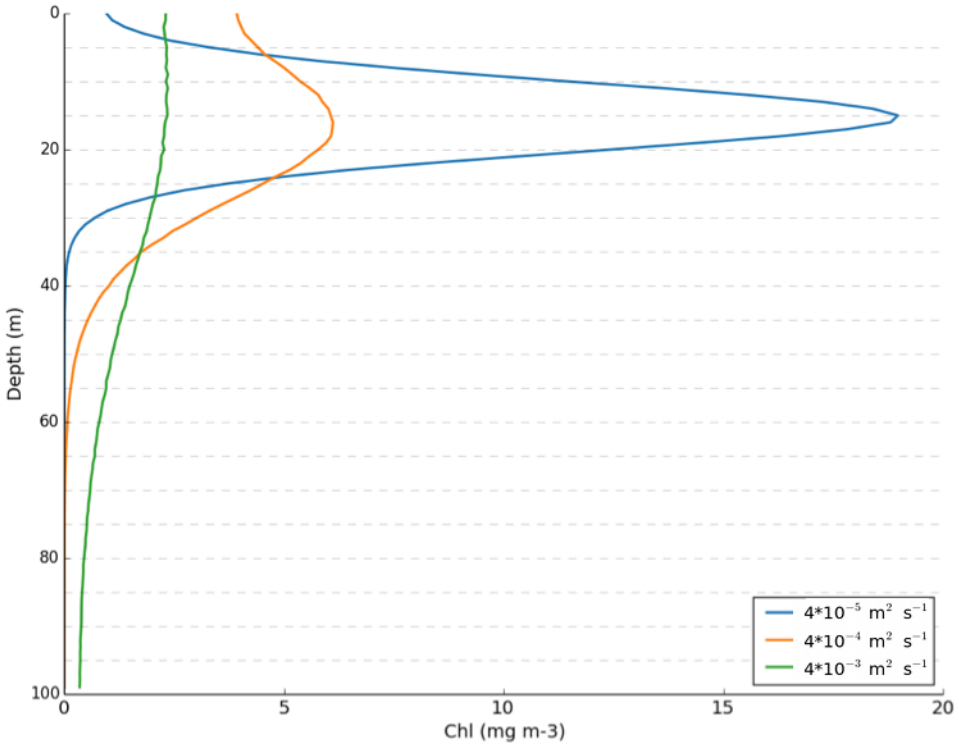

Figure 67: Steady state vertical chlorophyll profiles for a 100 m deep mixed layer, a constant surface irradiance of 200 W m^{-2}, and 3 different mixing rates

These profiles can be estimated using a four-parameter shifted Gaussian model, as described in Platt et al. (1988). This model uses four parameters to describe the shape of the chlorophyll profile: the background chlorophyll

concentration (B_0, mg m^{-3}), the total chlorophyll concentration beneath the curve (h, mg m^{-2}), the width of the peak (σ, mg m^{-3}), and the depth of the chlorophyll maximum (z_m, m).

$$B(z) = B_0 + \frac{h}{\sigma\sqrt{2\pi}} e^{-\left(\frac{(z-z_m)^2}{(2\sigma^2)}\right)} \tag{3.9}$$

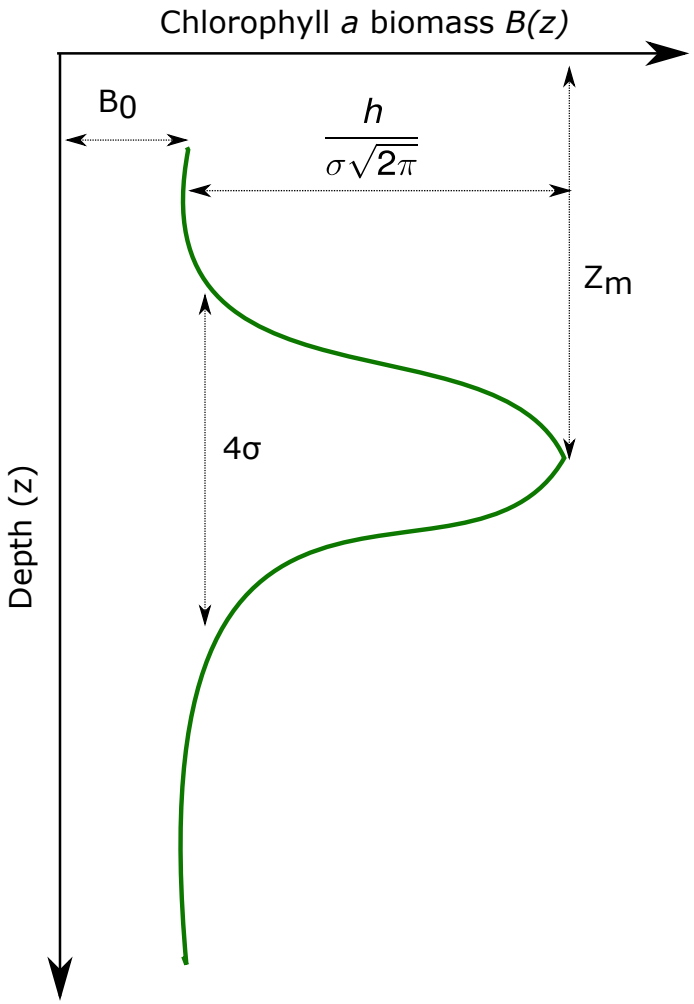

Figure 68: A shifted Gaussian curve showing the four parameters (B_0, h, σ and Z_m) used to describe vertical chlorophyll profiles. Redrawn from Platt et al. (1988)

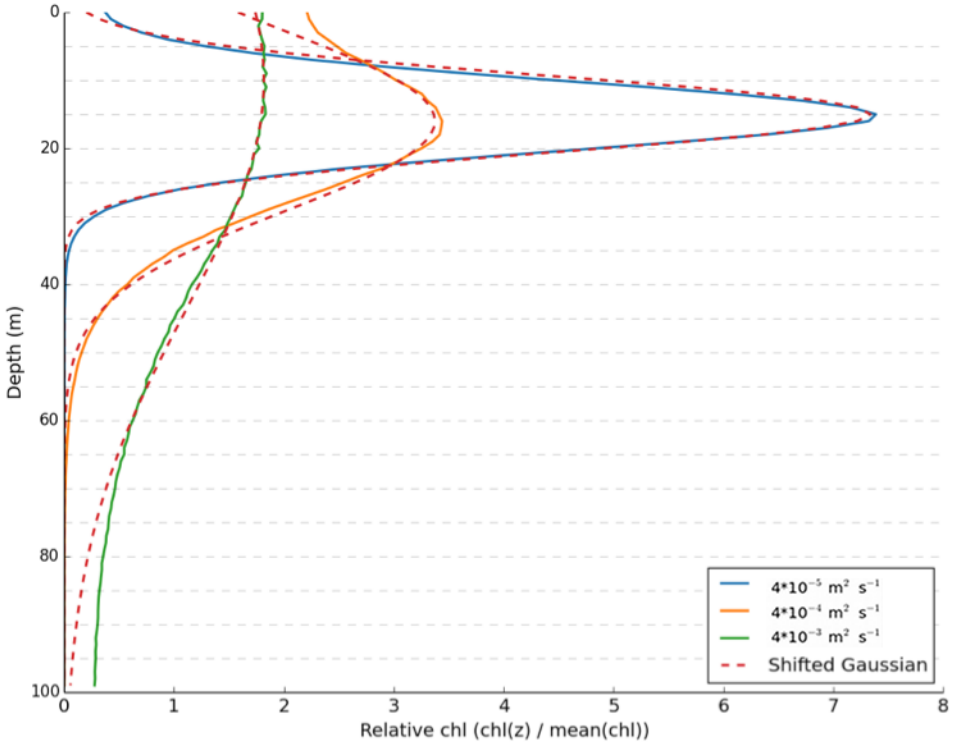

Figure 69: Relative chlorophyll distribution predicted by the steady state model, compared to the fitted function (see text). Parameter values: B_o = 0.0 mg m^{-3}, h = 103, 110, 155 mg m^{-2}, σ = 5.6, 13.0, 34.0 mg m^{-3} and Z_m = 15, 16, 10 m for *Kturb* = 4•10^{-5}, 4•10^{-4}, 4•10^{-3} m^2 s^{-1}, respectively.

Figure 69 shows the shifted Gaussian curves fitted to the relative chlorophyll distribution predicted by the fixed-slab model, run to steady state, under the 3 different mixing rates. The function of this curve can be used as a shape function, S_{Chl}, to modify the calculation of the new production, P_c, throughout the mixed layer:

$$\sum Pc = \int_{z=mld}^{z=0} S_{Chl}(z) \cdot \theta_{Chl} \cdot \frac{\alpha_P \cdot I(z) \cdot V_{PT}}{\left(V_{PT}{}^2 + \alpha_P{}^2 \cdot I(z)^2\right)^{0.5}} \qquad (3.10)$$

The full explanation of the terms in these equations can be found in Chapter 2.

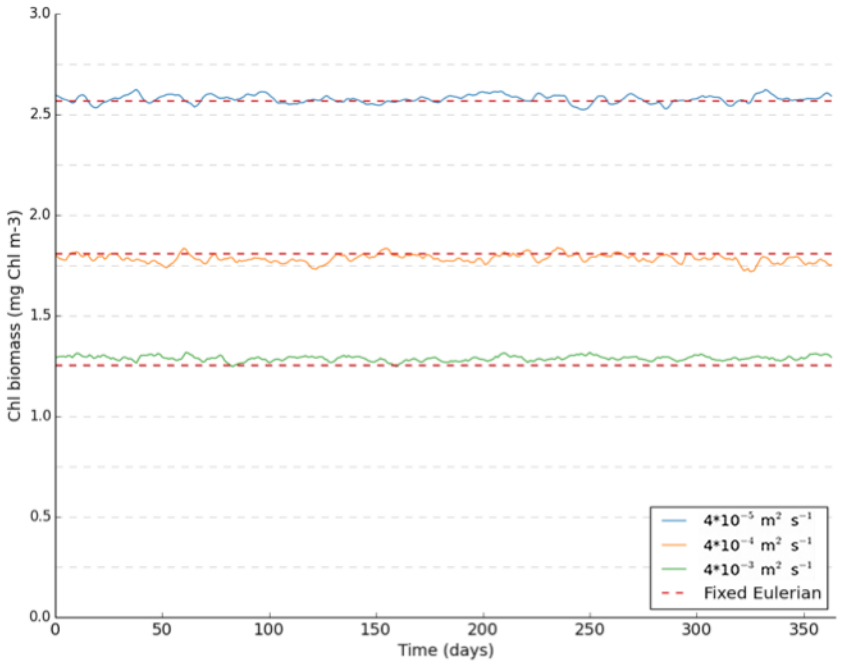

Figure 70: The steady state predictions of chlorophyll biomass for the Eulerian and Lagrangian formulations, and also the prediction from the Eulerian model with the vertical distribution applied (fixed Eulerian model).

Figure 70 shows the 'fixed' Eulerian model predictions of steady state chlorophyll for each of the three mixing rates. It demonstrates that the difference between the Eulerian model and equivalent Lagrangian simulations using moderate to low mixing rates can be accounted for by the vertical profile of phytoplankton, thus indicating that individual differences due to photoacclimation have little or no impact on the overall rates of primary production.

3.6 Sensitivity analysis of the full ecosystem

The previous sections (3.4 and 3.5) have demonstrated the relationship between the mixing rates and both the individual chl-to-carbon ratios of the phytoplankton, and their vertical distribution through the mixed layer. In this final section, the response of the seasonal cycle of chlorophyll and chl-to-carbon to changes in the mixing rates, the choice of the light attenuation model, the mixed layer depth, and the surface irradiance are investigated, using the full OWS I model.

3.6.1 Mixing rates and choice of attenuation model

The random walk algorithm is parameterised using the vertical turbulence diffusivity, K_{turb}, as described in Chapter 2. This is a function of both the depth of the mixed layer, and the surface wind speed, which follows a sinusoidal function based on 5 year averaged ERA 40 data. To investigate the response of the ecosystem to changes in the mixing rate, the surface wind speeds were decreased by increasing orders of magnitude. The values on the plots show the average annual wind speeds for each model run – each simulation still employed the seasonal cycle of wind speed shown in Chapter 2, but the daily values were decreased by a scaling factor (i.e. 10, 100 and 1000, which resulted in average annual wind speeds of 1 m s^{-1}, 0.1 m s^{-1} and 0.01 m s^{-1}, respectively). The simulation was run for both light attenuation models: the Anderson (1993) model, which calculates attenuation for each metre, depending on the chlorophyll above each depth, and the Evans and Parslow (1985) model, which calculates attenuation based on the average concentration of phytoplankton in the entire mixed layer.

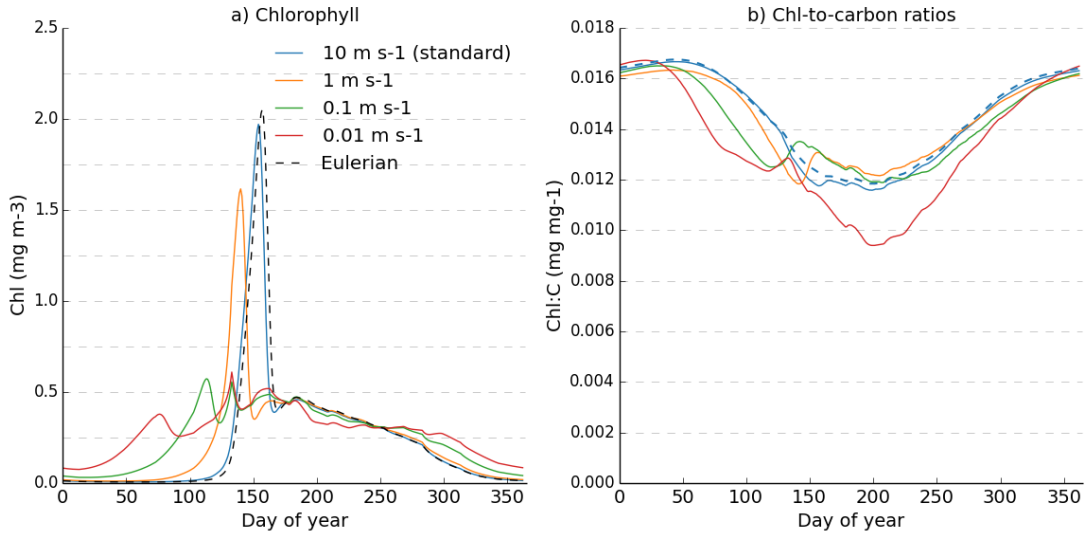

Figure 71: Seasonal cycle of averaged chlorophyll biomass for Lagrangian models with a range of wind speeds. Light attenuation using Anderson (1993). Wind speeds shown are the average values for the seasonal cycle over the year.

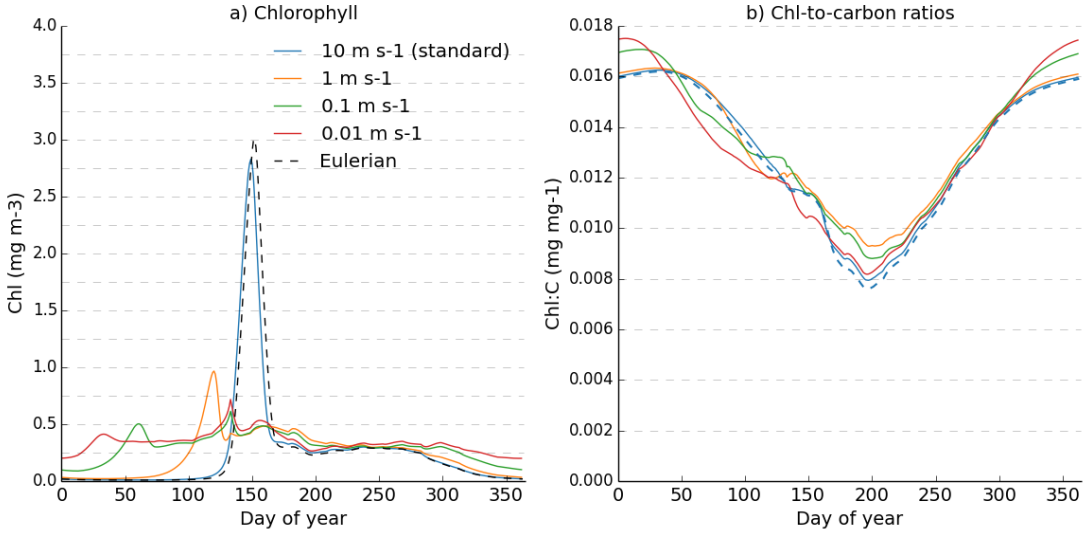

Figure 72: Seasonal cycle of averaged chlorophyll biomass for Lagrangian models with a range of different wind speeds. Light attenuation using Evans and Parslow (1985).

Figure 71 and Figure 72 show that a decrease in the rate of mixing results in an increase in the predicted chlorophyll over winter, and a decrease in the magnitude of the peak of the spring bloom for both types of light attenuation model. The reduction in the rate of mixing results in a strong vertical profile of phytoplankton (profiles are shown in Figure 73 and Figure 74), with a greater concentration of phytoplankton being located in the region of the mixed layer that is the most conducive to growth (i.e. not enough irradiance for photoinhibition to occur, but sufficient for both a high level of chlorophyll production and light fixation). This results in a higher overall rate of production, which explains the high level of chlorophyll over winter, compared to the standard model, where the chlorophyll falls close to zero over winter. In addition, changing the mixing rates appears to have little effect on the average chl-to-carbon ratios for all cases, except the simulation using the Anderson (1993) light attenuation model under a mixing rate based on a surface wind speed of 0.01 m s^{-1}, which shows a significant decrease in the average chl-to-carbon ratio over summer. The reason for this decrease is explained in section 3.4.1: chlorophyll production is downgraded when the achieved rate of photosynthesis is less than the light-harvesting capacity. Reducing the mixing rate results in a higher rate of production earlier in the year, which lowers the concentration of DIN, and therefore reduces the rate of photosynthesis. A reduction in the reduced rate of photosynthesis reduces the amount of chlorophyll production, even at low irradiances, because it reduces the ratio

between the achieved rate of production and the light-harvesting capacity of the phytoplankton individual.

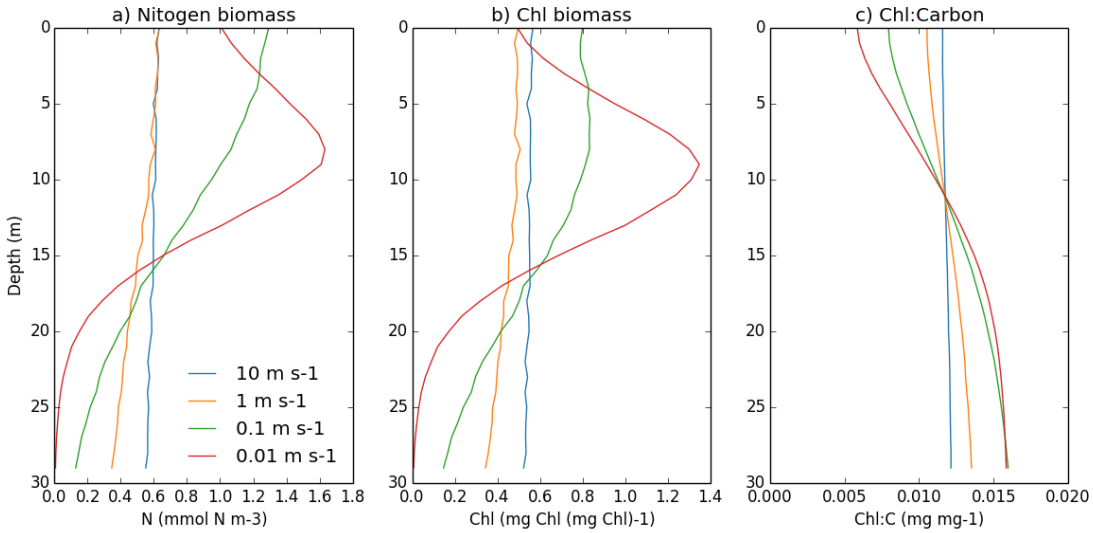

Figure 73: Average vertical profiles of phytoplankton nitrogen, chlorophyll and chl-to-carbon ratios for day 150:250 for the simulations using the Anderson (1993) model of light attenuation

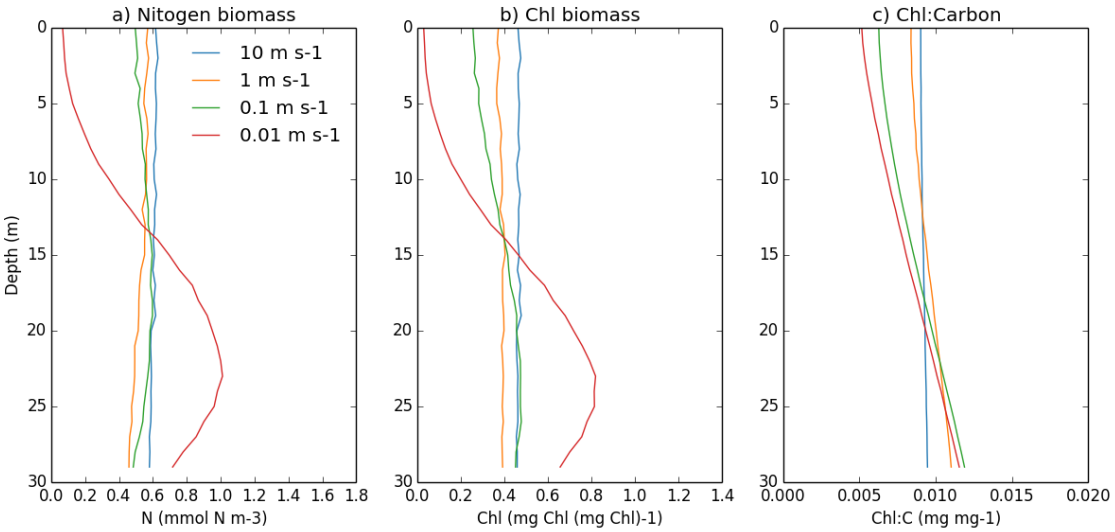

Figure 74: Average vertical profiles of phytoplankton nitrogen, chlorophyll and chl-to-carbon ratios for day 150:250 for the simulations using the Evans and Parslow (1985) model of light attenuation

The choice of light attenuation model clearly has a large effect on the vertical structure of the phytoplankton for scenarios with low to moderate mixing. In order to accurately represent phytoplankton growth in low to moderate mixing rates, the light attenuation model should therefore take account of the

phytoplankton biomass at each depth, rather than using an average concentration.

To further test the conclusion in section 3.5 that the change in primary production under lower mixing rates results from the vertical profile of phytoplankton, rather than a change in chl-to-carbon ratios, a simulation was run using a fixed ratio of chl-to-carbon.

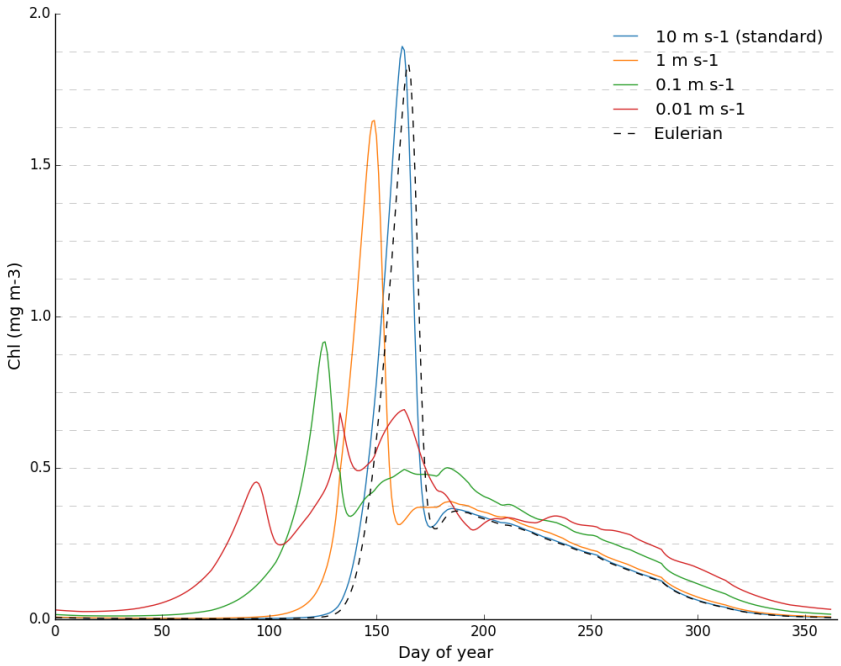

Figure 75: The OWS India simulation using the different cycles of wind speed as in Figure 71:Figure 74 but with a constant ratio of chl-to-carbon (0.01 mg mg^{-1}). Light attenuation as in Anderson (1993)

Figure 75 shows that changing the rate of mixing for a model with phytoplankton with a fixed chl-to-carbon ratio has a very similar effect on the predictions of average chlorophyll as for the same model with a variable chl-to-carbon ratio (Figure 71). This shows that differences in model predictions from changes to the mixing rate are due to vertical profiles of phytoplankton rather than photoacclimation in the full model, as well as for a fixed slab version.

3.6.2 Water turbidity

The fixed slab model in section 3.4.5 suggested that there is little relationship between the range of individual chl-to-carbon ratios and the turbidity of the

water for the model using the Evans and Parslow light attenuation. The same simulation was run with the full OWS I model, with the background attenuation being increased from the standard value of 0.04 m^{-1} to 0.08, 0.16 and 0.32 m^{-1}. In all cases, the Eulerian and Lagrangian models showed very similar predictions of both chlorophyll and chl-to-carbon ratios, suggesting that, as for the fixed slab model, increasing the turbidity of the water does not result in a increase in the individual variability of the chl-to-carbon ratios.

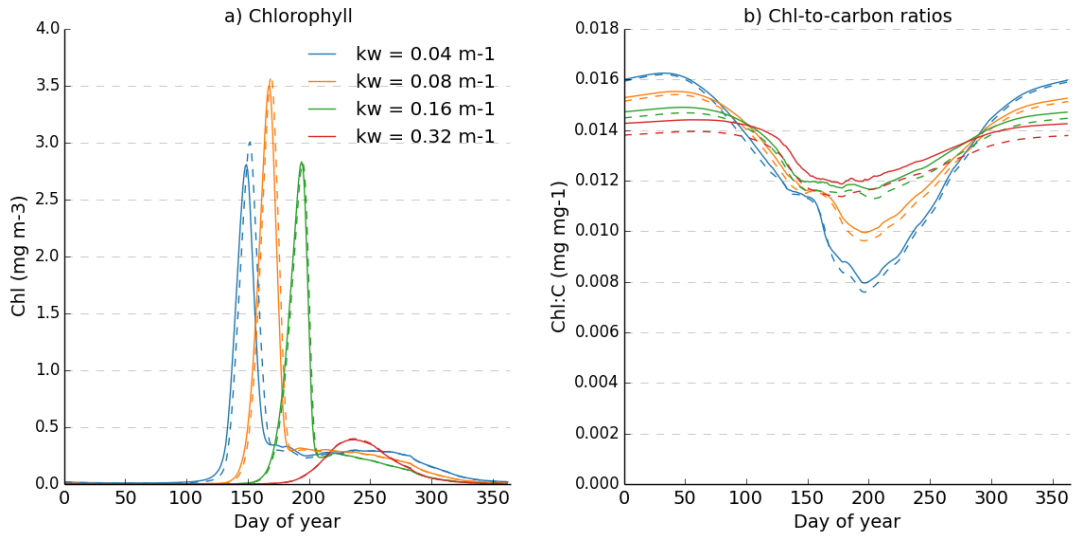

Figure 76: Seasonal cycle of chlorophyll in Lagrangian and Eulerian models with different levels of attenuation (Evans and Parslow attenuation model)

3.6.3 Surface irradiance

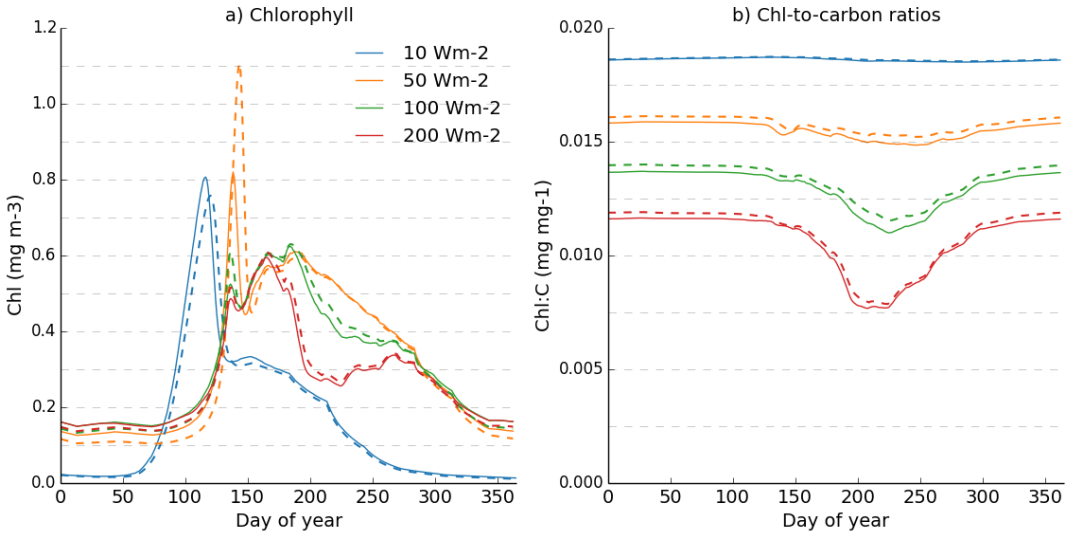

Figure 77: Seasonal cycle of a) chlorophyll and b) Chl:C for a simulation with the full seasonal cycles of mixed layer depth and mixing, but with the surface irradiance held at a constant value. Anderson attenuation.

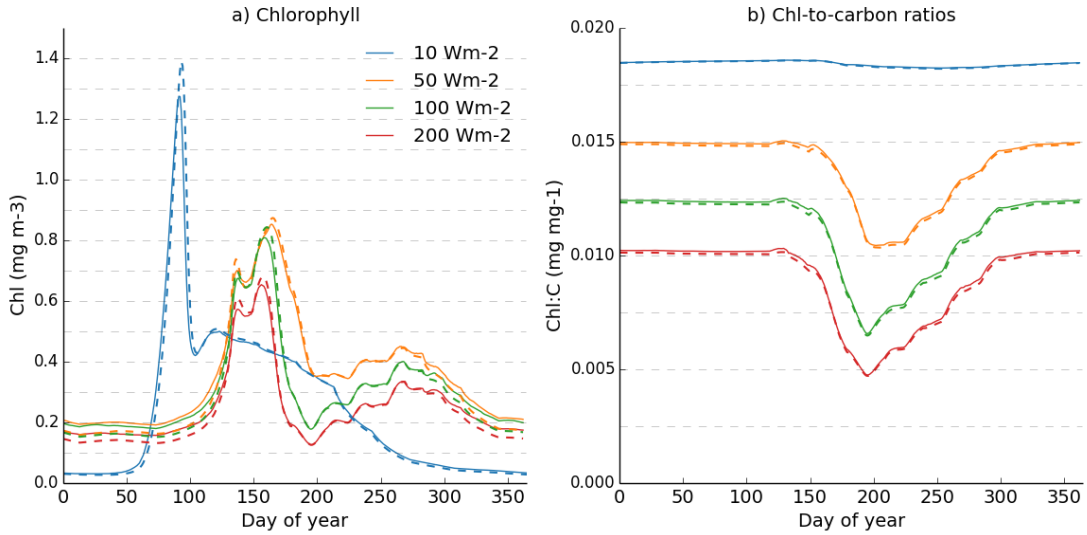

Figure 78: Seasonal cycle of a) chlorophyll and b) Chl:C for a simulation with the full seasonal cycles of mixed layer depth and mixing, but with the surface irradiance held at a constant value. Evans and Parslow attenuation.

One point of interest in both Figure 77 and Figure 78, is that the seasonal cycle of chlorophyll for a constant irradiance of 10 W m^{-2} looks very similar to the seasonal cycle predicted with a seasonally and diel varying irradiance. This demonstrates the importance of the conditions at the beginning of the year to the timing and magnitude of the peak of the spring bloom, which is discussed

in more detail in the next chapter. However, the average irradiance over the first 50 days of the full OWS India model is ~ 10 W m^{-2}, which accounts for the beginning of the cycle looking the same. After that, the phytoplankton concentration is controlled by the loss rates, and growth is limited by the DIN concentrations, so the phytoplankton are not overly affected by increases to the irradiance at this point.

3.6.4 Mixed layer depth

In the final simulation, I ran the full OWSI model, but with a fixed mixed layer depth. The resulting seasonal cycles of chlorophyll biomass showed a slight difference between the Eulerian and Lagrangian model version, which appeared to increase with the depth of the mixed layer (Figure 79).

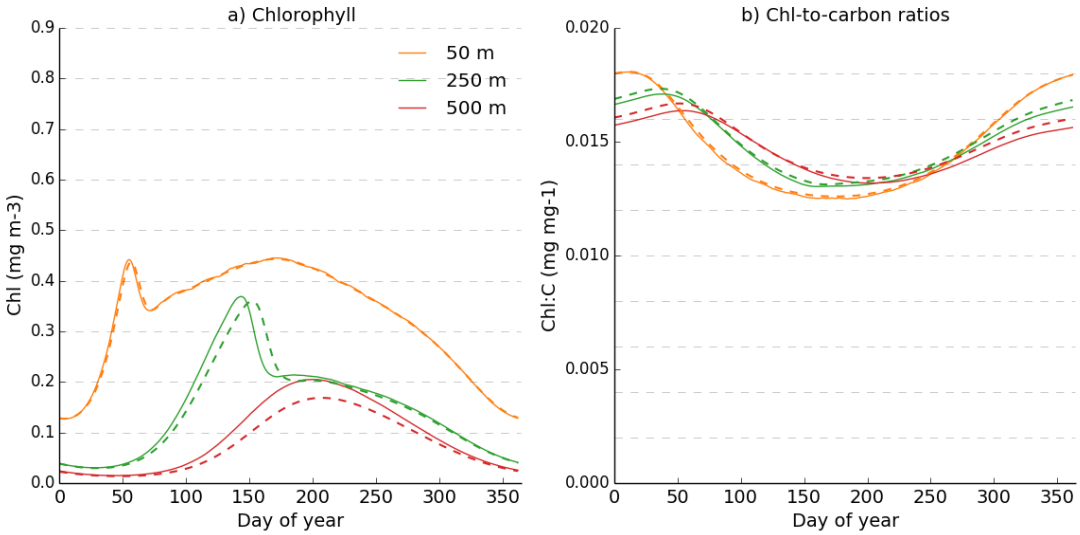

Figure 79: Predicted seasonal cycle of chlorophyll biomass for OWSI model, using a fixed mixed layer depth. Solid line shows Lagrangian model, dashed line the Eulerian equivalent. The mixing rate is constant throughout the simulation (10 m s^{-1})

The increase in divergence between the Eulerian and Lagrangian models with an increase in the depth of the mixed layer results from the degree to which the phytoplankton growth is light limited. Section 3.6.3 demonstrated that the phytoplankton are not light limited over the summer, and that their growth is controlled by other factors i.e. nutrient concentration and grazing. Therefore, increasing the mixed layer depth decreases the average irradiance in the mixed layer, which increases the extent to which phytoplankton growth is limited by irradiance. The more light limited the phytoplankton are, the greater

effect a non-uniform distribution of phytoplankton will have, which explains, the greater divergence between the Eulerian and Lagrangian models when the mixed layer depth is increased to 500m in Figure 79.

The results in this section show that the results for the fixed slab model (section 3.4) also hold true for the full OWS India model. The Eulerian and Lagrangian model implementations will only diverge as a result of a non-uniform distribution of phytoplankton throughout the mixed layer in the Lagrangian model, resulting from low mixing rates. In addition, the effect of a vertical profile of phytoplankton is dependent on the degree to which phytoplankton growth is limited by the surface irradiance: it will have more impact at low irradiances, or when the mixed layer is very deep. Variability in physiology as a result of individual phytoplankton super-individuals acclimating to their local irradiance, on the other hand, appears to have little affect on the model output. Even when the individual phytoplankton showed a wide range of chl-to-carbon ratios, the divergence between the Eulerian and Lagrangian models could be accounted for by the vertical distribution of phytoplankton.

In addition, this section has demonstrated the importance of identifying the correct timescales for models of primary production. For example, for this model, it appears that growth happens on a timescale much faster than that of acclimation, and so exerts a stronger control over the response of overall rates of primary production to changes in turbulence. The timescales of mixing, T_M, growth, T_G, and acclimation, T_A, can be estimated from:

$$T_M = \frac{H^2}{k_{turb}}, T_G = \frac{1}{\mu_{sp}}, T_A = \frac{1}{\theta_{Chl,sp}} \tag{3.11}$$

where μ_{sp} and $\theta_{Chl,sp}$ represent the average daily specific production (gross) rate, and specific rate of change in θ_{Chl} for the super-individuals, respectively.

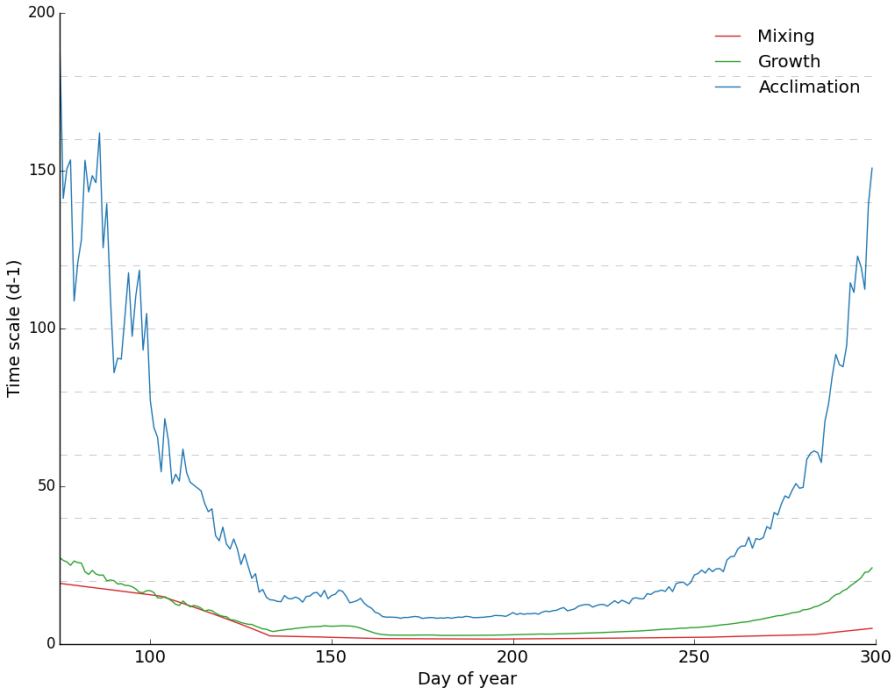

Figure 80: The timescales associated with mixing, growth and acclimation for the OWS India model

Figure 80 shows how close the timescales of growth and mixing are, especially in the time leading up to the spring bloom. Small changes in the rate of mixing during this time will have large effects on the vertical structure of the phytoplankton, which, because growth is light limited, will strongly affect the rates of primary production. On the other hand, the timescales of acclimation are much slower than the mixing, and a significant reduction in the mixing would be required to bring them closer. However, as this would also strongly affect the growth, it shows that the accurate representation of growth, and the resulting vertical phytoplankton profiles, is more important than representing photoacclimation.

It's important to note that these results do not suggest that photoacclimation does not have an impact on the rates of primary production. Both the Eulerian and Lagrangian models demonstrate a clear annual cycle of average chl-to-carbon ratios in response to the seasonal cycle of irradiance. However, the results do suggest that photoacclimation impacts overall rates of primary production on a seasonal, rather than a daily or hourly, timescale.

3.7 Conclusion

There were three main aims to this chapter: firstly to discover whether there are any differences between Eulerian and Lagrangian implementations of phytoplankton models, secondly to understand whether these differences are due to acclimation, and finally to understand the relationship between acclimation and mixing rates. The simulations have shown that:

1. Although the phytoplankton in the Lagrangian model do show a large range of photoacclimative properties, the average chl-to-carbon ratio predicted does not differ significantly from that predicted by the Eulerian model.
2. Photoacclimation happens slowly. Phytoplankton do not have time to acclimate to the ambient irradiance at any particular time, instead they acclimate to the average irradiance experienced over a longer period of time (days). In the short term, this results in the range of photoacclimative properties observed in the Lagrangian model, but also explains why the average of these does not differ from the those predicted by the Eulerian model.
3. Divergence between Eulerian and Lagrangian models results from changes in the vertical distribution of phytoplankton in the water column, and not from photoacclimation. For this model, this is achieved by slowing the mixing rate, allowing those phytoplankton near the surface more time to grow, and those near the base more time to decline. However, it is possible to approximate this using an Eulerian model and a function describing how the vertical profile of phytoplankton changes with depth.

It is important, however, to view these results in context. The rate at which the phytoplankton adjust to changes in their light environment is controlled by the chosen model of photoacclimation. The model chosen for this study, described in Geider et al. (1997), calculates chlorophyll synthesis based on the rate of photosynthesis, therefore assuming that phytoplankton do not synthesise chlorophyll in the dark. This assumption explains why the phytoplankton particles appear to be acclimating to the average irradiance in the euphotic zone, rather than over the mixed layer as a whole (Figure 56). However, Ross & Geider (2009) point out that this assumption does not produce

photoacclimation dynamics that allow for a sufficiently rapid response to shifts from high to low light. They developed a cell-based model in which carbon accumulated by phytoplankton during the day, can then be utilised after sunset, allowing them to continue to synthesise chlorophyll for some time into the night. They showed that this approach increased the performance of the model, in particular with regards to the response time of phytoplankton to changes from high to low irradiance.

Although the question of whether the model accurately represents the phytoplankton light shift dynamics will obviously impact on the vertical distribution of phytoplankton light-harvesting properties, the results here have suggested that the vertical distribution of phytoplankton has a greater impact on overall rates of primary production. Increasing understanding of mixing rates in the ocean and how these impact on the vertical distribution of phytoplankton – even within a fully mixed layer – will help to further the accuracy of future ecosystem models. Also of interest for this field are the development of new techniques to predict vertical profiles from satellite measurements, for example, Richardson et al. (2003) have developed an approach to predict phytoplankton profiles, using the four-parameter Gaussian curve described in section 3.5, based on environmental variables such as the depth of the water column, the season, and the geographical location.

It is also important to note that, even though the chapter has shown no advantage to the use of Lagrangian models in terms of their accuracy in predicting primary production, it has also shown their great utility for the creation and testing of hypotheses. It suggests that the place for Lagrangian models in marine ecology is for the testing of ecosystem theory, on which Eulerian models for prediction can then be based. This idea will be further tested in the next chapter, where the Lagrangian model is used to explore the mechanisms that control the spring bloom in the North Atlantic, to see if the use of this method can resolve some of the controversy that current exists in the literature regarding this important phenomenon.

Chapter 4: Using a Lagrangian phytoplankton model to test the controls of the spring bloom

4.1 Introduction

The North Atlantic is a key region for carbon sequestration, accounting for an estimated 25% of the global oceanic CO_2 uptake (Bagniewski et al., 2011). The phytoplankton spring bloom in the North Atlantic contributes significantly to carbon export, playing an important role in the annual dynamics of the phytoplankton community (Lindemann & St John, 2014). There has therefore been a great deal of research focussed on understanding the drivers of the spring bloom, in order to aid prediction of the system's response to changes in environment pressure, whether that be ephemeral phenomena, such as eddies and fronts, or long-term changes in climate.

The canonical study for the explanation of the mechanisms driving the spring bloom was performed by Sverdrup (1953). Sverdrup's critical depth hypothesis (CDH) proposes that in order for the spring bloom to occur, vertically averaged phytoplankton growth rates have to exceed phytoplankton loss rates. This can only occur if the vertically averaged irradiance through which the phytoplankton are mixed is above some critical value. There therefore exists a critical depth, above which the average irradiance exceeds the level required for positive net growth. If the phytoplankton are mixed below this depth, net growth cannot occur, and the population will decline. At the end of the winter, the water column stratifies due to the reduction in mixing rates combined with an increase in net surface heat flux, from the seasonal increase in irradiance. Once the depth of the fully mixed portion of the surface layer shoals above the critical depth, positive net growth can occur, and conditions are favourable for a spring bloom.

Despite being published over 60 years ago, Sverdrup's paper is still cited over 50 times a year (Sathyendranath et al., 2015), due, in part, to its elegant way of summarising a complex oceanographic process with a simple mathematical

model. Although the simplicity of the model has attracted its fair share of criticism (e.g. Evans & Parslow (1985); Smetacek & Passow (1990)) no suitable alternative was suggested until Huisman et al. (1999) proposed that a reduction in mixing rates could also result in a spring bloom (the critical turbulence hypothesis, CTH). Although Sverdrup had indicated that a reduction in turbulence could enable a population to survive even if they were being mixed beyond the critical depth, Huisman et al. (1999), and later Taylor & Ferrari (2011), were able to quantify the turbulence below which positive production could occur, regardless of the depth to which the phytoplankton are mixed. However, the CTH was not intended to replace the CDH, Huisman et al. suggested that each hypothesis described an independent mechanism by which the spring bloom could be initiated.

Behrenfeld (2010) and later Behrenfeld & Boss (2014), offered a different explanation, which they termed the disturbance-recovery hypothesis (DRH). They proposed that the seasonal increases in phytoplankton biomass were a result of disturbances to the balance between phytoplankton growth and loss through grazing. During the winter, the phytoplankton and zooplankton are mixed down to greater depths, essentially diluting their respective concentrations. This results in fewer encounter rates, lower specific grazing losses, and effectively decouples the phytoplankton-zooplankton balance. The reduction in specific grazing loss results in an increase of specific phytoplankton growth, irrespective of the available resources, with positive net growth being apparent during the winter. This growth continues, until the zooplankton populations are able to recover, and once again keep pace with the phytoplankton production (i.e. the phytoplankton-zooplankton balance recouples).

In this chapter, I use the Lagrangian model to test each of these hypotheses. My main aim is to reconcile these theories, showing that, rather than being alternatives to the critical depth hypothesis, the critical turbulence and disturbance-recovery hypotheses describe mechanisms by which the critical depth can be altered. In essence, I extend the critical depth hypothesis to include scenarios with reduced mixing, and scenarios with a disturbance to the phytoplankton-zooplankton balance.

Although in the previous chapter, I have demonstrated little predictive advantage in the use of a Lagrangian model over the use of an Eulerian model, I have also demonstrated the utility of the Lagrangian model for analysis of the individual life-histories of the phytoplankton super-individuals. This justifies the use of a Lagrangian model for this study. In addition, the Lagrangian model offers more precision in regards to the irradiance experienced by the super-individuals in the water column, because it calculates the irradiance at each, exact depth, rather than integrating through the water column using a discrete number of depth intervals. I demonstrate that the critical depth predicted by an Eulerian model using 1 metre intervals is significantly deeper than that predicted by a Lagrangian model, for this reason.

4.1.1.1 The spring bloom

One of the difficulties in reconciling the various hypotheses that describe the controls on the initiation of the spring bloom is the lack of consistency of terms in the literature. For example, the onset of the spring bloom can refer to the point where the net phytoplankton growth first becomes positive (Behrenfeld, 2010), or when the surface chlorophyll concentrations first exceed a threshold value (Cole et al., 2015). Llort et al. (2015) circumvented this problem by splitting the spring bloom into three, distinct stages: the onset, the point where net growth first becomes positive; the climax, where growth rate is at its maximum; and the apex, where total biomass reaches its peak. I follow this convention for this study, focussing only on the onset of the spring bloom, and the mechanisms that determine its timing.

4.1.2 Testing the hypotheses surrounding the initiation of the spring bloom

Franks (2014) proposed that in order to properly test the critical depth model, it is necessary to investigate both phytoplankton growth rates and the water column mixing rates. This was previously attempted through the use of an Eulerian NPZ model, which was forced with vertical mixing, by Lévy (2015). She ran a suite of simulations, starting from a simple representation of Sverdrup's assumptions, and gradually increasing complexity, in order to investigate how the adding complexity affected the timing of the onset of the theoretical

bloom (as calculated from the point where the mixed layer shoaled above the predicted critical depth) compared to the modelled bloom. She found that even the model that used the simplified assumptions proposed by Sverdrup showed a time lag of 1 week between the theoretical and modelled spring bloom. She also observed that, although the loss rate remained constant between winter and spring, suggesting that grazing plays little part in the timing of the spring bloom, if she included a seasonal cycle of mixed layer depth where the mixed layer deepened during the autumn, the model predicted positive growth rates due to the phytoplankton and zooplankton being significantly diluted by water entrained from below. She concluded that in order to fully understand bloom dynamics, it is necessary to simulate the full seasonal cycle, in order to account for the evolution of the physical parameters from the previous summer.

This model differs from the work carried out by Lévy, in that I am using a full ecosystem, including representation of photoacclimation, with Lagrangian phytoplankton. I carry out an in-depth study of each of the three main hypotheses that describe mechanisms controlling the timing of the onset of the spring bloom. Rather than simplify the model to fit with Sverdrup's assumptions, I derive an analytical equation to predict the critical depth, based on my model parameterisations (i.e. non-linear phytoplankton loss rate, non-linear P-I curve). I then demonstrate that the analytical predictions, and those obtained numerically with the model are the same. The inclusion of non-linear terms means that the critical depth is not a constant value in a dynamic simulation (i.e. one where the phytoplankton are not in steady-state), and I show that taking this into account allows for the theoretical and actual predictions of the onset of the spring bloom in the OWSI model to match, exactly. At the end of the first section, I show the sensitivity of the predicted critical depth to the parameterisation of the phytoplankton loss rate.

In the second section, I investigate the disturbance-recovery hypothesis. This essentially proposes that the spring bloom results from a decoupling between phytoplankton and zooplankton due to lowered concentrations over winter, so I run two scenarios, one with decoupling, one without, to see how this affects the initiation of the spring bloom. I demonstrate that, as predicted by Behrenfeld & Boss (2014), dilution of the phytoplankton and zooplankton populations results in a reduction of the specific loss rate, and therefore an

increase in the specific rate of net growth. However, if the change in the rate of loss is taken into account when calculating the critical depth, the timing of the onset of the spring bloom is still completely predictable.

For the first two sections, I used the assumption that the phytoplankton are fully mixed within the water column at any one time, so used the random position movement algorithm (the depth of each super-individual is set to a random point between the surface and the base of the mixed layer every 30 minute time step). For the final section, I investigate the critical turbulence hypothesis, which states that if the turbulence falls below a certain level, a spring bloom can develop, regardless of the depth of the mixed layer. In order to allow for changes to the mixing rate, I use the random walk model of movement (both types of movement rules are fully described in Chapter 2). This allows me to investigate how reductions in the mixing rate affect the timing of the spring bloom. I demonstrate that, contrary to Huisman et al. (1999), reducing the turbulence does not result in a bloom, irrespective of the mixed layer depth, instead it increases the value of the critical depth. There is a clear, hyperbolic relationship between the rate of turbulence and the critical depth – as the turbulence moves towards 0, the critical depth moves towards infinity. I further show that, if the vertical profile of phytoplankton resulting from a reduced rate of turbulence is known, it is possible to predict the critical depth, and therefore the onset of the spring bloom.

4.1.3 Objectives

1. Demonstrate the existence of the critical depth, as defined by Sverdrup, using a fixed slab model
2. Demonstrate how a Lagrangian model can be used to calculate the daily critical depth, and how this is affected by changes to the phytoplankton loss rates
3. Use the model to investigate the relationship between the critical depth and the point at which net growth becomes positive (i.e. the point at which a bloom could potentially develop)
4. Show how the critical depth hypothesis can be extended to include the critical turbulence and disturbance-recovery hypotheses

4.2 The critical depth hypothesis

In this section, I use the Lagrangian model to perform an in-depth analysis of the critical depth hypothesis. Firstly, I derive an analytical equation to determine the critical depth for a simulation, and then use the model to provide a numerical test of the equation. I then compare the predicted critical depth in a fixed slab, steady state model, to the critical depth predicted in a dynamic model. Next, I use the full OWS India model (described in Chapter 2) to determine which variables have the greatest impact on the critical depth, before moving on to evaluate whether the mixed layer depth shoaling above the critical depth triggers the spring bloom. Finally, I investigate the sensitivity of the critical depth to the parameters controlling the rate of phytoplankton loss.

4.2.1 Deriving an analytical equation to predict the critical depth

The critical depth hypothesis proposes that when the mixed layer depth shoals above some critical depth, the spring bloom is initiated. This critical depth is defined as the depth at which the integrated rates of phytoplankton growth are equal to the integrated rates of phytoplankton loss. Sverdrup described an equation that could be used to predict the critical depth for any surface irradiance:

$$\frac{Z_{cr}}{1-e^{k_{par}Z_{cr}}} = \frac{1}{k_{par}}\frac{I_0}{I_c} \tag{4.1}$$

where Z_{cr} represents the critical depth (m), k_{par} the light attenuation coefficient (m^{-1}), I_0 the surface irradiance, and I_c the compensation irradiance. The compensation irradiance is the irradiance at which the rate of photosynthesis exactly balances the rate of the sum of the losses in a phytoplankton cell.

However, one of the assumptions for Sverdrup's equation is that the relationship between photosynthesis and irradiance should be linear, whereas my model uses a non-linear Smith function to represent photosynthesis:

$$\overline{Pc}_{MLD} = \theta_{chl} \cdot \int_{z=0}^{z=H} \frac{\alpha_P \cdot I(z) \cdot V_{PT}}{\left(V_{PT}{}^2 + \alpha_P{}^2 \cdot I(z)^2\right)^{0.5}} \quad (4.2)$$

where:

$$I(z) = I_0 \cdot \exp(-k_{par} \cdot z) \quad (4.3)$$

Eq. (4.2) calculates the integrated rate of photosynthesis for a mixed layer, $\overline{Pc}_{MLD}$, from the chl-to-carbon ratio, θ_{Chl}, the initial slope of the P-I curve, α_{chl}, the maximum growth rate at the current temperature, V_{PT}, and the irradiance through the water column, *I(z)*.

In order to find an equation to predict the critical depth, I first needed to derive an analytical solution for the integral in equation (4.2) together with equation (4.3). This has already been done in Anderson et al. (2015), who used a trigonometric transformation and then integration by parts to give:

$$\overline{Pc}_{(MLD)} = \frac{V_{PT}}{k_{par} \cdot H} \ln\left(\frac{x_0 + \left(V_{PT}{}^2 + x_0{}^2\right)^{0.5}}{x_H + \left(V_{PT}{}^2 + x_H{}^2\right)^{0.5}}\right) \quad (4.4)$$

where $x = \alpha_P \cdot I(z)$, and x_0 is *x(z=0)* and x_{MLD} is *x(z=H)*.

The final step was to use equation (4.4), with the intention of finding the mixed layer depth at which the predicted integrated rate of photosynthesis would equal the loss rate i.e. when $\overline{Pc}_{(MLD)} = m$, where *m* represents the average daily phytoplankton loss (assumed to be constant with depth). This depth represents the critical depth, Z_{cr}:

$$Z_{cr} = \frac{\theta_{chl,\text{int}} \cdot V_{PT} \cdot \ln\left(\frac{x_0 + \left(V_{PT}{}^2 + x_0{}^2\right)^{0.5}}{x_{cr} + \left(V_{PT}{}^2 + x_{cr}{}^2\right)^{0.5}}\right)}{k_{par} \cdot m} \quad (4.5)$$

Equation (4.5) assumes that the irradiance at the base of the mixed layer is known. For deeper mixed layers (i.e. greater than 50 m), the irradiance at the base of the mixed layer will be close to zero, so I set x_{cr} to a small value, just above zero ($1e^{-3}$ W m^{-2}), to prevent division by zero errors. This assumption

would not be suitable for mixed layer depths shallower than ~50m, however, the irradiance at the base of the mixed layer can be estimated for models with shallower mixed layers, by numerically integrating equation (4.2) with equation (4.3).

Equation (4.5) shows that the critical depth is affected by four variables: the surface irradiance, I_0, the chl-to-carbon ratio, θ_{chl}, the attenuation coefficient, k_{par}, and the phytoplankton loss rate, m. Increases to the surface irradiance and the chl-to-carbon ratio will increase the critical depth, whereas increases to the attenuation coefficient and phytoplankton loss rate will decrease it.

I used the model to provide a numerical test of equation (4.5) by firstly using the equation to predict the critical depth for a particular scenario, then running a model version of that scenario at increasing mixed layer depths, until I found the depth at which the phytoplankton population could no longer survive. For these model runs, I used a fixed slab model, with a constant surface irradiance. In order to ensure that the phytoplankton were fully mixed through the water column, I used the random position movement method (described in Chapter 2), which randomises the position of the phytoplankton super-individuals each time step (30 mins). In the first instance, I wanted to simplify the model as much as possible, and so I removed the non-linear mortality terms (mortality, grazing), and just used a linear mortality term, as per Sverdrup. As the critical depth depends on the irradiance, the chl-to-carbon ratio, the light attenuation coefficient, and the phytoplankton loss rate, I set these variables to constant values. That way, I could use these values along with equation (4.5) to predict the critical depth for the scenario. I investigated two scenarios, using the parameter values: θ_{chl} = 0.02 mg chl (mg C)$^{-1}$, k_{par} = 0.04 m^{-1}, m = 0.1 d^{-1}, for I_0 = 10 W m^{-2} and I_0 = 20 W m^{-2}. In addition, I removed the nutrient limitation term from the growth equation, so that phytoplankton growth was unaffected by the external concentration of nutrient, simulating growth in nutrient replete conditions.

Using these parameters with Equation (4.5) gave predicted critical depths of 141.7 m and 271.6 m for surface irradiances of 10 W m^{-2} and 20 W m^{-2}, respectively. I tested these predictions by setting up the same scenarios in the model, and running it at a range of different mixed layer depths: between 140 and 142m for the surface irradiance of 10 W m^{-2} and between 270 and 272 m

for the surface irradiance of 20 W m^{-2}. If the equation were working as expected, then the phytoplankton would be expected to decline in simulations with a mixed layer depth greater than the predicted critical depth, and would be expected to increase in simulations with a mixed layer depth shallower than the predicted critical depth.

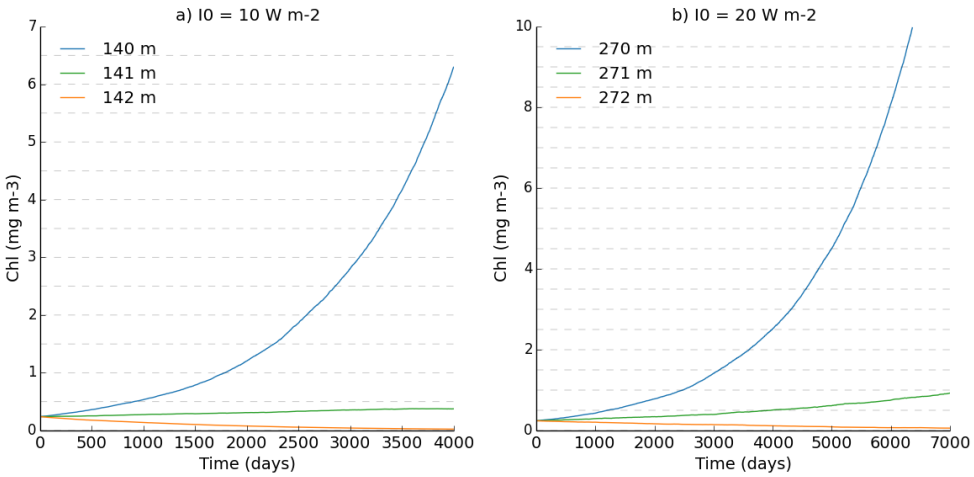

Figure 81: The predicted integrated chlorophyll biomass for fixed slab simulations with a constant irradiance, mixed layer depth, light attenuation coefficient and chl-to-carbon ratio, under a range of different mixed layer depths.

Figure 81 shows that, for both scenarios, the critical depth predicted by equation (4.5), is equal to the critical depth predicted by the model. This demonstrates that I can use the analytical equation to predict the critical depth for a fixed slab model, using a constant irradiance, linear mortality, and fixed values for chl-to-carbon and light attenuation.

4.2.2 Non-linear loss terms and critical depth

Having demonstrated that the analytical equation calculates the same critical depth as that determined numerically by a model with only linear mortality, I next investigated how non-linear phytoplankton loss terms affect the predicted critical depth. I first looked at steady-state solutions provided by a fixed-slab model, before investigating a dynamic model with a seasonal cycle of forcing, where the phytoplankton are in a state of continuous flux.

Predicting the critical depth using equation (4.5) requires knowledge of the total rate of phytoplankton loss, m (d^{-1}). If m is a linear term, as in the previous

section, then this is simple, however, calculating m in simulations with non-linear mortality and grazing is more complicated. The total phytoplankton loss rate then becomes a function of both the phytoplankton and zooplankton concentration, because increases in phytoplankton concentration will increase the specific rate of loss, and decreases in phytoplankton concentration will decrease the specific phytoplankton loss rate.

I used the model to estimate the values for m in simulations with a mixed layer depth close to the critical depth. I started with the same scenario as above, θ_{chl} = 0.02 mg chl (mg C)$^{-1}$, k_{par} = 0.04 m^{-1}, no nutrient limitation, and I_0 = 10 W m^{-2}, but this time, I used the phytoplankton mortality rates, as for OWS India, and also reintroduced the zooplankton (the full equations can be found in Chapter 2). I started by using equation (4.5) to calculate the predicted critical depth based on the respiration alone (linear loss, p_1 = 0.02 d^{-1}), and then took this depth as a starting point. I then ran simulations at decreasing mixed layer depths, until I found the depth at which the phytoplankton reached a steady state, and did not die out. In order to achieve this with a model with a deep mixed layer, I had to run the model for a very long time (65,000 days, or 178 years). This is because changes in the depth of the mixed layer makes very small changes to the average irradiance level. This can be demonstrated by calculating the difference in average irradiance between a mixed layer of 100m and 101m, and between a mixed layer depth of 700m and 701m, by integrating the irradiance function in equation (4.3). Increasing the mixed layer depth from 100 to 101m decreases the average irradiance from 2.454 W m^{-2} to 2.432 W m^{-2}, a decrease of 0.024 W m^{-2}, whereas increasing the mixed layer depth from 700 to 701 m decreases the average irradiance from 0.3571 W m^{-2} to 0.3566 W m^{-2}, a decrease of 0.0005 W m^{-2}. This demonstrates that as the depth of the mixed layer becomes deeper, the proportional difference in an increase or decrease by 1 metre becomes smaller (i.e. 1 metre becomes a smaller fraction of the mixed layer depth). Therefore, the resulting increase or decrease in the average irradiance also becomes smaller, and it becomes more difficult to observe changes in the phytoplankton at a population level.

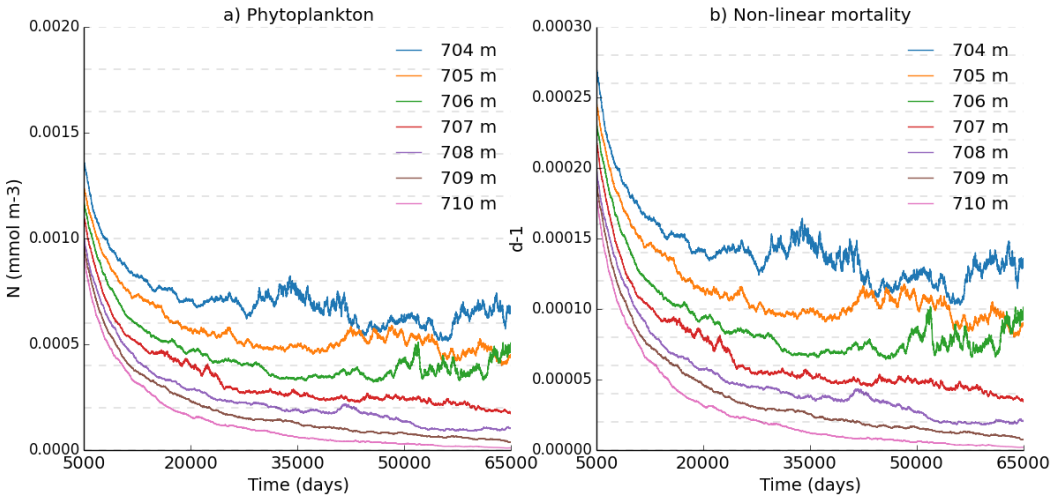

Figure 82: The predicted a) phytoplankton biomass and b) phytoplankton non-linear mortality for a fixed slab model with a constant irradiance (10 Wm^{-2}), a fixed chl-to-carbon ratio (0.02), and the full loss rates used in the OWSI model

Figure 82 shows how both the phytoplankton concentration and the daily non-linear mortality rate respond to different mixed layer depths. It suggests that the critical depth, as predicted by the model, lies between 706 and 707 m. It also shows how the non-linear mortality rate increases along with the increase in phytoplankton biomass. Unlike the scenario with the linear mortality (Figure 81), decreasing the mixed layer depth does not result in a continual increase in phytoplankton biomass, as the increase in the non-linear mortality rate prevents this from happening. Instead, the concentration of phytoplankton biomass reaches a new, higher, steady-state value. The steady-state values for the non-linear mortality are very low – less than 0.0002 d^{-1}, compared to 0.02 d^{-1} for the respiration, which supports findings by Platt et al. (1991), who found that when they calculated a generalised loss term to determine critical depth, it was dominated by the respiratory costs of phytoplankton growth and metabolism.

Figure 82 only shows the model predicted critical depth; it gives no information about the behaviour of the model around that depth. The time scales are extremely long, due to the size of the changes when the mixed layer is at the critical depth, and are therefore not biologically relevant, where changes to the mixed layer depth are important on time scales of days. An indication of how changes around the critical depth can impact the biology can

be give by running the model to steady state at close to the critical depth, and then deepening the mixed layer depth, and observing the changes to the predictions of phytoplankton biomass. The biomass was normalised to the value predicted at steady state, in order to remove changes due to dilution by the deepening of the mixed layer, and Figure 83 shows how an increase of 200 m only results in a 4% decline in phytoplankton biomass.

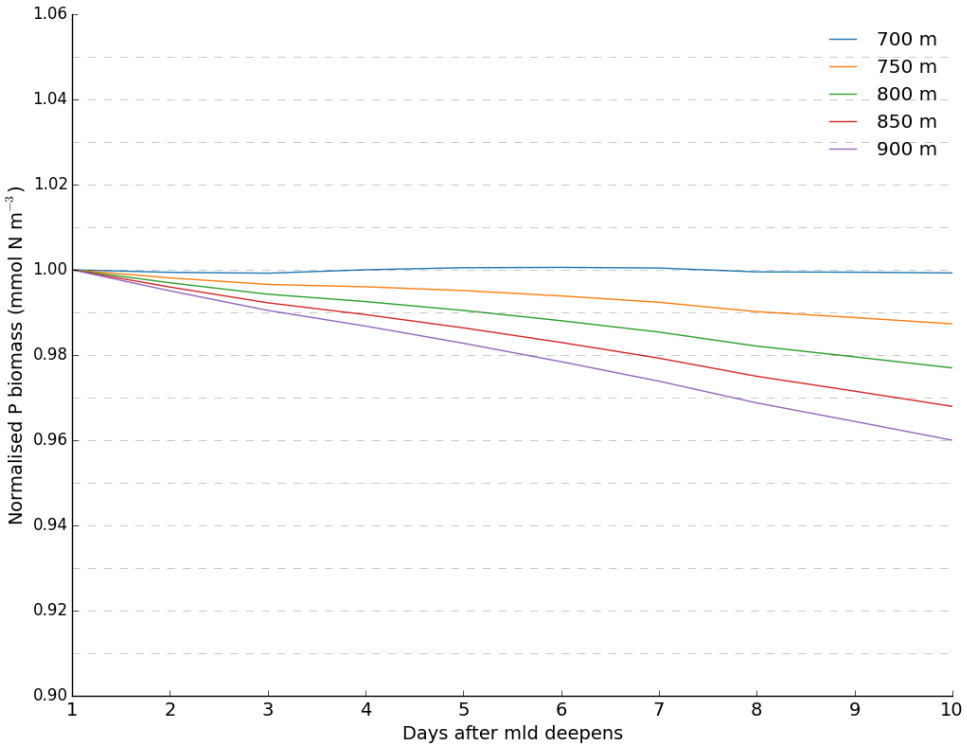

Figure 83: The decline of the steady state phytoplankton population, when the mixed layer depth is deepened, using the same conditions as in Figure 75.

However, steady-state simulations such as these may not be representative of conditions in the open ocean. The ocean is a highly dynamic environment, and marine systems are in a state of continuous flux. Changes in the concentrations of phytoplankton and zooplankton, resulting from changes to the depth of the mixed layer, can have a sudden impact on the specific grazing rates, and therefore the predicted critical depth. This is explained in more detail in the next section.

4.2.3 Calculating the compensation irradiance

I can demonstrate how dynamic scenarios can impact upon the predicted critical depth by using the model to predict the compensation irradiance, I_C. The compensation irradiance is the irradiance at which phytoplankton photosynthesis exactly balances phytoplankton loss. It is an important parameter in the definition of the critical depth, because the critical depth is the mixed layer depth at which the average irradiance from the surface to the base of the mixed layer is equal to the compensation irradiance. It is generally believed to be a constant, based on phytoplankton physiology, and is estimated either from laboratory experiments, or estimated from satellite pictures of chlorophyll (e.g. Siegel et al. (2002)). However, in dynamic scenarios, the rates of grazing and non-linear phytoplankton mortality change according to the concentrations of phytoplankton and zooplankton, which would change the value of the compensation irradiance.

4.2.3.1 Calculating I_c analytically

Sverdrup's original model was based on the assumption that the phytoplankton growth is linearly dependent, with slope α, on the irradiance. As mentioned earlier, the relationship between the compensation irradiance, the constant mortality rate, and α_P is:

$$I_C = \frac{m}{\alpha P} \tag{4.6}$$

However, my model uses a non-linear *P-I* curve, so the equation to determine the compensation irradiance is derived through rearranging equation (4.4) (solution kindly provided by Prof. Tom Anderson and Dr. Adrian Martin):

$$I_C = \frac{V_{PT}}{\alpha_P}\left[\frac{{\theta_{Chl}}^2 \cdot {V_{PT}}^2}{m^2} - 1\right]^{\frac{1}{2}} \tag{4.7}$$

I calculated the analytical solution for a simulation with a constant chl-to-carbon ratio, $\theta_{chl} = 0.02\ (\text{mg Chl (mg C}^{-1}))$, a constant loss rate, m = 8.3 e^{-4} h^{-1} (0.02 d^{-1}), and the model value for $\alpha_P = 0.12\ (\text{gC (gChl)}^{-1}\ \text{h}^{-1}\ (\text{W m}^{-2})^{-1}$, using both equations (4.6) and (4.7). (Note that, because production is a function of

θ_{Chl} in my model, the actual form of the equation (4.6) used is $I_C = \frac{m}{\alpha_P \cdot \theta_{Chl}}$).

Both equations (4.6) and (4.7) predict a compensation irradiance of 0.3472 for the scenario outlined above.

The reason that both equations predict the same solution is that phytoplankton experiencing very low irradiance will only experience the very beginning of the *P-I* curve, which is linear. More precisely, when $\alpha_P \cdot I \ll V_{PT}$, so when $I \ll \frac{V_{PT}}{\alpha_P}$. Therefore, for a model run at a low irradiance i.e. without saturated growth, the initial slope of the P–I curve, α_P, can be used in Sverdrup's original formulation.

4.2.3.2 Calculating I_c numerically

There are three possible ways that I can predict the compensation irradiance from the model:

1. Replicating a laboratory experiment, by running a single, stationary phytoplankton super-individual at decreasing levels of irradiance, until I find the lowest level of irradiance at which it can survive
2. The critical depth can also be described as the point above which the average irradiance (i.e. calculated from the surface down to the critical depth) is equal to the compensation irradiance. Therefore, if I use the model to calculate the critical depth for a particular scenario, as described in section 4.2.1, I can then determine the compensation irradiance by calculating the average irradiance over the entire mixed layer.
3. Running a fixed slab model, and calculating the net growth (photosynthesis – total loss) at each depth in the water column. The compensation irradiance is the irradiance at the depth where net growth is zero.

If I_c is a constant determined only by phytoplankton physiology, then all three of these methods should, theoretically, produce the same result.

Determining the compensation irradiance in a laboratory involves growing phytoplankton cells under low irradiances, in order to find the lowest

irradiance at which they can survive. In order to simulate this with the model (Method 1), I used a fixed slab model with a single, stationary phytoplankton cell. As I was only interested in the effects of a single irradiance level (i.e. the surface irradiance, no attenuation) I used a very shallow mixed layer (1 metre) to represent the phytoplankton remaining at the surface. I also assumed no nitrogen limitation, as this does not feature in eq. (4.4). I ran each simulation until the phytoplankton either declined to (or very close to) 0, or reached a steady, positive, state. If the phytoplankton did not die out, I repeated the simulation, with a slightly lower irradiance.

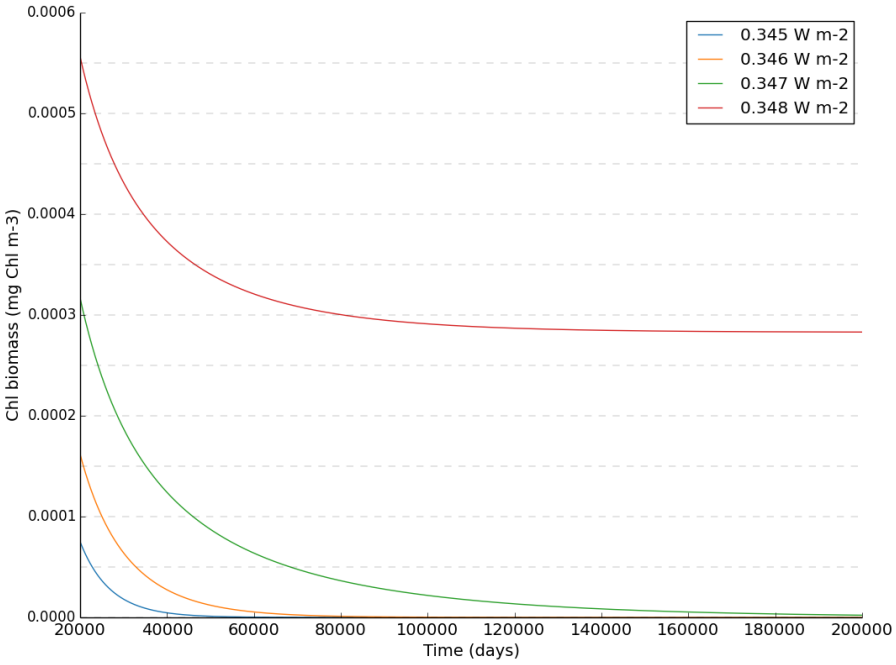

Figure 84: Predicted steady-state chlorophyll under a range of different irradiances for phytoplankton in a 1 metre mixed layer (no nutrient dependence, no mixing)

Figure 84 shows that the first irradiance level that allows the phytoplankton to reach a steady state (i.e. photosynthesis at a rate high enough to balance their loss rate) is 0.347 W m^{-2}. This is the same value as predicted by both forms of the analytical equation (linear and non-linear) in the previous section.

The next method of calculating the compensation irradiance is to calculate the integrated irradiance between the surface and the mixed layer depth, if the mixed layer depth is equal to the critical depth (Method 2). In section 4.2.1, I

calculated the critical depth for a particular scenario (θ_{Chl} = 0.02 mg chl (mg C)$^{-1}$, k_{par} = 0.04 m^{-1}, and I_0= 10 W m^{-2}) using a fixed-slab model, and the random position movement algorithm. The model predicted a critical depth of 706 m (the deepest depth at which the phytoplankton reached a steady-state). The average irradiance over this depth, calculated by finding the average of the function describing the attenuation of irradiance with depth (described in section 4.2.2) is 0.354 W m^{-2}.

The final way to measure the compensation irradiance is by finding the irradiance at the depth in the water column where phytoplankton growth and loss is in exact balance (Method 3). To do this, I ran a simulation with a fixed mixed layer depth and irradiance, and then calculated the net phytoplankton growth rate at each 1 metre interval, finding the point at which this became negative, and then taking the compensation irradiance to be the irradiance 1 metre above this point. This provides a slight underestimation of the true compensation irradiance, which would be somewhere in between these two depths. Doing this shows that I_c is not a constant value. For example, a simulation with a mixed layer depth of 100m and a surface irradiance of 10 W m^{-2} will predict a compensation irradiance of 2.1 W m^{-2}, whereas a simulation with a mixed layer depth of 500m and a surface irradiance of 10 W m^{-2} will predict a compensation irradiance of 0.52 W m^{-2}. This is because deeper mixed layers, with the same surface irradiance, have lower average irradiances over the entire depth. This reduces the average rate of photosynthesis, which results in lower concentrations of phytoplankton. As the phytoplankton concentration decreases, the specific rate of non-linear mortality and grazing will also decrease, meaning that the phytoplankton require a lower rate of photosynthesis in order to balance out the rate of loss. The irradiance at which the rates of growth and loss are in balance (i.e. the compensation irradiance) is therefore also reduced. This demonstrates that the compensation irradiance, and therefore the critical depth, is not a constant, because it is a function of the phytoplankton (and zooplankton) concentration, which changes over time.

4.2.3.3 Comparing the Lagrangian results with Eulerian results

I ran the simulations for sections 4.2.2 and 4.2.3.2 with the Eulerian model, in order to compare and understand any differences.

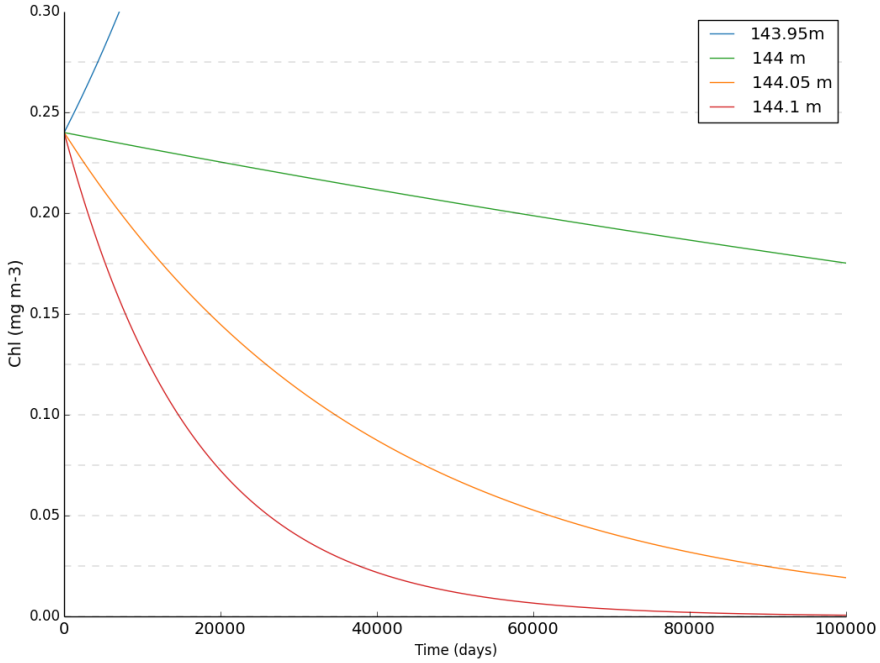

Figure 85: Predicted chl biomass for the completely Eulerian version of the model, for a constant irradiance (10 W m^{-2}), a fixed mixed layer depth, constant θ_{Chl} (0.02 mg mg-2), and a linear loss rate (0.1 d^{-1})

Figure 85 shows the results predicted by the Eulerian model for the scenario described in section 4.2.1 (I_0 = 10 W m^{-2}, θ_{Chl} = 0.02 mg Chl (mg C)$^{-1}$, m = 0.1 d^{-1} and k_{par} = 0.04 m^{-1}). The analytical equation predicted a critical depth of 141.67m, and this was demonstrated numerically with the Lagrangian model. However, the Eulerian model predicts a deeper critical depth (~144 m). This results from the way that the Eulerian model is implemented, as it integrates from the surface to the base of the mixed layer depth in 1-metre steps; there is no attenuation in the first metre. The Lagrangian model, on the other hand, calculates the exact attenuation at any point in the water column, leading to a greater precision in the predictions. Rounding the depth of each super-individual up to the nearest metre in order to calculate its ambient irradiance causes the model predictions to converge (i.e. increases the critical depth predicted by the Lagrangian model). In the same way, increasing the precision of the Eulerian model, by integrating over steps of 0.1 m decreases the critical depth predicted by the Eulerian model to ~141 m.

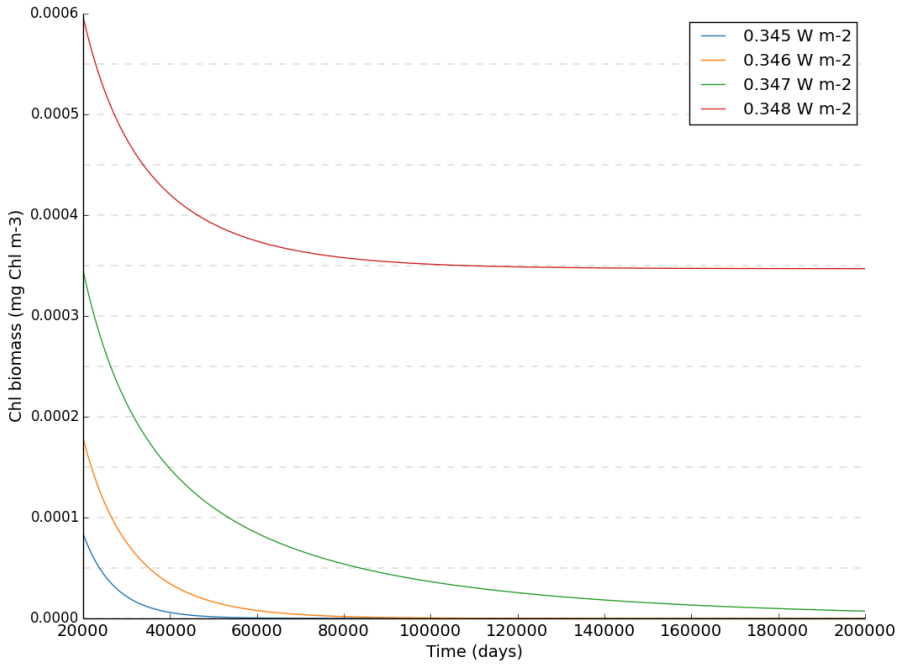

Figure 86: Compensation irradiance, as predicted by the Eulerian model

Using the Eulerian model to predict the compensation irradiance based on method 1 (section 4.2.3.2) produces an identical result to the Lagrangian model. This is because both models assume that the phytoplankton super-individual is at the surface, and so there is no light attenuation.

4.2.4 Calculating the critical depth over the build up to the spring bloom for Station India

In the section 4.2.1, I introduced the analytical equation to calculate critical depth, and in section 4.2.2, I showed that, for a fixed-slab, steady state model, the only phytoplankton loss term that affects the critical depth significantly is the linear respiration rate. In this section, I show the controls on critical depth in a dynamic model, and demonstrate the relationship between the mixed layer depth, the critical depth, and the net phytoplankton growth rate.

Calculating the critical depth requires knowledge of the attenuation coefficient, k_{par}. In order for this to be a constant value throughout the water column, I calculated attenuation as in Evans and Parsons (1985), who used a single value for k_{par}, based on the average phytoplankton biomass (nitrogen) in the water column:

$$k_{par} = k_w + k_c \cdot P_{conc} \quad (4.8)$$

where k_w represents the light attenuation coefficient for water, k_c represents the light attenuation due to chlorophyll, and P_{conc} is the phytoplankton nitrogen biomass (mmol N m^{-3}).

This gave a slightly different annual cycle of phytoplankton and dissolved inorganic nutrients than using the Anderson (1993) model:

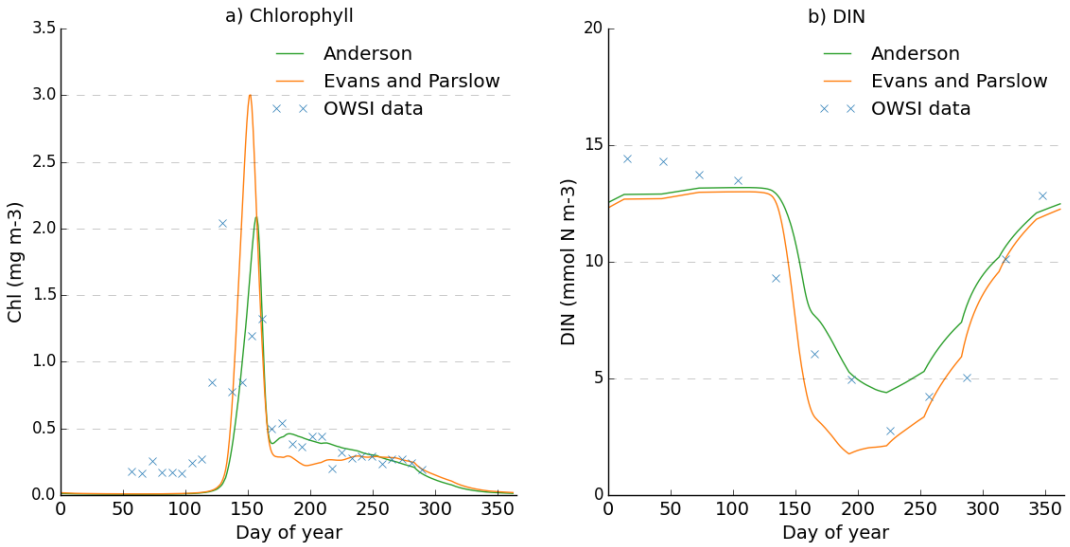

Figure 87: The seasonal cycle of a) chlorophyll and b) dissolved inorganic nitrate for the full Station India Model, using the Anderson 1993 model compared to the model using the Evans and Parslow 1985 model. Both simulations use the randomisation movement method.

The predicted seasonal cycle of phytoplankton using the Evans & Parslow (1985) model of attenuation shows increased production compared to the model that uses the model of attenuation from Anderson (1993). These results are very similar to plots produced by the EMPOWER model, ((Anderson et al., 2015), which includes settings for both the Evans and Parslow (1985), and Anderson (1993) methods of light attenuation. The Anderson (1993) model shows a decrease in predicted production, due to the increase in attenuation in the surface layers. The increase in production in the spring, shown by the increased magnitude of the spring bloom, in the Evans and Parslow model, results in a lower concentration of DIN over the summers, leading to the

reduced chlorophyll concentration shown here, compared to the Anderson model.

As shown in section 4.2.1, there are four variables that effect the value of the critical depth: the light attenuation, k_{par}; the chl-to-carbon ratio, θ_{Chl}; the surface irradiance, I_0; and the total phytoplankton mortality rate, m. For the first set of simulations, I investigated the relationship of each of these variables to the predicted critical depth, over the period of the run-up to the spring bloom (i.e. the first 100 days of the year). I used equation (4.5) to calculate the predicted critical depth for each day, using updated values for each of the four variables, taken from the model at run-time. I used the annual cycle of irradiance, however, in order to simplify the analysis, I removed the diel cycle of irradiance, setting the daily irradiance to the average over the 24 hours.

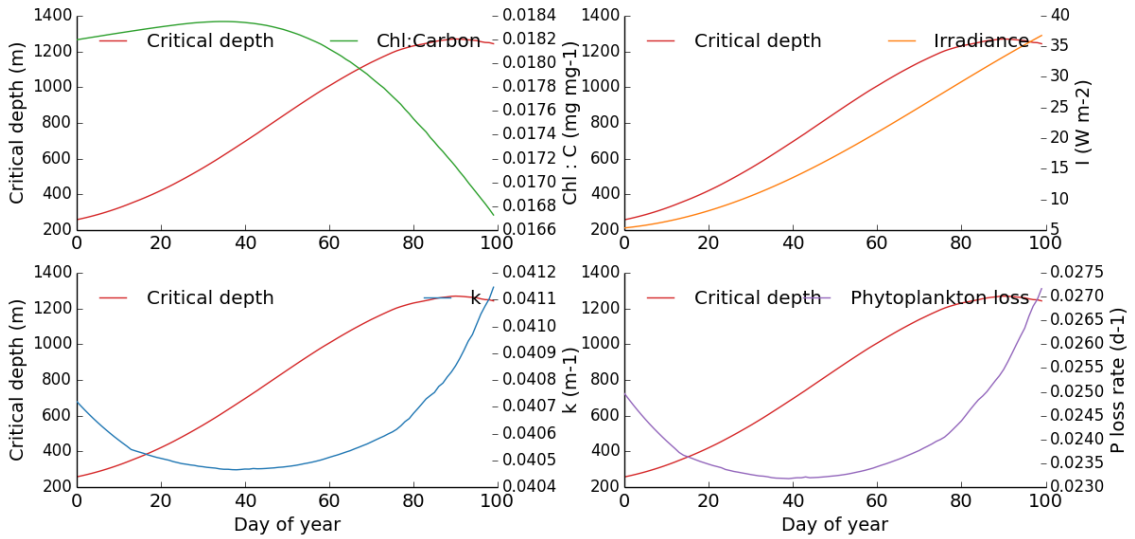

Figure 88: Relationship between the variables that influence the critical depth (I, chl:carbon, k, m) over the first 100 days of the Station India model, with no diel cycle of irradiance

Figure 88 suggests a correlation between the critical depth and each of the four variables investigated. In order to further test how each variable affected the predicted critical depth, I ran the model three more times, each time setting a different variable to a constant value. The light attenuation I set to 0.04 d^{-1} (attenuation due to water only), in order to see how removing self-shading affected the predicted critical depth. The chl-to-carbon ratio I set to the average value over the 100 days in the full model (0.018 mg mg^{-1}). In order to use a constant for mortality, I applied a linear term for mortality, which I parameterised to the average rate of phytoplankton loss over the first 100

days of the year in the full model (0.024 d^{-1}). However, applying this rate of loss over the full annual cycle resulted in levels of chlorophyll over the summer that were outside the workable boundaries of the model (i.e. too high), so I only applied this linear mortality rate over the first 100 days of year 3 (the section of data being analysed). I wanted to see if setting any of these variables to a constant value affected the way that the predicted critical depth changed over the first 100 days. If the increase in critical depth shown in Figure 88 resulted from a change in one of these variables, then setting it to a constant value would change the slope of the plot of critical depth against time.

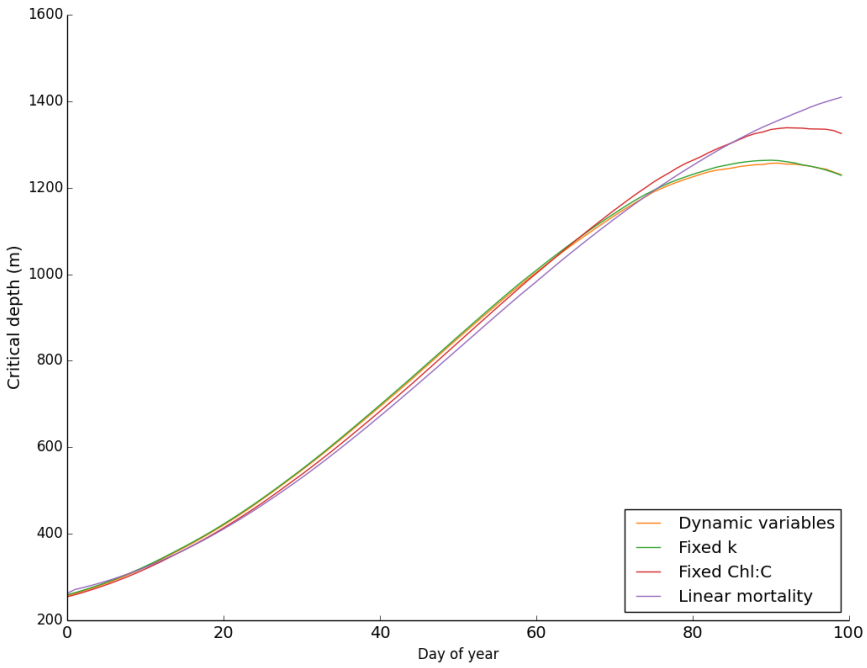

Figure 89: Predicted critical depth for a simulation with a) all variables using dynamic variables, b) fixed k, c) fixed Chl:C, and d) linear mortality

The results in Figure 89 are somewhat unexpected. The predicted critical depth does not appear to be significantly affected by setting any of the variables to a constant value. There is also little difference in the first day where the mixed layer depth is shallower than the critical depth – day 36, day 35, day 37, and day 37 for the simulations with all dynamic variables, constant k_{par}, constant chl-to-carbon and linear mortality, respectively. There are, however, some small variations:

1. Using a fixed value for chl-to-carbon results in a deeper predicted critical depth after day 80. This is because, as the irradiance increases, the chl-to-carbon ratio decreases in the dynamic model, which reduces the rate of photosynthesis. A reduced rate of production results in a shallower critical depth.
2. Removing the non-linear mortality (i.e. setting the mortality to a constant, linear rate, shown by the purple line), prevents the predicted critical depth from becoming shallower around day 90, as it does in the model that includes non-linear mortality. This is because, as the phytoplankton concentration increases, a non-linear rate of mortality results in a higher specific rate of loss, and therefore a shallower predicted critical depth.

Figure 89 suggests that the main control on the predicted critical depth in the model is the surface irradiance. I tested this by running the simulation again, but this time with constant values for θ_{Chl}, k_{par}, and with a constant, linear mortality rate.

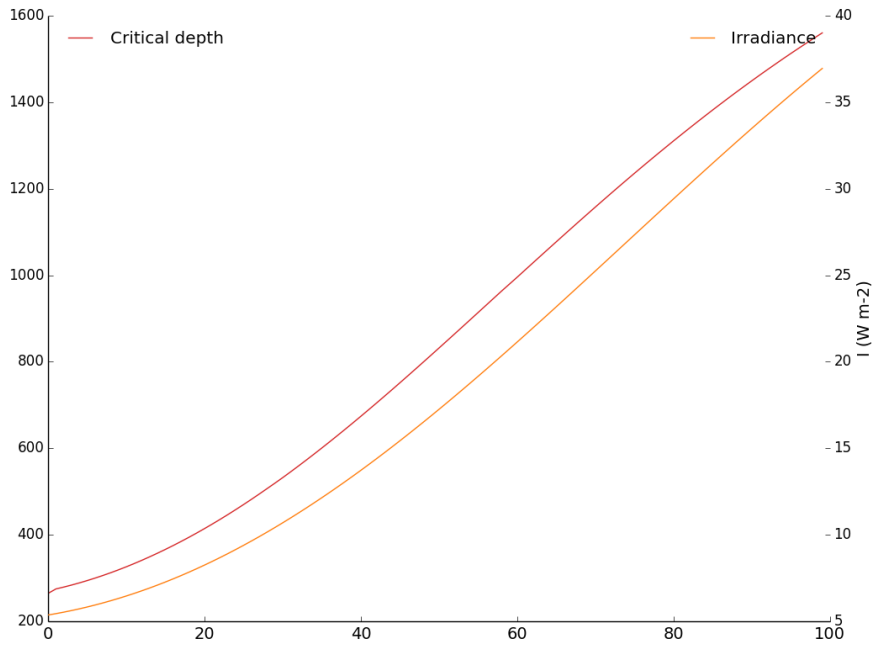

Figure 90: The relationship between critical depth and irradiance for a model with fixed θ_{Chl}, k_{par}, linear mortality

Figure 89 and Figure 90 show that the increase in predicted critical depth over the first 80 days of the year is almost entirely due to the increase in irradiance. After this, the predicted critical depth starts to decrease, due to the increase in phytoplankton concentration resulting in a higher specific phytoplankton loss rate, although this is tempered by the reduction in the rate of photosynthesis that results from the lower ratio of chlorophyll to carbon due to the seasonal increase in surface irradiance. The critical depth deepens beyond the mixed layer depth on day 37.

4.2.5 Determining whether the spring bloom is triggered by the mixed layer depth shoaling above the critical depth

In order for the spring bloom to take place, the rate of production in the mixed layer needs to exceed the rate of loss (Siegel et al., 2002; Sverdrup, 1953). Therefore, as defined by Llort et al. (2015), the initiation of the spring bloom is the point where the net phytoplankton production first becomes positive. The critical depth hypothesis proposes that this occurs when the mixed layer depth shoals above the critical depth, and in this section, I test this hypothesis by using the analytical model to calculate the daily predicted critical depth for the OWS India model, and comparing this to the model predictions of net specific phytoplankton growth rates.

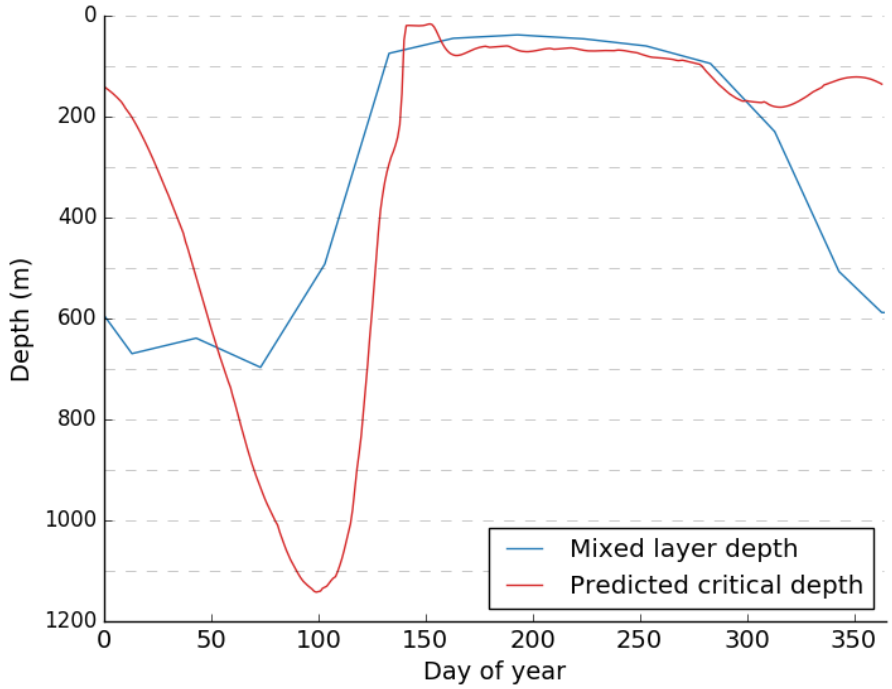

Figure 91: The predicted critical depth (calculated through the use of the analytical equation described in (4.5)) for the OWS India model.

Figure 91 shows the predicted annual cycle of critical depth for OWS India, based on the phytoplankton loss rates predicted by the model. The critical depth is calculated for each time step, and then averaged over 24 hours, in order to find the daily average critical depth. This is a more accurate method than using the daily averaged irradiance in order to calculate the critical depth, the reasoning for which is explained in section 4.2.5.1. At the beginning of the year, the critical depth is less than 200 m, which is shallow compared to the mixed layer depth, which is deeper than 600 m. At this point, the critical depth is controlled by the irradiance, because both phytoplankton and zooplankton production are very low. As the year progresses, increases in irradiance start to increase the critical depth, until it deepens past the mixed layer depth. Around day 100, it then starts to shallow once more, due to a combination of the decreases in mixed layer depth resulting in an increase of averaged irradiance across the water column, and an increase in phytoplankton production resulting in an increase in the turbidity of the water column, plus an increase in the mortality rate both from natural mortality and grazing. The peak of the phytoplankton spring bloom, around day 140, results in the critical depth shallowing above the mixed layer depth once more, suggesting that light

limitation could play a part in controlling the magnitude of the peak of the spring bloom. Over the summer, the critical depth is very shallow, due to the shallow mixed layer depth and the high concentration of phytoplankton both reducing the available light, and increasing the total phytoplankton loss rate. The critical depth then remains relatively shallow as the mixed layer depth deepens, until the increase in seasonal irradiance, the following year.

4.2.5.1 Calculating critical depth based on daily averaged irradiance versus daily averaged critical depth

I ran the full OWS India model, using the random position movement algorithm, without the diel cycle of irradiance, for 3 years, and took the data from the first 100 days of the last year. I calculate the predicted critical depth, using the full model, and plotted this against the mixed layer depth, to find the point where the mixed layer depth shoaled above the critical depth. I also plotted the net nitrogen-specific grown rate (growth – loss), noting in particular where this became positive. If the critical depth hypothesis is correct, then the net growth rate should become positive at the point where the mixed layer depth and critical depth cross.

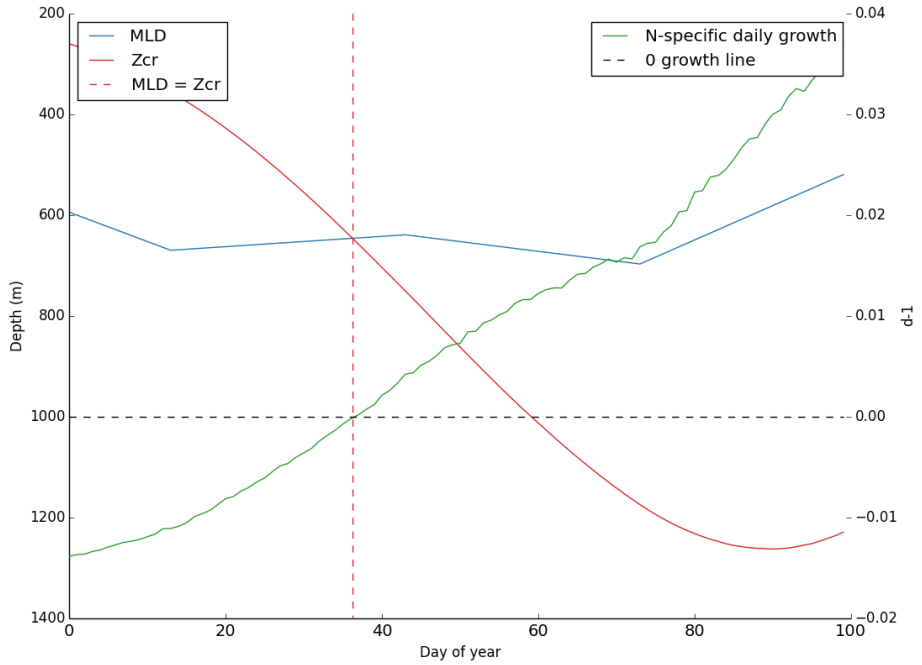

Figure 92: The predicted critical depth (analytical equation) and the net specific growth rate for the first 100 days of a simulation parameterised for OWS India, but with no diel cycle and the irradiance set to the daily averages for OWS India

Figure 92 shows that the net specific growth rate becomes positive (green line crosses dashed line) at the same time that the critical depth becomes deeper than the mixed layer depth (red line crosses blue line). It is interesting to note that it is the critical depth deepening below the mixed layer depth due to the increase in irradiance that results in the net phytoplankton growth rate becoming positive, rather than the mixed layer depth physically shoaling above the critical depth. At the point where the net growth becomes positive, the mixed layer depth is still deep (> 500m). This suggests that the spring bloom is driven by the seasonal increase in irradiance rather than by the shoaling of the mixed layer.

For the next simulation, I reintroduced the diel cycle of irradiance. Since I wanted to calculate a daily value for the critical depth, I could either calculate it based on the daily averaged irradiance, or I could calculate the critical depth based on the model output for each time step, and then calculate the average critical depth over each day.

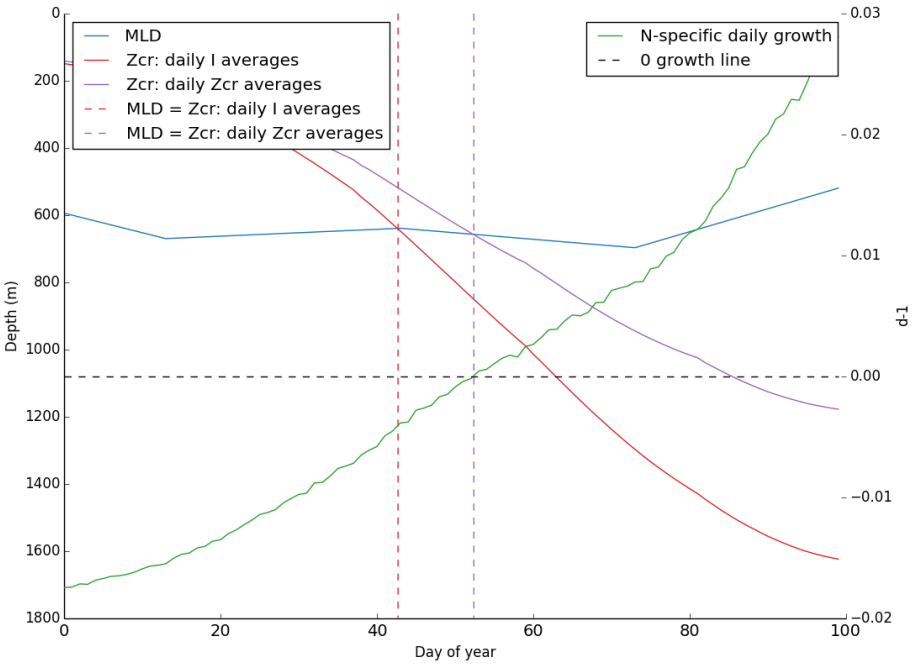

Figure 93: The model predicted critical depth and net daily n-specific growth rates for the first 100 days of the simulation with a diel cycle

Figure 93 shows the predicted critical depth for the same simulation, calculated in two different ways. The red line shows the daily critical depth calculated using the daily averaged irradiance for a simulation with a full diel cycle of irradiance, and the purple line shows the daily averaged critical depth, calculated from the critical depth predicted for each time step, from a model with a full diel cycle of irradiance. The predictions of daily critical depth using the daily averaged irradiance are deeper than those that are predicted using the average of the critical depths calculated each time step, because of the non-linear relationship between the rate of photosynthesis and the irradiance. Sverdrup proposed the use of the daily averaged irradiance to calculate critical depth, as he was using a model with a linear dependence of photosynthesis on irradiance.

4.2.6 The sensitivity of the critical depth

The critical depth is dependent on parameters that are notoriously difficult to measure, such as the rate of respiration. Here, I investigate how sensitive the critical depth, and therefore the point at which net production becomes

positive, is to changes in the rates of respiration and mortality. Firstly, I determine the important loss terms over the period of interest (i.e. the first 100 days of the year) by plotting the specific rates of respiration, non-linear mortality, mixing, and grazing.

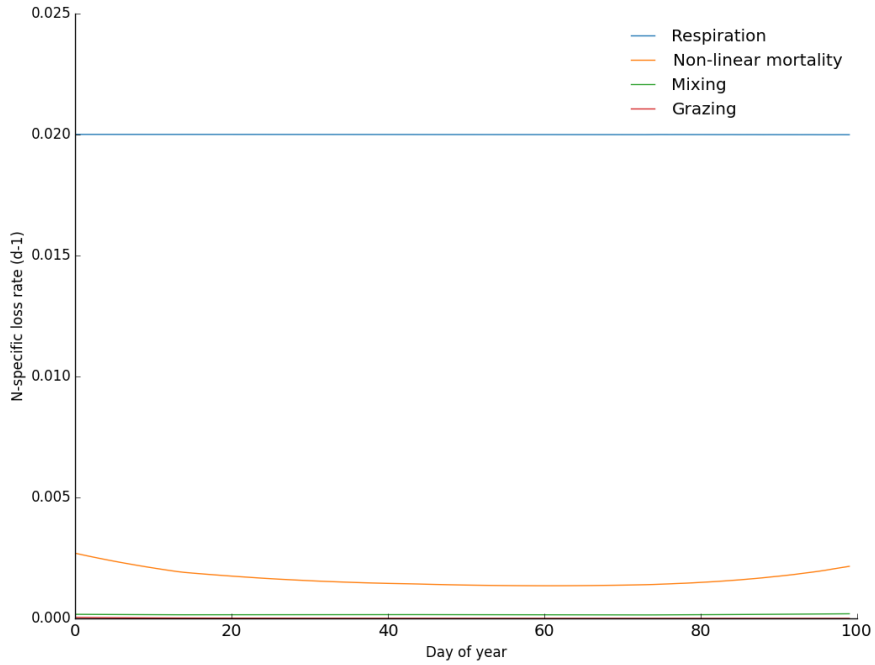

Figure 94: The nitrogen specific phytoplankton loss rate of the first 100 days of the year in the Station India model, separated into losses from grazing, respiration, mortality and mixing

Figure 94 shows that the main source of phytoplankton loss over the first 100 days of the year for the Station India model comes from the linear respiration. Due to the low concentrations of phytoplankton resulting from the deep mixed layer, and lower irradiance, the non-linear mortality rate is very low, and the grazing rates are negligible. Therefore, I focussed on the phytoplankton loss parameters p_1 (respiration) and p_2 (non linear mortality).

For the first set of simulations, I ran the model, with the full ecosystem and seasonal cycle, but using values for p_1 ranging from 0.0025 to 0.04 d^{-1} (standard value = 0.02 d^{-1}) . Figure 95 shows the predicted critical depth compared to the phytoplankton net growth rate when the respiration is halved and doubled (i.e. p_1 = 0.01, 0.02 and 0.04 d^{-1}). The simulation was run for three years, and the data in Figure 95 are taken from the final year.

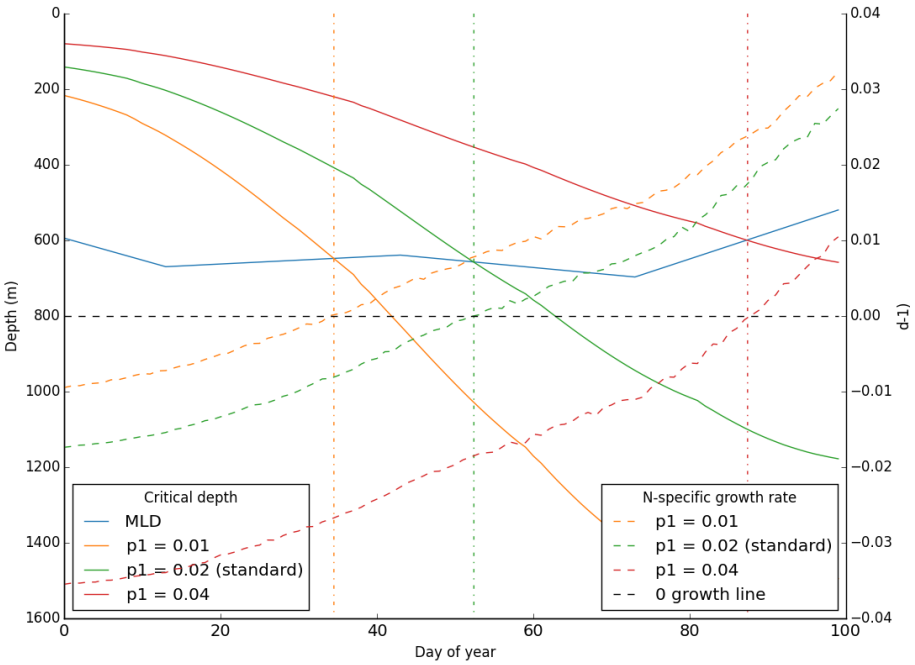

Figure 95: The predicted critical depth and daily specific growth rates for simulations with respiration rates of p_1 = 0.01, 0.02 and 0.04 d-1

Figure 95 shows the daily-predicted critical depth for each simulation, over the first 100 days (solid red, orange and green lines), along with the daily net specific growth rates (dashed red, orange and green lines). This demonstrates the sensitivity of the predicted critical depth to the linear rate of respiration (p_1). An increased rate of respiration leads to a shallower critical depth, because a higher rate of phytoplankton loss requires a higher rate of phytoplankton photosynthesis, in order to ensure the survival of the phytoplankton population. This can only be achieved with a higher rate of integrated irradiance, which comes from a shallower mixed layer depth. Doubling or halving the respiration rate impacts upon the point at which the mixed layer depth (solid blue line) shallows above the critical depth, and therefore the point at which net production becomes positive. The other important features of Figure 95 are the points where the mixed layer depth shallows above the critical depth (solid blue line crosses solid red, orange, green lines), and the points where the net growth rate becomes positive (dashed red, orange and green lines cross dashed black lines). In all cases, net

production does not become positive, until the mixed layer is shallower than the critical depth.

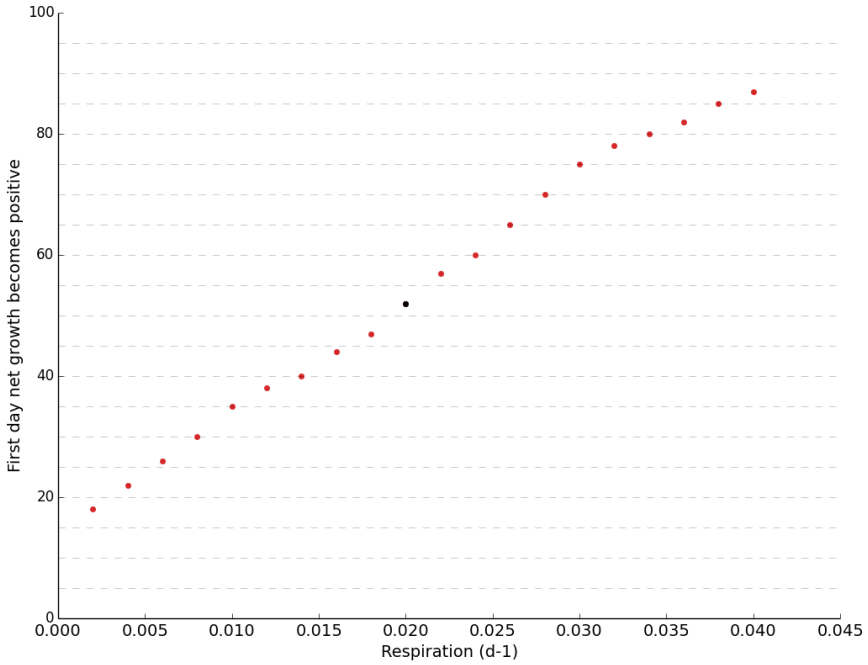

Figure 96: Relationship between rate of respiration and the first day where the net growth becomes positive after the winter

Figure 96 shows how the day on which the net phytoplankton growth rate becomes positive changes is proportional to the rate of respiration.

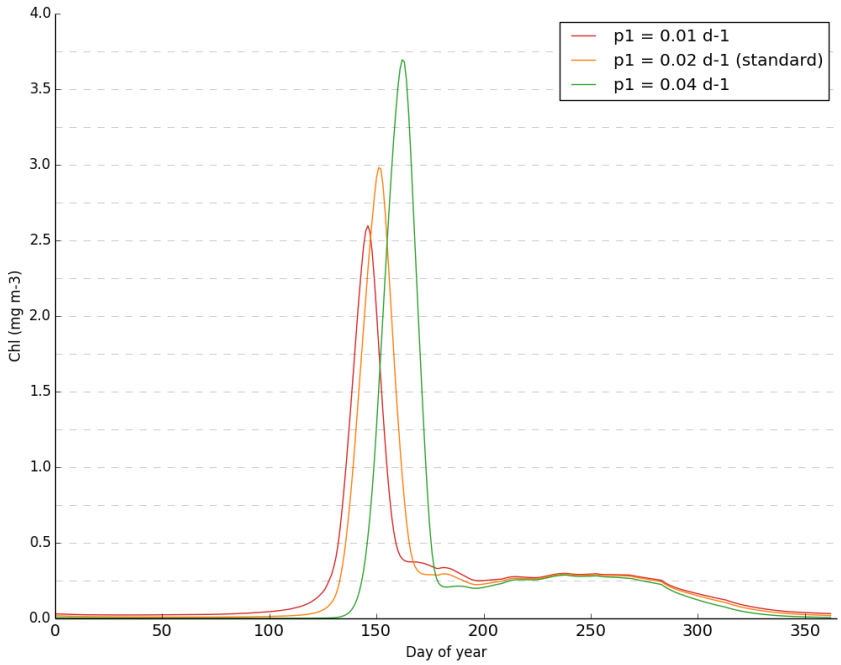

Figure 97: The annual cycle of predicted chlorophyll biomass for simulations with varying rates of respiration (p_1 = 0.01, 0.02 and 0.04 d-1)

Figure 97 shows how halving and doubling the rate of respiration affects the predicted annual cycle of integrated chlorophyll. Decreasing the rate of respiration results in a spring bloom peak that is both earlier, and smaller in magnitude. The predicted critical depth is deeper, because the daily loss rate is lower, and therefore a lower rate of production will balance respiration (i.e. a decreased compensation irradiance). This means that the mixed layer will shallow above the critical depth earlier in the year, resulting in an earlier spring bloom

I next repeated the experiment, but this time I doubled and halved the non-linear mortality rate (p_2). Although the non-linear mortality does appear to be a significant source of phytoplankton loss in Figure 94, increases and decreases to the parameter value do not appear to have a significant effect on either the predicted critical depth, or the point at which the net production becomes positive (Figure 98).

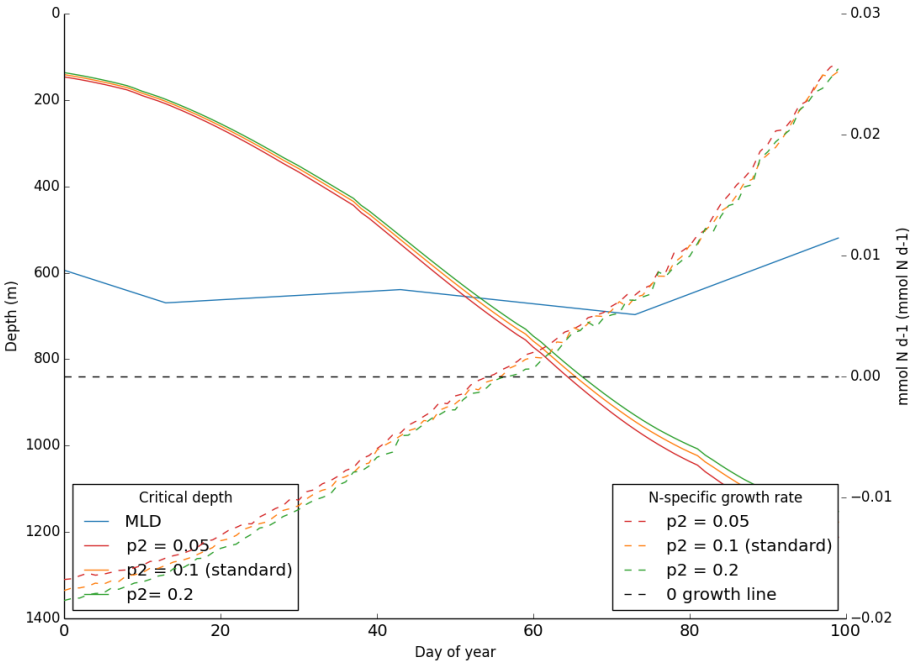

Figure 98: The predicted critical depth and daily specific growth rates for simulations with non-linear mortality rates of p_2 = 0.05, 0.1 and 0.2 d-1

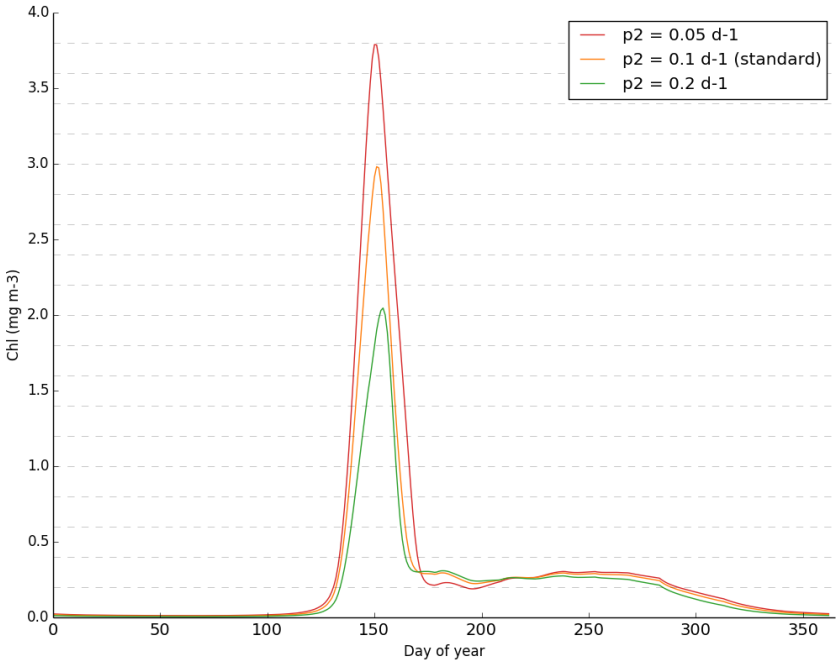

Figure 99: The annual cycle of predicted integrated chlorophyll biomass for simulations with varying rates of non-linear mortality (p_2 = 0.05, 0.1 and 0.2 d-1)

Figure 99 shows the predicted annual cycle for each of the simulations with the different values for p_2, and suggests that changes in non-linear mortality affect the magnitude of the spring bloom, but not the timing. Plotting the chlorophyll concentration over the first 100 days, shows this more clearly.

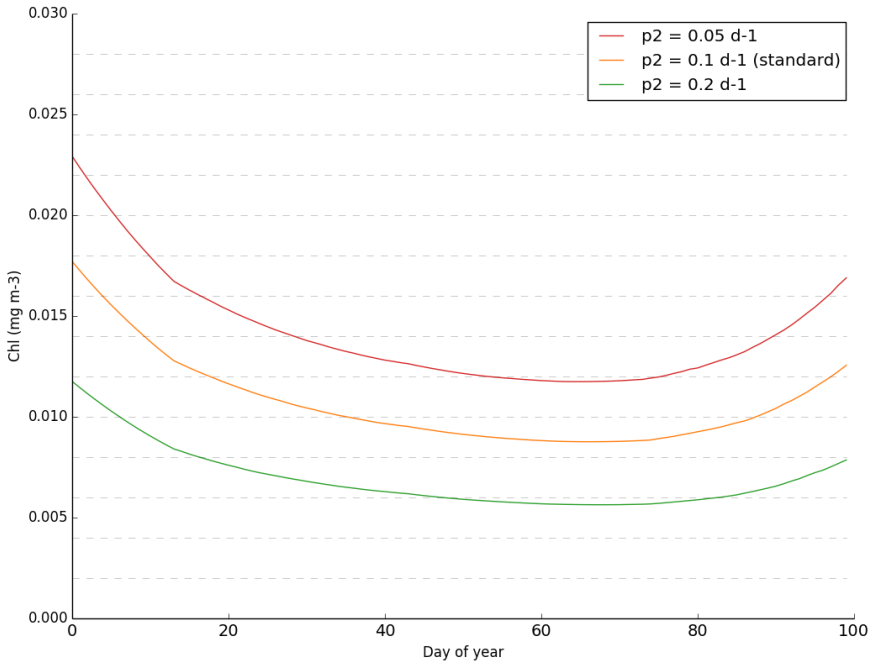

Figure 100: The first 100 days of predicted integrated chlorophyll biomass for simulations with varying rates of non-linear mortality (p_2 = 0.05, 0.1 and 0.2 d^{-1})

Figure 100 clearly shows that changes to the value used for p_2 affects the magnitude of the spring bloom, but not the timing.

I repeated these simulations, although this time doubling and halving the half saturation constant for phytoplankton non-linear mortality, k_p, but neither the timing or the magnitude of the spring bloom appeared to be sensitive to this parameter (Figure 101 and Figure 102).

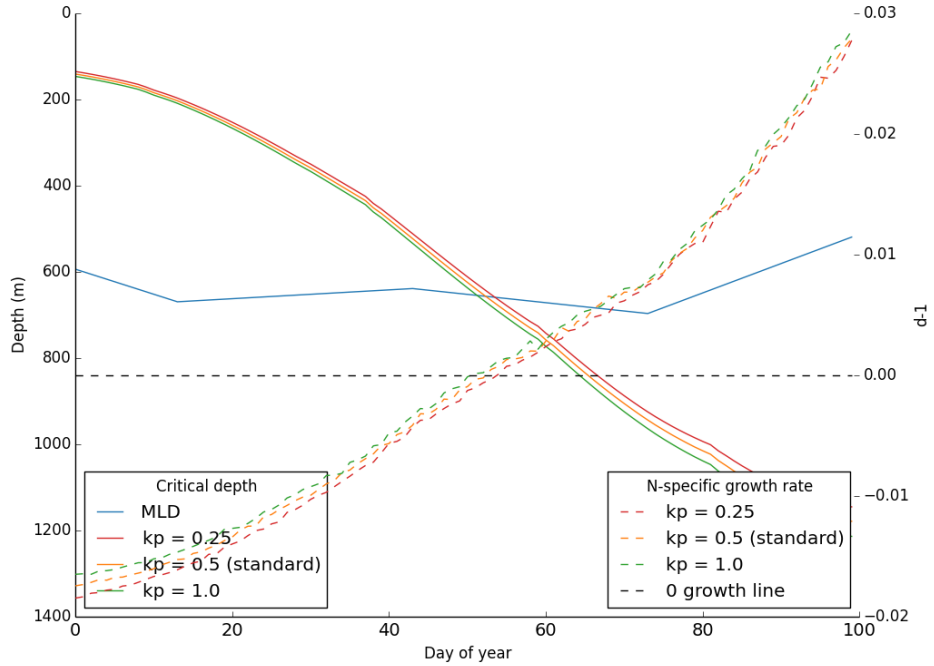

Figure 101: The predicted critical depth and daily specific growth rates for simulations with half-saturation constants of k_p = 0.25, 0.5 and 1.0 d-1

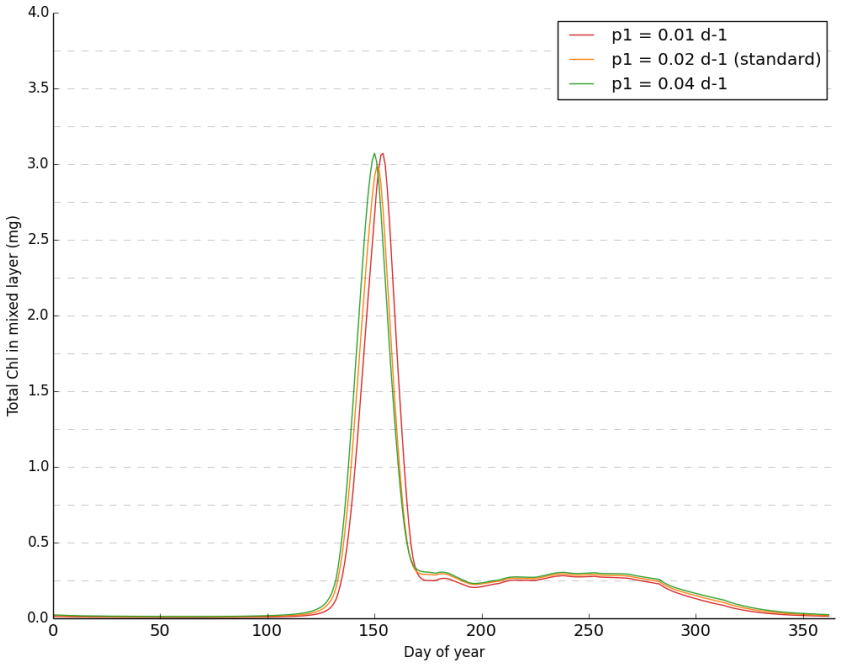

Figure 102: Predicted seasonal cycle of integrated chlorophyll for the simulations with k_p = 0.25, 0.5 and 1.0

Figure 94 suggested that there were two significant sources of phytoplankton loss over the time leading up to the initiation of the spring bloom: respiration, p_1 (linear), and non-linear mortality, p_2. However, performing a sensitivity analysis on these two parameters has demonstrated that, whilst the magnitude of the spring bloom can be affected by p_2, the timing of the bloom is almost entirely controlled by the value chosen for p_1.

This section has demonstrated that there is a predictable critical depth, as proposed by Sverdrup, for the mixed layer, above which net phytoplankton production can become positive, an essential condition for the start of the spring bloom. I have further demonstrated that the critical depth is not a constant value, but depends upon the phytoplankton and zooplankton concentrations.

4.3 The disturbance-recovery hypothesis

In this section, I use the model to investigate the disturbance-recovery hypothesis, as proposed by (Behrenfeld & Boss, 2014). The disturbance-recovery hypothesis states that the spring bloom is a result of decoupling between phytoplankton growth and loss, during times of extremely low phytoplankton concentrations, due to deep mixed layers, polar nights, eddies, or other physical processes. I investigated this hypothesis by running two versions of the OWS India model: the first with a constant mixed layer depth of 200m, and the second with a constant mixed layer depth of 200m, but that deepened to 500m for the last day of the year. This should have the effect of reducing the concentration of phytoplankton, and, in theory, decoupling the phytoplankton growth and loss. If, as according to the critical depth hypothesis, the spring bloom is purely a product of mechanical factors, i.e. the shoaling of the mixed layer above the critical depth, then these two simulations should produce similar predictions of the timing of the spring bloom.

Both simulations included the seasonal cycle of forcing (e.g. temperature and wind speed) and full ecosystem parameterised for OWS India. The simulations were run for three years, and the data in Figure 103 were taken from year 3.

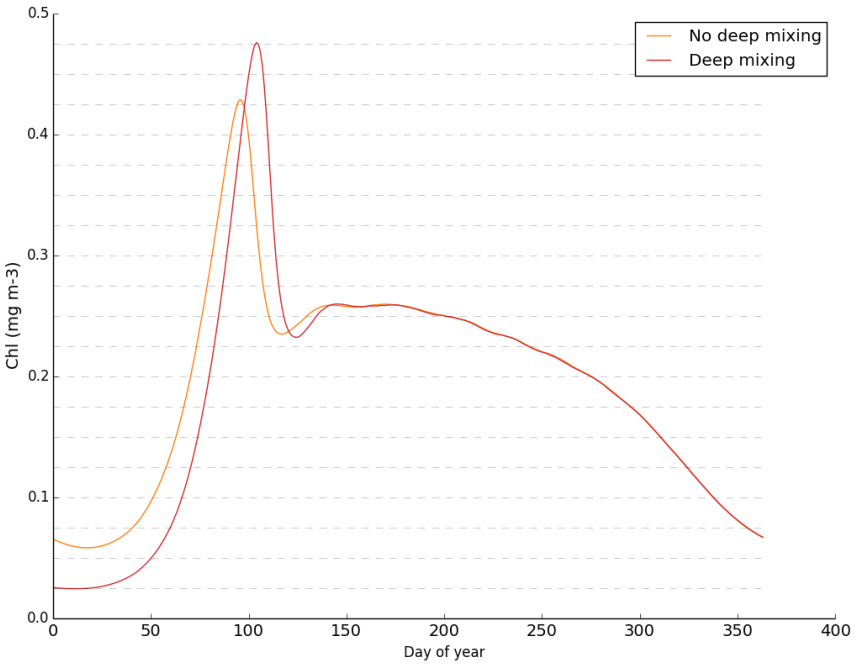

Figure 103: Predicted seasonal cycle of integrated phytoplankton chlorophyll for a simulation with a fixed mixed layer depth of 200m for two scenarios: the first with a constant mld for the entire simulation, and the second with the mld deepening to 500m for the final day of the year.

In Figure 103, the model with the single day of deep mixing shows a delay in the peak of the spring bloom. The phytoplankton and zooplankton concentrations are diluted by the mixed layer deepening, and then a large amount of biomass is detrained and lost from the simulation when the mixed layer depth shallows back to 200 m. This dilution means that the specific non-linear loss rate on the phytoplankton is reduced, and the decreases in the zooplankton population mean that it takes longer for grazing to catch up with phytoplankton growth.

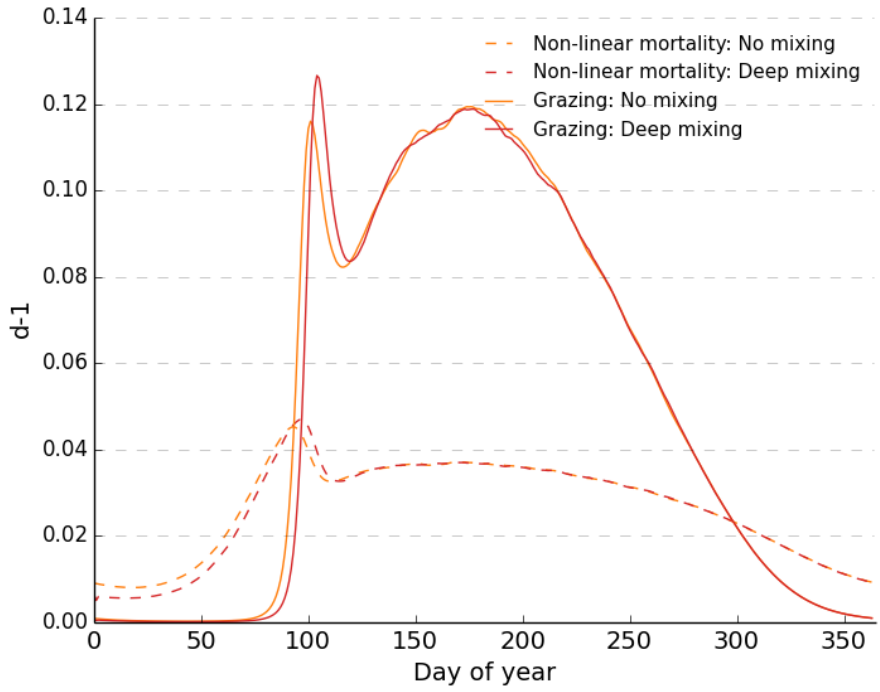

Figure 104: Specific rates of grazing and non-linear mortality for the OWS India model, set with a fixed mixed layer depth (200 m), and the simulation with the mixed layer depth set to 200m, but deepening to 500 m for the last day of the year.

Figure 104 shows how the specific rates of grazing and non-linear mortality change over the course of the year. The dilution of the phytoplankton and zooplankton on the last day of the previous year has reduced the specific grazing rates and non-linear mortality of the phytoplankton in the simulation with the deep mixing (red lines). After the peak of the spring bloom, the grazing and non-linear mortality have caught up with the phytoplankton, and the two model predictions converge.

This dependence on the non-linear loss rates appears to be contrary to the findings in section 4.2, where I demonstrated that the linear loss rate has the greatest impact on the critical depth and therefore the timing of the initiation of the spring bloom. However, I also demonstrated that there is a difference between predicted critical depths from steady-state simulations i.e. the deepest mixed layer depth to which the model predicts a positive steady-state value for the phytoplankton concentration (where concentrations decrease to such a level that non-linear loss rates fall close to zero), and the predicted critical depth for a particular moment during a simulation, where the

phytoplankton may not be in steady-state. Non-linear mortality and grazing losses have a far greater importance in dynamic scenarios.

As in the previous section, I can calculate and plot the predicted critical depth against the mixed layer depth, and compare this to the point when the net specific phytoplankton growth becomes positive. This reveals that although the peak of the spring bloom is delayed by the deep mixing, the spring bloom is initiated (point where net growth becomes positive) earlier (Figure 105). This demonstrates the difference between basing the timing of the bloom on specific growth rate or on biomass accumulation. For the simulation with the day of deep mixing, the bloom is initiated earlier, but allowed to proceed for longer, so that the peak appears after the peak of the bloom for the simulation with no deep mixing.

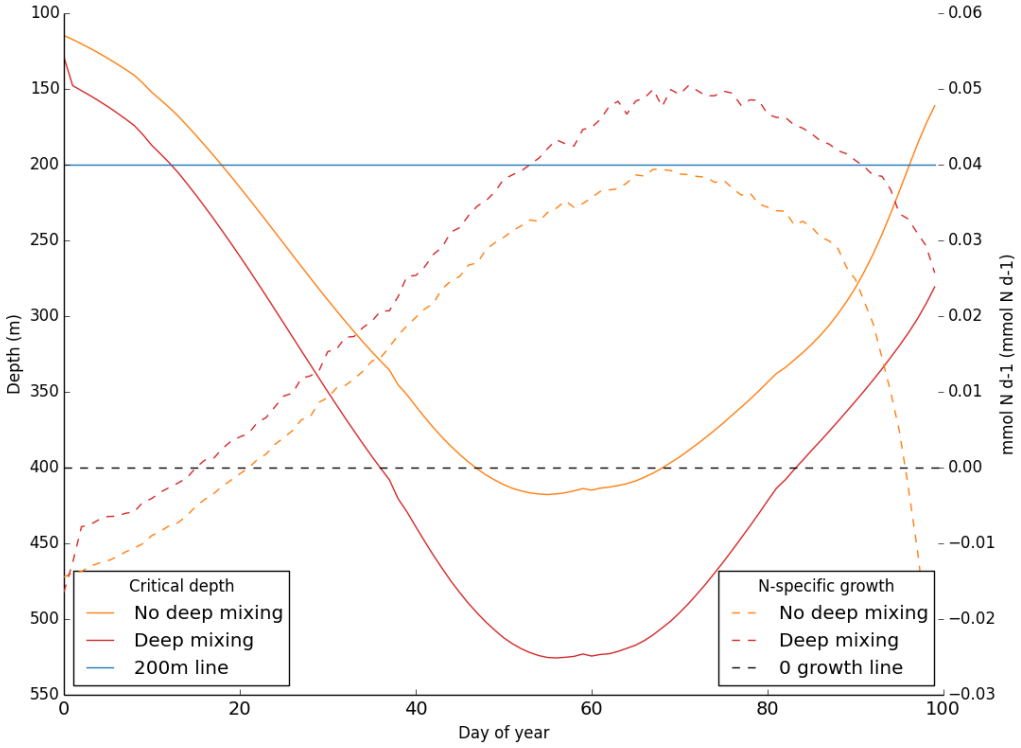

Figure 105: The predicted critical depth and net growth rate for the first 100 days of a fixed slab model, with a constant mld (200m), and a full seasonal cycle of forcing, for two scenarios: the first with a constant mld for the entire simulation, and the second with the mld deepening to 500m for the final day of the year.

This has demonstrated some important points. Firstly, as suggested by Behrenfeld (2010) and Behrenfeld & Boss (2014), measurements of the

maximum chlorophyll concentrations may not give a good indication as to the timing of the initiation of the spring bloom i.e. the model with the single day of deep mixing shows an earlier positive net growth rate of phytoplankton, but a later peak in chlorophyll concentration. Secondly, the critical depth and disturbance-recovery hypotheses are not mutually exclusive. Instead, the disturbance-recovery hypothesis describes a mechanism that can affect the predicted critical depth: reductions in phytoplankton and zooplankton concentrations lead to reductions in the non-linear loss rates, which change the critical depth. For both scenarios in Figure 105, the net production does not become positive until after the mixed layer depth has shoaled above the predicted critical depth.

4.4 Critical turbulence

Huisman et al. (1999) proposed that there are two independent mechanisms that drive the development of phytoplankton blooms: the classical critical depth theory, which is relevant for well-mixed environments, and the critical turbulence theory, which applies in cases with low to moderate mixing, and low turbidity. The critical turbulence hypothesis states that if the mixing rate falls below some critical value, then the resulting vertical profile of phytoplankton will allow sufficient phytoplankton growth near the surface to ensure that a bloom can develop, regardless of the depth of the mixed layer. Therefore if the mixing rate is below the critical value, the growth dynamics are independent of processes further down in the water column and the production by the phytoplankton should not be affected by changes to the mixed layer depth.

Up until now, I have been using the random position movement algorithm, in order to ensure that the phytoplankton super-individuals are fully mixed through the water column. However, in order to investigate the critical turbulence hypothesis, the mixing rate needed to be changed in some quantifiable and meaningful manner, so the simulations in this section use the random walk movement algorithm (described in Chapter 2). Figure 106 shows the predicted cycle of chlorophyll for the random walk model, compared to the model using the random position movement algorithm.

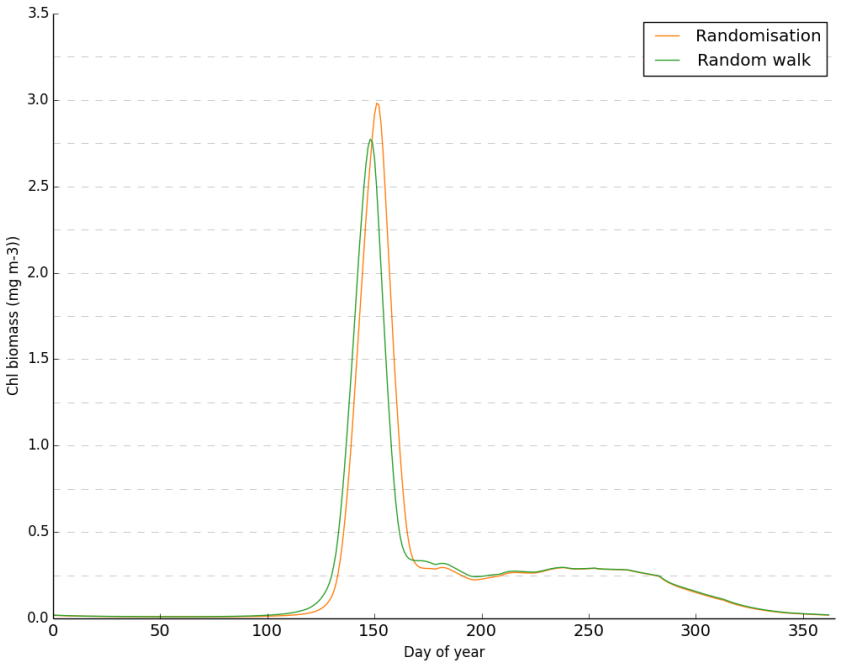

Figure 106: The annual cycle of chlorophyll predicted by the model using the random position movement algorithm (30 minute time step) and the random walk algorithm

The random walk model predicts a spring bloom peak that occurs earlier and is of a higher magnitude than the random position model. The differences between the predictions from the random walk and random position movement algorithms result from the non-homogeneous vertical profile of phytoplankton in the random walk model. This occurs because the mixing rate is not high enough to overcome the phytoplankton growth rates, and the phytoplankton near the surface have more time to grow. Figure 107 shows the average vertical chlorophyll profile from the surface to 500m for both movement algorithms, over the first 100 days of the year (data taken from year 3 of a 3 year simulation).

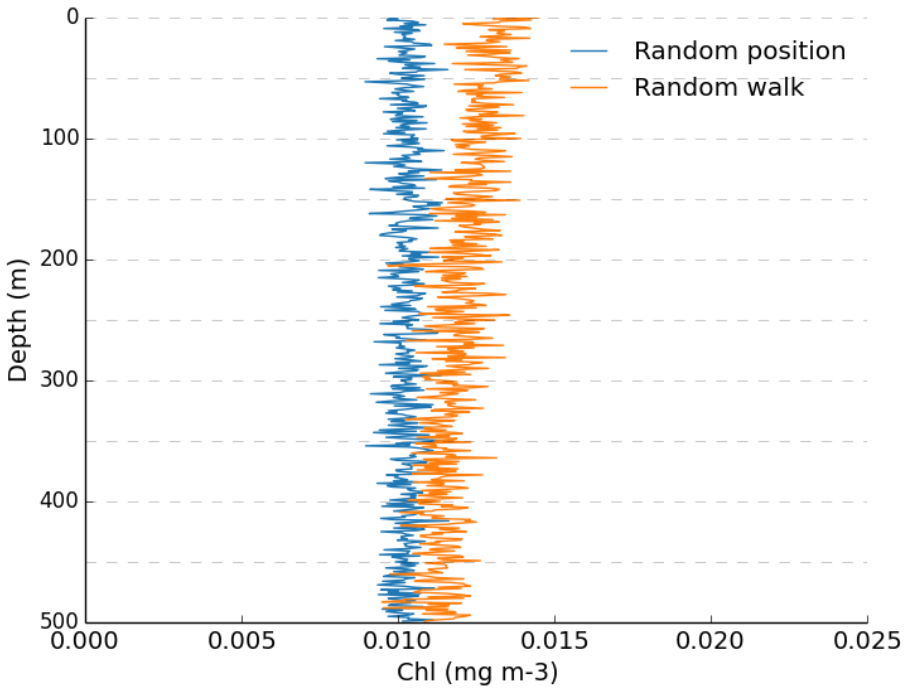

Figure 107: Comparison of the average vertical profile of chlorophyll over the first 100 days of the year of the OWS I model, using the random position and random walk movement algorithms

The differences in the vertical profiles of chlorophyll in Figure 109 are not a result of differences in the mixing rates. Plotting the diffusivity coefficient for the random walk model, and the assumed diffusivity for the random position model (how this is obtained is described in Chapter 2), shows that the random walk model has a higher rate of mixing over the first 100 days of the year (Figure 110). However, as explained in Chapter 2, even when the random position and random walk movement algorithms use the same diffusivity, they are not directly comparable, because there is a degree of relatedness between each step in the random walk model. Reducing the mixing rate in the random walk model increases the proximity of one step to the last, whereas reducing the mixing rate in the random position model (by increasing the time step) increases the length of time spent at each depth, but has no effect on the relationship between one step and the next.

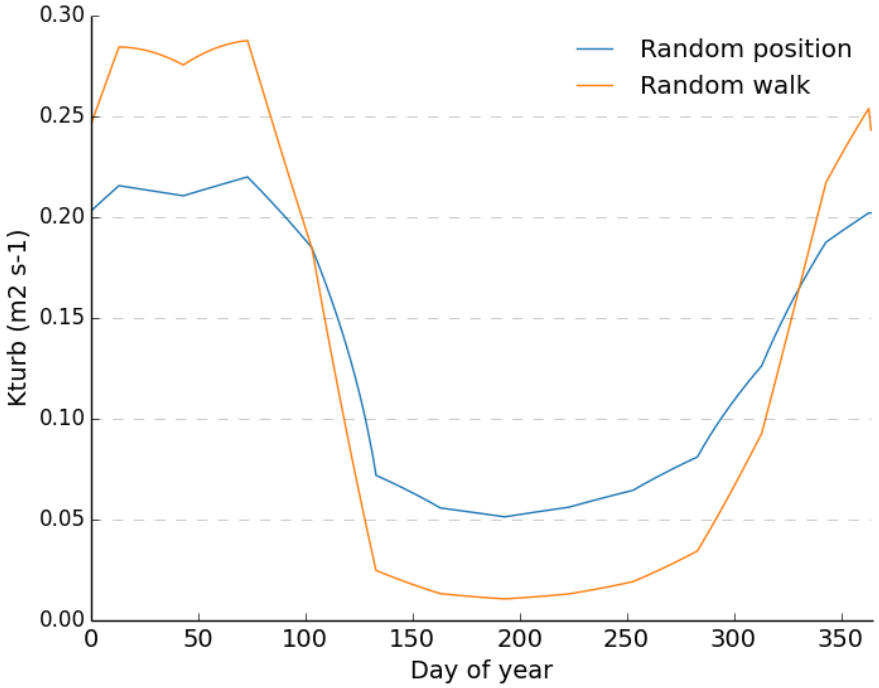

Figure 108: Seasonal cycle of diffusivity coefficients for the random walk model and the random position model with a time step of 30 mins

The change in the timing of the peak of the spring bloom in the random walk model shown in Figure 107 suggests that there could have been a change to the timing of the initiation of the bloom. I therefore examined the net growth rate and predicted critical depth over the first 100 days of the year, in order to deduce whether the point where the net phytoplankton growth first becomes positive happens when the mixed layer depth is equal to the critical depth.

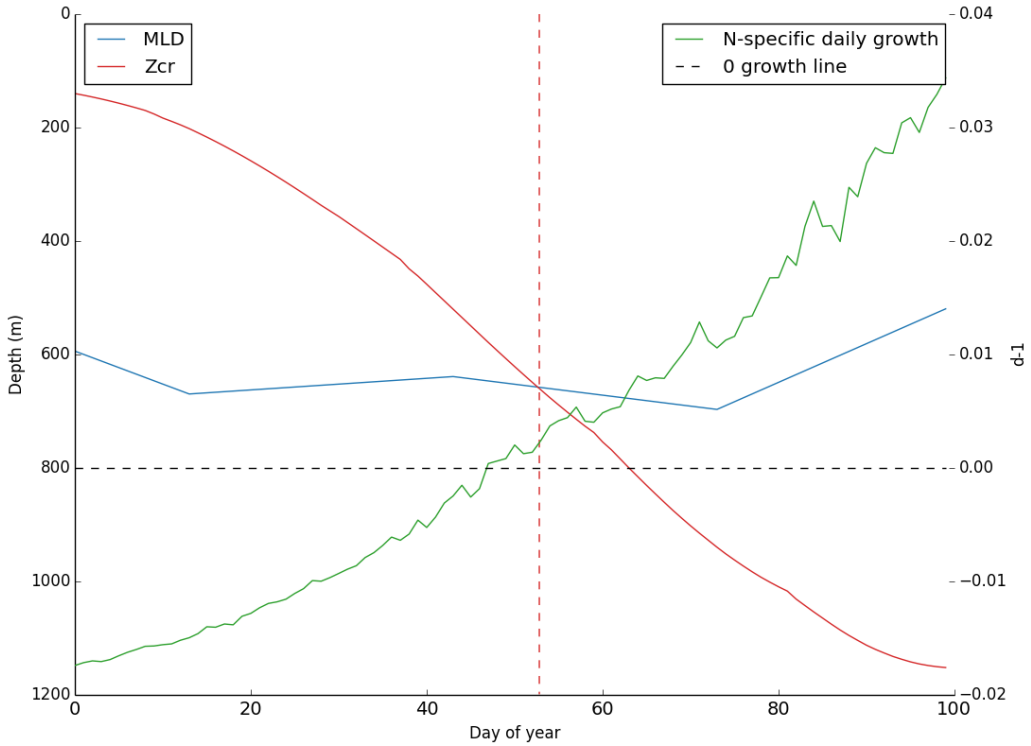

Figure 109: The predicted critical depth and net growth rate for the first 100 days of the year for the OWS I simulation, using the random walk model

Figure 109 shows that there is a lag between the net growth becoming positive (i.e. green line crosses the dashed line, day 47) and the critical depth deepening below the mixed layer depth (blue line crosses the red line, day 53). This would suggest that there is positive net phytoplankton growth, even though the mixed layer depth is deeper than the critical depth. This is happening because, as shown in Figure 107, the phytoplankton are not evenly distributed throughout the mixed layer, thus violating one of the assumptions of the critical depth hypothesis i.e. that mixing is high enough to result in an even distribution of phytoplankton. According to the critical turbulence hypothesis, this means that the mixing rate on day 47 is below the critical value, allowing a bloom to occur.

4.4.1 Calculating the critical turbulence for a fixed slab model

In order to investigate the critical turbulence, I set up a fixed slab model with a mixed layer depth deeper than the critical depth, and reduced the mixing rate

until the phytoplankton were able to reach a positive steady-state (i.e. not die out). In section 4.2.2, I demonstrated that the critical depth for a model using the random position movement algorithm (time step of 30 minutes) with a surface irradiance of 10 W m^{-2}, an attenuation coefficient, k_{par}, of 0.04 m^{-1}, no nutrient dependence, and with a constant ratio of phytoplankton chl-to-carbon (0.02 mg mg^{-1}) is 706 m. I ran the above scenario with the random walk model, but increased the mixed layer depth to 800 m, to ensure that all the phytoplankton died out. The turbulence diffusivity was based on a surface wind speed of 10 m s^{-1}, and was equal to 0.32 m s^{-1}. I then imposed decreasing values for K_{turb} on the model – usually K_{turb} is calculated as a function of the mixed layer depth, but I overrode this – until I found the rate of mixing below which the phytoplankton could reach a positive steady state. This was the critical turbulence, $K_{turb,cr}$ and, for this model scenario, $K_{turb,Cr}$ = 0.18 m^2 s^{-1}. This is a factor of ten higher than the value found by Huisman et al. in their model, however, they were investigating a model with a far higher level of background turbidity (0.2 m^{-1}). Increasing k_{par} to 0.2 m^{-1} for the above scenario, decreased the critical turbulence to 0.003 m^2 s^{-1}.

I could then use the model to test the assertion by Huisman et al., that once the mixing rate falls below the critical value, the phytoplankton production should be unaffected by changes to the mixed layer depth, I ran the simulation with increasing mixed layer depths, but with the same, imposed value for K_{turb} (0.18m^2 s^{-1}).

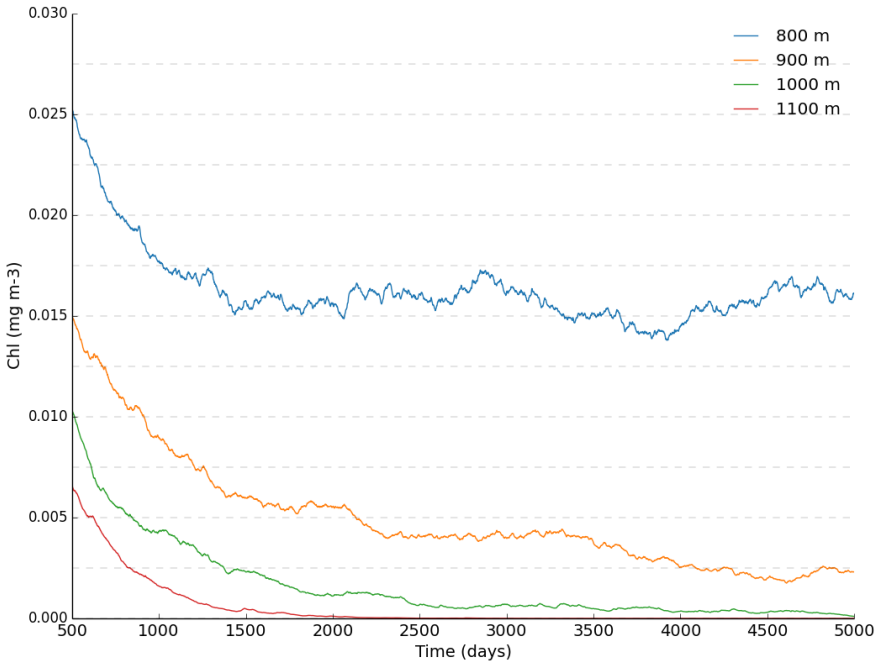

Figure 110: Predicted chlorophyll biomass for a simulation with a fixed diffusivity (0.18 m s^{-2}), fixed irradiance (10 W m^{-2}), fixed chl-to-carbon (0.02 mg Chl (mg C)$^{-1}$), and a fixed attenuation coefficient (0.04)

Figure 110 shows that even though the rate of turbulence is below the critical value necessary to allow a bloom when the mixed layer depth is at 800 m, deepening the mixed layer depth below 1000 m results in all of the phytoplankton dying out. There is still, it seems, a critical depth below which phytoplankton cannot survive, reducing the mixing rate has just deepened it. Instead of the critical depth and the critical turbulence being two independent mechanisms, the value of the critical depth is a function of the mixing rate (or rather, of the vertical profile of phytoplankton, which is a function of the mixing rate).

I investigated the relationship between the mixing rate and the critical depth by running a series of simulations for different mixing rates, under two different surface irradiances: 5 W m^{-2} and 10 W m^{-2}. The critical time in the OWS India model that determines the timing of the spring bloom and the magnitude of its peak is over the first 100 days. During this time, the daily average surface irradiance varies from ~5 W m^{-2} to ~12 W m^{-2}, and the mixing rate (diffusivity coefficient) is shown in Figure 108. In order to further relate these

results back to the full OWS India model, I reintroduced the variable chl-to-carbon ratio, and the nutrient limitation term in the photosynthesis equation. For each simulation, I used the model to predict the critical depth, by finding the deepest mixed layer depth at which the phytoplankton could still reach a positive steady-state.

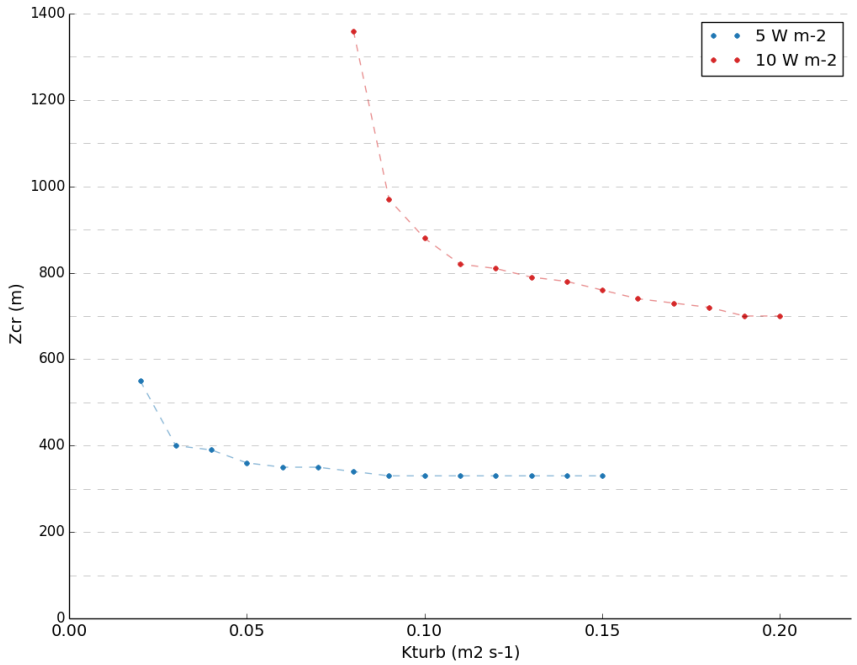

Figure 111: Critical depth predicted by a fixed slab model by finding the depth at which the phytoplankton could just survive (i.e. reach a positive steady) for a range of mixing rates, under constant surface PARs of 5 and 10 W m-2

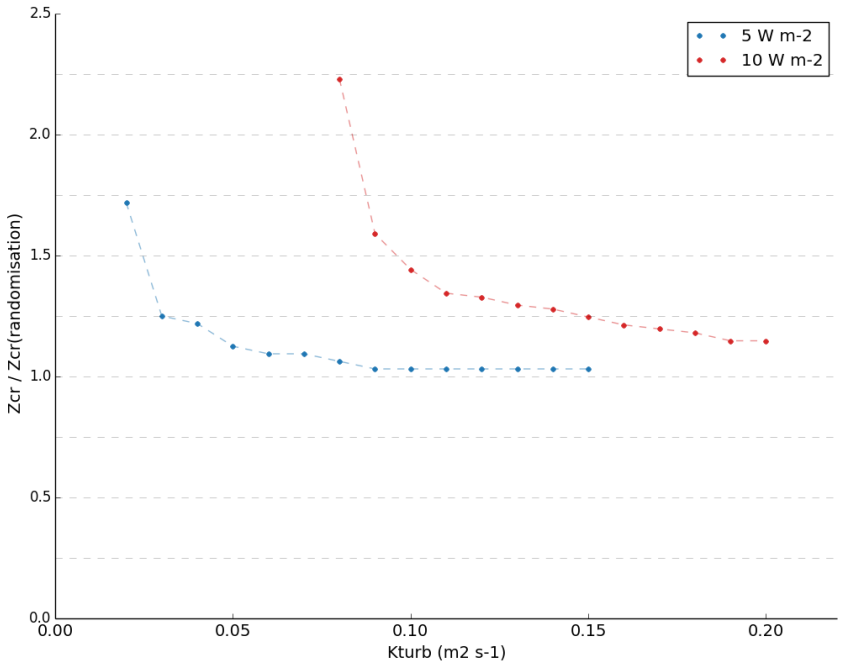

Figure 112: The critical depths predicted in Figure 111 normalised to the critical depth predicted by a model using the randomisation movement

Figure 111 shows the critical depths predicted by the fixed slab model, for a range of different mixing rates, under the two different surface PARs. It shows two important features: firstly, the relationship between the predicted critical depth and the mixing rate is hyperbolic, as the mixing moves towards 0, the critical depth will move towards infinity. At 0 mixing, the phytoplankton maintain their position in the water column, so the depth of the mixed layer will have no effect on the growth rate. Therefore, there will be no depth at which net production will become negative. Conversely, as the mixing moves towards infinity, the critical depth will reach a minimum, which equates to the value calculated using Sverdrup's original assumptions. Secondly, increases in the surface irradiance have a large effect on the shape of the curve describing the relationship between mixing and critical depth. This can be more clearly seen in Figure 112, where I have plotted each predicted critical depth normalised to the minimum possible critical depth for that scenario (i.e. the critical depth for a simulation with the random position movement algorithm, and a time step of 30 mins). A much lower mixing rate is needed to change the critical depth when the surface irradiance is 5 W m^{-2}, than when the surface

irradiance is 10 W m^{-2}. This means that it is not only the extent to which the turbulence is decreased that is of importance, but also the time of year. Low mixing rates earlier in the year could have less impact on the timing of the bloom, because, although the critical depth could potentially be deepened, it could still not be by enough to provoke a bloom.

These results vary from those predicted by Huisman et al. (1999), in that they show an hyperbolic relationship between the rate of turbulence and the depth at which no blooms are possible, whereas Huisman et al. suggested that the critical turbulence for a particular surface irradiance is a constant, below which blooms can develop, regardless of the depth of the water column and, above which, bloom development is dependent on the depth of the water column, as per Sverdrup. However, the first points plotted for both the scenarios with I_0 = 5 W m^{-2} and I_0 10 W m^{-2} in Figure 111 (K_{turb} = 0.02 and 0.08 m^2 s^{-1}, respectively), represent the lowest diffusivities at which the model could reasonably predict a critical depth. Below these values, the predicted critical depth moved beyond 15,000 metres, which is deeper than the deepest part of the ocean. This could explain the difference in the results obtained by Huisman et al., because they only investigated whether blooms were possible in mixed layer depths down to 1000m.

4.4.2 Calculating the critical depth for non-homogeneous phytoplankton profiles

For the final part of this section, I demonstrate that it is possible to predict the critical depth for a scenario with a non-homogeneous distribution of phytoplankton, if the vertical phytoplankton profile is known. I use the random walk model, with the value for K_{turb} calculated from a relatively low wind speed of 2.5 m s^{-1} (25% of the average value observed at OWS India). I used a low wind speed because I wanted the rate of mixing to be low enough to cause sufficient divergence from the predictions from the random position model.

The predicted critical depth for a scenario with a surface irradiance of 5 W m^{-2}, an attenuation coefficient, k_{par}, of 0.04 m^{-1}, no nutrient dependence, and with a constant ratio of phytoplankton chl-to-carbon of 0.02 mg Chl mg C^{-1} is 358 m. Running the random walk model with the mixing based on a surface wind speed of 2.5 m s^{-1} (K_{turb} = 0.0358 m^2 s^{-1}) results in positive steady state

phytoplankton population, with an average specific rate of production (gross) of 0.025 d^{-1}. This is above the linear respiration rate (0.02 d^{-1}), so this population will survive. To predict the critical depth, I took the normalised vertical chlorophyll profile of the steady state phytoplankton (the absolute value at each depth divided by the mean value over the mixed layer), and then fit a polynomial to the resulting profile (Figure 113).

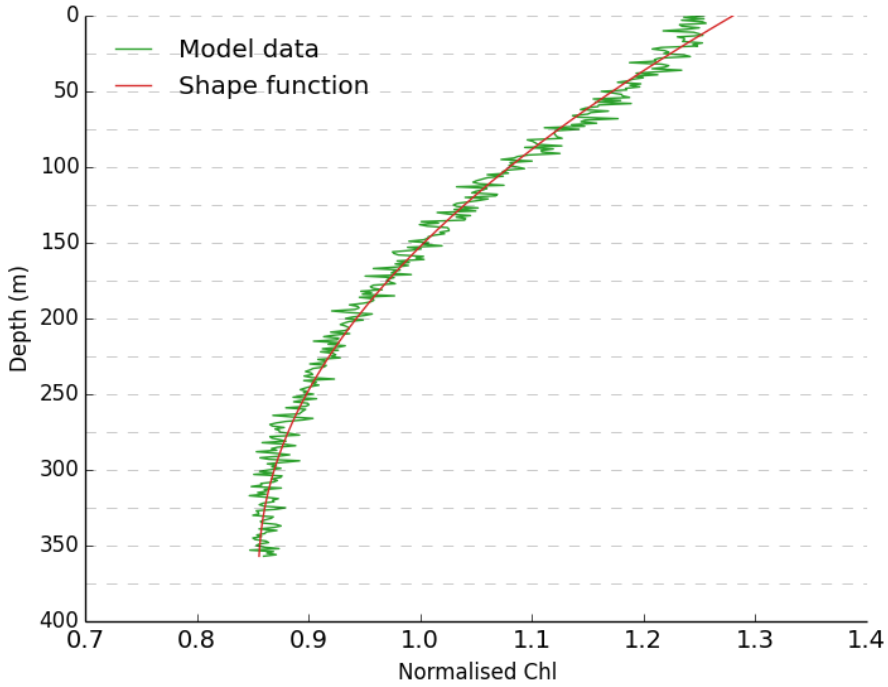

Figure 113: The normalised vertical chlorophyll profile from a simulation with a mixed layer depth of 358 m, surface irradiance of 5 W m^{-2}, surface wind speed 2.5 m s^{-1} (k_{turb} = 0.0358 m^2 s^{-1}), chl-to-carbon ratio of 0.02 mg Chl (mg $C^{)-1}$, no nutrient dependence, and k_{par} = 0.04 m^{-1}

The function of the curve shown in Figure 113 can then be used as a shape function to modify the calculation of the new production throughout the mixed layer. The shape function for the curve in Figure 113 is:

$$S_{chl} = \left(3.2e^{-6} \cdot z^2\right) - \left(2.3e^{-3} \cdot z\right) + 1.3 \qquad (4.9)$$

I could then estimate the average daily gross specific production in the mixed layer for scenarios with the same relative distribution, by numerically integrating equation (4.10), modifying the production at each depth by the shape function:

$$\sum Pc = \int_{z=mld}^{z=0} S_{Chl}(z) \cdot \theta_{Chl} \cdot \frac{\alpha_{Chl} \cdot I(z) \cdot V_{PT}}{\left(V_{PT}{}^{2} + \alpha_{Chl}{}^{2} \cdot I(z)^{2}\right)^{0.5}} \quad (4.10)$$

The depth for which equation (4.10) is equal to the linear rate of respiration (0.02 d^{-1}) is then the predicted critical depth. For the above scenario, this was 440 m.

I tested this prediction by running the scenario again, but this time with a mixed layer depth of 440 m. As the diffusivity coefficient is a function of the mixed layer depth, increasing the mixed layer to 440 m increased K_{turb} to 0.044 $m^2\ s^{-1}$. The phytoplankton were able to maintain a steady state at a depth of 440 m, with an average production rate of 0.020 d^{-1}, which is equal to the linear respiration rate, and a good indication that the method has been successful in predicting the critical depth. Increasing the mixed layer depth beyond 440 m resulted in the phytoplankton population declining.

4.5 Conclusions

In this chapter, I have tested three main hypotheses surrounding the controls of the initiation of the spring bloom, using a Lagrangian phytoplankton model with a full seasonal cycle. I have shown that these hypotheses can be reconciled if some of Sverdrup's original assumptions are relaxed. Although the study has successfully achieved its aims, it has also demonstrated that an Eulerian model using an appropriate step for integrations (i.e. 0.1 m) and that captured the same vertical profile of phytoplankton would have produced the same result.

The critical depth hypothesis was first formulated over 60 years ago, and has been hotly debated ever since. Testing the hypothesis is complicated due to the difficulties surrounding the necessary empirical measurements, such as the compensation irradiance, and the point where the net growth first becomes positive after winter. Siegel et al. (2002) proposed that laboratory measurements of compensation irradiance taken from the lowest irradiance at which a phytoplankton cell can survive are not necessarily applicable to oceanic environments, and my results have backed this up, showing how the compensation irradiance is not constant in dynamic scenarios, due to the changing rates of grazing and non-linear mortality. In addition, there has been

some controversy in the literature surrounding the definition of the start of the spring bloom. Behrenfeld (2010), Behrenfeld et al. (2013), and Behrenfeld & Boss (2014) suggested that peak chlorophyll concentration may not be a good indicator of the timing of the initiation of spring bloom, and my model has demonstrated this. Decreasing the concentration of phytoplankton by deepening the mixed layer at the start of the year will result in a delayed peak chlorophyll measurement, even though the net growth rate will become positive sooner. Finally, Sverdrup's assumption of phytoplankton that are evenly distributed throughout the mixed layer does not hold true for mixed layers with moderate turbulence rates, so accurately predicting the critical depth also requires knowledge about the rates of turbulence and mixing (Franks, 2014).

Traditionally, the critical depth hypothesis views the spring bloom as resulting from the mixed layer depth shoaling above the critical depth, but my model has shown that this is not necessarily the case. Increases to surface irradiance can increase the critical depth, so that net growth can occur even when the mixed layer is still deep (> 500m). This would account for studies that observe positive net phytoplankton growth without any mixed layer stratification, such as Behrenfeld (2010) who looked at a nine-year satellite record of phytoplankton biomass in the subarctic Atlantic, and found that in no case was positive net growth delayed until the mixed layer had shoaled significantly. Also, the model has given some indication as to how changes in external forcing and phytoplankton physiology can influence the critical depth. The critical depth is highly sensitive to the respiration rate, making this a crucial parameter in its definition. Also, increases in winter mixing that deepen the mixed layer and dilute the concentrations of both phytoplankton and zooplankton will reduce the specific non-linear phytoplankton loss rates, resulting in a decreased critical depth. Finally, if the turbulent mixing is reduced sufficiently to allow a nonhomogeneous vertical phytoplankton profile to develop, then both the timing of the initiation of the spring bloom and its peak will occur earlier.

There is plenty of opportunity for further research surrounding this topic, in particular regarding the parameterisation of the rates of respiration. These are usually parameterised as a constant, linear function of the biomass, which has

previously been criticised in the literature. Smetacek & Passow (1990) stated that maintenance respiration varies with growth rate, and that studies have shown that some species of diatoms show very low rates of respiration when grown at low irradiances. Lindemann et al. (2015) used a Lagrangian phytoplankton model to demonstrate that including variable rates of respiration (and sinking) in response to changes in irradiance allowed the model to capture the observed phytoplankton concentrations during deep mixing, and the timing and onset of the spring bloom at OWS Mike, in the North Atlantic. Fixed rates of respiration could only achieve the same result when using unrealistic model parameters. Also, this chapter focussed on the controls of the initiation of the spring bloom only, not on the timing and magnitude of its peak. Although I have shown that the point at which net growth becomes positive is predictable, given information regarding the turbulence, and the balance between the rates of growth and loss, the onset of the spring bloom does not necessarily impact upon the magnitude of its peak. In fact, the significant lag between the onset and the peak of the bloom shown in section 4.2.4 (> 50 days), raises the question of whether the net growth becoming positive is the sole mechanism controlling the climax and the peak of the spring bloom, or whether other factors have to come into play to result in the rapid increase in accumulated biomass that typifies the spring bloom.

Sverdrup's hypothesis was a mathematical simplification of a complex ocean phenomenon, which stated that phytoplankton blooms cannot take place, unless the conditions are favourable for positive net growth. This chapter has demonstrated that this theory is still valid, providing that additional factors, such as the turbulence and the balance between growth and loss, are taken into account. In addition, like Chapter 3, it has shown the utility of vertical phytoplankton profiles for the use of accurately predicting rates of photosynthesis for mixed layers with moderate mixing rates, providing further evidence that improving the accuracy of phytoplankton models could be improved by an increase in empirical observations regarding the vertical structure of phytoplankton in the mixed layer.

Chapter 5: Discussion

Ocean primary production constitutes an important link in the cycling of carbon between living and organic stocks, regulating the global climate through the removal of carbon dioxide from the atmosphere. At the same time, photosynthesis by oceanic phytoplankton is controlled by the availability of light and nutrients, which are, in turn, regulated by physical processes such as ocean circulation, mixed-layer dynamics, and the solar cycle. Understanding the relationships between the ocean biology and the climate depends upon the accuracy to which changes in the ocean ecosystems can be detected (Behrenfeld et al., 2006). Numerical and computational models can provide insight into these relationships, and recent technological advances in computer hardware, software, and data storage have allowed researchers to greatly expand their range of modelling tools. However, as Einstein is believed to have once said, "…everything should be as simple as it can be, but not simpler" (Prausnitz, 2002). In other words, before embarking on the construction of a complicated model of a system, it is important to be satisfied that a simpler model would not be just as suitable for the job at hand. In addition, if a more complex simulation will provide differing predictions to an equivalent simpler formulation, it is important to understand what is driving the differences between the two formulations.

The present study has focussed on gaining understanding into the potential differences between two marine ecosystem formulations: one that models all phytoplankton biomass as a homogeneous concentration (Eulerian), and the other which allows for the tracking of individual variability in phytoplankton individuals as they are mixed through the changing light field (Lagrangian). In addition, two ecological questions are investigated via Lagrangian modelling studies: whether the individual response of phytoplankton to their local irradiance affects the overall rates of primary production, and whether understanding the mechanisms that control the timing of the onset of the spring bloom requires knowledge about mixing rates, and individual phytoplankton growth rates.

Lagrangian models represent primary production as a number of particles, each of which experiences a different light history as they are vertically mixed through the surface layer of the ocean. It is a complex approach, requiring a number of decisions regarding its implementation, and a number of these were approached in Chapter 2. The resulting model included Lagrangian phytoplankton, a full ecosystem, with explicit state variables for zooplankton, detritus, and dissolved inorganic nitrate, with new techniques employed for dealing with the interactions between the Eulerian and Lagrangian components of the model. In order to obtain the model parameters, in particular, the parameters controlling photoacclimation, the model was set up for Ocean Weather Station in the North Atlantic. Empirical data were used to parameterise the turbulent mixing, and therefore also the random walk model that determined how the phytoplankton were redistributed each time step. In Chapter 3, the model was used for an intercomparison study, which was the first study of its kind to directly compare equivalent Eulerian and Lagrangian formulations of a full ecosystem model that included a seasonal, and diel, cycle of forcing. The results were unexpected – the two models demonstrated very similar predictions, and further investigation, through the use of controlled, fixed-slab models showed that the phytoplankton were moved through the mixed layer too fast to have time to acclimate to their local irradiance. Finally, in Chapter 4 three hypotheses surrounding the mechanisms controlling the timing of the onset of the spring bloom in the North Atlantic were investigated. Again, this study was the first of its kind to investigate the spring bloom using such a detailed Lagrangian ecosystem model, and was able to reconcile the three hypotheses under the one concept of critical depth. Although the model achieved the aims successfully, the same results could have been obtained through the use of an Eulerian model, given information about the vertical structure of phytoplankton, and also if using appropriate intervals for integration.

The following paragraphs will provide a summary of the key findings and give suggestions for further work.

5.1 Fundamental assumptions of Lagrangian modelling

This section investigated some of the fundamental assumptions underpinning Lagrangian models, such as how the ecosystem is structured, the manner in

which the particles are redistributed, how the numbers of particles are managed i.e. particle splitting, and the interactions between the phytoplankton and the rest of the model.

5.1.1 Structure of the ecosystem

Choosing the appropriate framework for the ecosystem is a balance between complexity and computational cost, and the necessary detail for the question at hand. Simulating the entire ecosystem on a Lagrangian basis, a method which is employed for the WB model (Barkmann & Woods, 1996a; Woods & Barkmann, 1993a; Woods & Barkmann, 1993b; Woods & Barkmann, 1994), and subsequent models based on it (i.e. Sinerchia et al. (2012)) is a highly complex, non-trivial undertaking, involving a great deal of computational expense. In addition, one of the aims of the current study, was to strip the model back to its fundamental components, in order to both investigate how different variables, (e.g. turbulence, grazing), influenced phytoplankton growth, and also to enable comparison with an equivalent Eulerian model. Therefore, the Lagrangian phytoplankton were implemented in an otherwise Eulerian ecosystem, a method previously seen in Broekhuizen (1999); Cianelli et al. (2009); Cianelli, D'Alcala, Saggiomo, & Zambianchi (2004). However, these previous studies chose not to represent interactions between the phytoplankton and zooplankton, instead implicitly including grazing through an increase in the mortality term. This was insufficient for the aims of the current study, which required explicit representation of the interplay between the phytoplankton and zooplankton in order to understand how the balance between zooplankton and phytoplankton populations affected the seasonal cycles of primary production, as well as the consequences of individual phytoplankton response for the ecosystem as a whole. The Eulerian ecosystem in which the Lagrangian phytoplankton were simulated therefore included explicit zooplankton, nutrients and detritus, in a manner which has not previously been seen in the literature. Essentially, Lagrangian phytoplankton were implemented in an otherwise Eulerian model that assumed complete homogeneity of dissolved nutrients, zooplankton, and detritus. This method is not without its issues, in particular, handling the interactions between the Lagrangian phytoplankton and Eulerian zooplankton was not a trivial matter, and the method for this is fully explained in section 0. Overall, though, the

model was highly successful, achieving both aims of creating an environment for Lagrangian phytoplankton that allowed for investigation of the interplay between the phytoplankton and the other components of the ecosystem, whilst also producing results that were directly comparable to an Eulerian equivalent.

5.1.2 Particle movement rules

The choice of particle movement rules is crucial to the model, because it determines the timescales at which the phytoplankton are mixed. The relationships between the timescales of mixing and the timescales of growth and acclimation determine whether it is necessary to represent primary production using a Lagrangian framework, which is fully explored in section 5.2. The particle movement rules need to redistribute the phytoplankton in a way that meaningfully represents the mixing timescales in the mixed layer, whilst avoiding any inconsistencies of distribution that could artificially influence the model predictions.

5.1.2.1 Random position movement algorithm

The simplest method of redistributing the phytoplankton particles is to update their depth to a new random position between the surface and the base of the mixed layer each time step. Woods (2005) proposes that this is a valid method for scenarios with time steps that are much greater than the turbulence time scale, and it is used in several models that are based on his WB model (e.g. Sinerchia et al., 2012; Woods & Barkmann, 1993a,b, 1994). Whether this would be a valid method for OWS India, where the mixed layer depth can reach to greater than 600m, can be determined by calculating the time scale of turbulence, T_M (s), which can be estimated using the diffusivity coefficient, K_{turb} ($m^2\ s^{-1}$), and the depth of the mixed layer, H (m):

$$T_M = \frac{H^2}{K_{turb}} \tag{5.1}$$

For the mixing time scale to be on the order of a time step of 30 minutes for a mixed layer depth of 600m would require a turbulent diffusivity of 200 $m^2\ s^{-1}$. For comparison, the turbulent diffusivity calculated for the random walk algorithm (discussed in more detail in section 5.1.2.3) for a mixed layer depth of 600 m and a surface wind speed of 10 m s^{-1} would be 0.24 $m^2\ s^{-1}$, almost 3

orders of magnitude smaller, and representing an estimated mixing time of ~ 17 days. Although time scales of mixing in the ocean, especially in large, turbulent eddies, have been observed at rates as fast as 0.5 h, these are on the order of 10m, rather than 600m (Denman & Gargett, 1983).

In addition, further detailed analyses that included comparisons with the Eulerian model, along with investigations into the individual rates of acclimation, demonstrated that the concept behind the random position movement algorithm is flawed. There is no difference in predictions between the Eulerian model and the random position model, because, on average, the phytoplankton particles experience the same conditions. Essentially, the phytoplankton particles in the random position model can be seen as random samples drawn from an Eulerian model each time step. There is no difference in the predictions of primary production, or average chl-to-carbon ratios. Therefore, there is no modelling scenario for which a Lagrangian model that utilises the random position movement algorithm would be a useful choice. However, a random position movement could be used to obtain the rates of growth and loss from a Lagrangian model, for use in an Eulerian model. One of the difficulties in creating equivalent Eulerian and Lagrangian models is how to apply average loss rates to individual phytoplankton particles. Knowing that Eulerian models and Lagrangian random position models are equivalent allows for average rates of loss to be determined from Lagrangian models where the rates of loss and grazing are applied on an individual, rather than an average, basis.

5.1.2.2 Random walk algorithm

The alternative to the random position movement algorithm is to implement a random walk, where the phytoplankton particles move a predetermined distance each time step in a random direction. As this was a 0D model that considered only vertical movement, the phytoplankton could move up or down. Although there has been a great deal of research in the literature with regards to the physicality of the random walk, in terms of how to determine the step length, and how to prevent accumulation of particles in regions with lower rates of mixing, few studies have investigated how the implementation of a random walk can affect the model predictions of primary production.

Most random walks involve some form of the Brownian motion equation:

$$Z_{t+1} = Z_t \pm \sqrt{2K_{turb} \cdot \partial t} \quad (5.2)$$

where K_{turb} represents the turbulent diffusivity, Z_t represents the current depth, and Z_{t+1} the depth at the end of the time step. This model formulation was revised by (Visser, 1997), due to the fact that for mixed layers with non-uniform diffusivity, particles would accumulate in the areas with the lowest diffusivity, and his revised model formulation (and the extended version described by (Ross & Sharples, 2004)) forms the base of many Lagrangian phytoplankton models (e.g. Broekhuizen (1999); Cianelli et al. (2009); Nagai et al. (2003); Ross et al. (2011a); Ross et al. (2011b)). The current study assumed a uniform diffusivity throughout the mixed layer, so used a simpler version of the Visser (1997) model that neglected the expression for redistributing particles from areas of low turbulence, although this could easily be added to allow the model to simulate profiles of diffusivity. The model described in Visser (1997) also included an additional random element through multiplying the step length calculated in equation (5.2) by a random process between 0 and 1. The study compared the random walk described in Visser (1997), to a simple, Brownian motion equation, as shown in equation (5.2), and used in (Falkowski & Wirick (1981). The Visser (1997) implemented was deemed to be the better choice, due to the introduction of the random element to the step length, ensuring an even sampling of the entire model space, unlike the Falkowski and Wirick (1981) random walk, which moved in steps of the same length each time step. The random walk model was fully tested in order to ensure that the phytoplankton were randomly distributed, and the appropriate boundary conditions (i.e. reflecting at both boundaries) were chosen. Both the random walk and the choice of boundary conditions were successful at evenly redistributing the phytoplankton throughout the mixed layer.

5.1.2.3 Rates of turbulence

Surface water mixing in the ocean is driven by energy from wind, waves, Langmuir circulations, or convection - gravitational instability caused by a cooling of the ocean's surface (Franks, 2014). Representing all of these difference processes with a single parameter is a daunting task. Nevertheless, a parameter that reasonably estimates the rate of mixing in the surface layer is essential in order to determine meaningful mixing timescales. This section therefore examines the formulation for turbulence used in the current model,

evaluating its success at reproducing mixing in the North Atlantic in terms of previous studies, and of empirical evidence.

Parameterisations of turbulent diffusivity in previous studies have ranged from complex methods, such as 2nd-order turbulence closure models (e.g. Nagai et al. (2003)), and non-hydrostatic convection models (Lindemann et al., 2015) to the use of constant values (Cianelli et al., 2004; Dippner, 1993; Dippner, 1998; Dusenberry, 2000; Ross et al., 2011a; Ross et al., 2011b). This study required a method that was simple enough to allow the model to be stripped back to its fundamental assumptions, but that would still produce a value for diffusivity that was reasonable for the location, and representative of the seasonal cycle. Therefore, as in Lizon et al. (1998), who parameterised a simple turbulence model with empirical tidal measurements, and in Yamazaki & Kamykowski (1991), who used a simple Ekman model, based on surface wind speed only, to define both the eddy diffusivity and the depth of the mixed layer, this study used a simple turbulence model, parameterised by data. However, unlike Yamazaki & Kamykowski (1991), the turbulence model in this study used empirical measurements of mixed layer depth, along with the surface wind speeds, to calculate turbulence, as described in the KPP model for boundary layer scenarios described in Large et al. (1994). In addition, while Yamazaki & Kamykowski (1991) only investigated several constant values for wind speed, this study investigated the effects on mixing of a full seasonal cycle of empirical measurements of surface wind forcing. Changes to the mixing as a consequence of changes to the surface wind forcing could be investigated, as well as how changes to the mixed layer depth influenced rates of mixing.

The model of turbulence used in this study used several simplifying assumptions, the consequences of which will be addressed here. Firstly, the model assumed that the rate of mixing was vertically constant, which is something that is not seen in the ocean, where the rate of mixing tends to increase towards the middle of the mixed layer, and decrease towards the boundaries. In addition, mixing in the ocean is not constant over a diel cycle – surface warming during the day will suppress mixing, whereas cooler conditions at night will increase it. Phytoplankton in the ocean are also subjected to lateral mixing, and ephemeral phenomena such as fronts and eddies. The aims of the current study were to understand the relationship between acclimation and mixing, rather than the creation of an accurate model

of the phytoplankton primary production in the North Atlantic. The use of a more complex model, as a Large Eddy Simulation model, could potentially provide differing predictions of primary production. Nevertheless, the current study provides a good first step towards understanding the complex relationship between individual phytoplankton response and overall rates of primary production.

5.1.3 Grazing and non-linear mortality

How to best represent grazing by zooplankton in Lagrangian phytoplankton models is a question that has not yet been satisfactorily answered. As a result, most models choose to not explicitly represent zooplankton, instead implicitly representing grazing through use of a higher rate of mortality (e.g. Broekhuizen, 1999; Daniela Cianelli et al., 2009; D. Cianelli et al., 2004; Hellweger & Kianirad, 2007; Lindemann, Backhaus, & St John, 2015). However, as mentioned in section 5.1.1, one of the aims of this study was to investigate the interplay between the phytoplankton and the zooplankton, so explicit zooplankton needed to be included.

As mentioned in section 5.1.1, previous models have either only included grazing implicitly, or included fully Lagrangian phytoplankton. Neither of these options was deemed as suitable: the former as it would not have allowed for the dynamic interplay between phytoplankton and zooplankton, including the seasonal variation in specific grazing rates, and the latter due to its complexity which would complicate comparison with an Eulerian model, so a middle ground solution was devised. This involved including explicit Eulerian zooplankton that would graze on the Lagrangian phytoplankton. However, implementing the interaction between these Eulerian zooplankton and the Lagrangian phytoplankton was fraught with difficulties. The grazing equations are in terms of concentrations of phytoplankton, and these need to be applied to the phytoplankton super-individuals in a meaningful manner. As each super-individual represents a quantity of biomass, it first seemed logical to apply these equations on an individual basis i.e. the grazing on each individual would be determined by the use of a non-linear function, and then the overall rates of grazing could be calculated through summing all of the individual rates. However, there were two problems to this: firstly, the overall loss rates then became sensitive to the threshold for particle splitting (particle splitting is

discussed in section 5.1.4), and secondly, it caused difficulties when it came to creating an equivalent Eulerian model, because the loss rates were not equivalent. A novel solution that successfully links the Eulerian zooplankton with the Lagrangian phytoplankton was therefore devised. The grazing rates are based on the concentration of phytoplankton biomass over the entire mixed layer, as in the Eulerian model. This translates into an absolute value of biomass to be lost every time step. This is then proportionally applied to each phytoplankton super-individual, according to its biomass. The grazing rates in the Eulerian and Lagrangian models are therefore comparable. However, as explained in Chapter 2, there are potential sources of error with this method. The grazing pressure ought to be relatively higher on large phytoplankton and lower for smaller phytoplankton, but this is not the case. This increases pressure on the smallest phytoplankton individuals, and reduces pressure on the largest, creating a positive feedback that results in the larger individuals increasing in size, whilst the smallest die out. In an extreme scenario, the largest individual could eventually dominate the simulation. Implementing particle splitting (section 5.1.4) alleviates this effect, but could be seen as not addressing the underlying cause of the issues. However, overall, this was a successful method of linking the two different model components.

5.1.4 Particle splitting

Lagrangian phytoplankton models can either use a fixed number of particles, or need to include some method of controlling the number of particles in the simulation. Too many particles can be difficult to model, whereas too few could lead to inaccuracies due to some parts of the mixed layer being devoid of phytoplankton. Previous studies have controlled the numbers of particles in one of three ways: using a constant number (Nagai et al., 2003; Ross et al., 2011a; Ross et al., 2011b), including particle splitting designed to represent cell division (Hellweger & Kianirad, 2007), or using particle division as a mechanism purely to control the number of particles in the simulation by employing a minimum number (Barkmann & Woods, 1996a; Woods & Barkmann, 1993b; Woods & Barkmann, 1994), or both a minimum and maximum number (Broekhuizen, 1999).

The current study uses a dynamic mixed layer cycle, which results in phytoplankton particles being lost through detrainment when the mixed layer

shallows. A constant number of particles would therefore not be appropriate, as the particles lost through detrainment need to be replaced. In addition, the use of non-linear growth rates that are applied proportionally to particles (explained in section 0) would result in an uneven distribution of biomass, without some method to control the size of the particles. Unlike the previous methods that employed particle splitting, there was no maximum number of particles prescribed, instead, a maximum particle size was established, and the number of particles in the simulation allowed to reach its natural value. The maximum size to which the particles could grow was determined through the sensitivity analysis in Chapter 2. Particle splitting is purely a method for controlling the number of super-individuals in the simulation, and is not meant to represent the biological process of cell division.

The model was not particularly sensitive to the threshold for particle splitting, which determined the numbers of super-individuals in the simulation. Even for mixed layer depths of > 600m, total particle numbers of ~2000 produced a sufficient level of precision, with an acceptable level of noise. This is similar to the number used by (Barkmann & Woods, 1996b; WOODS & BARKMANN, 1993; Woods & Barkmann, 1994), who initialised their model with 4000 particles, noting a minimum value of ~800. It is significantly more, however, than the number recommended in (Dippner, 1991), who performed a sensitivity analysis using a Lagrangian model, concluding that increasing the number of particles above 10 resulted in little change to the model predictions. (Nagai et al., 2003; Ross et al., 2011a; Ross et al., 2011b) used up to 80,000 particles for simulations with a mixed layer depth greater than 60m, but this was in order to have a statistically significantly number at each depth, for the purposes of analysis.

The particles in the model split into two, equally sized new particles, and introducing a random component to this (i.e. the particles being of unequal size) did not influence the results in any way.

5.2 Modelling growth and acclimation in Lagrangian phytoplankton

One reason behind the use of Lagrangian models is the belief that phytoplankton acclimate to their light environment, which will cause

divergence between Lagrangian and Eulerian models. This section used novel approaches in order to investigate this. First, a model intercomparison study was performed, which, like the studies performed by McGillicuddy (1995) and Lande & Lewis (1989) demonstrated no difference in the predictions of primary production between each model formulation. However, two studies differed in their explanations of the results, and this was resolved through the use of an in-depth study that used a fixed slab model to thoroughly investigate the rates of acclimation in the individual phytoplankton. Acclimation happens at a much slower rate than mixing, so phytoplankton do not have time to acclimate to their local irradiance as they are being mixed through the mixed layer. In addition, it was demonstrated that the timescales of importance are actually those of the mixing and the rate of phytoplankton growth. Changes to the turbulent diffusivity can result in the mixing rate becoming insufficient to overcome the phytoplankton growth rates, resulting in an non-uniform vertical structure of phytoplankton, which increases the overall rate of primary production. As growth occurs on a faster timescale than acclimation, this has a far stronger response to changes in the mixing rate.

5.2.1 Model intercomparison study

There were two objectives behind setting up the model for OWS India: firstly, to obtain the parameters for the photoacclimation equations, and secondly to investigate the consequences of photoacclimation on the ecosystem as a whole. This was the first study to perform a model intercomparison between Eulerian and Lagrangian representations of a full marine ecosystem that included both explicit zooplankton, and mixing based on empirical data. The results of the study showed that there was little difference between the predictions of both primary production and chl-to-carbon ratios between the Eulerian and Lagrangian models.

5.2.1.1 Photoacclimation parameters

One of the reasons why different studies have produced different results is the way in which photoacclimation is represented. Previous studies (notably the models by Lande & Lewis (1989); Wolf & Woods (1988), which were investigated in McGillicuddy (1995) have used different formulations for the rate of change in the photoacclimative properties of the phytoplankton. In

order to address this issue, this study used the growth model described in Geider (1997), in which the photoacclimative properties (the ratio between chlorophyll and carbon) are not modelled directly, but instead result from the differing rates of production of pigment and biomass, dependent on the external conditions (i.e. irradiance, nutrients). However, the behaviour of the model is highly dependent on its parameterisation, and the rate at which the phytoplankton acclimate is controlled by the maximum chl-to-carbon ratio, which varies between species: smaller phytoplankton functional groups, such as cyanobacteria and dinoflagellates, show low values for thetacmax, and larger groups, such as diatoms, show higher values Geider et al. (1997). In addition, estimates are often obtained in the laboratory, and these can vary from those measured in the ocean. The initial values used for the model, as used in Taylor et al. (1997); Yool et al. (2011); Yool et al. (2013) of 0.05 mg Chl mg C^{-1} resulted in overall ratios of chl-to-carbon that were too high, by a factor of two, for OWS India. Satellite measurements taken by Behrenfeld et al. (2005) suggest a maximum ratio of ~0.017 for that region of the ocean, and changing the maximum chl-to-carbon ratio to 0.02 mg Chl mg C^{-1} gave a much better representation of the seasonal observations of chl-to-carbon.

5.2.1.2 Fixed slab models

The investigations with the fixed slab models demonstrated the real strength of Lagrangian implementations. Not only could the effects on overall growth by changes to external forcing be investigated, but also the changes in individual phytoplankton as they moved through the mixed layer could be tracked. The model successfully demonstrated why there is little difference between the Lagrangian and Eulerian implementations – even at low to moderate mixing rates, the phytoplankton do not have time to significantly acclimate to their local irradiance.

5.2.1.3 Vertical phytoplankton profiles

One observation from the experiments was that the mixing that was parameterised for OWS India resulted in vertical profiles of phytoplankton, even though the mixed layer was fully mixed (section 5.1.2.3). Investigations into these vertical profiles showed that when the mixing rate was slowed to significantly affect the overall rates of primary production, these changes to

the rates of production were almost entirely due to the vertical profile of phytoplankton, rather than from the chl-to-carbon ratios of the phytoplankton.

5.2.1.4 Sensitivity of the ecosystem

Testing the entire marine ecosystem using the same scenarios as for the fixed slab experiments produced some interesting results. First of all, the growth of the phytoplankton over the summer is not controlled by the irradiance, but by the nutrient concentration and the loss rates. Secondly, the formation of a vertical profile of phytoplankton has the most effect when the phytoplankton growth is light limited, so when the mixed layer is deep, and/or the surface irradiance is low. This would be observed in early spring.

5.3 The main controls on the timing of the initiation of the spring bloom

Franks (2014) proposed that the critical depth hypothesis could not be properly tested by a model that did not included information about the rates at which the phytoplankton were mixed through the water column. Therefore the model was used to investigate the critical depth, critical turbulence, and disturbance-recovery hypotheses, for OWS India. The aims were twofold: to investigate which hypothesis best describes the controls of the spring bloom at OWS India, and to evaluate the suitability of a Lagrangian model to achieve this aim.

Critical depth, defined as the depth above which the integrated net growth was equal to 0, was calculated from the full ecosystem model, based on the predicted rates of growth and loss. This is something that has previously not been seen in the literature, where predictions of critical depth are based on constant parameters, such as the compensation irradiance. However, the non-linearity of phytoplankton loss rates mean that the critical depth will change as a function of the concentrations of both phytoplankton, and the zooplankton that graze on them. In addition, the daily critical depth was calculated in a number of different ways: without a diel cycle of irradiance, with a diel cycle, but using the daily averaged irradiance, and with a diel cycle of irradiance, but calculating the average critical depth over the day. This latter method was shown to provide the most accurate estimate, demonstrating that Sverdrup's

recommendation for using the average irradiance over the course of each day to calculate the critical depth introduces errors if the relationship between irradiance and photosynthesis is non-linear. In addition, an analytical equation for the critical depth was devised, and the critical depths predicted by the model matched those provided by the equation.

The predicted critical depth and the modelled day of the onset of the bloom were shown to match exactly, which has not previously been achieved in the literature. The study carried out by Lévy (2015), which used a 1D NPZ model to investigate critical depth, found a lag between the predicted (i.e. using Sverdrup's theory) and the modelled day of the onset of the bloom, even when the model adhered to all of the assumptions in Sverdrup's theory (i.e. constant rate of loss with depth, no grazing, linear dependence of photosynthesis on irradiance). This was attributed to the fact that Sverdrup's equations were solved for steady-state conditions, but the results from the current study suggest the use of a constant for the compensation irradiance, and the loss of accuracy through integrating an Eulerian model over 5 m intervals, could also affect the accuracy of the predicted critical depth. For example, the current demonstrated that an Eulerian model that integrated over 1 m intervals would predict a critical depth that differed from the Lagrangian predictions by ~2%, due to the loss in accuracy through integration. If the model integrated over smaller intervals (i.e. 0.1 m), the two predictions would converge.

The study yielded several interesting findings about the timing on the onset of the spring bloom in the North Atlantic:

1. The spring bloom is triggered by the increase in irradiance deepening the depth at which the mixed layer can sustain net production, rather than by the mixed layer shoaling. There is little change in the depth of the mixed layer at the point where production first becomes positive – it is still > 500m deep. This is an important result, because it provides an explanation as to how net growth can become positive in the absence of significant mixed layer stratification, as observed by Boss & Behrenfeld (2010); Townsend et al. (1994).

2. The timing of the onset of the spring bloom is controlled by the phytoplankton respiration (linear loss rate), whereas the magnitude of its peak is more strongly controlled by grazing (non-linear loss rate).

This is because the non-linear losses are very low at the beginning of the year, due to the deep winter mixing, which dilutes the concentrations of both phytoplankton and zooplankton. However, non-linear rates would have more impact on the timing of the onset of the spring bloom for scenarios without deep winter mixing, where the concentrations of zooplankton and phytoplankton were maintained over winter (as proposed in the disturbance-recovery hypothesis).

3. The critical depth and critical turbulence hypotheses do not describe independent mechanisms that control the onset of the spring bloom. If the timescale of growth is faster than the timescale of mixing, then the mixing is not sufficient to overcome to phytoplankton growth rate, and a vertical profile will start to form. This increases the overall growth rate of the phytoplankton population, which decreases the critical depth. This critical depth is still predictable, given information regarding the vertical structure of the phytoplankton, although it quickly becomes very deep – i.e. deeper than the depth of the deepest point of the ocean – meaning that, for all intents and purposes, there is no critical depth.

4. The predicted values for the critical depth are very deep, making the concept only relevant for regions with of high turbidity (increases to turbidity decrease the critical depth, by reducing the average irradiance, and therefore the rate of primary production), or with very deep mixed layers. This backs up results by Platt et al., (1991) who predicted the critical depth for various locations in the ocean, concluding that, except at the highest latitudes, it was very deep. They suggested that it is therefore possible that almost any surface mixed layer would satisfy the Sverdrup criterion.

The model has demonstrated that the timing of the spring bloom can be predicted, given certain information about the conditions. For regions with deep winter mixing, and therefore very low phytoplankton concentrations in early spring, the timing of the onset of the bloom is determined by the rate of respiration. For regions without deep winter mixing, and where a phytoplankton population is maintained throughout the winter, grazing rates play a much stronger role in controlling the onset of the spring bloom. However, it is important to note that the timing of the onset of the bloom does

not yield information regarding how rapidly phytoplankton biomass might accumulate (Platt et al., 1991), and therefore might have limited use for predicting the magnitude of the peak of the phytoplankton bloom, which is generally of greater use in terms of carbon export.

5.4 Future research

This study has highlighted several areas in which Lagrangian models could be useful for advancing knowledge in this field:

1. Include variability in the rates of photoacclimation. One important question that this study has highlighted is regarding the rates of photoacclimation. The study has suggested that phytoplankton acclimate very slowly to changes in their local irradiance, responding on seasonal, rather than diel cycles. However, only one functional group was represented, with a low maximum chl-to-carbon ratio, which would be typical of a small phytoplankton species, such as a dinoflagellate or cyanobacteria. Implementing the model with Lagrangian phytoplankton with a range of different photoacclimative traits could demonstrate the potential advantages to differing rates of acclimation, by determining the traits that become dominant in response to changes in external forcing. For example, Lewandowska et al. (2015) proposed that the timing of the spring bloom is not only determined by factors such as light, nutrients and grazing, but also by the photoacclimative properties of the phytoplankton. In addition, they stated that without the necessary combination of traits for a particular location and time, the spring bloom could not take place. They concluded that variability in photoacclimative and growth traits is essential in order to accurately model the spring bloom.

2. Investigate whether the results would change, if the phytoplankton were allowed to synthesise chlorophyll at night. In the cell-based phytoplankton growth model described in Ross & Geider (2009), phytoplankton cells can accumulate reserves of carbon during the day, which allows them to synthesise chlorophyll, in the absence of sunlight, over night. This effectively allows the phytoplankton cells to photoacclimate over the full 24-hour period, rather than just during the

day, when they are in the euphotic zone. This would be likely to result in different dynamics, in particular in terms of the average state of photoacclimation of the cells, as they would adjust to the average irradiance in the entire mixed layer, rather than just in the euphotic zone (as described in section 3.4.2). Implementing a completely cell-based model would also constitute a good next step from the model in the current study, which would then form a useful basis for comparison, starting, as it does, from a fully Eulerian model, and then moving to a Lagrangian equivalent.

3. Improving the representation of respiration. This study has demonstrated that for regions with deep winter mixing, such as the North Atlantic, the main control on the timing of the onset of the spring bloom is the phytoplankton rate of respiration. This tends to be assumed to be proportional to phytoplankton biomass in phytoplankton models, a technique that has been criticised (e.g. Smetacek & Passow (1990)). A modelling study performed by Lindemann et al. (2015) investigated the effect of including variable rates of phytoplankton respiration, and buoyancy, into ecosystem models. They demonstrated that the use of variable rates for respiration and sinking enabled their model to fit all of the observations (concentration during winter mixing, and timing and magnitude of the onset of the spring bloom), whereas using fixed rates only allowed the model to fit the observations when using unrealistic parameter values. It would be useful to see how incorporating variable rates of phytoplankton respiration into the current model would influence both the seasonal cycle of phytoplankton, and the predictions relating to the timing of the spring bloom.

4. This study has only focussed on one ocean site – the North Atlantic, in a region that is characterised by deep winter mixing. However, the model predictions suggest that in regions without deep winter mixing, the timing of the spring bloom would be determined more by the grazing rates than by the rates of acclimation. In addition, Cole et al., (2015) suggested that the mechanisms in the North Atlantic are not representative of the ocean basins as a whole, making it a poor choice for developing general theories surrounding the controls of spring

blooms. Testing other sites in the ocean, such as the North Pacific or the Southern Ocean, could enhance our understanding of the mechanisms that control phytoplankton blooms on a global basis. However, in order to properly investigate other sites, the model should be extended to include vertical profiles of nutrients and zooplankton, in order to allow for sub-surface chlorophyll maximum and zooplankton vertical migration.

5.5 Conclusion

This study has investigated two linked applications for marine ecosystem models: predicting the seasonal patterns of primary production, and gaining understanding about individual cellular processes such as photoacclimation. It might be expected that photoacclimation in Lagrangian models would have an impact on seasonal cycles, however, the timescales of mixing did not permit photoacclimation, resulting in no difference in seasonal predictions between the Lagrangian and Eulerian models. Therefore, the use of a Lagrangian approach did not demonstrate any advantage in terms of the accuracy of predictions, when set up for Ocean Weather Station India. However, this was the only ocean site investigated, and these findings need to be tested for locations that display different characteristics, such as a deep chlorophyll maximum, or a stratified water column. Overall, though, this study has demonstrated that Eulerian ecosystem models, as for example applied in biogeochemical modelling studies, do not suffer deficiencies due to their not representing the interaction of phytoplankton with their physico-chemical environment at the individual cell level.

Additionally, this study has demonstrated the utility of Lagrangian models for the purpose of testing current ecological theory. It is only by running a Lagrangian model that it was possible to investigate the time scales of acclimation and mixing in a dynamic environment. In particular, it has shown that, as the timescale for growth is faster than that of acclimation; reducing the mixing rate will affect the vertical profile of phytoplankton in the water column, before having a significant effect on individual chl-to-carbon ratios. This suggests that the accuracy of future models could benefit from improved parameterisation of the rates of mixing, and how these affect the vertical structure of phytoplankton through the mixed layer. For example, Behrenfeld

et al. (2006) found a clear link between net primary production and climate resulting from changes in water column stratification. Climatic changes that resulted in surface warming increased the density contrast between the surface layer and the underlying nutrient rich waters, thereby suppressing nutrient exchange through vertical mixing, and decreasing net primary production. A recent study by Wijffels et al. (2016) showed that the constant planetary radiation imbalance over the years 2006 to 2015 have resulted in a steady rise in ocean heat content, and therefore it is critical for future research to focus on how, if this trend continues, this could affect both the vertical structure of the ocean, and the overall rates of primary production.

The study also demonstrated that, as proposed by Franks (2014), knowledge about the rates of turbulent mixing are crucial for proper testing of the critical depth hypothesis (and therefore also the critical turbulence and disturbance-recovery hypotheses). As described above, reductions to the rate of mixing result in changes to the vertical profile of phytoplankton, which deepen the critical depth. In addition, it has demonstrated that, as proposed by Platt et al. (1991), the critical depths are deep, which means that, in order for net phytoplankton growth to occur, stratification of the mixed layer does not need to occur. Seasonal increases in the surface irradiance are sufficient to result in the critical depths deepening beyond that of the mixed layer. Most importantly, it has indicated that the different hypotheses for the control of the spring bloom are just describing the different processes that determine it. Sverdrup's hypothesis is correct, in that it is possible to accurately describe the point at which net production becomes positive, based on the rates of growth and loss. However, as this point tells us little about the magnitude, or even timing of the peak of phytoplankton production, it is unlikely to have a great deal of predictive power.

.

Bibliography

Anderson, T. R. (1993). A spectrally averaged model of light penetration and photosynthesis. *Limnology and Oceanography*, *38*(7), 1403–1419.

Anderson, T. R., Gentleman, W., & Yool, A. (2015). EMPOWER-1.0: an Efficient Model of Planktonic ecOsystems WrittEn in R. *Geoscientific Model Development Discussions*, (1), 53–140. http://doi.org/10.5194/gmdd-8-53-2015

Anning, T., MacIntyre, H. L., Pratt, S. M., Sammes, P. J., Gibb, S., & Geider, R. J. (2000). Photoacclimation in the marine diatom Skeletonema costatum. *Limnology and Oceanography*, 1807–1817.

Antonov, J. I., Seidov, D., Boyer, T. P., Locarnini, R. A., Mishonov, A. V., Garcia, H. E., … Johnson, D. R. (2010). World Ocean Atlas 2009, Volume 2: Salinity. S. Levitus, Ed. *NOAA Atlas NESDIS*, *69*.

Bagniewski, W., Fennel, K., Perry, M. J., & D'Asaro, E. A. (2011). Optimizing models of the North Atlantic spring bloom using physical, chemical and bio-optical observations from a Lagrangian float. *Biogeosciences*, *8*(5), 1291–1307.

Barkmann, W., & Woods, J. D. (1996a). On using a Lagrangian model to calibrate primary production determined from in vitro incubation measurements. *Journal of Plankton Research*, *18*, 767–788.

Barkmann, W., & Woods, J. D. (1996b). On using a Lagrangian model to calibrate primary production determined from in vitro incubation measurements. *Journal of Plankton Research*, *18*(5), 767.

Béchet, Q., Shilton, A., & Guieysse, B. (2013). Modeling the effects of light and temperature on algae growth: State of the art and critical assessment for productivity prediction during outdoor cultivation. *Biotechnology Advances*, *31*(8), 1648–1663.

Behrenfeld, M. J. (2010). Abandoning Sverdrup's critical depth hypothesis on phytoplankton blooms. *Ecology*, *91*(4), 977–989.

Behrenfeld, M. J., & Boss, E. S. (2014). Resurrecting the ecological underpinnings of ocean plankton blooms. *Annual Review of Marine Science*, *6*, 167–194.

Behrenfeld, M. J., Boss, E., Siegel, D. A., & Shea, D. M. (2005). Carbon-based ocean productivity and phytoplankton physiology from space. *Global Biogeochemical Cycles*, *19*(1). Retrieved from http://onlinelibrary.wiley.com/doi/10.1029/2004GB002299/full

Behrenfeld, M. J., Doney, S. C., Lima, I., Boss, E. S., & Siegel, D. A. (2013). Annual cycles of ecological disturbance and recovery underlying the subarctic Atlantic spring plankton bloom. *Global Biogeochemical Cycles*, *27*(2), 526–540.

Behrenfeld, M. J., O'Malley, R. T., Siegel, D. A., McClain, C. R., Sarmiento, J. L., Feldman, G. C., … Boss, E. S. (2006). Climate-driven trends in contemporary ocean productivity. *Nature*, *444*(7120), 752–755.

Boss, E., & Behrenfeld, M. (2010). In situ evaluation of the initiation of the North Atlantic phytoplankton bloom. *Geophysical Research Letters*, *37*(18). Retrieved from http://onlinelibrary.wiley.com/doi/10.1029/2010GL044174/pdf

Brock, T. D. (1981). Calculating solar radiation for ecological studies. *Ecological Modelling*, *14*(1), 1–19.

Broekhuizen, N. (1999). *Simulating motile algae using a mixed Eulerian-Lagrangian approach : does motility promote dinoflagellate persistence or co-existence with diatoms ?* (Vol. 21). Oxford, ROYAUME-UNI: Oxford University Press.

Chiswell, S. M. (2011). Annual cycles and spring blooms in phytoplankton: don't abandon Sverdrup completely. *Marine Ecology Progress Series*, *443*, 39–50.

Cianelli, D., D'Alcala, M. R., Saggiomo, V., & Zambianchi, E. (2004). Coupling mixing and photophysiological response of Antarctic plankton: a Lagrangian approach. *Antarctic Science*, *16*, 133–142.

Cianelli, D., Sabia, L., d'Alcalà, M. R., & Zambianchi, E. (2009). An individual-based analysis of the dynamics of two coexisting phytoplankton species in the mixed layer. *Ecological Modelling*, *220*(19), 2380–2392.

Cole, H. S., Henson, S., Martin, A. P., & Yool, A. (2015). Basin-wide mechanisms for spring bloom initiation: how typical is the North Atlantic? *ICES Journal of Marine Science: Journal Du Conseil*, fsu239.

Copernicus Marine Service. (2016). North Atlantic Surface Chlorophyll Concentration from Satellite observations. Retrieved from http://marine.copernicus.eu/web/69-interactive-catalogue.php?option=com_csw&view=details&product_id=OCEANCOLOUR_ATL_CHL_L3_NRT_OBSERVATIONS_009_036

Cullen, J. J., & Lewis, M. R. (1988). The kinetics of algal photoadaptation in the context of vertical mixing. *Journal of Plankton Research*, *10*(5), 1039–1063.

Denman, K. L., & Gargett, A. E. (1983). Time and space scales of vertical mixing and advection of'phytoplankton in the upper ocean. *OCEANOGRAPHY*, *28*(5). Retrieved from http://mediteran.aslo.net/lo/toc/vol_28/issue_5/0801.pdf

Dippner, J. W. (1991). *A Lagrangian Model of Phytoplankton Growth Dynamics: A Sensitivity Analysis*. Office for Official Publications of the European Communities.

Dippner, J. W. (1993). A Lagrangian model of phytoplankton growth dynamics for the Northern Adriatic Sea. *Continental Shelf Research*, *13*, 331–350.

Dippner, J. W. (1998). Competition between different groups of phytoplankton for nutrients in the southern North Sea. *Journal of Marine Systems*, *14*(1-2), 181–198.

Dubinsky, Z., & Stambler, N. (2009). Photoacclimation processes in phytoplankton: mechanisms, consequences, and applications. *Aquatic Microbial Ecology*, *56*, 163–176.

Dusenberry, J. A. (2000). Steady-state single cell model simulations of photoacclimation in a vertically mixed layer: implications for biological tracer studies and primary productivity. *Journal of Marine Systems*, *24*, 201–220. http://doi.org/10.1016/s0924-7963(99)00086-x

Einstein, A. (1905). ON THE MOVEMENT OF SMALL PARTICLES SUSPENDED IN STATIUNARY LIQUIDS REQUIRED BY THE MOLECULAR-KINETIC THEORY 0F HEAT. Retrieved from http://old.stat.duke.edu/courses/Spring12/sta357/refs/Eins1905EN.pdf

Eppley, R. W. (1972). Temperature and phytoplankton growth in the sea. *Fish. Bull*, *70*(4), 1063–1085.

Evans, G. T., & Parslow, J. S. (1985). A model of annual plankton cycles. *Biological Oceanography*, *3*, 327–347.

Falkowski, P. G., & Raven, J. A. (2013). *Aquatic photosynthesis*. Princeton University Press. Retrieved from http://books.google.com/books?hl=en&lr=&id=kUCrAQAAQBAJ&oi=fnd&pg=PP1&dq=aquatic+photosynthesis&ots=bn3Bm9Wm4w&sig=l5KeO-VpxDHKGrNQ7SBj4D4H9cY

Falkowski, P., & Wirick, C. (1981). A simulation model of the effects of vertical mixing on primary productivity. *Marine Biology*, *65*, 69–75.

Fasham, M. J. R., Ducklow, H. W., & McKelvie, S. M. (1990). A nitrogen-based model of plankton dynamics in the oceanic mixed layer. *Journal of Marine Research*, *48*(3), 591–639.

Fennel, K., Wilkin, J., Levin, J., Moisan, J., O'Reilly, J., & Haidvogel, D. (2006). Nitrogen cycling in the Middle Atlantic Bight: Results from a three-dimensional model and implications for the North Atlantic nitrogen budget. *Global Biogeochemical Cycles*, *20*(3). Retrieved from http://onlinelibrary.wiley.com/doi/10.1029/2005GB002456/full

Flynn, K. J. (2001). A mechanistic model for describing dynamic multi-nutrient, light, temperature interactions in phytoplankton. *Journal of Plankton Research*, *23*, 977–997. http://doi.org/10.1093/plankt/23.9.977

Flynn, K. J., Marshall, H., & Geider, R. J. (2001). A comparison of two N-irradiance interaction models of phytoplankton growth. *Limnology and Oceanography*, *46*(7), 1794–1802.

Franks, P. J. (2014). Has Sverdrup's critical depth hypothesis been tested? Mixed layers vs. turbulent layers. *ICES Journal of Marine Science: Journal Du Conseil*, fsu175.

Franks, P., & Marra, J. (1994). A simple new formulation for phytoplankton photoresponse and an application in a wind-driven mixed-layer model. *Marine Ecology Progress Series. Oldendorf*, *111*, 143–153.

Fulton, E. A., Smith, A. D., & Johnson, C. R. (2003). *Effect of complexity on marine ecosystem models*. Retrieved from http://eprints.utas.edu.au/1119/

Geider, R. J., MacIntyre, H. L., & Kana, T. M. (1996). A dynamic model of photoadaptation in phytoplankton. *Limnology and Oceanography*, 1–15.

Geider, R. J., MacIntyre, H. L., & Kana, T. M. (1998). A dynamic regulatory model of phytoplanktonic acclimation to light, nutrients, and temperature. *Limnology and Oceanography*, 679–694.

Geider, R., MacIntyre, H., & Kana, T. (1997). Dynamic model of phytoplankton growth and acclimation: responses of the balanced growth rate and the chlorophyll a: carbon ratio to light, nutrient-limitation and temperature. *Marine Ecology Progress Series. Oldendorf*, *148*, 187–200.

Gran, H. H., & Braarud, T. (1935). A quantitative study of the phytoplankton in the Bay of Fundy and the Gulf of Maine (including observations on hydrography, chemistry and turbidity). *Journal of the Biological Board of Canada*, *1*, 279–467.

Hellweger, F. L., & Kianirad, E. (2007). Accounting for intrapopulation variability in biogeochemical models using agent-based methods. *Environmental Science & Technology*, *41*, 2855–2860.

Huisman, J., van Oostveen, P., & Weissing, F. J. (1999). Critical depth and critical turbulence: two different mechanisms for the development of phytoplankton blooms. *Limnology and Oceanography*, *44*(7), 1781–1787.

Joint, I., Pomroy, A., Savidge, G., & Boyd, P. (1993). Size-fractionated primary productivity in the northeast Atlantic in May–July 1989. *Deep Sea Research Part II: Topical Studies in Oceanography*, *40*(1), 423–440.

Kamykowski, D., Yamazaki, H., & Janowitz, G. S. (1994). A Lagrangian model of phytoplankton photosynthetic response in the upper mixed layer. *Journal of Plankton Research*, *16*, 1059–1069. http://doi.org/10.1093/plankt/16.8.1059

Lalli, C., & Parsons, T. R. (1997). *Biological Oceanography: An Introduction: An Introduction*. Butterworth-Heinemann. Retrieved from

http://books.google.com/books?hl=en&lr=&id=c6J5hlcjFaAC&oi=fnd&pg=PP2&dq=lalli+and+parsons&ots=RFgjT60nq0&sig=Xi-PXI1rLZkQX37pm2Y4j3xLMns

Lande, R., & Lewis, M. R. (1989). Models of photoadaptation and photosynthesis by algal cells in a turbulent mixed layer. *Deep Sea Research Part A. Oceanographic Research Papers*, *36*(8), 1161–1175. http://doi.org/doi: DOI: 10.1016/0198-0149(89)90098-8

Large, W. G., McWilliams, J. C., & Doney, S. C. (1994). Oceanic vertical mixing: A review and a model with a nonlocal boundary layer parameterization. *Reviews of Geophysics*, *32*, 363–404.

Lévy, M. (2015). Exploration of the critical depth hypothesis with a simple NPZ model. *ICES Journal of Marine Science: Journal Du Conseil*, fsv016.

Lewandowska, A. M., Striebel, M., Feudel, U., Hillebrand, H., & Sommer, U. (2015). The importance of phytoplankton trait variability in spring bloom formation. *ICES Journal of Marine Science: Journal Du Conseil*, fsv059.

Lima, I. D., & Doney, S. C. (2004). A three-dimensional, multinutrient, and size-structured ecosystem model for the North Atlantic. *Global Biogeochemical Cycles*, *18*(3). Retrieved from http://onlinelibrary.wiley.com/doi/10.1029/2003GB002146/full

Lindemann, C., Backhaus, J. O., & St John, M. A. (2015). Physiological constrains on Sverdrup's Critical-Depth-Hypothesis: the influences of dark respiration and sinking. *ICES Journal of Marine Science: Journal Du Conseil*, fsv046.

Lindemann, C., & St John, M. A. (2014). A seasonal diary of phytoplankton in the North Atlantic. *Frontiers in Marine Science*, *1*, 37.

Li, W. K. W., & Harrison, W. G. (2001). Chlorophyll, bacteria and picophytoplankton in ecological provinces of the North Atlantic. *Deep Sea Research Part II: Topical Studies in Oceanography*, *48*(10), 2271–2293.

Lizon, F., Seuront, L., & Lagadeuc, Y. (1998). Photoadaptation and primary production study in tidally mixed coastal waters using a Lagrangian model. *Marine Ecology Progress Series*, *169*, 43–54.

Llort, J., Lévy, M., Sallée, J.-B., & Tagliabue, A. (2015). Onset, intensification, and decline of phytoplankton blooms in the Southern Ocean. *ICES Journal of Marine Science: Journal Du Conseil*, fsv053.

Longhurst, A. R. (1998). *Ecological Geography of the Sea*. Academic Press. Retrieved from https://books.google.com/books?hl=en&lr=&id=MFHK18F5aCsC&oi=fnd&pg=PR11&ots=MfakG1-cDx&sig=T_a2RVkdy0DVeaWKYKRXpzAlR8I

MacIntyre, H. L., Kana, T. M., Anning, T., & Geider, R. J. (2002). PHOTOACCLIMATION OF PHOTOSYNTHESIS IRRADIANCE RESPONSE CURVES AND PHOTOSYNTHETIC PIGMENTS IN MICROALGAE AND CYANOBACTERIA1. *Journal of Phycology*, *38*, 17–38. http://doi.org/10.1046/j.1529-8817.2002.00094.x

Marra, J. (1978). Phytoplankton photosynthetic response to vertical movement in a mixed layer. *Marine Biology*, *46*, 203–208. http://doi.org/10.1007/bf00390681

McGillicuddy, D. J. (1995). One-dimensional numerical simulation of primary production: Lagrangian and Eulerian formulations. *Journal of Plankton Research*, *17*(2), 405–412. http://doi.org/10.1093/plankt/17.2.405

Moore, Cm., Suggett, D. J., Hickman, A. E., Kim, Y.-N., Tweddle, J. F., Sharples, J., … Holligan, P. M. (2006). Phytoplankton photoacclimation and

photoadaptation in response to environmental gradients in a shelf sea. *Limnology and Oceanography*, *51*, 936–949.

Nagai, T., Yamazaki, H., & Kamykowski, D. (2003). A Lagrangian photoresponse model coupled with 2nd-order turbulence closure. *Marine Ecology Progress Series*, *265*, 17–30.

Nogueira, E., Woods, J. D., Harris, C., Field, A. J., & Talbot, S. (2006). Phytoplankton co-existence: Results from an individual-based simulation model. *Ecological Modelling*, *198*(1-2), 1–22.

Oschlies, A., & Garcon, V. (1999). An eddy-permitting coupled physical-biological model of the North Atlantic: 1. Sensitivity to advection numerics and mixed layer physics. *Global Biogeochemical Cycles*, *13*, 135–160.

Paskyaci, M. B., & Fer, I. (2010). Ocean near-surface boundary layer: processes and turbulence measurements. Retrieved from http://web.gfi.uib.no/publikasjoner/rmo/RMO-2010-1.pdf

Patara, L., Visbeck, M., Masina, S., Krahmann, G., & Vichi, M. (2011). Marine biogeochemical responses to the North Atlantic Oscillation in a coupled climate model. *Journal of Geophysical Research: Oceans (1978–2012)*, *116*(C7). Retrieved from http://onlinelibrary.wiley.com/doi/10.1029/2010JC006785/full

Pinchasov-Grinblat, Y., Hoffman, R., & Dubinsky, Z. (2011). The Effect of Photoacclimation on Photosynthetic Energy Storage Efficiency, Determined by Photoacoustics. *Open Journal of Marine Science*, *1*(02), 43.

Platt, T., Bird, D. F., & Sathyendranath, S. (1991). Critical depth and marine primary production. *Proceedings of the Royal Society of London. Series B: Biological Sciences*, *246*, 205–217.

Platt, T., Sathyendranath, S., Caverhill, C. M., & Lewis, M. R. (1988). Ocean primary production and available light: further algorithms for remote sensing. *Deep Sea Research Part A. Oceanographic Research Papers*, *35*(6), 855–879.

Prausnitz, F. (2002). *Roger Sessions: how a' difficult' composer got that way*. Oxford University Press on Demand.

Reed, R. K. (1977). On estimating insolation over the ocean. *Journal of Physical Oceanography*, *7*(3), 482–485.

Richardson, A. J., Silulwane, N. F., Mitchell-Innes, B. A., & Shillington, F. A. (2003). A dynamic quantitative approach for predicting the shape of phytoplankton profiles in the ocean. *Progress in Oceanography*, *59*(2), 301–319.

Riley, G. A. (1942). The relationship of vertical turbulence and spring diatom flowerings. *J. Mar. Res*, *5*, 67–87.

Riley, G. A. (1946). Factors controlling phytoplankton populations on Georges Bank. *J. Mar. Res*, *6*(1), 54–73.

Ross, O. N., & Geider, R. J. (2009). New cell-based model of photosynthesis and photo-acclimation: accumulation and mobilisation of energy reserves in phytoplankton. *Marine Ecology Progress Series*, *383*.

Ross, O. N., Geider, R. J., Berdalet, E., Artigas, M. L., & Piera, J. (2011a). Modelling the effect of vertical mixing on bottle incubations for determining in situ phytoplankton dynamics. I. Growth rates.

Ross, O. N., Geider, R. J., & Piera, J. (2011b). Modelling the effect of vertical mixing on bottle incubations for determining in situ phytoplankton dynamics. II. Primary production. *Marine Ecology Progress Series*, *435*, 33–45.

Ross, O. N., & Sharples, J. (2004). Recipe for 1-D Lagrangian particle tracking models in space-varying diffusivity. *Limnol. Oceanogr.: Methods*, *2*, 289–302.

Ross, O. N., & Sharples, J. (2007). Phytoplankton motility and the competition for nutrients in the thermocline. *Marine Ecology Progress Series*, *347*, 21–38.

Sathyendranath, S., Ji, R., & Browman, H. I. (2015). Revisiting Sverdrup's critical depth hypothesis. *ICES Journal of Marine Science: Journal Du Conseil*, *72*(6), 1892–1896. http://doi.org/10.1093/icesjms/fsv110

Sathyendranath, S., Stuart, V., Nair, A., Oka, K., Nakane, T., Bouman, H., … Platt, T. (2009). Carbon-to-chlorophyll ratio and growth rate of phytoplankton in the sea. *Mar. Ecol. Prog. Ser*, *383*(7). Retrieved from http://www.researchgate.net/profile/Heather_Bouman/publication/240809575_Carbon-to-chlorophyll_ratio_and_growth_rate_of_phytoplankton_in_the_sea/links/543fb1cb0cf2be1758cf088c.pdf

Scheffer, M., Baveco, J. M., Deangelis, D. L., Rose, K. A., & Vannes, E. H. (1995). Super-Individuals a Simple Solution for Modeling Large Populations on an Individual Basis. *Ecological Modelling*, *80*, 161–170.

Siegel, D. A., Doney, S. C., & Yoder, J. A. (2002). The North Atlantic spring phytoplankton bloom and Sverdrup's critical depth hypothesis. *Science*, *296*(5568), 730–733.

Sinerchia, M., Field, A. J., Woods, J. D., Vallerga, S., & Hinsley, W. R. (2012). Using an individual-based model with four trophic levels to model the effect of predation and competition on squid recruitment. *ICES Journal of Marine Science: Journal Du Conseil*, *69*, 439–447. http://doi.org/10.1093/icesjms/fsr190

Smetacek, V., & Passow, U. (1990). Spring bloom initiation and Sverdrup's critical-depth model. *Limnology and Oceanography*, *35*, 228–234.

Smith, E. L. (1936). Photosynthesis in relation to light and carbon dioxide. *Proceedings of the National Academy of Sciences of the United States of America*, *22*(8), 504.

Soetaert, K., & Herman, P. M. (2008). *A practical guide to ecological modelling: using R as a simulation platform*. Springer Science & Business Media. Retrieved from https://books.google.co.uk/books?hl=en&lr=&id=6y1WMbp2DfcC&oi=fnd&pg=PA1&dq=soetaert+a+practical+guide+to+ecological+modelling&ots=QwpcQxi3r9&sig=dsT44PmpVbs5GE9oQ8F--ZcCuD0

Spitz, Y. H., Moisan, J. R., & Abbott, M. R. (2001). Configuring an ecosystem model using data from the Bermuda Atlantic Time Series (BATS). *Deep Sea Research Part II: Topical Studies in Oceanography*, *48*(8), 1733–1768.

Sverdrup, H. U. (1953). On conditions for the vernal blooming of phytoplankton. *Journal Du Conseil*, *18*(3), 287–295.

Taylor, A. H., Geider, R. J., & Gilbert, F. J. H. (1997). Seasonal and latitudinal dependencies of phytoplankton carbon-to-chlorophyll a ratios: results of a modelling study. *Oceanographic Literature Review*, *44*(11). Retrieved from http://yadda.icm.edu.pl/yadda/element/bwmeta1.element.elsevier-a3ff237c-1c04-369d-9d04-ba5bedc4d7b3

Taylor, J. R., & Ferrari, R. (2011). Shutdown of turbulent convection as a new criterion for the onset of spring phytoplankton blooms.

Townsend, D. W., Cammen, L. M., Holligan, P. M., Campbell, D. E., & Pettigrew, N. R. (1994). Causes and consequences of variability in the timing of

spring phytoplankton blooms. *Deep Sea Research Part I: Oceanographic Research Papers*, *41*, 747–765.

Townsend, D. W., Keller, M. D., Sieracki, M. E., & Ackleson, S. G. (1992). Spring phytoplankton blooms in the absence of vertical water column stratification. *Nature*, *360*, 59–62.

Tuljapurkar, S., & Caswell, H. (1997). *Structured-population models in marine, terrestrial, and freshwater systems*. Springer.

Vichi, M., Pinardi, N., & Masina, S. (2007). A generalized model of pelagic biogeochemistry for the global ocean ecosystem. Part I: Theory. *Journal of Marine Systems*, *64*(1), 89–109.

Visser, A. W. (1997). Using random walk models to simulate the vertical distribution of particles in a turbulent water column. *Marine Ecology Progress Series*, *158*, 275–281.

Wijffels, S., Roemmich, D., Monselesan, D., Church, J., & Gilson, J. (2016). Ocean temperatures chronicle the ongoing warming of Earth. *Nature Climate Change*, *6*(2), 116–118.

Wolf, K., & Woods, J. D. (1988). *Toward a theory on biological-physical interactions in the world ocean*. Dordrecht ; London: Kluwer Academic.

Woods, J., & Barkmann, W. (1993). Diatom demography in winter-simulated by the Lagrangian Ensemble method. *Fisheries Oceanography*, *2*(3-4), 202–222.

Woods, J., & Barkmann, W. (1993b). The plankton multiplier-positive feedback in the greenhouse. *Journal of Plankton Research*, *15*(9), 1053.

Woods, J., & Barkmann, W. (1994). Simulating plankton ecosystems by the Lagrangian Ensemble method. *Philosophical Transactions: Biological Sciences*, *343*(1303), 27–31.

Woods, J. D. (2005). The Lagrangian Ensemble metamodel for simulating plankton ecosystems. *Progress in Oceanography*, *67*, 84–159. http://doi.org/10.1016/J.Pocean.2005.04.003

Woods, J. D., & Onken, R. (1982). Diurnal variation and primary production in the ocean preliminary results of a Lagrangian ensemble model. *Journal of Plankton Research*, *4*(3), 735–756. http://doi.org/10.1093/plankt/4.3.735

Woods, J., Perilli, A., & Barkmann, W. (2005). Stability and predictability of a virtual plankton ecosystem created with an individual-based model. *Progress in Oceanography*, *67*, 43–83. http://doi.org/10.1016/J.Pocean.2005.04.004

Yamazaki, H., & Kamykowski, D. (1991). The vertical trajectories of motile phytoplankton in a wind-mixed water column. *Deep Sea Research Part A. Oceanographic Research Papers*, *38*, 219–241. http://doi.org/10.1016/0198-0149(91)90081-P

Yool, A., Popova, E. E., & Anderson, T. R. (2011). Medusa-1.0: a new intermediate complexity plankton ecosystem model for the global domain. *Geoscientific Model Development*, *4*, 381–417.

Yool, A., Popova, E. E., & Anderson, T. R. (2013). MEDUSA-2.0: an intermediate complexity biogeochemical model of the marine carbon cycle for climate change and ocean acidification studies. *Geoscientific Model Development*, *6*, 1767–1811.

Yool, A., Popova, E. E., & Coward, A. C. (submitted). Future change in ocean productivity: Is the Arctic the new Atlantic? *J. Geophys. Res.*

Zonneveld, C. (1998). A cell-based model for the chlorophyll a to carbon ratio in phytoplankton. *Ecological Modelling*, *113*(1), 55–70.